LASER INDUCED FLUORESCENCE AND ENERGY TRANSFER IN CERTAIN RARE EARTH IONS DOPED IN LaF_3 SINGLE CRYSTALS

A Thesis Submitted
In Partial Fulfilment of the Requirements
for the Degree of
DOCTOR OF PHILOSOPHY

By
B. RAMI REDDY

to the
DEPARTMENT OF PHYSICS
INDIAN INSTITUTE OF TECHNOLOGY, KANPUR

JULY, 1980

TO MY BROTHER BOMMA REDDY SAMBI REDDY

I.I.T. KANPUR
CENTRAL LIBRARY
Acc. No. A 67014

10 SEP 1981

PHY-1980-D-RED-LAS

POST GRADUATE OFFICE
I.I.T Kanpur.
Submitted on 31.7.80

CERTIFICATE

This is to certify that the work presented in this thesis is the original work of Mr. B. Rami Reddy done under my supervision and it is not submitted elsewhere for a degree.

Putcha Venkateswarlu 30/7/80

(Putcha Venkateswarlu)
Senior Professor of Physics
Indian Institute of Technology
Kanpur, (U.P.) India

POST GRADUATE OFFICE
This thesis has been approved for the award of the Degree of Doctor of Philosophy (Ph.D.) in accordance with the regulations of the Indian Institute of Technology Kanpur
Dated: 9.6.1981

ACKNOWLEDGEMENTS

I am very grateful to Professor P. Venkateswarlu for introducing me to the field of solid state spectroscopy and for his constant encouragement and help during my stay here. I once again thank Smt. and Dr. Venkateswarlu for their hospitality.

I am also thankful to Dr. G.N. Rao with whom I associated for some time during the earlier part of my stay here.

I thank Drs. A. Sivaram and U.V. Kumar for helping me to get acquainted with the spectrometer. I thank Dr. G. Chakrapani for extending his co-operation. Thanks are due to Drs. H. Jagannath, D. Narayana Rao and Bansilal for their help. I acknowledge the help received from Mr. Bh.A.R.B. Raju and Mr. Jagir Singh.

I thank Mr. V.N. Sarma and Mr. S.K. Basu for their company and co-operation.

I thank Mr. N.V.G. Swamy for his help in the laboratory. It gives me pleasure to thank Mr. Piar Singh, Mr. D.S. Rawat, Mr. S.L. Yadav and Mr. Kuldip Singh Ubhey who were very helpful during the course of my work. I also acknowledge Mr. R.K. Garg, Mr. Bahadur Singh, Mr. P. Tewari and Mr. S.K. Anand.

ACKNOWLEDGEMENTS

I am very grateful to Professor P. Venkateswarlu for introducing me to the field of solid state spectroscopy and for his constant encouragement and help during my stay here. I once again thank Smt. and Dr. Venkateswarlu for their hospitality.

I am also thankful to Dr. G.N. Rao with whom I associated for some time during the earlier part of my stay here.

I thank Drs. A. Sivaram and U.V. Kumar for helping me to get acquainted with the spectrometer. I thank Dr. G. Chakrapani for extending his co-operation. Thanks are due to Drs. H. Jagannath, D. Narayana Rao and Bansilal for their help. I acknowledge the help received from Mr. Bh.A.R.B. Raju and Mr. Jagir Singh.

I thank Mr. V.N. Sarma and Mr. S.K. Basu for their company and co-operation.

I thank Mr. N.V.G. Swamy for his help in the laboratory. It gives me pleasure to thank Mr. Piar Singh, Mr. D.S. Rawat, Mr. S.L. Yadav and Mr. Kuldip Singh Ubhey who were very helpful during the course of my work. I also acknowledge Mr. R.K. Garg, Mr. Bahadur Singh, Mr. P. Tewari and Mr. S.K. Anand.

My sincere thanks are due to Professor R.K. Asundi and Dr. B.N. Khanna who have gone through the manuscript and suggested some modifications.

I acknowledge Mr. R.K. Bajpai, Mr. Kalyan Das and Mr. Ganguly for their help.

I thank Ms. C. Komala for the neat and patient typing of the manuscript and Mr. H.K. Panda for the careful cyclostyling work.

I thank all my friends for their good company.

The financial assistance from the INSA is gratefully acknowledged.

B. Rami Reddy

CONTENTS vi

LIST OF FIGURES x

LIST OF TABLES xvi

SYNOPSIS xviii

CHAPTER 1

INTRODUCTION

1.1 General 1

1.2 Ion-lattice interaction 3

1.3 Laporte-forbidden transitions 5

1.4 Polarization in crystals 7

1.5 Relaxation 9

1.6 Energy transfer 12

1.6.1 Radiative energy transfer 12

1.6.2 Non-radiative energy transfer 13

1.6.3 Exchange interaction 13

1.6.4 Ion-ion interaction 14

1.7 Resonance energy transfer 14

1.8 Phonon-assisted non-radiative energy transfer 17

1.9 Macroscopic case of energy transfer 19

1.10 Migration of excitation 23

1.11 Energy up-conversion 23

REFERENCES 29

CHAPTER 2

EXPERIMENTAL DETAILS

ABSTRACT 32

2.1 Introduction 33

2.2 Excitation source 33

2.3 Optics for collecting the signal 36

2.4 Spectrophotometer 37

2.5 Recording the spectra 38

2.6 Calibration 38

2.7 Excitation spectra 41

2.8 Decay time measurements 41

2.9 Dewar for low temperature work 44

2.10 Crystals used 44

CHAPTER 3

LASER INDUCED FLUORESCENCE AND SITE SYMMETRY

ABSTRACT 47

3.1 Introduction 48

3.2 Proposed crystal structure for Lanthanum Trifluoride 50

3.3 Selection rules 57

3.4 Salient features in the fluorescence spectra 64

3.5 Fluorescence spectra 66

3.6 Fluorescence originating from $^3P_0$ 73

1. Fluorescence terminating in $^3H_4$ 79
2. Fluorescence terminating in $^3H_5$ 83
3. Fluorescence terminating in $^3H_6$ 86
4. Fluorescence terminating in $^3F_2$ 89
5. Fluorescence terminating in $^3F_3$ 92
6. Fluorescence terminating in $^3F_4$ 94

3.7 Fluorescence originating from $^3P_1(^1I_6)$ 97

3.8 Room temperature fluorescence 100

3.9 Fluorescence originating from $^3P_2$(LNT) 105

3.10 Resonance fluorescence from $^1D_2$ multiplet 106

3.11 Excitation spectra 114

3.12 Conclusion 122

REFERENCES 123

CHAPTER 4

ENERGY TRANSFER STUDIES

ABSTRACT 125

4.1 Radiative energy transfer 126

4.1.1 General 126

4.1.2 Oscillator strength (f) 129

4.1.3 Evaluation of the f-number 129

4.2 Non-radiative energy transfer 138

4.2.1 Introduction 138

4.2.2 Experimental 140

4.2.3 Results 142

(a) $LaF_3:Pr^{3+}$ 142

(b) $LaF_3:Nd^{3+}$ (Impurity Pr^{3+}) 145

(c) $LaF_3:Dy^{3+}$ (Impurity Pr^{3+}) 148

(d) $LaF_3:Ho^{3+}$ (Impurity Pr^{3+}) 152

4.2.4 Discussion 152

(i) $LaF_3:Nd^{3+}$ 152

(ii) Efficiency of energy transfer 159

(iii) $LaF_3:Dy^{3+}$ 160

(iv) $LaF_3:Ho^{3+}$ 165

4.2.5 Conclusion 166

REFERENCES 168

CHAPTER 5

ENERGY UP-CONVERSION STUDIES

ABSTRACT 170

5.1 Introduction 171

5.2 Experimental results and discussion 181

5.2.1 Fluorescence from D multiplet 181

5.2.2a Fluorescence from R multiplet 181

5.2.2b Concentration quenching of R level Fluorescence 187

5.2.3 Fluorescence from S multiplet (Room temperature) 191

5.2.4 Energy up-converted fluorescence from E multiplet 196

5.2.5 Energy up-converted fluorescence from L multiplet 203

5.2.6 Rate equation model 215

5.3 Conclusion 220

REFERENCES 221

LIST OF FIGURES

Figure		Page
1.1	Optically positive and negative crystals	8
1.2	Diagrams of phenomena caused by ion-ion coupling or up-conversion of radiation	27
2.1	Block diagram of the experimental set-up	34
2.2	Schematic diagram of the wavelength marker circuit	39
2.3	Emitter follower	43
2.4	Cold finger dewar used for work at liquid nitrogen temperature	45
3.1	(a) D^3_{6h} and (b) D^4_{3d} crystal structures of LaF_3	51
3.2	C^3_{6v} structure of LaF_3	55
3.3	Energy level diagram of $LaF_3:Pr^{3+}$ showing the observed fluorescence groups	72
3.4	Fluorescence spectrum of $LaF_3:Pr^{3+}$ at LNT; $^3P_0 \rightarrow {}^3H_4$ group	80
3.5	Partial energy level diagram of $LaF_3:Pr^{3+}$ showing the fluorescence transition group $^3P_0 \rightarrow {}^3H_4$ at LNT	81
3.6	Fluorescence spectrum of $LaF_3:Pr^{3+}$ at LNT $^3P_0 \rightarrow {}^3H_5$ group	84
3.7	Partial energy level diagram of $LaF_3:Pr^{3+}$ showing the fluorescence transition group $^3P_0 \rightarrow {}^3H_5$ at LNT	85
3.8	Fluorescence spectrum of $LaF_3:Pr^{3+}$ at LNT, $^3P_0 \rightarrow {}^3H_6$ group	87

3.9 Partial energy level diagram of $LaF_3:Pr^{3+}$ showing the fluorescence transition group $^3P_0 \longrightarrow {}^3H_6$ at LNT 88

3.10 Fluorescence spectrum of $LaF_3:Pr^{3+}$, $^3P_0 \rightarrow {}^3F_2$ group 90

3.11 Partial energy level diagram of $LaF_3:Pr^{3+}$ showing the fluorescence transition group $^3P_0 \longrightarrow {}^3F_2$ 91

3.12 Partial energy level diagram of $LaF_3:Pr^{3+}$ showing the fluorescence transition group $^3P_0 \longrightarrow {}^3F_3$ at LNT 93

3.13 Fluorescence spectrum of $LaF_3:Pr^{3+}$ at LNT, $^3P_0 \longrightarrow {}^3F_4$ group 95

3.14 Partial energy level diagram of $LaF_3:Pr^{3+}$ showing the fluorescence transition group $^3P_0 \longrightarrow {}^3F_4$ at LNT 96

3.15 Fluorescence spectrum of $LaF_3:Pr^{3+}$ at LNT, $^3P_1(^1I_6) \longrightarrow {}^3F_3$ and $^3P_2 \longrightarrow {}^3F_4$ groups 98

3.16a Fluorescence spectrum of $LaF_3:Pr^{3+}$ observed only at RT showing transitions from phonon coupled levels of $^3P_0$ and $^3P_1$ to $^3F_3$ levels 102

3.16b Partial energy level diagram of $LaF_3:Pr^{3+}$ showing transitions from $^3P_1$ and phonon coupled levels of $^3P_0$ terminating in $^3F_3$ observed at RT. 103

3.17 Fluorescence spectrum of $LaF_3:Pr^{3+}$ at RT, $^3P_1(^1I_6) \longrightarrow {}^3H_5$, $^3P_0 \longrightarrow {}^3H_5$ and $^3P_1(^1I_6) \rightarrow {}^3H_6$ groups 104

3.18	Fluorescence spectrum of $LaF_3:Pr^{3+}$ at LNT, $^1D_2 \longrightarrow {}^3H_4$ group	109
3.19	Partial energy level diagram of $LaF_3:Pr^{3+}$, showing the fluorescence transition group, $^1D_2 \longrightarrow {}^3H_4$ at LNT	110
3.20	Fluorescence spectrum of $LaF_3:Pr^{3+}$ at LNT, $^1D_2 \longrightarrow {}^3H_5$ group	111
3.21	Partial energy level diagram of $LaF_3:Pr^{3+}$ showing the fluorescence transition group, $^1D_2 \longrightarrow {}^3H_5$ at LNT	112
3.22	Excitation spectrum of 4791.5 Å showing from $^3H_4$ to $^3P_0$, $^3P_1$ ($^1I_6$) levels at LNT	115
3.23	Excitation spectrum of 7888 Å showing transitions from $^3H_4$ to $^1D_2$ levels at LNT	116
3.24	Excitation spectrum of 5218 Å showing transitions from $^3H_4$ to $^3P_1(^1I_6)$ levels at RT.	118
3.25	Observed excitation transitions of $LaF_3:Pr^{3+}$ at room and liquid nitrogen temperatures	121
4.1	Self-absorption in $LaF_3:Pr^{3+}$ at LNT (Radiative energy transfer) of 4791.5 Å	127
4.2	Variation of line centre intensity of the self-reversed line (4791.5 Å) with x at LNT	134
4.3	Variation of hump separation^2(S^2) of the self-reversed line at 4791.5 Å of the $^3P_0 \longrightarrow {}^3H_4$ group with x at LNT	136

4.4 Partial energy level diagrams of Pr^{3+}, Nd^{3+}, Dy^{3+} and Ho^{3+} in LaF_3 141

4.5 Fluorescence spectrum of LaF_3:Pr^{3+} at LNT 143

4.6 Excitation spectrum of 5985.4 Å transition of LaF_3:Pr^{3+} at LNT 144

4.7 Fluorescence spectrum of LaF_3:Nd^{3+} (Impurity Pr^{3+}) at LNT. 146

4.8 Excitation spectrum of LaF_3:Nd^{3+} (Impurity Pr^{3+}) at LNT (of 5946.4 Å). 147

4.9 Fluorescence spectrum of LaF_3:Dy^{3+}(Impurity Pr^{3+}) at LNT 149

4.10 Excitation spectrum of 5946.4 Å transition of LaF_3:Dy^{3+} (Impurity Pr^{3+}) at LNT 150

4.11 Excitation spectrum of 5695 Å (F Y) transition of LaF_3:Dy^{3+} (Impurity Pr^{3+}) at LNT. 151

4.12 Non radiative transition probabilities at 77°K for several excited states of Er^{3+} in LaF_3 plotted as a function of energy gap to the next-lower multiplet. 154

4.13 Possible ion-pair transitions between energy levels of $Pr^{3+}(^3P_0 \rightarrow {}^1D_2)$ and Nd^{3+} (Z→X) in LaF_3. 156

5.1 Partial energy level diagram of LaF_3:Nd^{3+} showing the observed fluorescence groups at room and/liquid nitrogen temperature when D levels are resonantly excited. 180

5.2 Fluorescence spectrum of LaF_3:Nd^{3+} at LNT, R→Z group 182

5.3	Excitation spectrum of $LaF_3:Nd^{3+}$ at LNT (Ex. Spec. 8656 Å).	183
5.4	Possible ion-pair transitions between the energy level of $LaF_3:Nd^{3+}$ (D — R; Z — W)	186
5.5	Fluorescence spectrum of $LaF_3:Nd^{3+}$ for four different concentrations at room temperature, R → Z group	188
5.6	Possible ion-pair transitions between the energy levels of $LaF_3:Nd^{3+}$ (R — W; Z — W).	189
5.7	Fluorescence spectrum of $LaF_3:Nd^{3+}$ observed only at room temperature, S → Z group	192
5.8	Excitation spectrum of 7905.3 Å (S Z) at RT showing transitions from Z to D levels	193
5.9	Fluorescence spectrum of $LaF_3:Nd^{3+}$ at LNT, E → Z group	197
5.10	Fluorescence spectrum of $LaF_3:Nd^{3+}$ at LNT, E → X group	198
5.11	Excitation spectrum of $LaF_3:Nd^{3+}$ at LNT (Ex. Spec. 5232.2 Å).	199
5.12	Two probable mechanisms for the production of up-converted fluorescence. (a) The ETU process (b) The STEP process.	201
5.13	Fluorescence spectrum of $LaF_3:Nd^{3+}$ at LNT, L → Y group	204
5.14	Fluorescence spectrum of $LaF_3:Nd^{3+}$ at LNT, L → S group	205
5.15	Fluorescence spectrum of $LaF_3:Nd^{3+}$ at LNT L → A group	206

5.16 Excitation spectrum of $LaF_3:Nd^{3+}$ at LNT (Ex. Spec. 3801.6 Å). 207

5.17 Observed (a) decay and (b) delay times respectively for several concentrations of $LaF_3:Nd^{3+}$ measured at room temperature of the up-converted L fluorescence 210

5.18 ETU process 212

LIST OF TABLES

Table		Page
3.1	Character table of C_{2v} symmetry	61
3.2	Character table of C_2 symmetry	61
3.3	Character table of C_s symmetry	61
3.4	Splitting of various J levels under C_{2v}, C_2 and C_s symmetries	62
3.5	Selection rules under C_{2v} symmetry	63
3.6	Selection rules under C_2 symmetry	63
3.7	Selection rules under C_s symmetry	63
3.8	The energy levels of Pr^{3+} in LaF_3	67
3.9	Fluorescence of Pr^{3+} in LaF_3 at LNT	74
3.10	Fluorescence of Pr^{3+} in LaF_3 at RT	101
3.11	Resonance fluorescence from $^1D_2$ levels	107
3.12	$^3H_4 \rightarrow {}^3P_0$, $^3P_1(^1I_6)$ excitation transitions of $LaF_3:Pr^{3+}$ at LNT.	117
3.13	$^3H_4 \rightarrow {}^1D_2$ excitation transitions of $LaF_3:Pr^{3+}$ at LNT.	117
3.14	$^3H_4 \rightarrow {}^3P_1(^1I_6)$ excitation transitions of $LaF_3:Pr^{3+}$ at RT	119
4.1	Some possible resonant and non-resonant ion-pair transitions between $Pr^{3+}(^3P_0 \rightarrow {}^1D_2)$ and Nd^{3+} $(Z \rightarrow X)$ ions doped in LaF_3	158
4.2	Some possible non-resonant (phonon-assisted) ion-pair transitions between $Pr^{3+}(^3P_0 \rightarrow {}^1D_2)$ and Dy^{3+} $(Z \rightarrow Y)$ ions doped in LaF_3.	161

4.3	Some possible non-resonant ion-pair transitions between $Dy^{3+}(F \rightarrow Y)$ and Pr^{3+} ($^3H_4 \rightarrow {}^1D_2$) ions doped in LaF_3.	164
5.1	The energy levels of $LaF_3:Nd^{3+}$	174
5.2	Fluorescence of $LaF_3:Nd^{3+}$	178
5.3	Excitation transitions of $LaF_3:Nd^{3+}$ at LNT	184
5.4	Decay times of R and S levels measured at room temperature	184
5.5	Some possible ion-pair transitions between energy levels of $LaF_3:Nd^{3+}$ (D — R; Z — W).	184
5.6	Possible ion-pair transitions between energy levels of $LaF_3:Nd^{3+}$(R — W; Z — W).	190
5.7	Excitation transitions of $LaF_3:Nd^{3+}$ at RT	194
5.8	Possible energy matchings for ETU process (D + Y — Z + E)	202
5.9	Possible energy matchings for STEP process (Z — D ; Y — E)	202
5.10	Delay and decay times of L levels measured at room temperature	209
5.11	Energy combinations for ETU process (D + R — Z + L)	213
5.12	Energy combinations for ETU process (three body interaction).	214

SYNOPSIS

LASER INDUCED FLUORESCENCE AND ENERGY TRANSFER IN CERTAIN RARE EARTH IONS DOPED IN LaF_3 SINGLE CRYSTALS

B. Rami Reddy
Department of Physics
Indian Institute of Technology, Kanpur
India

The study of rare earth (RE) crystal spectra has been the subject of interest for a long time. Some of the RE ions doped in solid hosts are forming potential laser materials (e.g. SHIVA : Nd-glass laser). Global search has been going on for high efficient laser materials. A basic understanding of the energy levels of RE ions, their crystal spectra, deexcitation mechanisms and interaction of these ions with their neighbourhood (RE ions of similar/dissimilar kind and host lattice) is not only of academic interest but also useful in applied research. It is well known that energy transfer increases the population of certain energy levels and may even result in lasing action in certain crystalline and glass materials. The importance of energy up-conversion in photosynthesis has been realised recently. In the present thesis an attempt has been made to have a better understanding of the deexcitation and ion-ion interaction mechanisms of some of the singly/doubly doped RE ions, Pr^{3+}, Nd^{3+}, Dy^{3+} and Ho^{3+} in LaF_3 single crystals. With the advent of intense narrow

band lasers the understanding of weak ion-ion interactions has become feasible.

The first Chapter of the thesis deals with the general principles of RE crystal spectra, and the various relaxation and energy transfer processes that take place in such systems.

Experimental details are presented in the second Chapter. Fluorescence and excitation spectra have been recorded using CW Ar^+ and (pulsed) N_2 pumped dye lasers. A 0.75 m Jarrell-Ash spectrograph fitted with FW 130 photomultiplier, and picoammeter and strip chart recorder combination is used in recording the spectra. Decay times have been measured using a calibrated oscilloscope.

The results of the optical excitation and fluorescence spectra of $LaF_3:Pr^{3+}$ are discussed in the third Chapter. Vast data is presented which was not reported earlier. At liquid nitrogen temperature six fluorescence groups, $^3P_0 \rightarrow {}^3H_{4,5,6}$; $^3F_{2,3,4}$ have been observed. [Weak fluorescence arising from $^3P_1$ ($^1I_6$) levels is observed on excitation with CW Ar^+ laser]. All the proposed sites C_{2v}, C_2 and C_s have been tried to explain the salient features of the $^3P_0$ fluorescence. Though the three different site symmetries are able to explain a major part of the spectra, it is observed that only C_s site symmetry

has been able to account for all the observed polarized transitions. At room temperature strong fluorescence has been observed from $^3P_1$ ($^1I_6$) levels to $^3H_5$, and $^3F_3$ and weak fluorescence to $^3H_6$ levels. Some fluorescence transitions in the regions 5784-5824 Å and 6625-6912 Å have been observed only at room temperature whatever might be the excitation source. This suggests that there is a fast relaxation at liquid nitrogen temperature from $^3P_1(^1I_6)$ levels to $^3P_0$ level. At room temperature thermal population of $^3P_1(^1I_6)$ levels from $^3P_0$ level is also appreciable. Resonance fluorescence has been observed from $^1D_2$ levels to $^3H_{4,5,6}$ and $^3F_2$ levels. The intensity of the fluorescence groups obey Ofelt's theory.

The fourth Chapter discusses the energy transfer processes that have been observed in singly/doubly doped RE ions in LaF_3. The radiative transition at 4791.5 Å in $LaF_3:Pr^{3+}$ (1 percent) is found to be self-absorbed in the crystal medium itself (Radiative energy transfer). Oscillator strength of this transition is estimated to be 1.4×10^{-6}, which is in good agreement with the absorption value measured by Krupke.

When ^3P groups of levels are excited, no fluorescence emission is observed from $^1D_2$ levels of $LaF_3:Pr^{3+}$. Under the same excitation conditions we have

observed $^1D_2$ emission in $LaF_3:Nd^{3+}$, Pr^{3+} and $LaF_3:Dy^{3+}$, Pr^{3+} but not in $LaF_3:Ho^{3+}$, Pr^{3+}. On the basis of excitation spectra and decay time measurements, it has been concluded that the $^1D_2$ emission was possible by ion-pair relaxation. In this process the Pr^{3+} ion relaxes from $^3P_0$ to $^1D_2$ levels non-radiatively, simultaneously exciting the nearby Nd^{3+} or Dy^{3+} ion from the ground levels to higher excited levels. The efficiency of energy transfer in $LaF_3:Nd^{3+}$, Pr^{3+} is estimated to be 36 percent. It has been found from the energy level positions, that 3-4 phonons are needed for ion-pair relaxation to take place in $LaF_3:Ho^{3+}$, Pr^{3+}. If this process were to be operative this would be weaker by few orders of magnitude than resonant process. It has been suggested that the lack of resonance between the energy levels of these ions is a possibility for the absence of $^1D_2$ emission in $LaF_3:Ho^{3+}$, Pr^{3+}.

The fifth Chapter deals with the energy up-conversion processes that have been observed in $LaF_3:Nd^{3+}$. When the D levels are resonantly excited fluorescence is observed from R, S and D levels and energy up-converted fluorescence from E, K and L levels. We have found that the R levels are populated by ion-pair relaxation of the type, $D(1) + Z(2) \longrightarrow R(1) + W(2)$ (1 and 2 represent ions). It has been concluded, from decay time measurements, that the S levels (whose fluorescence was observed only at room

temperature) were populated thermally from R levels. Two processes, a sequential two photon excitation (STEP) and an energy transfer up-conversion (ETU) have been suggested for the population of E levels.

Delay and decay times have been measured of the induced L fluorescence for different concentrations of Nd^{3+} in LaF_3. The delay time has been found to decrease with increasing concentration of Nd^{3+} whereas the magnitude of the decay time is of the same order of magnitude as if measured intrinsically (on resonant excitation). The observed delayed nature of L fluorescence suggested ion-pair relaxation. From the energy level matchings it has been suggested that two ions one in R level and the other in D level undergo energy transfer interaction (ETU) leaving one ion in the L level and the other ion in the Z level. A rate equation model has been developed which could explain the delayed emission from L levels.

CHAPTER 1

INTRODUCTION

1.1 General

LASER has proved to be one of the most powerful sources of energy and has applications in various fields of science and engineering. Solid state lasers like Nd-glass, Ruby and others have come to exist as powerful tools for basic and applied research. Some of the rare earth (RE) ions are known to lase in different hosts. Therefore a thorough understanding of the energy levels of the rare earth ions, their decay mechanisms along with their interactions with the surrounding medium is not only of academic interest but also of practical use. A good amount of work has been going on in various schools of research in this direction and the present work is taken to understand specifically various features and phenomena associated with Pr^{3+}, Nd^{3+}, Dy^{3+} and Ho^{3+} in LaF_3.

Based on x-ray analyses different crystal structures [1], D^3_{6h} (C_{2v}), D^4_{3d} (C_2), D^4_{6h} (D_{3h}) and C^3_{6v} (C_s) have been suggested. The symbols in the parenthesis represent the site symmetry of La^{3+} ion. In such a case spectroscopic study of isovalent impurity rare earth ions will be helpful. So in the present study we have made an attempt to study the energy levels of Pr^{3+} in LaF_3 in detail. The site symmetry of Pr^{3+} in LaF_3 has been fixed (C_s) on the basis

of observed polarized spectra. So a brief description of RE ions and the effect of lattice on these ions and the characteristics of radiative processes in crystals (polarization) are discussed briefly in the first few pages of this Chapter. We have also made an attempt to study the relaxation processes of some of the energy levels of Pr^{3+} ion and their interactions with the co-dopant, Nd^{3+}, Dy^{3+} or Ho^{3+} ions in LaF_3. We have also observed blue fluorescence in LaF_3:Nd^{3+} on excitation with yellow laser line. The energy transfer and energy upconversion phenomena have therefore, been discussed in greater detail in the later pages of this Chapter.

Rare earth ions form a group of elements, which have in common a partially filled 4f-shell. They form mostly trivalent compounds and it is principally the properties of the trivalent ions which are important rather than those of neutral atoms. All trivalent ions have the Xe like rare gas shell of fifty four electrons in common and contain, in addition $4f^n$ electrons, with n ranging from 0 (La^{3+}) to 14 (Lu^{3+}). Considerable work [2] has been done on the crystal spectra of rare earths, particularly of the lanthanides. In triply ionized lanthanides, the f-electrons are active which are well shielded from the outside influence by $5s^2$ $5p^6$ electrons. Hence the interaction of the environment with 4f electrons

is weak and the ion retains its 'free-ion' properties even in solid hosts. The observed fluorescence lines of these ions are due to transitions among the levels of $4f^n$ configurations. These are forbidden transitions in a free ion but become allowed in crystal field due to admixing of states with opposite parity. This results in large lifetimes of the energy levels and consequently sharp spectral lines are observed. For a given ion while the structure of these groups of lines changes from host to host, the relative positions of their centres of gravity are very nearly the same.

1.2 Ion-lattice interaction

The Hamiltonian [3] of an ion embedded in a crystal lattice is given by

$$H = H_F + V_c \qquad (1)$$

where H_F is the free ion Hamiltonian and V_c represents the interaction of the ion with the crystalline environment. The free ion Hamiltonian is expressed as

$$H_F = \sum_{i=1}^{n} \left(-\frac{\hbar^2}{2m}\nabla_i^2 - \frac{Z_e^2}{r_i}\right) + \sum_{i<j}^{n} \frac{e^2}{r_{ij}} + \sum_{i=1}^{n} \xi_i (l_i \cdot S_i) \qquad (2)$$

In the zero order approximation the f-electrons are considered to be in a central field produced by the nucleus and the fifty four core electrons. In this approximation all states arising out of a given configuration have the same energy. The degeneracy is partly removed with the inclusion of interelectronic repulsion and spin-orbit interaction. For a free ion spherical symmetry exists, and each level is $(2J + 1)$ fold degenerate. On placing the ion in a crystal, the spherical symmetry is destroyed and each level splits under the influence of the electric field produced by the environment. Usually, the environment about the rare earth ion will possess a well defined symmetry (lower than spherical). The degree to which this degeneracy is removed will depend on the site symmetry of the rare earth ion. For odd electron systems there is a two-fold degeneracy (called Kramers degeneracy) in the energy states which cannot be removed by any electric fields. This degeneracy is removed only by the application of the magnetic field. The effect of V_c is treated as perturbation on the eigenvalues and eigenfunctions of H_F. The eigenfunctions of H_F are spherically symmetric. Hence V_c is expanded [3] interms of spherical harmonics or operators that transform like spherical harmonics. V_c is expanded in terms of tensor operators $c_q^{(k)}$ to give $V_c = \sum_{k,q,i} B_q^k (c_q^{(k)})_i$. The values of K and q are

limited by the point symmetry of the rare earth ion site, since the Hamiltonian must be invariant under the operations of the point symmetry group.

Crystals doped with rare earth ions emit fluorescence when they are excited into one of their excited states. This emission is due to transitions between energy levels of the same configuration. Selection rules don't permit E.D. transitions between the levels of the same configuration. But experimentally E.D. transitions are observed. These transitions are called Laporte-forbidden transitions because they donot obey the Laporte-rule. The transitions that are generally encountered in RE ion doped crystals are described below.

1.3 Laporte-forbidden transitions [4]

The spectral lines arising from the transitions between levels belonging to the same electronic configuration can be classified as follows:

1. Electric dipole transitions in a crystalline field having no centre of symmetry

Since the observed spectral lines are due to transitions between levels of the same electronic configuration, electric dipole transitions are not possible between these levels. But the crystal field mixes the levels of opposite parity at the non-centrosymmetric sites. For example $4f^n$ levels contain small admixture of $4f^{n-1}$ 5d levels. When such a mixing occurs electric dipole transitions are

allowed. The oscillator strengths of the forced electric dipole transitions are of the order of 10^{-6}.

2. Electric dipole transitions in a crystalline field having a centre of symmetry (vibrationally induced)

If a rare earth ion is at the centre of inversion, the crystal field can no longer mix the states of opposite parity. But mixing of states of different parities is also produced by lattice vibrations of odd symmetry that are coupled to the ionic system. As a consequence of this mixing certain vibrationally induced electric dipole transitions are allowed. The f-numbers of such transitions are temperature dependent.

3. Magnetic dipole transitions

These transitions are allowed between states for which $\triangle L = 0$, $\triangle S = 0$ and $\triangle J = 0, \pm 1$. The oscillator strengths are of the order of 10^{-8}.

Vibrationally induced magnetic dipole transitions and electric quadrupole transitions are insignificant in rare earth crystals and so are not considered in detail.

Most of the observed radiative transitions in crystals are polarized. In some crystals even unpolarized

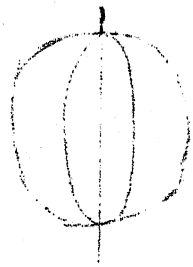
transitions are also observed. The polarization of the radiation depends upon the site symmetry of the ion in the crystal. Whether polarized transitions are observed in every crystal host or not is another question and is discussed in the later sections.

1.4 Polarization in crystals [5]

The vector surface for the velocity of light in any cubic crystal is a sphere. For any noncubic crystal it is not. Cubic crystals are optically isotropic. That is the vector surface of light is a sphere at any instant. All other crystals are anisotropic. In trigonal, tetragonal and hexagonal crystals the light travelling in a given direction is broken up into two rays, polarized at right angles to each other, travelling at different velocities. There are thus two vector surfaces. One is spherical, like the surface in ordinary glass, air and somewhat-less-ordinary cubic crystals, and is the ray-velocity surface of the ordinary ray. The other is an ellipsoid of revolution and is the ray velocity surface of the extraordinary ray. The spherical, ordinary ray-velocity surface coincides with the extraordinary ray-velocity surface at two points only. They are the ends of the axis of revolution of the ellipsoid, so that a cross section of the ordinary ray-velocity surface and the extraordinary ray-velocity surfaces look like Fig. 1a & b

according to whether the crystal is optically positive or negative (positive and negative are arbitrary).

(a) positive



(b) negative

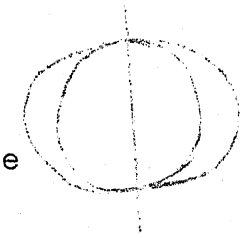


Fig.1.1 Optically positive and negative crystals

If the extraordinary ray is the slow ray, relative to the ordinary ray, then the ellipsoid will lie inside the sphere and the crystal will be said to be optically positive. If the extraordinary ray is the fast ray relative to the ordinary ray, then the ellipsoid will lie outside of the sphere, and the crystal will be said to be optically negative. Light travelling along the axis of revolution of the ellipsoid will have a single velocity. This direction is called the optic axis. Only along this direction does light pass through a crystal as though it were passing through an isotropic medium (ofcourse exceptions will be there). In every other direction light is broken up into two rays, both polarized, which travel with different velocities. The difference in velocity increases from zero along the optic axis to a maximum for propagation normal to the optic axis.

In general, the vibration direction of the polarized extraordinary ray is the plane defined by the

propagation direction (ray direction) and the optic axis. That of the ordinary ray is normal to this and normal to the propagation direction of the ray. Since these ray velocity figures have one optic axis, the tetragonal, trigonal and hexagonal crystals are said to be optically uniaxial. The optic axis will by symmetry, coincide with the c-axis in this case (4, 3 or 6 - fold respectively). The orthorhombic, monoclinic and triclinic crystals which have ray-velocity surfaces with two optic axes are said to be optically biaxial.

1.5 Relaxation

When an ion is excited it may come down to the lower level radiatively or non-radiatively. The relaxation of excited energy levels depends significantly on the immediate surroundings of the excited RE ions because, when the rare earth ions are placed in a crystal lattice they are subjected to a number of forces which are absent in the free ion. There can be resonant interactions among ions of the same or different kinds. There can be coupling between rare earth ions and host lattice so that the ions can transfer some or all of their energy to the crystal lattice vibrations. Therefore, ions in excited states, can relax radiatively as well as non-radiatively. The observed lifetimes of the excited states are the inverse of the sum of the probabilities

for all possible transitions (radiative and non-radiative) to all lower levels. That is,

$$\tau_i^{-1} = \sum_j w_{ij}^r + \sum_j w_{ij}^{nr} \qquad (3)$$

where w_{ij}^r (w_{ij}^{nr}) is the probability of radiative (non-radiative) transition from level i to j. The radiative relaxation of the lanthanide ions is mostly due to forced electric dipole transitions which become allowed because of configurational mixing. Magnetic dipole transitions are also encountered in radiative relaxation. The radiative [6] lifetime is obtained by calculating the total spontaneous emission probability or from combined measurements of the relative and absolute intensities in absorption and fluorescence spectra. Judd and Ofelt [7] have shown that the probabilities for an electric dipole transition can be expressed in terms of parameters which involve the strength of configuration interaction. Non-radiative decay by phonon/multiphonon process is related to the energy gap between the excited level and the next lower level. The multiphonon relaxation is found to depend exponentially on the energy gap. Miyakawa and Dexter [8] found a relation between multiphonon relaxation rate and the energy gap (ΔE) between the levels as

$$W_{mpr}(\triangle E) = W_{mpr}(0)\ e^{-\alpha \triangle E} \qquad (4)$$

where α is given by $\alpha = \frac{1}{\hbar w}\left\{ \ln\left[\frac{N}{g(n+1)}\right] - 1 \right\}$ (5)

In the above expression g is the electron-lattice coupling constant, n is the number of phonons excited at the temperature of the system, $\hbar w$ is the phonon energy which contributes significantly and N is the number of phonons emitted in the process, namely, $N = \frac{\triangle E}{\hbar w}$. Multiphonon transition rate for several excited states of Er^{3+} in LaF_3 host has been studied by Weber [9]. Riseberg and Moos [10] studied the multiphonon decay of the E ($^6F_{3/2}$) level of $LaBr_3:Dy^{3+}$ as a function of temperature. Their data were fitted by a theoretical model involving the stimulated emission of phonons by thermally populated phonon-modes. German and Kiel [11] have studied radiative and non-radiative transitions in $LaCl_3:Pr^{3+}$ and $PrCl_3$. A more refined model of the relaxation processes in the ^3P states is described which qualitatively explains the exceptionally large relaxation rates of the $^3P_2$ state and the much slower $^3P_1$ decay rate. According to this model $^3P_2$ first relaxes to $^1I_6$ which in turn relaxes to $^3P_1$. The phonon close to the cut off [8] frequency is found to play a dominant role in the relaxation process, and is supported by the observations of Fong et al. [12].

So far we have considered only the effect of lattice on the relaxation of excited energy levels. But the presence of other impurity ions, similar/dissimilar to the fluorescing ions in their vicinity affects the relaxation of these levels. This effect of other impurity ions on the relaxation of fluorescing ions is discussed separately in the later sections.

1.6 Energy transfer

The processes such as sensitization, quenching of fluorescence and energy transfer up-conversion depend significantly upon the interactions among the rare earth ions. Sometimes energy transfer may sensitize even crystalline and glass lasers [13]. Energy transfer may increase the population of excited levels of lanthanides by one or two orders of magnitude compared with the direct absorption of light by the rare earth ions. With the advent of intense narrow band lasers the understanding of such energy transfer mechanisms has become feasible. Energy transfer occurs in fluorescence when excitation energy of an ion is partly or completely transferred to a different ion. The energy transfer may occur without charge transport. The energy transfer can occur radiatively or non-radiatively.

1.6.1 Radiative energy transfer

When the transfer is radiative, the photons emitted by the 'sensitizer' (or donor) ions are absorbed by the

'activator' (or acceptor) so that transfer depends upon the size (or shape) of the sample and concentration of the dopants. Moreover depending on the degree of overlap between the emission spectrum of the sensitizer and the absorption spectrum of the activator the form of the emission spectrum changes with activator concentration. (Also see Sec.4.1).

1.6.2 Non-radiative energy transfer

When the transfer of energy is non-radiative, no change occurs in the form of the emission spectrum. This energy transfer takes place before the emission of radiation occurs from the excited state of the sensitizer and affects the lifetime and intensity of the emission spectra but there is no change in the form of the spectra. This transfer mechanism is independant of the size of the sample. There are two types of non-radiative energy transfer one by exchange interaction and the other by the ion-ion interaction.

1.6.3 Exchange interaction [14]

This occurs by the overlap of the electronic wavefunctions of the donor and acceptor ions and is consequently a very short range interaction, falling off exponentially with the distance between the ions. f-electron wavefunctions are localized in LaF_3 host and hence the overlap of wavefunctions does not occur in this case. So, this type of interaction is not considered in detail.

1.6.4 Ion-ion interaction

This transfer mechanism takes place by the overlap of the dipole (or quadrupole) field of the sensitizer (or donor) with the dipole (or quadrupole) field of the activator (or acceptor). This can happen in the following ways.

(a) A portion of the excitation energy may be transferred to a neighbouring ion (ion-pair decay).

(b) All of the excitation energy may be transferred from one ion to another, in a random walk fashion, until a sink is reached which is capable of dissipating the energy (Migration decay).

1.7 Resonance energy transfer

Initial formulations on energy transfer were due to Perrins [15], Förster [16] and Dexter [14]. Consider two molecules each with one excitable electronic state separated from its ground state with nearly equal energy. When there is a suitable interaction between the two electronic systems, the excitation will jump from one molecule to the other before one is able to emit a quantum of fluorescence. The mutual interactions are coulomb interactions of the van der Waals type between the two systems. Förster, first treated such a case quantum mechanically, for organic molecules in solutions. He assumed that the transitions in

the sensitizer and the activator are allowed by electric dipole. However, Dexter pointed out that this theory should be extended to include higher multipole and exchange interactions which are responsible for resonance energy transfer in all inorganic systems. The coulombic interaction between electrons and cores of ions S and A gives rise to the dominant cross relaxation process[φ]. The interaction energy H_{SA}, can be expanded in reciprocal powers of the inter-ionic distance. Then, H_{SA} can be written as the dipole-dipole term plus higher order terms as follows

$$H_{SA}(R) = \frac{e^2}{KR^3}\left[r_S \cdot r_A - \frac{3(r_S \cdot R)(r_A \cdot R)}{R^2}\right] + \text{higher order terms} \qquad (6)$$

where R, e and K are respectively the inter-ionic distance, magnitude of electronic charge and dielectric constant of the medium in which the ions are embedded. r_A is given by $r_A = \sum_i r_{Ai}$ where r_{Ai} is the vector from the nucleus to the electron i of the ion A and r_S is defined similarly. The electric dipole-dipole, dipole-quadrupole and quadrupole-quadrupole interaction energies are inversely proportional to the third, fourth and fifth powers respectively of the inter-ionic separation. Dexter derived the following expression for the probability of resonance

φ S represents the sensitizer and A the acceptor.

transfer per unit time that energy will be transferred between the two ions:

$$P(R) = \frac{2\pi}{\hbar} \left| \langle \psi_S^* \psi_A | H_{SA} | \psi_S \psi_A^* \rangle \right|^2 \int g_S(E) g_A(E) dE \qquad (7)$$

where ψ_S^* and ψ_S, ψ_A^* and ψ_A are the excited and ground state wave functions of the sensitizer S and the activatcr A ions respectively, and where H_{SA} is the interaction Hamiltonian. The integral is over the normalized emission band shape of the sensitizer and the absorption band of the activator in which the transitions $S \rightarrow S^*$ and $A \rightarrow A^*$ are represented by the line shape functions $g_S(E)$ and $g_A(E)$ each normalized in the sense $\int g(E) dE = 1$. The dependence of energy transfer rate on S-A separation as given by Dexter is expressed as

$$P_{SA}(R) = \frac{1}{\tau_0} \left(\frac{R_0}{R} \right)^S \qquad (8)$$

where S is a positive integer taking 6,8 and 10 respectively for electric dipole-electric dipole, electric dipole-electric quadrupole and electric quadrupole-electric quadrupole transitions. τ_0 is the actual lifetime of the sensitizer excited state, R is the separation between sensitizer and activator and R_0 is the critical transfer distance, for which, excitation transfer and spontaneous deactivation have equal probability. Kushida [17] made transition probability calculations of resonance energy

transfer, cooperative sensitization of luminescence and cooperative optical transitions and compared them with experimental values. Critical concentration of energy-acceptor ions is estimated for the case of Yb - Yb transfer. He has emphasized the importance of J - selection rule in the determination of the dominant interaction term in the resonance transfer and cooperative processes.

1.8 Phonon-assisted non-radiative energy transfer

If now we consider two ions with excited states of different energies, the probability for energy transfer should drop to zero where there is no overlap between the donor and acceptor transitions involved. However it is found experimentally that energy transfer can take place without electronic energy overlap provided that the over all energy conservation is maintained by production or annihilation of phonons with energies approximately $K\Theta_d$ or KT, where Θ_d is the Debye temperature of the host lattice. When the energy of one phonon is sufficient for energy conservation, the overlap integral should be replaced by [18]

$$\frac{3W_p}{4\pi^2\hbar\rho v^5}\left|\langle A^e|V|A^e\rangle - \langle S^e|V|S^e\rangle + \langle S^o|V|S^o\rangle - \langle A^o|V|A^o\rangle\right|^2 \qquad (9)$$

where S^o, S^e and A^o, A^e are ground and excited states of sensitizer and acceptor respectively. v and ρ are the velocity of sound and specific gravity of the host lattice. V represents the ion-lattice vibration interaction and n_p is the occupation number of phonon state. $n_p + 1$ states the occupation number of phonons in emission process while n_p corresponds to the absorption process.

This shows that the phonon-assisted non-radiative energy transfer depends on the difference of the matrix elements of the orbit-lattice interaction between the ground and excited states of a given ion and also on the difference between the matrix elements of the activator and sensitizer for a given state. If the energy of the sensitizer excited state is greater than the activator excited state, the energy transfer takes place only via sensitizer to activator. This assumes that no phonon can be absorbed at the working temperature. However, in energy transfer between rare earth ions, energy mismatch could be as high as several thousand cm^{-1}s. This is much higher than the Debye cut off frequency generally found in normally encountered hosts, so that multiphonon phenomena have to be considered here [8]. According to this theory the probability of phonon-assisted energy transfer (PAT) is

$$W_{PAT}(\triangle E) = W_{PAT}(0)\, e^{-\beta \triangle E} \qquad (10)$$

where ΔE is the energy gap between energy levels of donor and acceptor. β is a parameter determined by the strength of electron-lattice coupling. The above equation has the same form as was given by Miyakawa and Dexter for multiphonon relaxation as $W_{mpr}(\Delta E) = W_{mpr}(0)\, e^{-\alpha \Delta E}$ and $\beta = \alpha - \gamma$

where $$\gamma = \frac{1}{\hbar w} \ln \left(1 + \frac{g_S}{g_A}\right) \qquad (11)$$

Yamada et al [19] studied phonon assisted energy transfer process in Y_2O_3 host. Selzer [20] dealt phonon assisted energy migration process occuring between Pr^{3+} ions. A relation similar to equation (10) has been derived by Fong et al [12] recently.

1.9 Macroscopic case of energy transfer

Upto this point we have been dealing with the microscopic case of two ions interacting with one another. To discuss the case of real macroscopic samples with many ions and to obtain a link with experimental facts, a statistical analysis on the energy transfer is necessary. The average transfer efficiency can be computed on the basis of sensitizer-activator interaction. This was studied in some detail by Inokuti and Hirayama[14]. They considered a number of activators situated at random in a sphere around a sensitizer such that the activator concentration is constant

when the volume of the sphere and the number of activator ions considered goes to infinity. They obtained the following expression for the intensity decay of the emission of the sensitizer surrounded by many activators.

$$I(t) = \exp\left[- \frac{t}{\tau} - \Gamma\left(1 - \frac{3}{S}\right) \frac{C}{C_o} \left(\frac{t}{\tau_o} \right)^{3/S} \right] \quad (12)$$

where τ_o is the decay time of the sensitizer in the absence of activator, C is the activator concentration, C_o is the critical concentration and S is the parameter of the multipolar interaction. The comparison between the experimental and the theoretical decay curves has been widely used to determine the index of the multipolar interaction involved. This theory is valid only when there is no sensitizer-to-sensitizer transfer or activator-to-activator transfer. This means that it cannot be used when dealing with high rare earth concentrations for sensitizers and activators although it should be valid when studying concentration quenching for one type of ion only since equation (12) is derived by averaging the interactions of one ion with all others which then are of the same kind.

When random ions of type S are excited, each ion has the same probability of radiative decay resulting in a purely exponential decay for the ensemble of ions. When the activator ions are also present and randomly distributed

in the medium, some of the excited S ions will be sufficiently close to the A ion so that energy transfer will occur. Since transfer probability depends on inter-ionic distance the decay rate of individual S ion will vary with its distance to the A ion in a random way. Only ions with identical environment will have identical decay rates. Those donor ions which are near to the activator ions will decay rapidly, therefore, the decay rates increase soon after excitation. After the ions near the quenching centres have decayed, the ions with no activator with in a close distance remain excited and their decay will approach the radiative rate. Therefore energy transfer in absence of diffusion among the donor ions will be characterized by a non-exponential fluorescence decay with a rate approaching purely radiative rates at long times.

Another approach to the macroscopic case is the use of the well known rate equations which deal with population of ions in a given state. This was used as a phenomenological approach in studies of the laser systems. In the same manner rate equations were derived for the energy transfer between Yb^{3+} and Er^{3+} [21]. The applicability of these equations in relation to the Inokuti and Hirayama derivations has been discussed recently by Grant [22]. Based on the principles of quantum statistics, Grant

shows that the dependence of average transfer probability on concentration does not reflect the multipolar behaviour but rather the number of particles participating in the relaxation process and this was supported by Fong and Diestler [23]. With the assumption of random mixing, the energy transfer rate at low concentration is linear with concentration (C) as long as only pairwise interactions are considered. Quadratic or higher dependence on concentration, C can result from energy transfer between the sensitizer and two, three or more activator ions. Fong et al [12]believe that the many body transfer mechanisms are particularly important in the rare earth ions. The efficiency of energy transfer is given by

$$\eta_T = 1 - \frac{\eta}{\eta_o} \qquad (13)$$

where $\frac{\eta}{\eta_o}$ is the relative yield of donor luminescence. Many experiments have been performed to know about the interaction mechanism by measuring the radiative quantum efficiency of donor fluorescence.

The quantum efficiency under pulsed excitation can be obtained from an arbitrary time dependence of fluorescence by performing the following integration

$$\frac{\eta}{\eta_o} = \frac{1}{\tau_o} \int \phi(t)\, dt \qquad (14)$$

where $\tau_o = \int \phi_o(t)dt$

and $\phi_o(t)$ is the intrinsic time decay without energy transfer. The average transfer probability is given by

$$P = \frac{1}{\tau_o}\left(\frac{\eta_o}{\eta} - 1\right) \qquad (15)$$

where τ_o is the measured lifetime of the donor.

1.10 Migration of excitation

In many systems because of the resonant condition, the sensitizer-sensitizer transfer is more rapid than the sensitizer-acceptor transfer (when the concentration of the two ions are comparable) especially in rare earths where the stokes shift is small. Excitation energy may then be able to migrate among the sensitizers before passing to the activator ion, thus, decreasing the effective sensitizer-acceptor distance. This mechanism has been dealt in detail by many workers [24].

Another type of interaction mechanism is the magnetic dipole-magnetic dipole interaction. The Hamiltonian of such interaction is similar to that of electric dipole-electric dipole interaction. This type of interactions are not detected in optical measurements.

1.11 Energy up-conversion

Microscopic and macroscopic aspects of energy transfer have been dealt with briefly in the previous sections.

In some systems energy transfer causes up-conversion of radiation also. That is, when a particular group of energy levels are resonantly excited, fluorescence originating from energy levels, which are situated at much higher levels, is observed. This phenomenon is called here after, ''Energy Up-conversion''. Energy up-converted fluorescence can arise with or without energy transfer to a neighbouring ion. The processes such as ''Two photon excitation process'', ''Sequential two photon excitation process (STEP)'', and ''Infrared quantum counters (IRQC)'' require the involvment of single ion only. Bloembergen [25] has observed infrared quantum counter for the first time. The subject of IRQCs has been reviewed by Brown and Shand [26]. Successive multipole transfers as well as cooperative processes giving rise to energy up-converted fluorescence have been reviewed by Auzel [27]. Kinetics of up-conversion has been discussed by Wright [28]. Various energy transfer phenomena have been reviewed, recently by Reisfeld and Jorgensen [13].

The basic energy level diagram of IRQC (not shown) is a three level scheme where the ion is excited from level E_o to level E_1 by a signal of frequency ν_{01} and the transition from level E_1 to E_2 is provided by another frequency ν_{12} and then fluorescence is observed from E_2. The efficiency of IRQCs depends on the following :

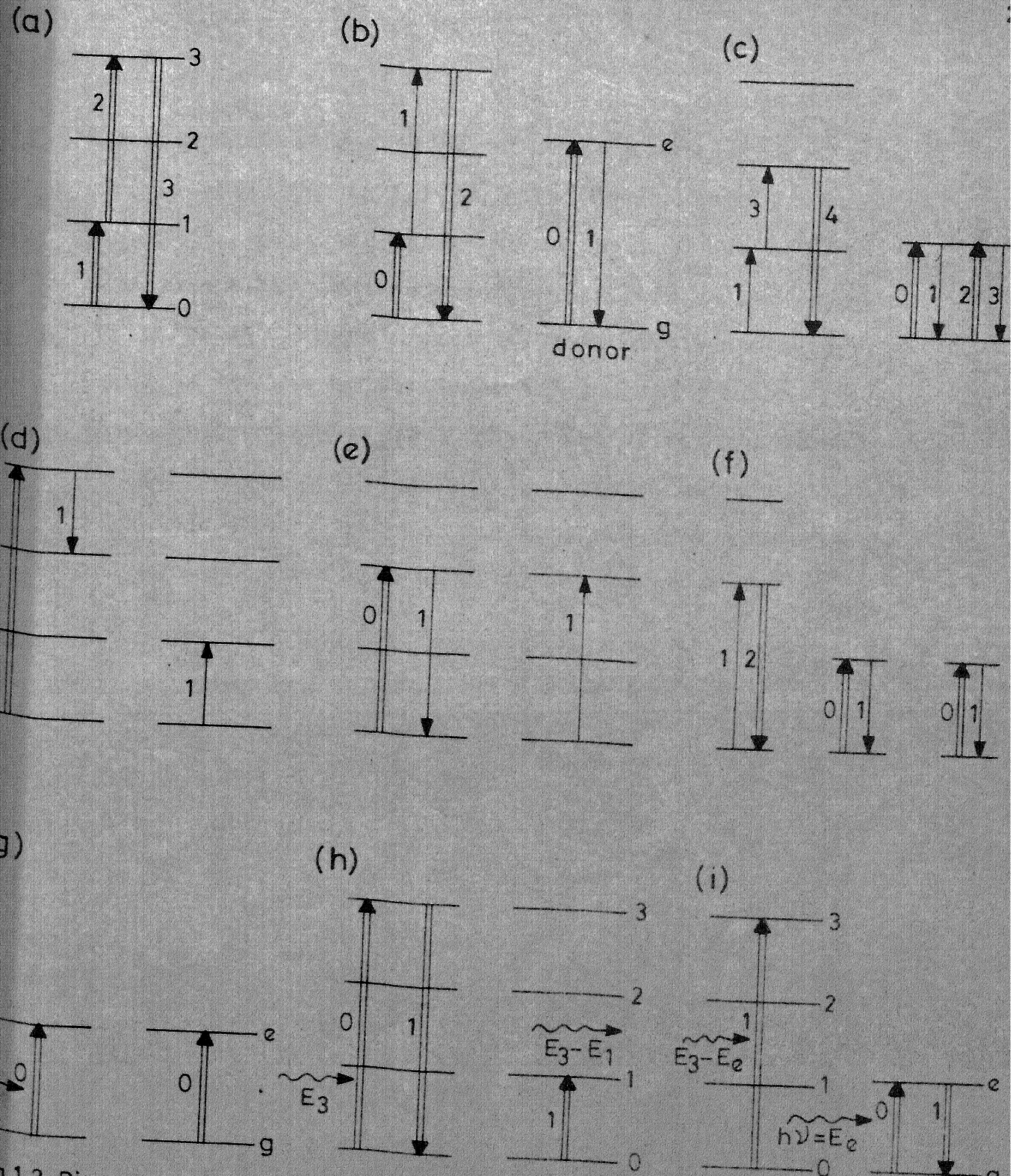
1. At normal temperatures the ground state E_o should contain all the ions in that state.

2. The level E_1 should not be populated thermally, otherwise the output is noisy.
3. The transition ν_{01} must be an allowed one.
4. The lifetime of E_1 should be long since this is to be picked up by another transition.
5. The absorption ν_{12} should be an allowed one.
6. The energy gap between E_1 and E_2 must be large.
7. The level E_2 must be fluorescing with high radiative efficiency.

This is not an ideal system because the long lifetime of E_1 is not compatible with a strong transition. An improved quantum counter scheme is a four level scheme, in which the ion is excited from E_0 to E_2, which rapidly relaxes to E_1 and then picked up by another photon to E_3. For this process to be observed the output frequency ν_{30} must be sufficiently isolated from the pump frequencies. The above conditions are favourable for the operation of not only IRQCs but also STEP. But in STEP process the exciting radiation is of single frequency [29]. These two processes are observed at low concentrations. At higher concentrations ''Energy transfer up-conversion (ETU)'' process is significant. Here two excited donor ions undergo a transfer leaving one ion in a higher excited state and the other in a lower state or the two excited ions may transfer their energy to a third ion. This

process is observed in singly as well as doubly doped systems [30].

Some schemes of ion-ion coupling or up-conversion of radiation are depicted in Fig. 1.2. Excited state absorption of the type proposed by Bloembergen is shown in Fig.1.2(a). In this, the ion is excited from level 0 to level 1 by infrared radiation and is tuned from 1 to 3 by a strong excitation source and then fluorescence from level 3 is observed. Another mechanism of up-conversion proposed by Esterowitz et al [31], in which the excitation from level 1 to level 3 is provided by an excited ion is shown in Fig.1.2(b). A different type of up-conversion is observed by Auzel [32], in which, two excited donors successively transfer their energy to an acceptor (Fig.1.2(c)). A fluorescence quenching process [33] by ion-pair decay is shown in Fig.1.2(d) and the migration of excitation [34] is shown in Fig. 12 (e). Fig.1.2(f) represents a cooperative excitation [35] mechanism, observed in doubly doped systems, in which two donors simultaneously transfer their energies to a third ion. Cooperative radiative transitions [36] are allowed where a single photon is absorbed or emitted by two ions (Fig.1.2(g)). Another type of cooperative process is presented in Fig.1.2 (h), where an excited ion emits a photon, whose energy is the difference between that of the initial excited level and a level on a neighbouring ion [37].



g.1.2 Diagrams of phenomena caused by ion-ion coupling or up-conversion of radiat
⟹ represents transitions induced by the radiation field and ⟶ represe
transitions caused by inter-ionic coupling. The sequence in time is indicated
by the numbers beside each transition with 0 represeting the earliest
event. Designation of levels is given beside the levels.

A combination of energy transfer and photon absorption [38] is shown in Fig.1.2(i). That is, an excited donor ion can transfer its energy to an acceptor ion at the same moment that the acceptor is absorbing a photon. Consequently, acceptor excitation is created that is equal to the sum of the donor and photon energies. Kushida [17] calculated efficiencies of several infrared to-visible conversion processes, as well as rates for resonance energy transfer and cooperative optical transition, and compared them with experimental values.

REFERENCES

1. V.K. Sharma, J.Chem.Phys. 54, 496 (1971).
2. G.H. Dieke: Spectra and Energy Levels of Rare Earth Ions in Crystals (Wiley-Interscience, N.Y.1968).
3. B.G.Wybourne, Spectroscopic Properties of Rare Earths (John Wiley and Sons, New York, 1965).
4. B. Di Bartolo: Optical Interactions in Solids, (John Wiley and Sons, 1968).
5. E.A. Wood,: Crystals and Light, D Van Nostrand Co., Inc., East West Edition (1964).
6. M.J. Weber, Phys.Rev. 157, 262 (1967).
7. B.R. Judd, Phys.Rev. 127, 750 (1962).
 G.S. Ofelt, J.Chem.Phys. 37, 511 (1962)
8. T. Miyakawa and D.L. Dexter, Phys.Rev. B1, 2961 (1970).
9. M.J. Weber, Phys.Rev. 156, 231 (1967); 157, 262 (1967).
10. L.A. Riseberg and H.W.Moos, Phys.Rev.Lett.19, 1423 (1967).
11. K.R. German and A.Kiel, Phys.Rev.B8,1846 (1973).
12. F.K. Fong, S.L. Naberhuis and M.M. Miller, J.Chem.Phys. 56, 4020 (1972).
 F.K. Fong, and W.A. Wassam, J.Chem.Phys.58,956 (1973).
13. R. Reisfeld and C.K.Jorgensen:Lasers and Excited States of Rare Earths (Springer Verlag, Berlin, 1977).
14. D.L. Dexter, J.Chem.Phys. 21, 836 (1953).
 M. Inokuti and F. Hirayama, J.Chem.Phys.43, 1978 (1965).
15. J.Perrin, 2 me Conseil de Chimie Solvay (Gauthier and Villar, Paris,1925), p.322.
 J.Perrin, C.R.Lebd.Seances Acad.Sci.,184,1097 (1927).
 F.Perrin, Ann. Chim. Physique 17, 283 (1932).
16. Th. Förster,: Discussions Faraday Society 27, 7 (1959).
17. T. Kushida, J.Phys.Soc.Japan 34, 1318; 34,1327 and 34,1334 (1973).
18. B. Di Bartolo: Optical Interactions in Solids(John Wiley and Sons, Inc., New York 1968),pp.456.
19. R. Orbach,:Optical Properties of Ions in Crystals Ed.H.M. Crosswhite and H.W. Moos (1967) pp.445.
20. N. Yamada, S.Shionoya and T. Kushida, J.Phys.Soc.Japan 32, 1577 (1972).
 P.M. Selzer, D.S. Hamilton,R.Flach and W.M. Yen, J. of Luminescence 12/13, 737-41 (1976).

21. T. Miyakawa and D.L. Dexter, Phys.Rev.B1, 70 (1970).

22. W.J.C. Grant, Phys.Rev. B4, 648 (1971).

23. F.K. Fong and D.J. Diestler, J.Chem.Phys.56,2875 (1972).

24. J.P. van der Ziel, L. Kopf and L.G.van Uitert,Phys.Rev. B6, 615 (1972).

W.B.Gandrud and H.W. Moos,J.Chem.Phys.49,2170 (1968).

M.J.Weber, Phys. Rev. B4, 2932 (1971).

25. N. Bloembergen, Phys. Rev.Lett. 2, 84 (1959).

26. M.R. Brown and W.A. Shand, :Adv.Quant.Electron.,ed. D.W. Goodwin (Academic Press, New York, 1970).

27. F.E.Auzel, Proc.IEEE 61, 758 (1973).

28. J.C.Wright : Topics in Applied Physics,Vol.15,ed. Fong (Springer-Verlag, Berlin, 1976).

29. D.J. Zalucha,J.A.Sell and F.K.Fong, J.Chem.Phys.60,1660(1974

30. D.J. Zalucha,J.C.Wright and F.K. Fong,J.Chem.Phys.59,997(197 and also Ref.29.

31. L.Esterowitz,J.Noonan,J.Bahler,Appl.Phys.Lett.10,126 (1967).

32. M.F. Auzel, Compt.Rend.262,1016 (1966); 263B,819 (1966).

33. D.L. Dexter, Phys.Rev. 108, 630 (1957).

34. D.L. Dexter and J.H. Schulman, J. Chem. Phys. 22, 1063 (1954).

35. F.W. Ostermayer & L.G. Van Uitert, Phys. Rev. B1, 4208 (1970).

B.M. Antipenko, A.V. Dmitryuk, G.O. Karapetyan, V.S. Zubkova, V.I. Kosyakov, A.A. Mak, N.V. Mikhailova, Opt. Spektrosk, 35, 540 (1973) [English Translation in Opt. Spectrosc. 35 315 (1973)].

L.D. Livanova, I.G. Saitkulov & A.L. Stolov, Sov. Phys. - Solid State 11, 750 (1969).

36. F. Varsanyi & G.H. Dieke, Phys. Rev. Lett. 7, 442 (1961).

E. Nakazawa & S. Shinoya, Phys. Rev. Lett. 25, 1710 (1970).

37. J.P. van der Ziel & L.G. Van Uitert, Phys. Rev. B8, 1889 (1973).

J.P. van der Ziel, and L.G. Van Uitert Sol. Stat. Commun. 7, 1819,(1969).

J.P. van der Ziel and L.G. Van Uitert, Phys. Rev. Lett. 21, 1334 (1968).

J.P. van der Ziel and L.G. Van Uitert, Phys. Rev. 186, 332 (1969).

J.P. van der Ziel and L.G. Van Uitert, Phys. Rev. 180, 343 (1969).

38. M. Altarelli, D.L. Dexter, Opt. Commun. 2, 36 (1970).

CHAPTER 2

EXPERIMENTAL DETAILS

ABSTRACT

Fluorescence and excitation spectra have been recorded using CW Ar^+ and pulsed N_2 pumped dye lasers. A 0.75 m Jarrell-Ash spectrograph, fitted with an ITT FW 130 photomultiplier has been used to record the spectra. The wavelengths are measured with an accuracy of 1.5 Å using picoammeter and strip chart recorder combination. Decay times have been measured using an oscilloscope. The crystals used for this study have been procured from Optovac Inc.

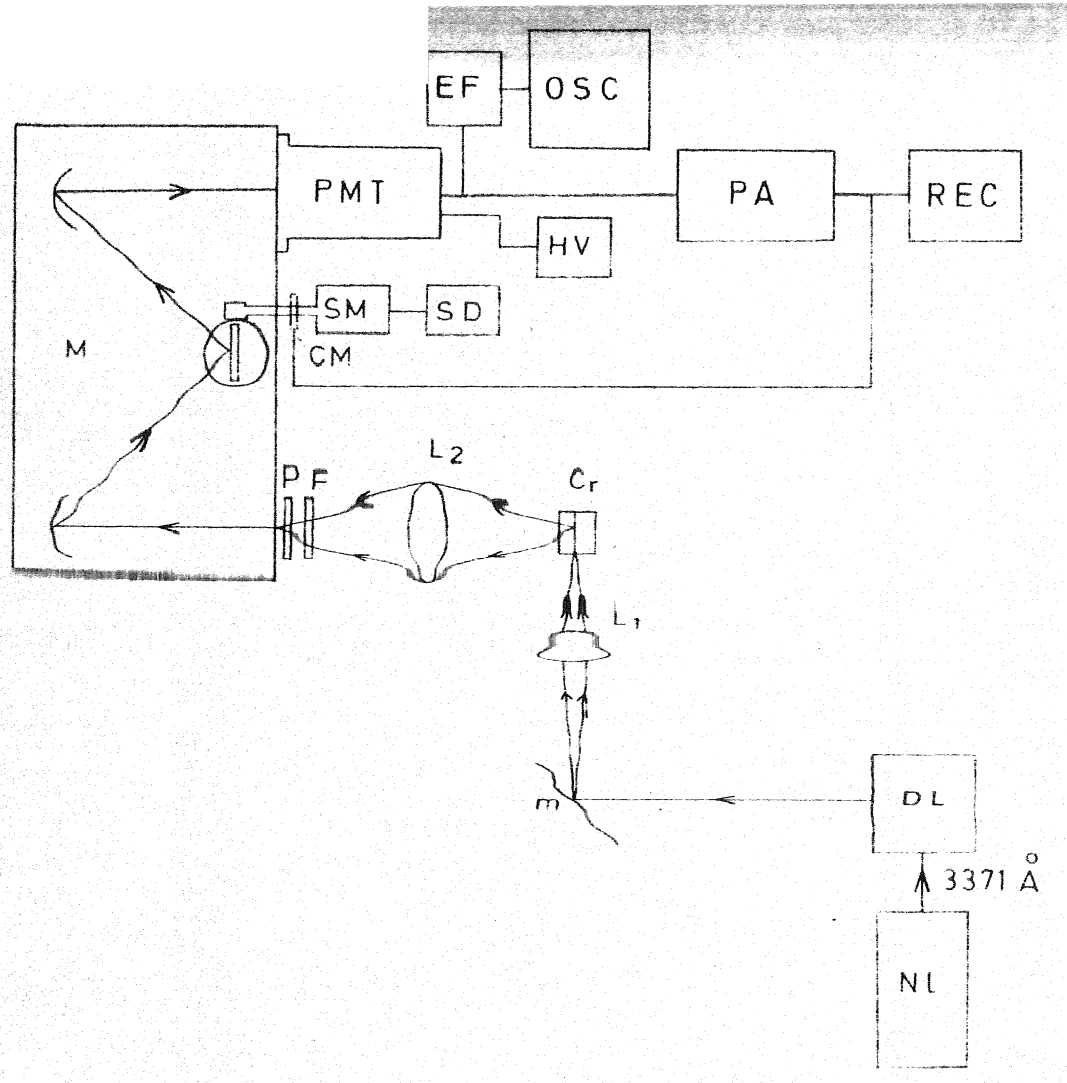
2.1 Introduction

The experiment involved is to excite fluorescence in $LaF_3:M^{3+}$ [where M^{3+}= Pr^{3+}, Nd^{3+}, Dy^{3+} or Ho^{3+}] using a laser beam and to record the fluorescence spectra, excitation spectra and the measurement of decay times of some of the fluorescing energy levels of M^{3+} ion(s) in the above mentioned single crystals. The block diagram of the experimental set up is given in Fig. 2.1. The experimental arrangement consists of an excitation source, optics for collecting the signal, spectrometer and recording system.

2.2 Excitation source

Molectron UV 1000 N_2 laser pumped DL300 dye laser is used to excite the crystals. The N_2 laser is capable of producing a peak output power of 1 MW at 3371 Å having a fixed pulse width of 10 nsec. It is operated at a repetition rate of 10 Hz though provision is there to vary the pulse rate from 5 Hz. to 50 Hz. The laser is operated at 22 KVDC and the pressure is maintained at 60 mm of mercury. The output is a rectangular beam of dimensions 25 mm x 6 mm.

The DL 300 dye laser is pumped transversely with horizontal N_2 laser beam. The focussing lens included in the dye laser focusses the beam to a line at the dye cell



NL = N_2 Laser
DL = Dye Laser
m = Mirror
L_1, L_2 = Convex lenses
C_r = Crystal
F = Filter
P = Polarizer
M = Monochromator
CM = Cam and Microswitch
SM = Stepper motor
SD = Stepper motor drive
PMT = Photomultiplier tube
HV = High voltage power supp
PA = Picoammeter
REC = Strip chart recorder
EF = Emitter follower
OSC = Oscilloscope

Fig. 2.1 Block diagram of the experimental set up

8 mm long by 0.2 to 0.5 mm high. The intracavity (not shown) consists of a grating, etalon, beam expanding telescope and an output mirror. The beam expanding telescope focusses the beam on the grating. The intracavity etalon is used to reduce the bandwidth and to improve frequency stability of the laser cavity. The grating selects a particular wavelength with in the emission band of the dye for amplification in the cavity. The grating is a glass replica blazed at 2.7 μm with 600 grooves per millimeter. To operate over the broad range of output wavelengths, orders 4 through 7 of the grating are used, there by maintaining high efficiency at all wavelengths. The grating is rotated by a sine drive to provide linear relationship between handcrank rotation and wavelength increment of the dye laser output. Each revolution of the grating shaft corresponds to 100 Å in first order and $\frac{100}{n}$ Å in nth order. A stepper motor (Step-Syn™ of Automatic Electric Co. India) is added to drive the grating shaft at fixed rates. The speed of the stepper motor can be varied by a stepper motor drive‡ in nine steps viz., 10, 5, 2, 1, 0.5, 0.25, 0.1, 0.05 and 0.025 rpm.

Various organic dyes in the visible and near ultraviolet regions of the optical spectrum can be excited to

‡ Stepper motor drive has been fabricated under a joint project of Lasers Laboratory, Dept. of Physics and Advanced Centre for Electronic Systems of Electrical Engg. Dept., IIT Kanpur.

lase with in their fundamental fluorescence bands of 200-600 Å width. Continuous tuning is achieved from 3600 Å to 7500 Å. A stirring magnet is provided within the curvette. A stirring motor is used to keep the magnet rotating. In this study Coumarin (7D 4MC) and Rhodamine 6G (R6G) dyes are used which lase in the regions 4400-4780 Å and 5680 - 6050 Å respectively. Each revolution of grating shaft changes the wavelength by about 17 Å and 20.5 Å respectively for the above dyes.

2.3 Optics for collecting the signal

The horizontal output of the dye laser is reflected vertically using an inclined aluminium coated mirror. A quartz lens of diameter and focal length each 2'' is used to focuss the beam to a point in the crystal. Fluorescence output is collected in a direction perpendicular to the direction of excitation using a lens of diameter and focal length each 2'' and is focussed on to the slit. Coloured glass filters (Corning) are used to check the wavelength and order of the spectra and is arranged in front of the slit whenever necessary. A polarizer supplied by Andhra Scientific Company, Machilipatnam is used in recording the polarized spectra and is arranged in front of the entrance slit. The slit widths (entrance and exit slits) are varied from 30 μ to 440 μ depending on the

strength of the signal.

2.4 Spectrophotometer

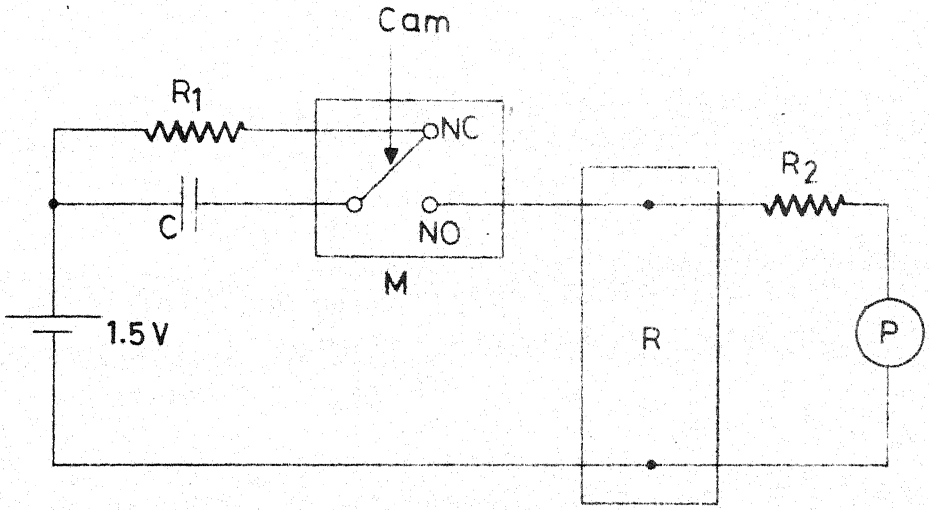
The fluorescence light is analysed using a 0.75 m Jarrell-Ash Model No. 75-000 plane grating spectrograph (f/6.3) which has an asymmetric Czerny-Turner mounting for the grating and a worm and gear arrangement to rotate the grating table. The grating used is blazed at 5000 Å and has 1200 grooves/mm. One revolution of the grating shaft results in 0.1 degree rotation of the grating. A mechanical counter on the spectrograph indicates the grating setting in hundredths of a degree. A stepper motor and stepper motor drive combination similar to the one described in Sec. 2.1 is used to rotate the grating shaft at a fixed rate. This results in different scanning speeds in the range from 52 Å/min to 1.3 Å/min. A precision bilateral slit (Jarrell-Ash No. 12-000) is mounted in place of the plate holder using the same clamping arrangement. A photomultiplier tube ITT FW 130 with S-20 response is used to detect the signals. PMT with its housing is fixed at the exit slit. Its dark current at 1500 V is about 1.5 nA. The high voltage required is obtained from a stabilized high voltage power supply.

2.5 Recording the spectra

While recording steady state fluorescence the current from PMT output is measured by a picoammeter (Keithley No.417), which has a full scale range variable between 3×10^{-5} amps to 3×10^{-14} amps and in 3, 1, 0.3 and 0.1 sequence. The d.c. component of the dark current of the PMT is subtracted out using the 'current suppress'. The picoammeter has an output 3 V for full scale deflection, which is used to drive the strip chart recorder (Varian Model No. G 14A-2). The recorder has two chart speeds of 2.5 and 10 cms/min. The spectra are recorded in fast speed and the speed of the shaft is chosen in such a way that a dispersion of 1 Å/mm or 2 Å/mm is obtained on the chart paper.

2.6 Calibration

Provision is made to obtain a marker on the chart paper for every rotation of the grating shaft (Fig. 2.2). A cam attached to the grating shaft closes the microswitch (Kesbo (India) No.MVR6) contact once every rotation and connects a 1.5 V dry cell across the recorder terminals through a capacitor. The capacitor allows only a sharp spike of voltage to pass through, at the instant the contact is closed. During the off period of the microswitch,



M = Microswitch (kesbo No. MVR-6)

NC = Normally closed contact

NO = Normally open contact

R = Recorder

P = Picoammeter

C = ~0.1 μF

R_1 = ~10 KΩ

R_2 = ~50 KΩ

Fig. 2.2 Schematic diagram of the wavelength marker circuit.

the capacitor is discharged through the resistor R_1 to make ready for the next marker. A resistor R_2 is inserted in the picoammeter output to prevent the shunting of the 1.5 V pulse by the low output impedence of the picoammeter. Since the input impedence of the recorder is as large as 1 MΩ this series resistance does not reduce the voltage received by the recorder to any significant extent. The calibration of the spectrometer thus consists of ascertaining the wavelengths corresponding to these marker positions. This is done by recording the spectra of some standard sources like low pressure discharges of He, Ne, Ar and Xe. These sources cover the regions of spectra recorded. The maximum inaccuracy involved is ± 1.5 Å for the wavelengths measured. Usually the spectral lines are recorded a number of times and an average of these values is given in the tables. Some preliminary work on the fluorescence spectrum of $LaF_3:Pr^{3+}$ using (Coherent Radiation No.52) Ar^+ laser excitation on a SPEX No.1400 double monochromator with an EMI No.9558 PMT was done by Professor P. Venkateswarlu at the University of California, Santa Barbara. The wavelengths obtained in this laboratory are in agreement with those recorded by Professor Venkateswarlu within the experimental errors. All the recordings which are made in this laboratory are presented in the thesis except the fluorescence group $^3P_1 \rightarrow {}^3F_3$

in the region 6409-6570 Å, which is from Professor Venkateswarlu's unpublished data.

2.7 Excitation spectra

While recording the excitation spectra the monochromator is fixed at a particular position, so that the PMT receives signals of a particular wavelength only. Then the excitation wavelength is changed continuously at a fixed rate. Whenever a particular wavelength is absorbed by the ion in the crystal, fluorescence is emitted by the ion. So a peak appears on the chart paper corresponding to that excitation. This type of recordings give information about the energy levels responsible for that particular fluorescence line.

2.8 Decay time measurements

It is convenient for practical purposes to introduce a term 'decay time' which characterizes the behaviour of the decay function. Let $\phi(t)$ represents the intensity of the decay curve at time, t. Since $\phi(t)$ is not in general an exponential function, there is no unique way of defining a decay time. One can define the mean duration time, τ_m of donor luminescence by

$$\tau_m = \int_0^\infty t\,\varphi(t)dt \Big/ \int_0^\infty \phi(t)dt$$

Another way of defining it is the '$\frac{1}{e}$ - decay time', τ_e or the time interval after which the donor luminescence has decreased by a factor of e from its value at t = 0. If the decay function happens to be purely exponential, then τ_m and τ_e coincide. Otherwise they are in general different. The aim of the present experiments is not to measure the decay times very accurately but to see the relative variations in decay times with concentration of impurity ions in the host lattice. So '$\frac{1}{e}$ - decay time' is measured in every case. For this purpose, the output of the photomultiplier tube is fed to an emitter follower (Fig. 2.3) and then to an amplifier (Tektronix Model 1121). The output of the preamplifier is given to an oscilloscope (Tektronix 545A) and the waveform is displayed on the scope. The emitter follower with large input impedance (20 kΩ to 1 MΩ) and an output impedance of 50Ω is used to avoid distortion of the pulse due to impedance mismatch. Saturation effects of the signals are eliminated by controlling the slit widths of the spectrometer. We have used calibrated scope to measure the decay times. Calibration error that could appear is very small. But some error is there due to the finite width of the signal trace (because the signals are noisy). The maximum error that could appear in all measurements is about 10 percent. Each decay time is measured couple of times and an average value is taken.

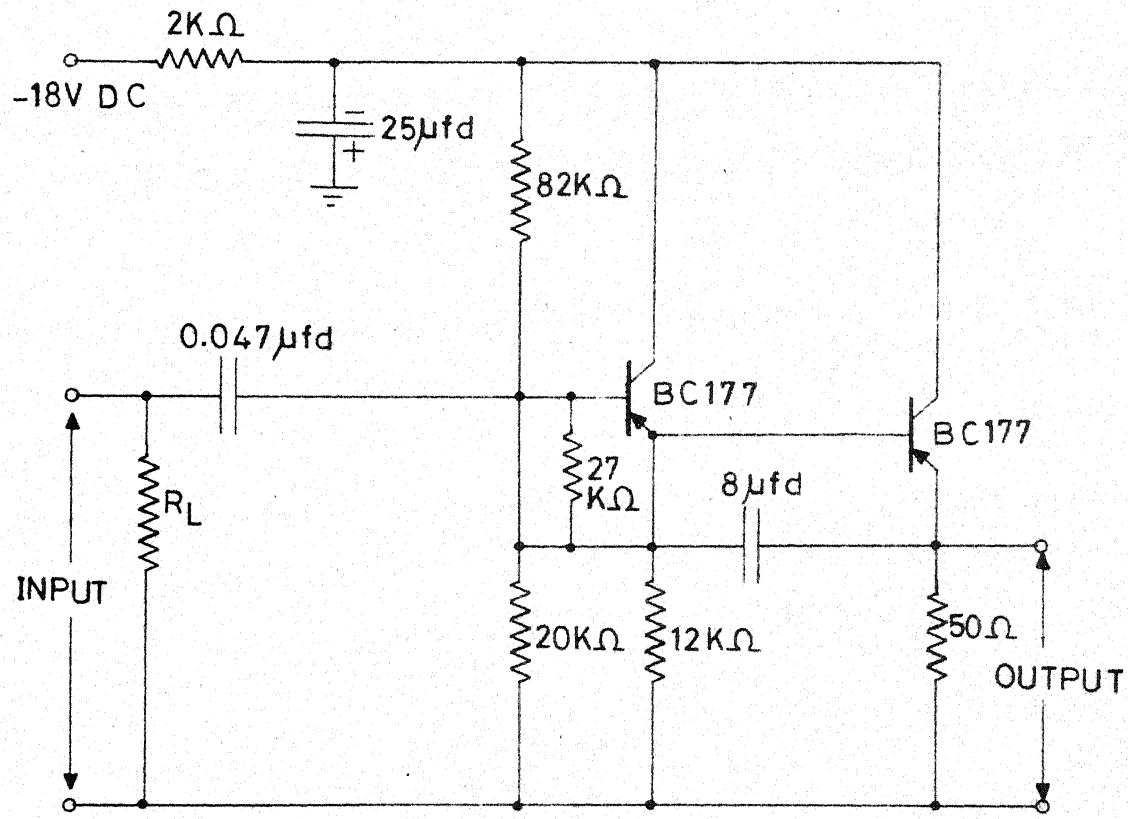


Fig. 2.3 Emitter follower.

2.9 Dewar for low temperature work

A demountable (pyrex B-55 joint) cold finger dewar has been fabricated for the low temperature work. The upper half of the dewar is double-walled with inner-wall terminating in a glass-to-metal seal (Kovar seal). A non porous copper block is soldered to the tip of the Kovar seal (Fig. 2.4). The crystal is mounted on the copper block in such a way that there is maximum contact with the copper block. To maintain good thermal contact a thin layer of grease is applied to the contact surface. The crystals are fixed to the copper block with quick fix. It is applied only to one edge of the crystal so that it does not affect the excitation and fluorescence intensity. The lower half of the dewar has three windows one at the bottom and two on the sides at right angles to each other. An outlet (through a stop-cock) is provided in the lower half for evacuation of the dewar. A vacuum of the order of 10^{-5} torr is created between the walls and then liquid nitrogen poured inside the dewar.

2.10 Crystals used

The single crystals of $LaF_3:Pr^{3+}$ (1 percent), $LaF_3:Nd^{3+}$ (2 percent) $LaF_3:Dy^{3+}$ (0.5 percent) and $LaF_3:Ho^{3+}$ (0.5 percent) obtained from Optovac Inc. have been loaned to us by the late Professor H.P. Broida, Department of Physics,

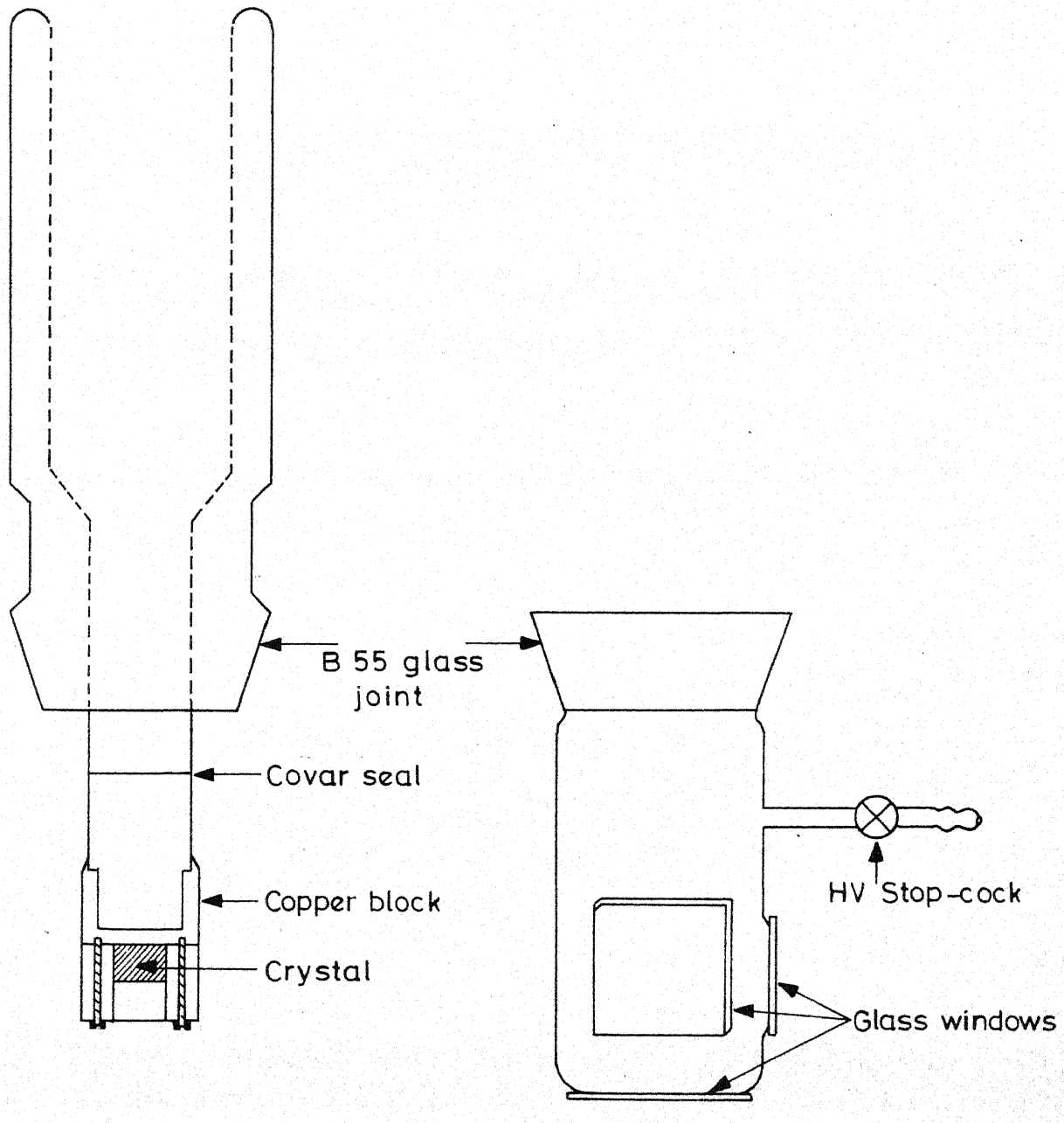


Fig. 2.4 Cold finger dewar used for work at liquid nitrogen temperature.

University of California, Santa Barbara. All the above crystals on excitation have shown the presence of Pr^{3+}. [In the last three crystals Pr^{3+} is present as an unintentional dopant]. The $LaF_3:Dy^{3+}$ crystal also contains very small concentration of Nd^{3+} (unintentional dopant). The other crystals of $LaF_3:Nd^{3+}$ with Nd concentrations (0.01, 0.1, 0.5, 5 and 20 percent) have been obtained from Optovac Inc.

CHAPTER 3

LASER INDUCED FLUORESCENCE AND SITE SYMMETRY

ABSTRACT

Polarized fluorescence spectra of $LaF_3:Pr^{3+}$ (one percent) has been recorded at room and liquid nitrogen temperatures using a N_2 laser pumped dye laser and an Ar^+ laser. Vast data has been observed which was not reported earlier. Fluorescence originating from $^3P_0$, $^3P_1$ ($^1I_6$), $^3P_2$ and on resonant excitation from $^1D_2$ levels is observed. Some transitions originating from phonon coupled levels of $^3P_0$ and $^3P_1$ ($^1I_6$) and terminating in $^3F_3$ and $^3H_6$ have been observed only at room temperature. Excitation spectrum has been recorded for at least one fluorescence line of each group. Analysis of polarized spectra indicates that Pr^{3+} ion occupies a C_s site rather than C_{2v} or C_2 site. A consistent set of species assignment has been made to most of the energy levels and to some of the phonons under C_s site symmetry.

3.1 Introduction

Praseodymium is the third element in the Lanthanide series. Triply ionized praseodymium has tw trons in the incomplete shell which contribute in all all of which have been observed either in absorption o fluorescence. The free ion energy levels are also kno [1,2]. Energy levels of Pr^{3+} in LaF_3 were established by Caspers et al.[3] and later by Carnall et al.[4] fr absorption and fluorescence experiments and are given i pages. The energy levels in the order of increasing energy are $^3H_{4,5,6}$, $^3F_{2,3,4}$, $^1G_4$, $^1D_2$, $^3P_0$, $^3P_1$ ($^1I_6$), $^3P_2$ and $^1S_0$. The energy levels of $^3P_1$ and $^1I_6$ are found to be superimposed. Vacuum-ultraviolet absorptio spectra of trivalent lanthanides in LaF_3 were recorded by Heaps et al.[5]. The level energies obtained by Carna et al [4] are slightly different from the values obtaine by Caspers et al [3] except the $^1D_2$ level energies in which there is a large discrepancy. The level energies of $^1D_2$ mentioned by Carnall et al [4] are supported by $^1D_2$ fluorescence and excitation spectra recorded in this laboratory. The values obtained for energy levels from the present fluorescence experiments are agreeing within the experimental errors with those of Caspers et al.[3] and Carnall et al.[4]. Absorption and fluorescence spectra of Pr^{3+} in LaF_3 were reported earlier by Wong et al [6]

and later fluorescence spectra were recorded by Yen et al [7]. Even then the data reported by them is not complete and no proper explanation was given which could explain the polarization of all the observed transition energies. The optical fluorescence analysis of $LaF_3:Pr^{3+}$ is very easy because the strongly fluorescing level is a single state (J=0). Keeping this in view a thorough reinvestigation of the fluorescence spectra was undertaken. When the ^3P group of levels are excited no fluorescence is observed from $^1D_2$ Stark multiplet. So fluorescence from $^1D_2$ is observed on resonant excitation. The details of fluorescence analysis are given under separate headings. The observed fluorescence consists of transitions originating from $^3P_0$, $^3P_1(^1I_6)$, $^3P_2$ and $(^1D_2)$ to lower multiplets. All these data are given in Tables 3.9-3.11. Fluorescence from $^3P_1(^1I_6)$ and $^3P_2$ to lower levels and some of the weaker lines arising from $^3P_0$ are not observed in this laboratory at liquid nitrogen temperature. These data are taken from the unpublished work of Professor Putcha Venkateswarlu who recorded the spectra using CW Ar^+ laser and SPEX No. 1400 spectrometer at the Department of Physics, Santa Barbara, California. These data are taken for the sake of completeness and the analysis is done by me.

3.2 Proposed Crystal structure for Lanthanum Trifluoride

Lanthanum trifluoride is an important optical material which has been the subject of numerous investigations. The study of magnetic susceptibility and Faraday rotation, NMR, EPR, Optical Spectroscopy of impurities in LaF_3, Optical-RF double resonance [8] the study of Raman spectra, Infrared and Lattice vibrations, photon-echo technique [9] and photo emission studies [10] have generated considerable interest. The crystal structure of LaF_3 has been the subject of controversy from the beginning and was reviewed by Sharma [11] earlier. In 1931 Oftedal [12] suggested a hexamolecular D^3_{6h} ($P6_3/mcm$) space group based on his X-ray results on a study of crystals of mineral tysonite (La, Ce, ...) F_3. He also observed that the actual structure deviated only slightly from the D^4_{6h} ($P6_3/mmc$) space group in which a bimolecular pseudocell would become the true unit cell. A projection of the unit cell on a plane perpendicular to the crystal z or c axis is shown in Fig. 3.1a. The results of Faraday rotation experiment by Van Vleck and Hebb [13] support this structure. Wong et al. [6] recorded the optical absorption and fluorescence spectra of Pr^{3+} in LaF_3 and suggested C_{2v} site symmetry. But it could not explain the appearance of unpolarized lines and weak lines. The

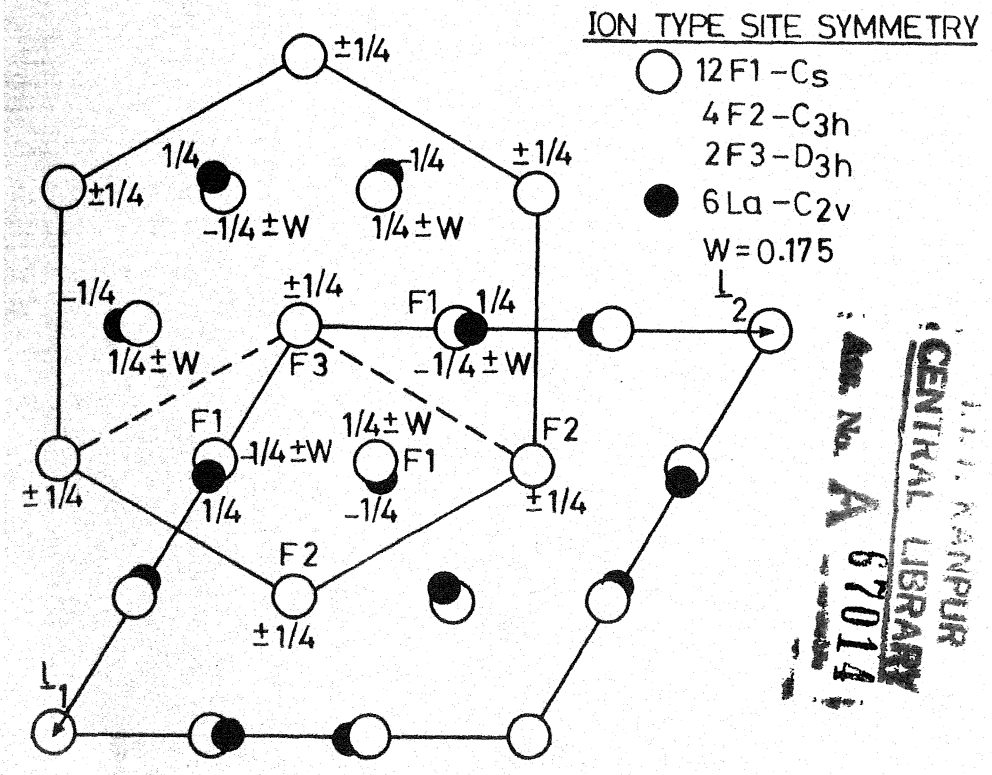


Fig. 3.1a D^3_{6h} crystal structure of LaF_3.

The solid lines indicate the hexamolecular unit cell, the dashed lines show the bimolecular cell (D^4_{6h}). The plane shown passes through $z = zt_3$. The projection of the particles in the hexagonal cell are shown on the plane perpendicular to z or crystal c axis and passing through the origin. (Phys. Rev. 171, 1051 (1968)).

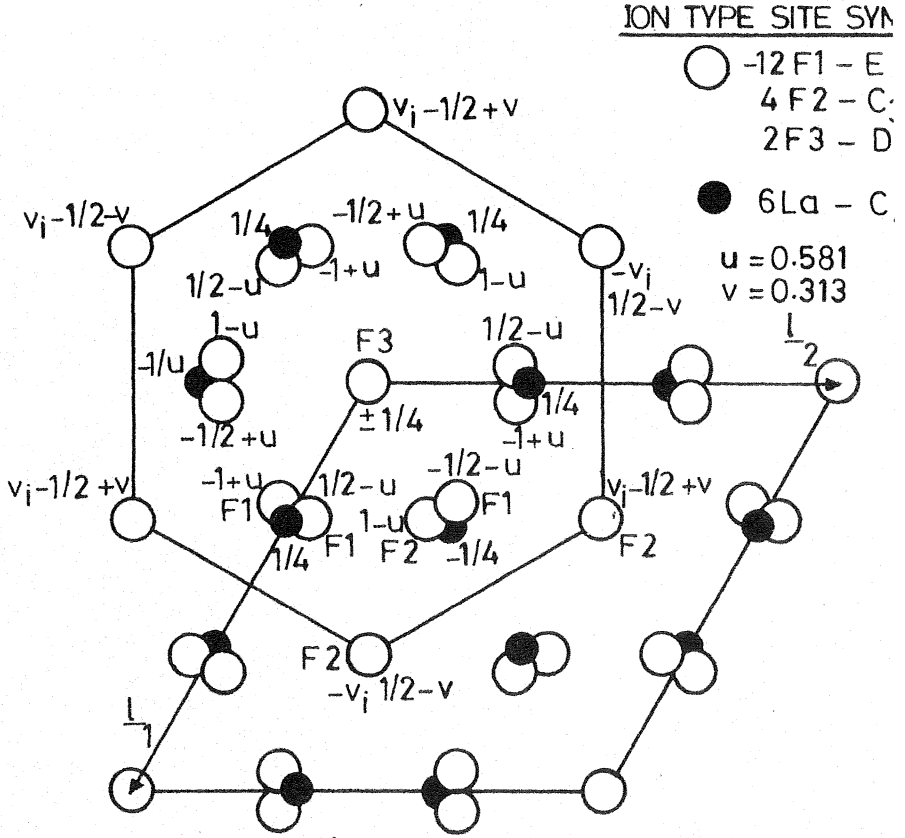


Fig. 3.1b D^4_{3d} crystal structure of LaF_3.

The plane shown passes through $z = \frac{1}{2}t_3$. The projection on this plane of the particles in the hexagonal unit cell ar indicated. (Phys. Rev. 171, 1051 (1968))

CENTRAL LIBRARY

results of F^{19} NMR experiment by Afanasiev et al [14] support this structure. Schlyter [15] reinvestigated the X-ray diffraction spectrum of tysonite and concluded that the true structure was the bimolecular D^4_{6h} space group. Krupke and Gruber [16] recorded the fluorescence spectra of Er^{3+} in LaF_3 and found that some of those lines are polarized in contrast with the expectation for Er^{3+} to be located at the site C_{2v}. They suggested a slight distortion towards a trigonal site D_{3h} to account for the polarization.

Mansmann [17] and Zalkin et al. [18] independently repeated the study and suggested the hexamolecular trigonal structure L^4_{3d}. A projection of the unit cell on a plane perpendicular to the crystal z or c axis is shown in Fig. 3.1b. Raman spectra of LaF_3 was recorded by Bauman and Porto [19] and by Venkateswarlu [19a] and the infrared spectra by Rast et al. [20] and later by Lowndes et al. [21]. Their results support the trigonal structure D^4_{3d} ($P\bar{3}C1$). The results of powder neutron diffraction studies by Cheetham et al [22] and thermal conductivity study by Hudson [23] support the trigonal, D^4_{3d} structure.

Three sets of equivalent fluorine positions exist for each proposed structure. They have been indicated respectively, as F_1, F_2 and F_3 type ions. The La ions

form a triangle at $Z = 1/4$ and $1/3$ lattice distance away from the origin and another triangle at $Z = -1/4$ (or $3/4$) separated by $C/2$ from the first and rotated by 60° with respect to the first triangle. The F_3 type fluorines are at the centres of the triangles formed by the La ions. The difference exists however in the positions $12F_1$ and $4F_2$ type fluorines. In D^3_{6h} structure the $12F_1$ fluorines are situated on vertical planes passing through the origin and the La ions. Each La ion is located equidistantly between the two F_1 fluorines. The F_1-F_1 separation is 0.65 C units. The La ion is 0.05 Å off the line joining the two F_1 type fluorines in these planes. In the D^4_{3d} structure, the $12F_1$ fluorines have been moved horizontally an amount approximately 0.03 Å from the vertical planes defined above. The F_2 fluorines in D^3_{6h} structure are located on the planes perpendicular to the crystal c axis at $Z = \pm 1/4$ c while in D^4_{3d} structure these two planes are 0.063 c units above and below the plane formed by the La ions.

The bimolecular structure D^4_{6h} proposed by Schlyter is (shown by dotted lines) obtained from D^3_{6h} by moving the La and F_1 type fluorine ions on C_3 symmetric axis. This in effect places the La, F_2 and F_3 ions in sites of D_{3h} symmetry while the F_1 type ions would find themselves in sites of C_{3v}. Electron diffraction studies by

Gries and Bevan [24] revealed that LaF_3 can crystallize in atleast two forms D_{3d}^4 ($P\bar{3}C1$) and D_{6h}^4 ($P6_3/mmc$). This behaviour usually correlates with the high F^- ion mobility at room temperature.

On the basis of their investigations of La^{139} NMR spectra, Anderson and Proctor [25] found the structure to be hexagonal with six magnetically inequivalent La ions occupying sites of symmetry C_s, C_2 or C_{2v} in a unit cell. Combining this with the positions of La ions determined by X-rays, they proposed C_{6v}^3 space group. Rango et al.[26] also found from neutron diffraction that the structure is C_{6v}^3 (Fig.3.2). F^{19} NMR observations of Lee and Sher [27] provided evidence for the presence of two types of fluorine nuclei in LaF_3. Baturin et al.[28] also found similar evidence in their F^{19} observations on La, Ce, Pr and Nd trifluoride powders. These experiments support D_{6h}^4 structure but are in fact indicative of gross symmetry at the fluorine sites. Since the difference in the environments of F_2 and F_3 type fluorines is only small, a measurable difference in the 'Chemical shifts' could not be produced at the magnetic field these experiments were carried out. A similar limitation occurs to the work of Goldman and Shen [29] who found one type of fluorine nuclei in LaF_3 to be in rapid motion and determined the ratio of slow to fast moving nuclei as 1:2 using pulsed NMR technique.

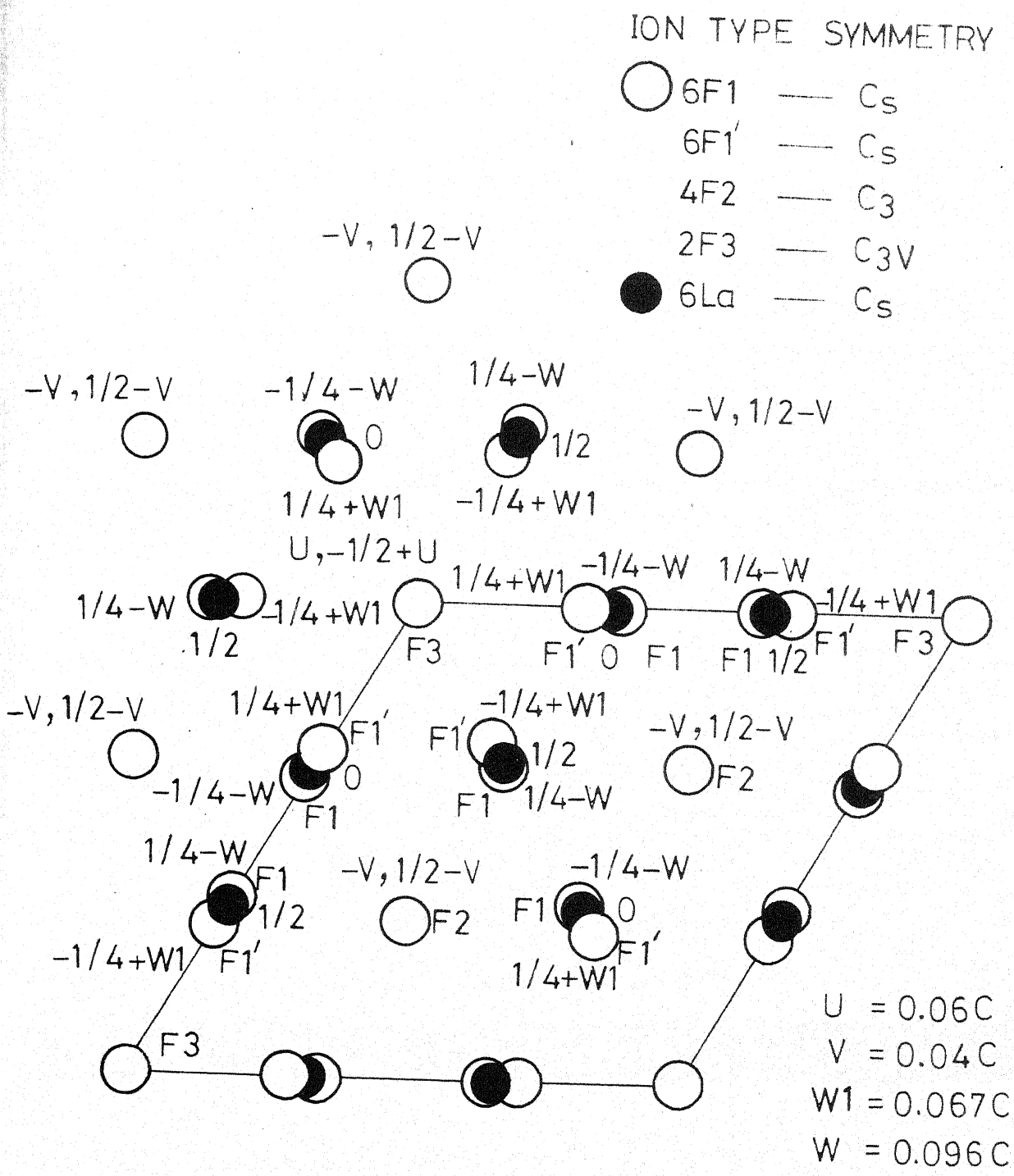


Fig. 3.2 C_{6v}^3 structure of LaF_3. The projection of the particles on the hexagonal cell is shown on a plane perpendicular to crystal c-axis and passing through half of La ions. (V. K. Sharma, Ph. D. Thesis, I. I. T. Kanpur, (1971)).

Anderson and Proctor [25] performed F^{19} measurements at higher magnetic fields and found evidence for four types of fluorines in the ratio 3:3:2:1. As such this observation supports C_{6v}^3 structure. But Anderson and Johansson [25a] report that Lee has shown the observed splittings of NMR lines to be due to the dipole-dipole interaction, which they had attributed to F_1 and F_1' fluorines so that there may be only three types of fluorines in the ratio 6:2:1 in agreement with D_{3d}^4 structure. EPR measurements on Ce^{3+}, Nd^{3+}, Dy^{3+}, Er^{3+} and Yb^{3+} in LaF_3 reported by Baker and Robins [30] revealed six magnetically inequivalent ions in a unit cell and indicated a site symmetry lower than C_{2v}. Each of these ions had an identical g-tensor such that one of the principal axes, Y was perpendicular to the C-axis and another, Z, made an angle θ with it which was different for the different RE ions. Templeton has suggested that the determination of the direction of the field gradient Y axis in relation to the crystal a-axis would be a method to distinguish between the two proposed structures. On doing this experiment they found the y-axis to be parallel to the a-axis which is consistent with La ions having C_2 symmetry in D_{3d}^4 ($P\bar{3}c1$) and contradicts it having C_s symmetry in C_{6v}^3 ($P6_3cm$) and concluded the most likely space group for LaF_3 to be D_{3d}^4. This ambiguity could be resolved if it is assumed that the crystal structure is

twinned on a submicroscopic scale in a balanced fashion. However they do not claim their determination of direction of the y-axis to be rigorous. From EPR measurements Sharma [11] found that the axis of the crystalline electric field to be perpendicular to the crystal c-axis and also to one of the cleavage planes (ac-plane) which contains the c-axis as has been reported for the other RE^{3+} ions by Schultz and Jeffrics [31]. X-ray measurements carried out by Sharma confirmed this cleavage plane to be the ac-plane. This shows that the y-axis is perpendicular to the crystal a-axis. The measurements made by Sharma[11], Schultz and Jeffrics [31] clearly support C_s site symmetry. Matthies and Welsch [32] determined the crystal field parameters for Pr^{3+} in LaF_3 from least squares fit. In their opinion the assumption of lowest site symmetry was justified. Assuming D^4_{3d} space group crystal field parameters for Ce^{3+} in LaF_3 were calculated by Starostin et al. [33].

3.3 Selection rules

When considering the energy levels of an ion in a crystal the representations of the free ion are reduced interms of the irreducible representations of the symmetry group of the crystal site in which ion finds itself. In the same way the representations of the electric dipole, magnetic dipole and electric quadrupole operators are reduced

in terms of the irreducible representations of this symmetry group. In general one component may belong to a certain representation, another component to another representation and so on. A transition between two representations is allowed if the product of the representations of the initial state by the representation of a component of the transition operator contains the representation of the final state. This is strictly related to the polarization and if the product $\Gamma_x \Gamma_i$, Γ_i being the representation of the initial state, contains the representation Γ_f of the final state, then the corresponding radiation is linearly polarized in the z-direction. Same selection rules are valid even if the transition is vibronic. Then the final representation is $\Gamma_f = \Gamma_{f'} \times \Gamma_v$ where $\Gamma_{f'}$ is the representation associated with the final Stark level and Γ_v is the representation of the phonon which is coupled to the Stark level. Same is valid for the initial level. If the representations of the initial and final Stark levels and phonon are known then the polarization of the transition can be determined from the selection rules. Or even if the representations of the initial level, transition moment (polarization) and final Stark level are known then the phonon representation is determined in the usual way.

In a rare earth ion because of the weakness of the crystalline fields the selection rules of the free ion have still some relevance. For magnetic dipole and electric quadruple transitions we have these approximate rules.

$$M1 : \Delta J = 0, \pm 1 ; J = 0 \not\leftrightarrow J = 0$$

$$E2 : \Delta J = 0, \pm 1, \pm 2; J = 0 \not\leftrightarrow J = 0, 1$$

Electric dipole transitions within an f^n configuration are allowed only through environmental perturbation. The selection rules which control the electric dipole lines are determined completely by the local field symmetry at the site of the ion.

Therefore in the analysis of the fluorescence spectra of Pr^{3+} in LaF_3, site symmetry of the ion is of prime consideration. The sites D_{3h}, C_{2v}, C_2 and C_s were proposed by the former workers. The D_{3h} site which contains doubly degenerate irreducible representations is not suited to explain the polarization of all the lines in our case. The π polarization refers to the electric vector parallel to the c-axis of the crystal, and σ polarization refers to the electric vector perpendicular to the c-axis, a π transition means the electric vector is perpendicular to the two fold axis (or to y-axis in the case of C_s). By this means one can determine the polarizations

of the optical transitions. The spectrum is recorded in three ways to distinguish electric and magnetic dipole transitions.

1. With propagation vector along the optic axis (a-spectrum)
2. With propagation vector and E vector perpendicular to optic axis (σ-spectrum).
3. With propagation vector and H vector perpendicular to optic axis (π-spectrum).

If a line appears in the axial spectrum and σ spectrum, the transition is an electric dipole. If a line appears in the axial spectrum and π spectrum, the transition is magnetic dipole. A line that appears in the π spectrum and not in the axial spectrum is an electric dipole while a line that appears in the σ-spectrum and not in the axial spectrum is a magnetic dipole.

The character tables for C_{2v}, C_2 and C_s groups and the irreducible representations of different J levels are given in Table 3.1-3.4. To distinguish the polarization nature of the transition moment components, the notation used by McClure et al [34] is followed. In this notation the perpendicular components of $E(E_\perp)$ and the parallel components of $H(H_{||})$ represent σ-polarization and the parallel components of $E(E_{||})$ and the perpendicular components of $H(H_\perp)$ represent π-polarization where E and

Table 3.1

Character Table of C_{2v} Symmetry

C_{2v}	E	C_2	$\sigma_v(zx)$	$\sigma_v(yz)$	
A_1	1	1	1	1	Z
A_2	1	1	-1	-1	R_z
B_1	1	-1	1	-1	X, R_y
B_2	1	-1	-1	1	Y, R_x

Table 3.2

Character Table of C_2 Symmetry

C_2	E	C_2	
A	1	1	T_z, R_z
B	1	-1	T_x, T_y R_x, R_y

Table 3.3

Character Table of C_s Symmetry

C_s	E	σ_h	
A'	1	1	X, Y, R_z
A''	1	-1	Z, R_x, R_y

Table 3.4

Splitting of the various J Levels under C_{2v}, C_2 and C_s Symmetries

J	C_{2v}	C_2	C_s
0	A_1	A	A'
1	$A_2 + B_1 + B_2$	A + 2B	$A' + 2A''$
2	$2A_1 + A_2 + B_1 + B_2$	3A + 2B	$3A' + 2A''$
3	$A_1 + 2A_2 + 2B_1 + 2B_2$	3A + 4B	$3A' + 4A''$
4	$3A_1 + 2A_2 + 2B_1 + 2B_2$	5A + 4B	$5A' + 4A''$
5	$2A_1 + 3A_2 + 3B_1 + 3B_2$	5A + 6B	$5A' + 6A''$
6	$4A_1 + 3A_2 + 3B_1 + 3B_2$	7A + 6B	$7A' + 6A''$

Table 3.5

Selection rules under C_{2v} Symmetry

a. Electric dipole

C_{2v}	A_1	A_2	B_1	B_2
A_1	σ		σ	π
A_2		σ	π	σ
B_1	σ	π	σ	
B_2	π	σ		σ

b. Magnetic dipole

C_{2v}	A_1	A_2	B_1	B_2
A_1		π	σ	π
A_2	π		π	σ
B_1	σ	π		π
B_2	π	σ	π	

Table 3.6

Selection rules under C_2 Symmetry

a. Electric dipole

C_2	A	B
A	σ	$\sigma\pi$
B	$\sigma\pi$	σ

b. Magnetic dipole

C_2	A	B
A	π	$\sigma\pi$
B	$\sigma\pi$	π

Table 3.7

Selection rules under C_s Symmetry

a. Electric dipole

C_s	A'	A''
A'	$\pi\sigma$	σ
A''	σ	$\pi\sigma$

b. Magnetic dipole

C_s	A'	A''
A'	π	$\pi\sigma$
A''	$\pi\sigma$	π

H represent the electric dipole and magnetic dipole transitions. The selection rules for electric dipole and magnetic dipole are given in Tables 3.5-3.7.

3.4 Salient features in the fluorescence spectra

(1) Self-absorption

In the fluorescence spectrum of Pr^{3+} in LaF_3 the 4791.5 Å line of the group $^3P_0 \rightarrow {}^3H_4$ is very strong and of magnetic dipole in nature. It is found to be self-absorbed in the crystal, whose oscillator strength is found to be 1.4×10^{-6}. Wong et al [6] did not observe self-absorption but found a weak line with π polarization in its place. Yen et al. [7] observed two lines at 4791.5 Å and 4794.9 Å the later being asymmetric. This was possibly due to self-absorption which they could not identify. Self-absorption is discussed separately (see Radiative energy transfer).

(2) Electric dipole transitions

Some electric dipole transitions are observed from $^3P_0$ (J=0) to $^3H_5$ (J = odd) and $^3F_3$ (J = odd) levels which are weak and very weak respectively. These support Ofelt [35] who proposed a theory on the intensity of the crystal spectra of rare earth ions. He said that for ions having an even number of f-electrons (assuming that even K,

J mixing is negligible) both σ and π electric dipole from (or to) a J = 0 level to (or from) an odd J level are prohibited. But the observation of fluorescence from $^3P_0$ to $^3H_5$ (which is not very weak) is probably possible by J mixing, that is mixing of wave functions belonging to $^3P_0$ and $^3P_1$ ($^1I_6$).

(3) Magnetic dipole transitions

Magnetic dipole transitions are observed for $\Delta J > 2$ (for $\Delta J = 6$ even), in some cases they are even strong, which is in contrast with the selection rules $\Delta J = 0, \pm 1$. Again the emission of magnetic dipole radiation from $^3P_0$ to the ground multiplets is probably due to the possible J mixing, that is, mixing of wave functions associated with the levels $^3P_0$ (J=0) and $^1I_6$ (J=6), in the crystal field. In general J mixing could produce weak lines where as strong lines are observed (oscillator strength of 4791.5 Å is 1.4×10^{-6}) in fluorescence 4791.5, 4895, 6001 and 7192 Å. The reason is not known.

(4) Resonance fluorescence

Fluorescence is observed from $^1D_2$, $^3P_1$ ($^1I_6$) and $^3P_2$ levels on resonance excitation. Four groups of lines are observed from $^1D_2$ to the lower multiplets. Three groups of lines are observed from $^3P_1$ ($^1I_6$) to lower

multiplets. It is observed that there is a fast relaxation at liquid nitrogen temperature from $^3P_1$ ($^1I_6$) levels to $^3P_0$.

(5) Site symmetry

There has been a controversy regarding the site symmetry of La^{3+} in LaF_3. C_{2v} site was supported by the X-ray and optical data [4]. Anderson and Proctor [25] on the basis of NMR measurements proposed C_2 site. Sharma [11] on the basis of EPR measurements found the site symmetry to be C_s. We tried to fix the site symmetry by analysing the fluorescence spectra of Pr^{3+} in LaF_3. On analysing the spectra we observed that C_s site symmetry is favoured for Pr^{3+} in LaF_3 to a greater extent than C_{2v} and C_2 sites. Using C_s site symmetry we are able to explain most of the weaker lines and phonons also.

3.5 Fluorescence spectra

Energy levels of Pr^{3+} in LaF_3 are given in Table 3.8 and shown in Fig. 3.3 alongwith the observed fluorescence groups. The fluorescence transitions are given in Tables 3.9-3.11. The observed wavelengths, their wavenumbers, relative intensity, polarization and nature of the transitions are given in columns through 1-5. The initial and terminal levels of the transitions are given in column 6. If a

Table 3.8

Energy levels of Pr^{3+} in LaF_3

SLJ	Caspers et al (cm^{-1})	Carnall et al (cm^{-1})	Present Values	Species (under C_s)
$^3H_4$	0	0	0	A''
	58	57	60	A'
	76	76	(81)	A''
	137	136	136	A'
	196	195	197	A'
	203	204	204	A'
	296	296	296	A''
	330	322	317	A''
	508	508	504	A'
$^3H_5$	2179		2181	A''
	2234		2230	A''
	2272		2273	A'
	2299		2298	A''
	2304		2305	A'
	2354		2358	A'
	2412			A''
	2431		2430	A'
	2457		2459	A'
	2469			A''
	2567			A'

Table 3.8 (contd...)

SLJ	Caspers et al (cm^{-1})	Carnall et al (cm^{-1})	Present values	Species (under C_s)
$^3H_6$	4219			
	4223	4223	4222	A"
	4266	4268	4266	A'
	4300	4305	4303	A"
	4385	4388	4383	A'
	4440	4440	4443	
	4508	4504	4506	A'
	4527	4529	4523	A'
	4552	4558	4551	A'
	4579	4581	4581	A'
	4591	4591	4596	A'
	4671	4573	4667	A"
	4776	4785		
$^3F_2$	5136	5137	5136	A'
	5182	5182	5182	A"
	5201	5201	5199	A'
	5275	5275	5276	A'
	5280	5280		A"
$^3F_3$	6465	6453	6453	A'
	6490	6495	6489	A"
	6497	6499	6498	A'
	6590	6587	6589	A'

Table 3.8 (contd....)

SLJ	Caspers et al (cm^{-1})	Carnall et al (cm^{-1})	Present Values (cm^{-1})	Species (under C_s)
$^3F_3$	6603	6602		A''
	6621	6622		A''
	6720	6722	6720	A''
$^3F_4$	6930	6927		A'
	6944	6946	6941	A''
	6982	6980	6980	A'
	6998	6998	6996	A''
	7029	7029	7025	A'
	7035	7035		A'
	7093	7093	7092	A''
	7105	7104	7103	A''
	7161	7165	7160	A'
$^1G_4$	9708	9716		
	9748	9751		
	9871	9876		
	9908	9912		
	9995	10005		
	10038	10042		
	10045	10048		
	10156	10163		
	10501	10449		

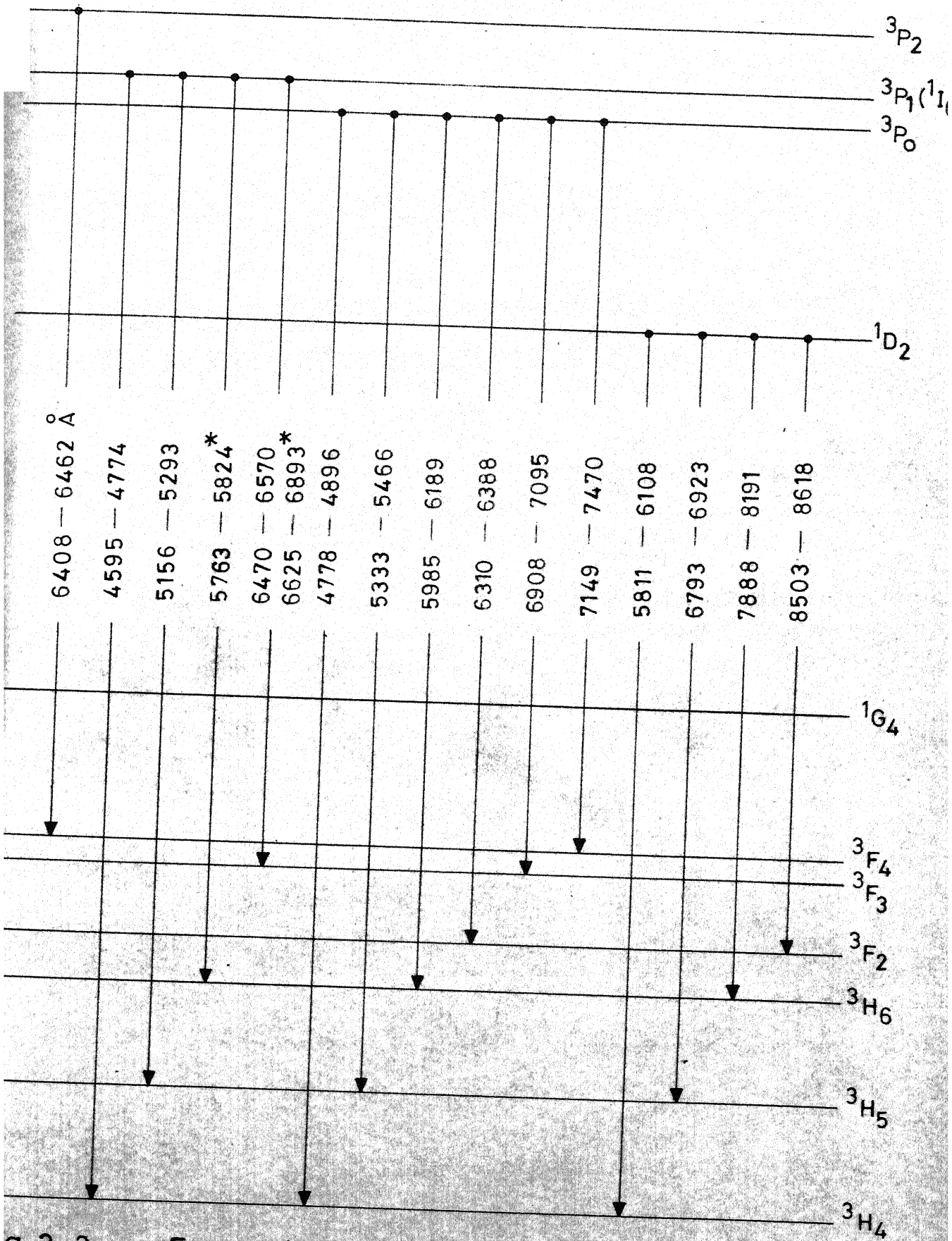
Table 3.8 (contd...)

SLJ	Caspers et al (cm^{-1})	Carnall et al (cm^{-1})	Present values (cm^{-1})	Species (under C_s)
$^1D_2$	16796			
	16820			
	16842			
	16874	16873	16872$^{\varphi}$	A''
	16897	16893	16893$^{\varphi}$	A''
		17083	17086$^{\varphi}$	A'
		17183	17183$^{\varphi}$	A'
		17204	17191$^{\varphi}$	A'
$^3P_0$	20925	20927	20925$^{\varphi}$	A'
$^3P_1$,	21469	21458		A''
$^1I_6$	21472	21475	21473$^{\varphi}$	
	21476	21479	21479$^{\varphi}$	
	21483	21484	21484$^{\varphi}$	
	21486	21487		A'
	21504	21498		A''
	21515	21516		A'
	21519	21522	21520$^{\varphi}$	A'
	21524	21529		A''
	21534	21536		A''

Table 3.8 (contd....)

SLJ	Caspers et al (cm^{-1})	Carnall et al (cm^{-1})	Present values (cm^{-1})	Species (under C_s)
$^3P_1$,	21547	21554	21556$^{\varphi}$	A''
$^1I_6$	21563	21567	21564$^{\varphi}$	A'
	21579	21580	21578$^{\varphi}$	
	21605			
$^3P_2$	22696	22691		A'
	22731	22714		A''
	22744	22734		A''
	22778	22772		A'
	22321	22819		A'
$^1S_0$		46986		

The values marked φ have been obtained from excitation spectra. Rest of the values given in the fourth column are obtained from fluorescence spectra.



g.3.3 Energy level diagram of $LaF_3:Pr^{3+}$ showing the observed fluorescence groups.(* observed only at RT)

transition is associated with a phonon, its energy is mentioned in that particular row and in the last column of the table. In $LaF_3:Pr^{3+}$ the strongest fluorescing level is $^3P_0$ (J=0) which remains as a singlet even in the crystal field. So assignment of representations to terminal Stark levels to which $^3P_0$ level fluoresces is very simple. Electronic transitions are analysed first and then the phonons involved in the vibronic transitions are analyzed. If a phonon is repeated several times consistency in the assigned representations is observed.

3.6 Fluorescence originating from $^3P_0$

Six fluorescence groups $^3P_0 \rightarrow {}^3H_{4,5,6}$, $^3F_{2,3,4}$ are observed at liquid nitrogen temperature. Since the fluorescing level at 20925 cm^{-1} is a singlet it is always represented by A_1 under C_{2v} site, by A under C_2 site and by A' under C_s site. It is to be noted that **only** C_s site has been used throughout in the analysis because it is able to explain the fluorescence satisfactorily. C_{2v} is considered in the analysis of $^3P_0 \rightarrow {}^3H_4$ to emphasize its failure in the analysis. Similarly C_2 is considered in the analysis of $^3P_0 \rightarrow {}^3F_{3,4}$ groups to show its failure in explaining those transitions.

Table 3.9

Fluorescence of Pr^{3+} in LaF_3 at LNT

π Electric vector parallel to c-axis

σ Electric vector perpendicular to c-axis

E Electric dipole transition

M Magnetic dipole transition

Wavelength (Å)	Energy (cm^{-1})	Int.	Pol.	Nat.	Transition Initial	Transition Final
4595.7	21753				21564+189	0
4642.4	21535				21536	0
4656.1	21471				21498	0+27
4663.2	21439				21498	60
4668.8	21413				21473	60
4686.5	21332				21473	0+141
4701.0	21266				21483	136+81
4728.9	21141				21458	317
4735.1	21113				21484	317+54
4743.1	21077				21458	298+83
4748.2	21055				21473	317+101
4761.5	20996				21498	504
4768.8	20964				21458	296+198
4773.6	20943				21473	504+26
4778.6	20921	w	σ	E	20925	0(4)
4791.5	20865	s	π(σ)	M	20925	60
4809.0	20789	s	π(σ)	M	20925	136
4823.1	20728	m	π	M	20925	197
4824.7	20721	m	π	M	20925	204
4831.8[φ]	20690		σ	E	20925	136+99

Table 3.9 (contd.....)

Wavelength (Å)	Energy (cm^{-1})	Int.	Pol.	Nat.	Transition Initial	Transition Final
4838.3[φ]	20663		σ	E	20925	204+58
						136+126
4846.3	20629	s	σ	E	20925	296
4851.1	20608	s	σ	E	20925	317
4856.5	20585	s	σ	E	20925	197+143
4866.0	20545		σ	E	20925	204+176
4872.1	20519		σ	E	20925	136+270
4876.0	20503				20925	197+225
4880.0	20486		π	E	20925	298+141
4885.7[φ]	20462		π		20925	317+146
4895.6	20421	s	πσ	ME	20925	504
5156.6	19387	vv	σ	E	21564	2181
5169.1	19340	vv	π		21520	2181
5181.8	19293	w			21520	2230
5194.0	19248	vv			21479	2230
5202.3	19217	vv	σ		22516	2298
5216.4	19165	vw	π	M	21520	2356
5229.4	19117	vv	σ	E	21578	2461
5240.0	19079	vv	σ	E	21536	2457
5252.8	19032	vv	π	M	21498	2469
5269.6	18971	vv			21536	2567
5276.9	18945	vv	π		21516	2567
5287.3	18908	vv	π		21473	2567
5293.2	18887	vv	σ		21458	2567
5333.5	18744	m	σ	E	20925	2181
5347.6	18695	vw	σ	E	20925	2230
5359.8[φ]	18652	vw	σ	E	20925	2273
5369.2	18620	m	π	M	20925	2305

Table 3.9 (contd....)

Wavelength (Å)	Energy (cm^{-1})	Int.	Pol.	Nat	Transition Initial	Transition Final
5384.3	18567	w	π	M	20925	2358
5389.7	18549		π	M	20925	2230+146
5397.7φ	18521		σ	E	20925	2305+99
5405.3	18495		π	M	20925	2430
5409.9	18479	w	π	M	20925	2305+141
5413.8φ	18466	w	π	M	20925	2459
5418.7φ	18449		σ	E	20925	2230+246
5427.0φ	18421		π	M	20925	2358+146
5432.9φ	18401		π	E	20925	2469+55
5442.9φ	18367		π	M	20925	2358+200
5466.3φ	18289		π	M	20925	2469+167
5985.4	16703	s	σ	E	20925	4222
6001.0	16659	s	πσ	ME	20925	4266
6014.3	16622	m	σ	E	20925	4303
6019.0φ	16609				20925	4222+94
6043.5	16542	w	π	M	20925	4383
6057.0φ	16505		σ	E	20925	4266+154
6065.7	16482	vw	σπ		20925	4443
6074.6φ	16457		σ	E	20925+55	4523
6082.0	16437		σ	E	20925	4383+105
6089.0	16419	m	π(σ)	ME	20925	4506
6095.0	16402	m	π	M	20925	4523
6105.5	16374	m	π	M	20925	4551
6116.9	16344	m	π	M	20925	4581
6122.3	16329	m	π	M	20925	4596
6126.5	16318				20925	4558+49
6137.6φ	16289				20925	4558+78
6149.1	16258	m	σ	E	20925	4667
6189.2	16153	w	π	M	20925	4667+105

4772

Table 3.9 (contd....)

Wavelength (Å)	Energy (cm^{-1})	Int.	Pol.	Nat.	Transition Initial	Transition Final
6309.7$^{\varphi}$	15844				20925+55	5136
6331.7	15789	w	σ(π)	E	20925	5136
6350.3	15743	w	σ	E	20925	5182
6357.3	15726	w	σ(π)	E	20925	5199
6368.6$^{\varphi}$	15698		π	E	20925	5199+28
6388.4	15649	w	σ(π)	E	20925	5276
6408.7	15599	vw	σ	E	22691	7092
6415.7	15582	sh	π		22691	(7109)
6421.8	15568	vw	σ	E	22734	(7165)
6430.1	15548	vw	σ	E	22714	(7165)
6442.8	15517	vw	πσ		22691	7092+81
6450.3	15499	vw	π	M	22691	7092+100
6454.3	15489	vw	π(σ)		22691	7104+98
6462.0	15471	vw	σπ		22691	(7165)+55
6469.9	15452	vw	σ	E	21564+340	6453
6481.1	15425	vw	π(σ)	M	21578+300	6453
6487.6	15410	vw	σ	E	21520+340	6453
6496.1	15390	vw	π	M	21529+315	6453
6501.1	15378	vw	σπ		21578+298	6498
6507.7	15362	vw	σ	E	21520+340	6498
6514.7	15346	vw			21529+315	6498
6519.5	15334	vw	σ	E	21516+315	6498
6533.3	15302	vw	σπ		21564+340	6602
6542.7	15280	sh	π	M	21556+313	6589
6570.1	15216	vw	σ	E	21487+318	6589
6908.0	14472	vw	π	M	20925	6453
6925.1$^{\varphi}$	14436	w	σ	E	20925	6489
6929.4	14427	w	π	M	20925	6498
6973.5	14336	vw	π	M	20925	6589

(Table 3.9 (contd.....)

Wavelength (Å)	Energy (cm^{-1})	Int.	Pol.	Nat.	Transition Initial	Transition Final
6986.3φ	14310	vw	π		20925	6453+162
7005.7φ	14270	vv	π		20925	6602+53
7025.6φ	14230	vv	π		20925	6498+197
7038.0	14205	vw	σ	E	20925	6720
7062.6φ	14155	vv	π		20925	6602+168
7069.0φ	14142	vv	π		20925	6589+194
7075.2φ	14130	vv	π		20925	6489+306
7081.1φ	14118	vv	π		20925	6489+318
7094.5φ	14092	vv	π		20925	6720+113
7149.3	13984	w	σ	E	20925	6941
7169.3	13945	w	π	M	20925	6980
7177.1φ	13929	vw	σ	E	20925	6996
7192.3	13900	s	π	M	20925	7025
7232.8	13822	w	σ	E	20925	7103
7262.8	13765	w	π	M	20925	7160
7296.2φ	13702		π		20925	7160+63
7312.2φ	13672				20925	7103+150
7333.6φ	13632				20925	7103+190
7345.7φ	13610				20925	7160+155
7367.3φ	13570				20925	7160+195
7428.7φ	13458		π		20925	7160+307
7470.1φ	13383		σ		20925	7160+382

The wavelengths marked φ and fluorescence originating from $^3P_1(^1I_6)$ and $^3P_2$ levels and terminating in $^3H_{4,5}$ and $^3F_{3,4}$ levels are not observed in this laboratory. These are taken from the unpublished work of Professor Venkateswarlu. Rest of the lines are observed by me and Venkateswarlu.

m	moderate	vv	very very weak
w	weak	sh	shoulder
s	strong	vw	very weak

3.6 (1) Fluorescence terminating in $^3H_4$

This level splits into 9 components in the crystal field. The Stark levels are represented by $5A' + 4A''$ under C_s site, and by $3A_1 + 2A_2 + 2B_1 + 2B_2$ under C_{2v} site. This observed fluorescence group falls in the region 4778-4897 Å (Fig. 3.4 and 3.5). In this group the transitions at 4778.6 Å (20921 cm^{-1}), 4846.3 Å (20629) and 4851.1 Å (20608 cm^{-1}) are σ-polarized and electric dipole (E.D.) in nature. The terminal levels of these transitions at 0, 296 and 317 cm^{-1} are represented by $A_1(B_1)$ under C_{2v} site and by A'' under C_s site. The transitions at 4823.1 (20728) and 4824.7 Å (20721 cm^{-1}) are π-polarized and magnetic dipole (M.D.) in nature. The terminal levels of these transitions at 197 and 204 cm^{-1} are represented by A_2 (B_2) under C_{2v} site and by A' under C_s site. The transitions at 4791.5[φ] Å (20865), 4809[φ] Å (20789) and 4865.6 Å (20421 cm^{-1}) are having both π-polarized and σ-polarized components, π-polarization being strong. These transitions are observed in the axial spectrum also. It is assumed that these transitions

φ The weak σ-components of 4791.5 and 4809 Å may arise due to erratic optics also. Even then there wouldn't be any change in species assignment under C_s symmetry. Again C_{2v} site fails to explain the $^3P_0 \rightarrow {}^3H_4$ group. C_2 site symmetry also fails to explain this group, because seven levels transform as A where as only five levels are allowed to be A, group theoretically.

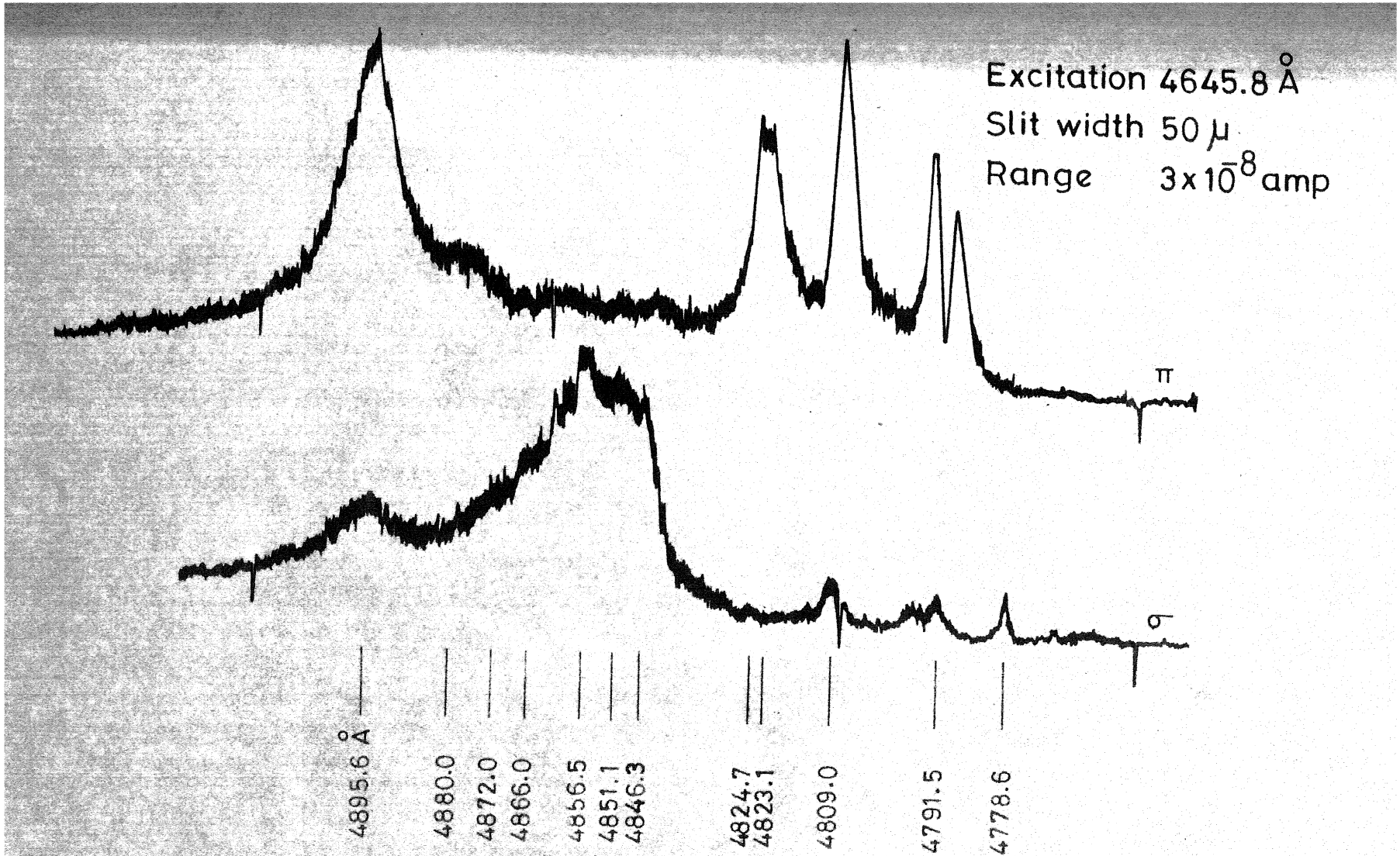
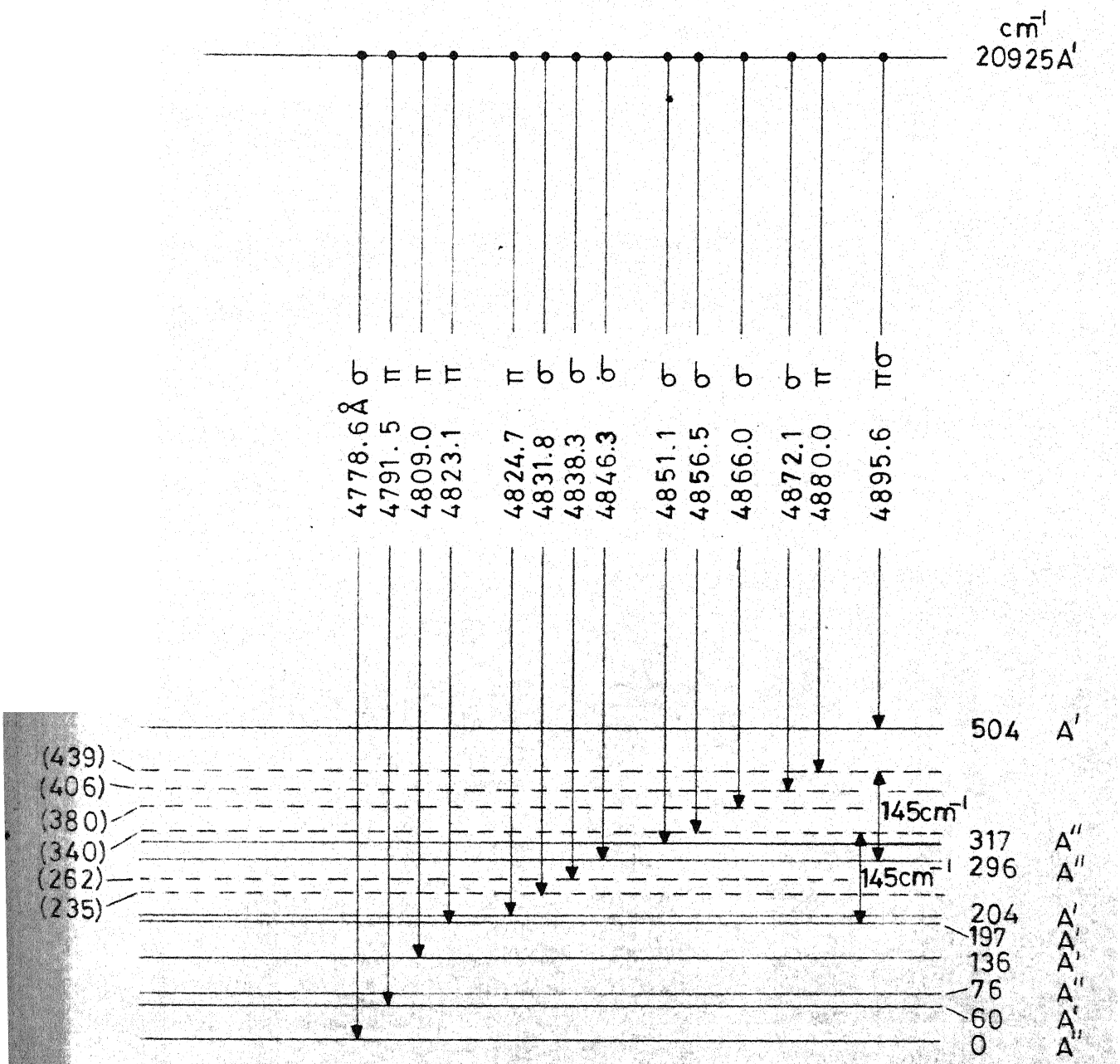


Fig . 3 . 4 Fluorescence spectrum of $LaF_3 : Pr^{3+}$ at LNT; $^3P_0 \longrightarrow {}^3H_4$ group.



3.5 Partial energy level diagram of $LaF_3: Pr^{3+}$ showing the fluorescence transition group $^3P_0 \rightarrow {}^3H_4$ at LNT.

are allowed by strong M.D. and weak E.D. moments. Under C_s site the terminal levels at 60,136 and 504 cm^{-1} are represented by A'. C_{2v} site cannot account for double polarization even if the transitions are to be allowed by E.D. and M.D. between the same levels. So the possibility of vibronic levels coinciding with the terminal Stark levels of the above transitions has been considered. Since the vibronic transitions are generally weak, it is assumed that the strong π-polarization is appearing only due to pure electronic transition. So the Stark levels at 60,136 and 504 cm^{-1} are represented by $A_2(B_2)$ under C_{2v} site. So far five levels are assigned with $A_2(B_2)$ species whereas only four are allowed group theoretically. This supports the failure of C_{2v} site in explaining the $^3P_0 \rightarrow {}^3H_4$ group. So far five levels are assigned with A' and three with A''. Therefore, the hitherto unassigned level at 76 cm^{-1} is represented by A'' under C_s site. With this, species assignment to all the Stark levels is over. Now, vibronic lines are analysed.

In fluorescence mostly vibronic transitions are observed on low energy side and are weak in intensity. The vibronic transitions at 4831.8 (20690), 4838.3 (20663), 4856.5 (20585), 4866 (20545) and 4872.1Å(20519. cm^{-1}) are σ-polarized and E.D. in nature. The Stark levels associated with these transitions have been already assigned with

species. The phonons involved in the above transitions respectively at 99,58,143, 176 and 270 cm^{-1} are represented by A'' . The vibronic transition at 4880 Å (20486 cm^{-1}) is π-polarized and not observed in the axial spectrum (E.D.). The phonon at 143 cm^{-1} coupled to the lower Stark level of this transition is an A'' since the Stark level at 296 cm^{-1} is also an A'' .

(2) Fluorescence terminating in $^3H_5$

This level splits into 11 components in the crystal field. The Stark levels are represented by $5A' + 6A''$. The fluorescence group falls in the region 5333-5466 Å (Fig.3.6 and 3.7). The transitions at 5333.5 (18744), 5347.6 (18695), and 5359.8 Å (18652 cm^{-1}) are σ-polarized and E.D. in nature. Therefore their terminal levels at 2181, 2230 and 2273 cm^{-1} are represented by A'' . The transitions at 5369.2 (18620), 5384.3 (18567), 5405.3 (18495) and 5413.8 Å (18466 cm^{-1}) are π-polarized and M.D. in nature. So their terminal levels at 2305, 2358, 2430 and 2459 cm^{-1} are represented by A' . The transition at 5432.9 Å (18401 cm^{-1}) is π-polarized and E.D. in nature. But the phonon at 55 cm^{-1} is an A'' (will be known from the analysis of 6074.6 Å line), consequently the Stark level at 2469 cm^{-1} is an A'' . The Stark level at 2298 cm^{-1} is an A'' (known after analysing the 6874.9 Å transition of $^1D_2 \rightarrow {}^3H_5$ group). The Stark level at 2412 cm^{-1} is known to

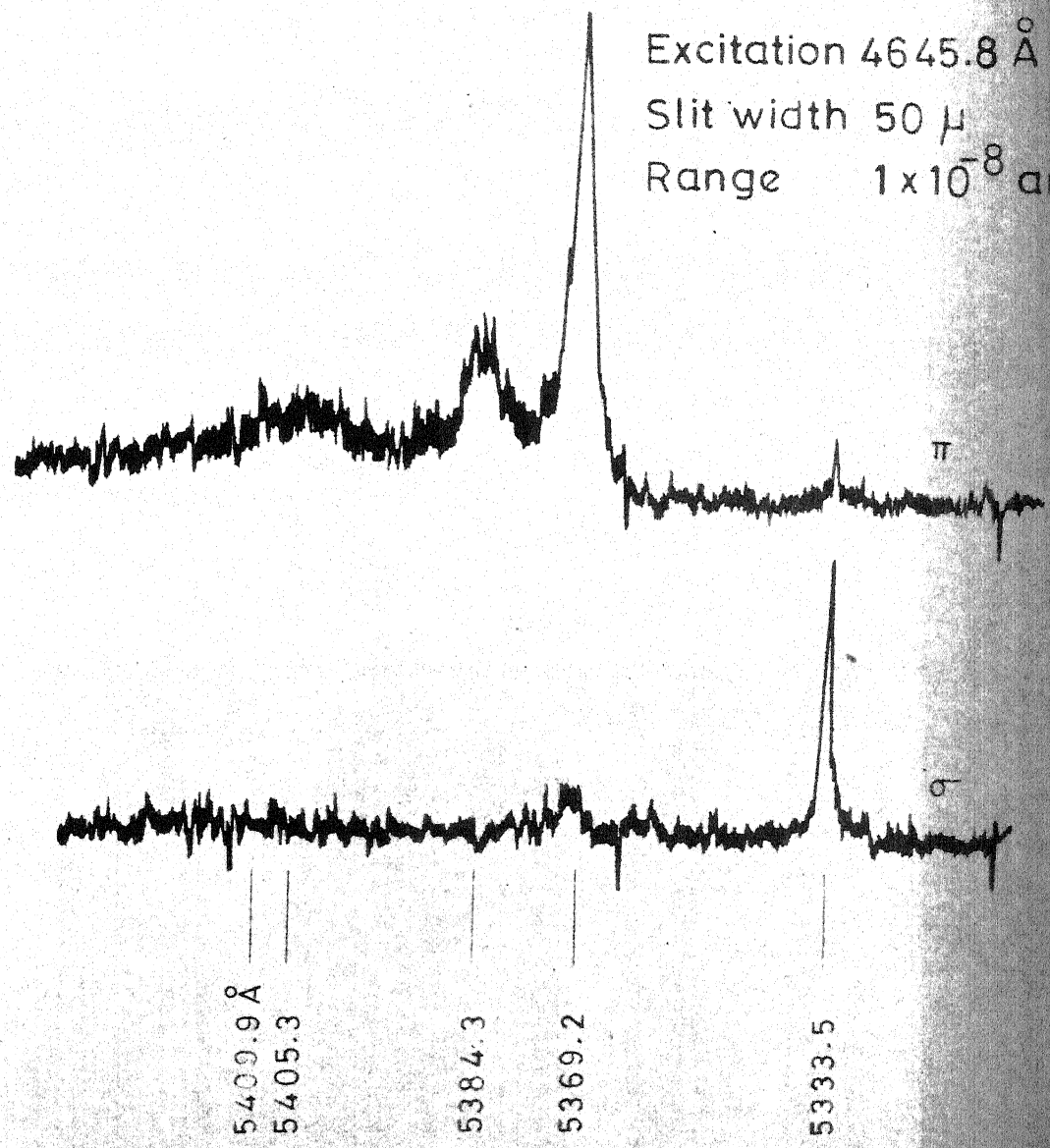
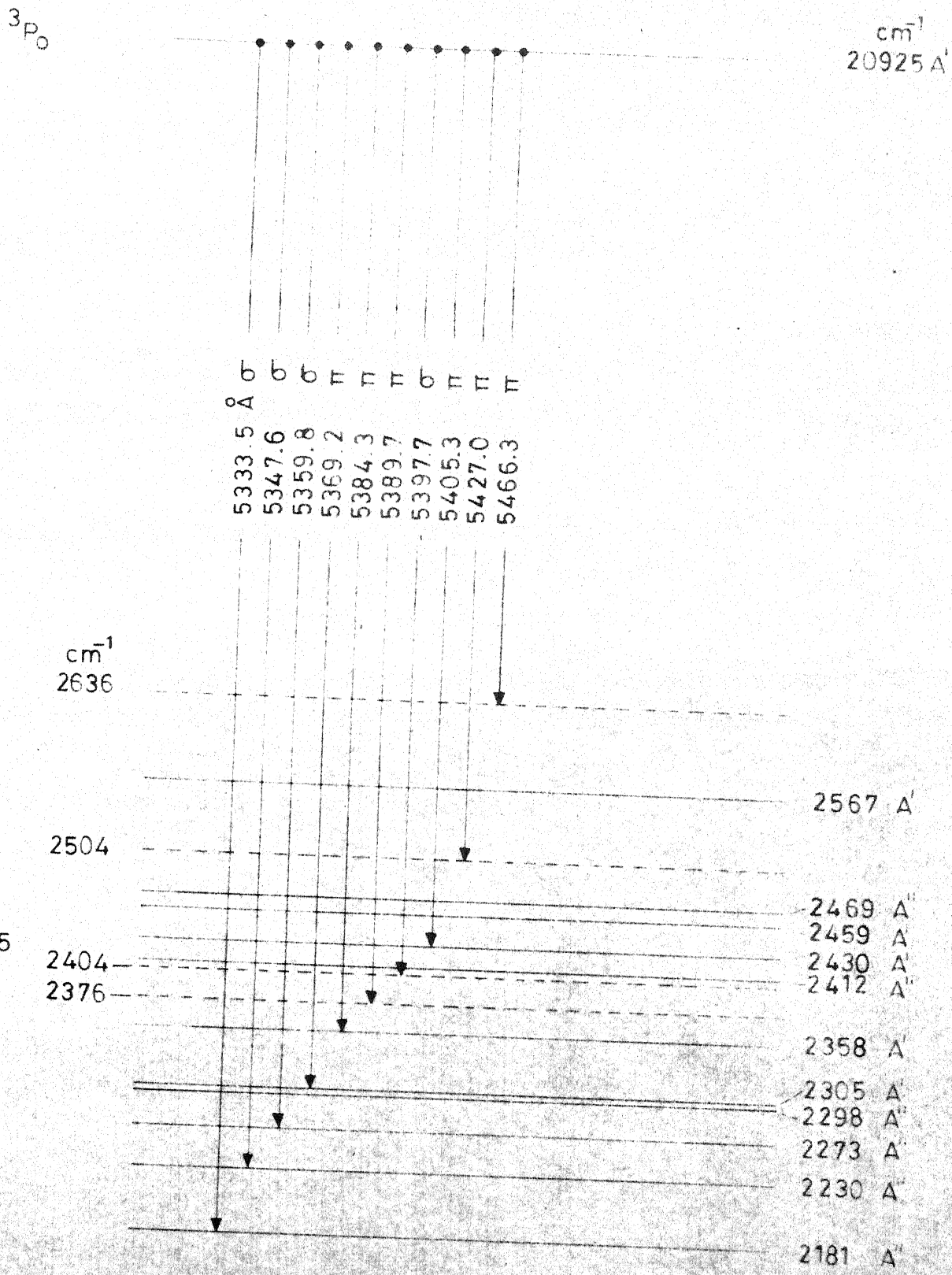


Fig. 3.6 Fluorescence spectrum of $LaF_3 : Pr^{3+}$ at LNT, $^3P_0 \rightarrow {}^3H_5$ group.



g. 3.7 Partial energy level diagram of $LaF_3:Pr^{3+}$ showing the fluorescence transition group $^3P_0 \rightarrow {}^3H_5$ at LNT.

be A'' (from the analysis of 5248.4 Å, Fig.3.17, see the Section 3.8, page 100) so far four levels are assigned with A' and six with A''. Therefore the level at 2567 cm^{-1} is represented by A'. Rest of the transitions in this group are vibronic. They are easily understood from the table.

(3) Fluorescence terminating in $^3H_6$

The level splits into 13 components in the crystal field. The Stark levels are represented by $7A' + 6A''$ under C_s symmetry. The fluorescence group falls in the region 5985-6189 Å (Fig.3.8 and 3.9). The transitions at 5985.4 (16703), 6014.3 (16622) and 6149.1 Å (16258 cm^{-1}) are σ-polarized and E.D. in nature. The terminal levels of these transitions at 4222, 4303 and 4667 cm^{-1} are represented by A''. The transitions at 6043.5 (16542), 6095 Å(16402 cm^{-1}), 6105.5 (16374), 6116.9 (16344) and 6122.3 Å (16329 cm^{-1}) are π polarized and M.D. in nature. So their terminal stark levels at 4383, 4523, 4551, 4581 and 4596 cm^{-1} are represented by A'. The transitions at 6001 Å (16659 cm^{-1}) and 6089 Å (16419 cm^{-1}) are having both the polarizations and observed in the axial spectrum also. The transition at 6001 Å (16659 cm^{-1}) is very sharp and is terminating in the level at 4266 cm^{-1}. To explain the multiple polarization under C_{2v} site the possibility of a vibronic level coinciding with that Stark level was considered.

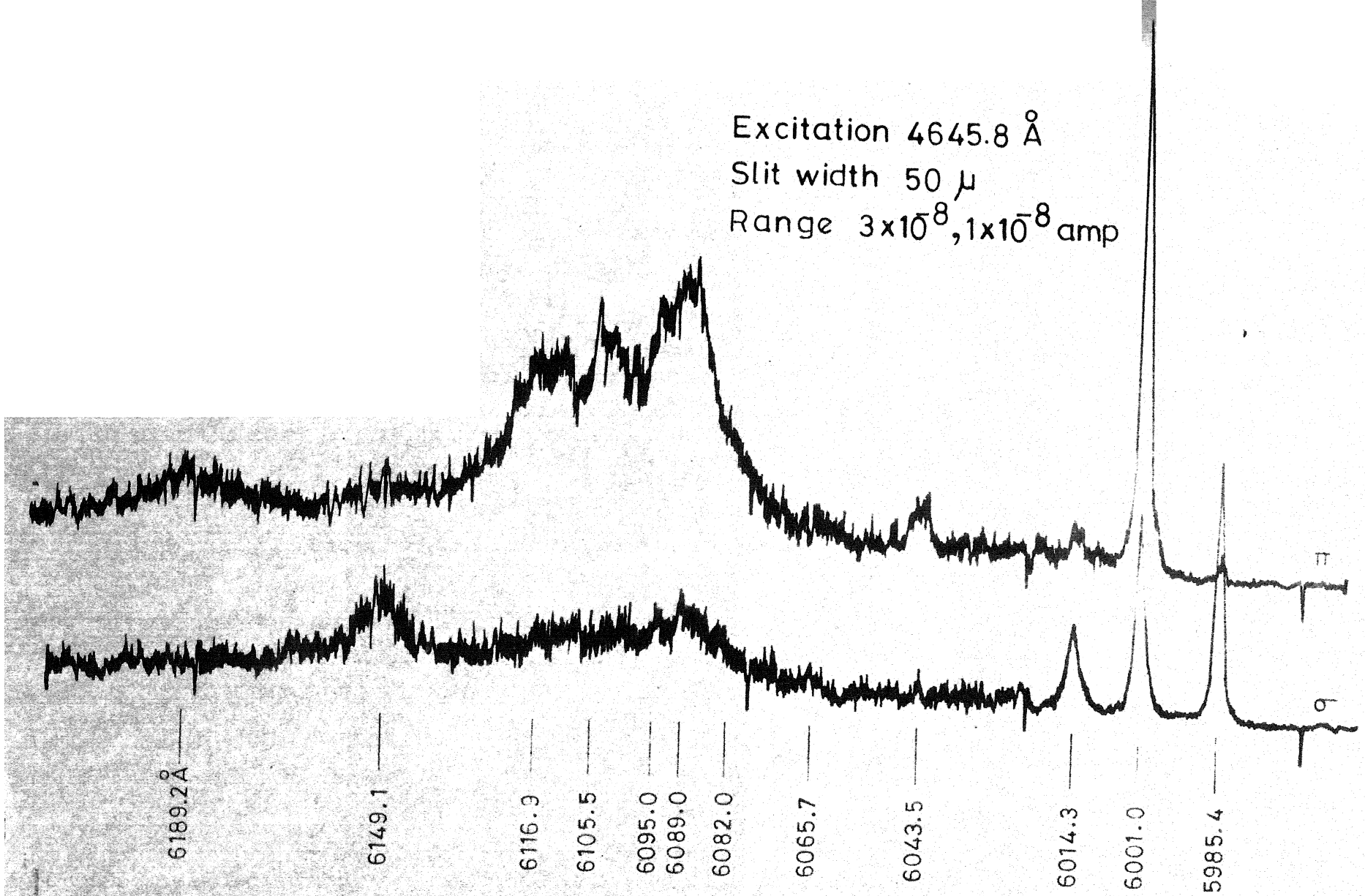


Fig. 3.8 Fluorescence spectrum of $LaF_3: Pr^{3+}$ at LNT, $^3P_0 \rightarrow {}^3H_6$ group.

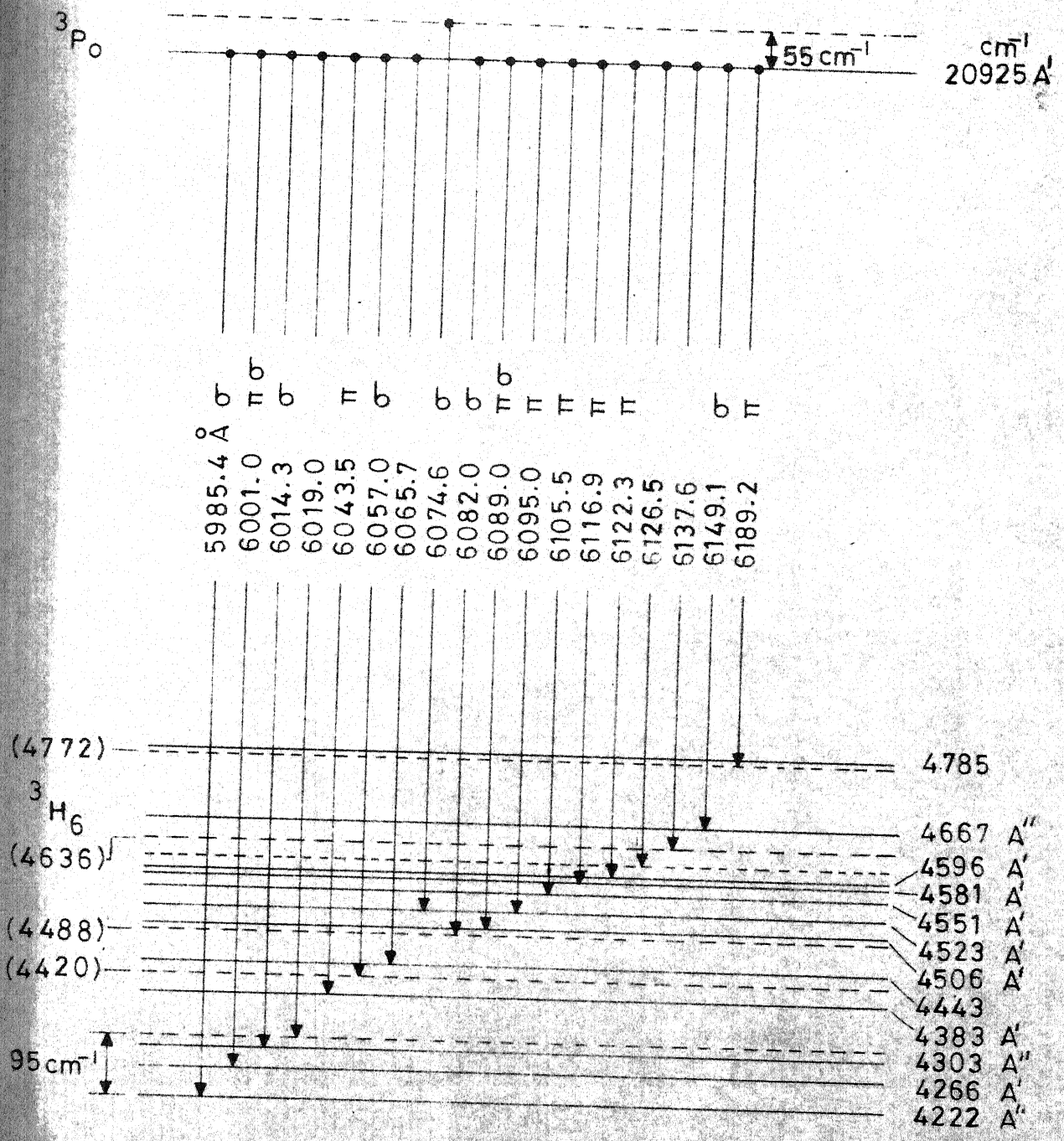


Fig. 3.9 Partial energy level diagram of $LaF_3 : Pr^{3+}$ showing the fluorescence transition group $^3P_0 \longrightarrow {}^3H_6$ at LNT.

We did not find any phonon(7,18-20) that could explain the observed transition. So C_{2v} site fails to explain the 6001 Å transition. Under C_s site the multiple polarization of 6001 Å and 6089 Å is explained easily. Since the π polarization is stronger these transitions are considered to be allowed by both E.D. and M.D. The terminal levels of these transitions at 4266 and 4506 cm^{-1} are represented by A'. The phonon at 154 cm^{-1} involved in the transition at 6057 Å (16505 cm^{-1}) is represented by A'' because the Stark level at 4266 cm^{-1} is an A'. The phonon at 55 cm^{-1} involved in 6074.6 Å (16457 cm^{-1}) transition is an A'' because the other two levels are of A' type species. Similarly, the phonon at 105 cm^{-1} involved in the 6082 Å (16437 cm^{-1}) transition is an A''.

(4) Fluorescence terminating in $^3F_2$

The level splits into 5 components in the crystal field. The levels transform as $3A' + 2A''$ under C_s site. The fluorescence group falls in the region 6310-6388 Å (Fig. 3.10 and 3.11). The transitions at 6331.7 (15789), 6357.3 (15726) and 6388.4 Å (15649 cm^{-1}) are having medium intense σ-polarized, and less intense π-polarized components. But the transition at 6350.3 Å (15743 cm^{-1}) is σ-polarized. All these transitions occur in axial spectrum also. This suggests that these transitions are allowed by pure E.D. Therefore the terminal Stark levels

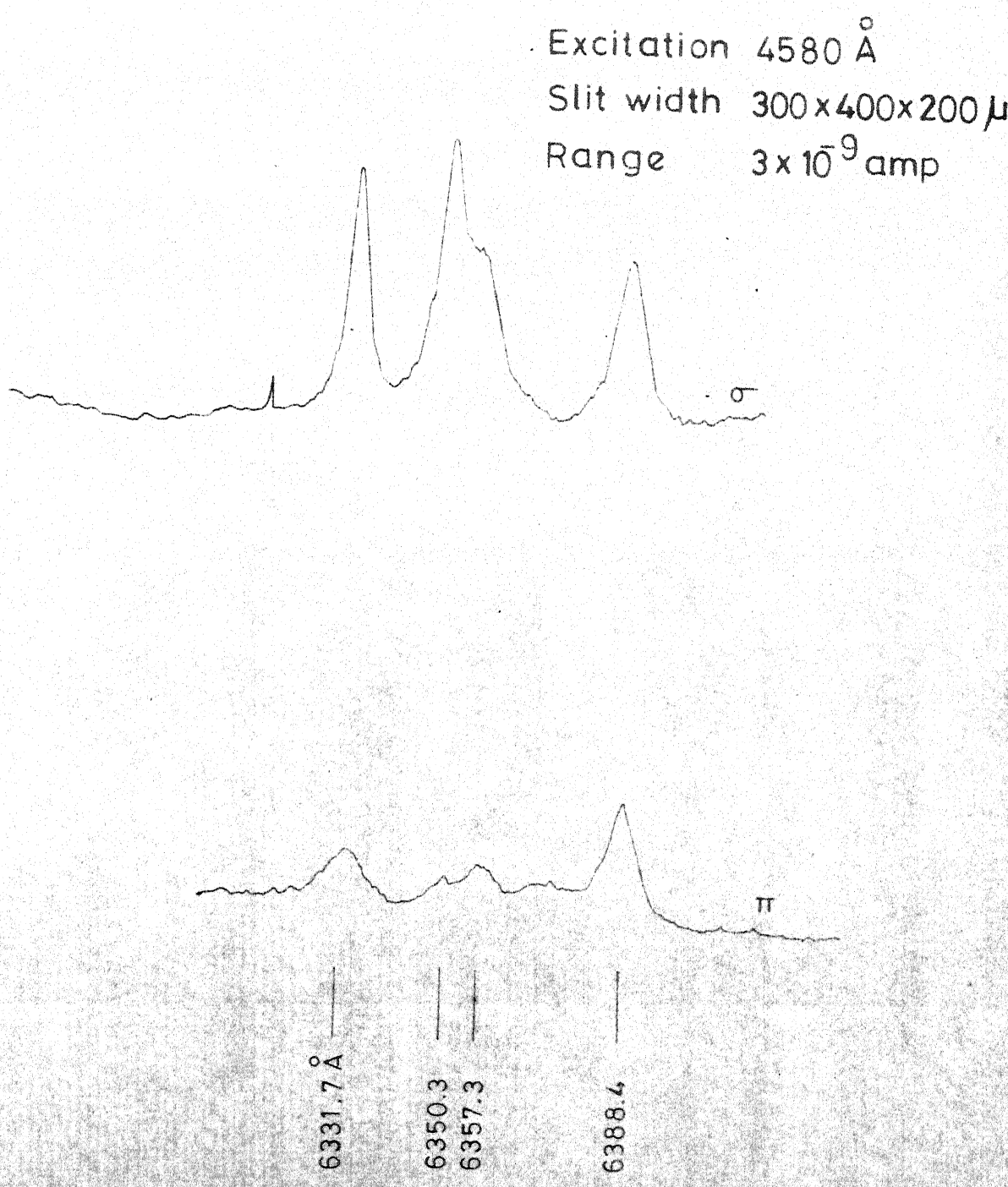


Fig. 3.10 Fluorescence spectrum of $LaF_3:Pr^{3+}$, $^3P_0 \longrightarrow {}^3F_2$ group.

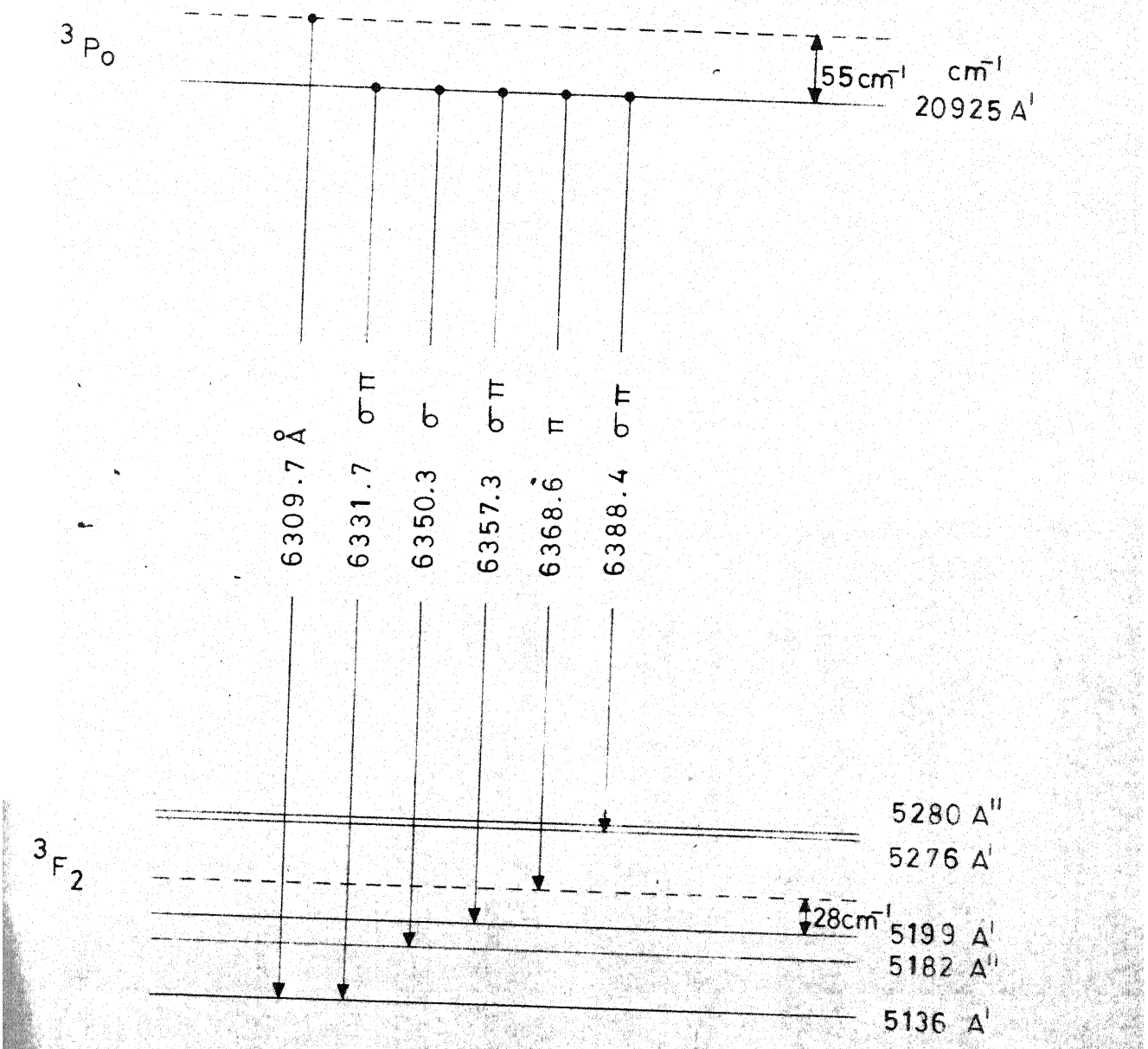


Fig. 3.11 Partial energy level diagram of $LaF_3:Pr^{3+}$ showing the fluorescence transition group $^3P_0 \longrightarrow {}^3F_2$.

of these transitions at 5136, 5199 and 5276 cm^{-1} are A' and the other two Stark components at 5182 and 5280 cm^{-1} are of A''.

(5) Fluorescence terminating in $^3F_3$

This level splits into 7 components in the crystal field. The components are represented by $3A' + 4A''$ under C_s site and $3A + 4B$ under C_2 site[φ]. This group falls in the region 6908-7095 Å (Fig.3.12). The transitions at 6908 (14472), 6929.4 (14427) and 6973.5 Å (14336 cm^{-1}) are π polarized and M.D. in nature. So their terminal Stark levels at 6453, 6498 and 6589 cm^{-1} are represented by A' under C_s site and by A under C_2 site. The transitions at 6925.1 (14436) and 7038 Å (14205 cm^{-1}) are σ-polarized and E.D. in nature. Their lower levels at 6489 and 6720 cm^{-1} are represented A'' under C_s site and by A under C_2 site. From the above analysis it is seen that five levels are represented by A whereas three are allowed group theoretically. This shows that C_2 site fails to explain this fluorescence group. Under C_s site, so far, 3 levels have been assigned with A' and 2 with A''. Therefore the remaining two levels at 6602 and 6622 cm^{-1}, hitherto left unassigned are represented

φ Earlier 'under salient features' the failure of C_2 site has been mentioned. So C_2 site is considered here to show its failure in explaining the $^3P_0 \rightarrow {}^3F_3$ and $^3P_0 \rightarrow {}^3F_4$ groups of lines in fluorescence.

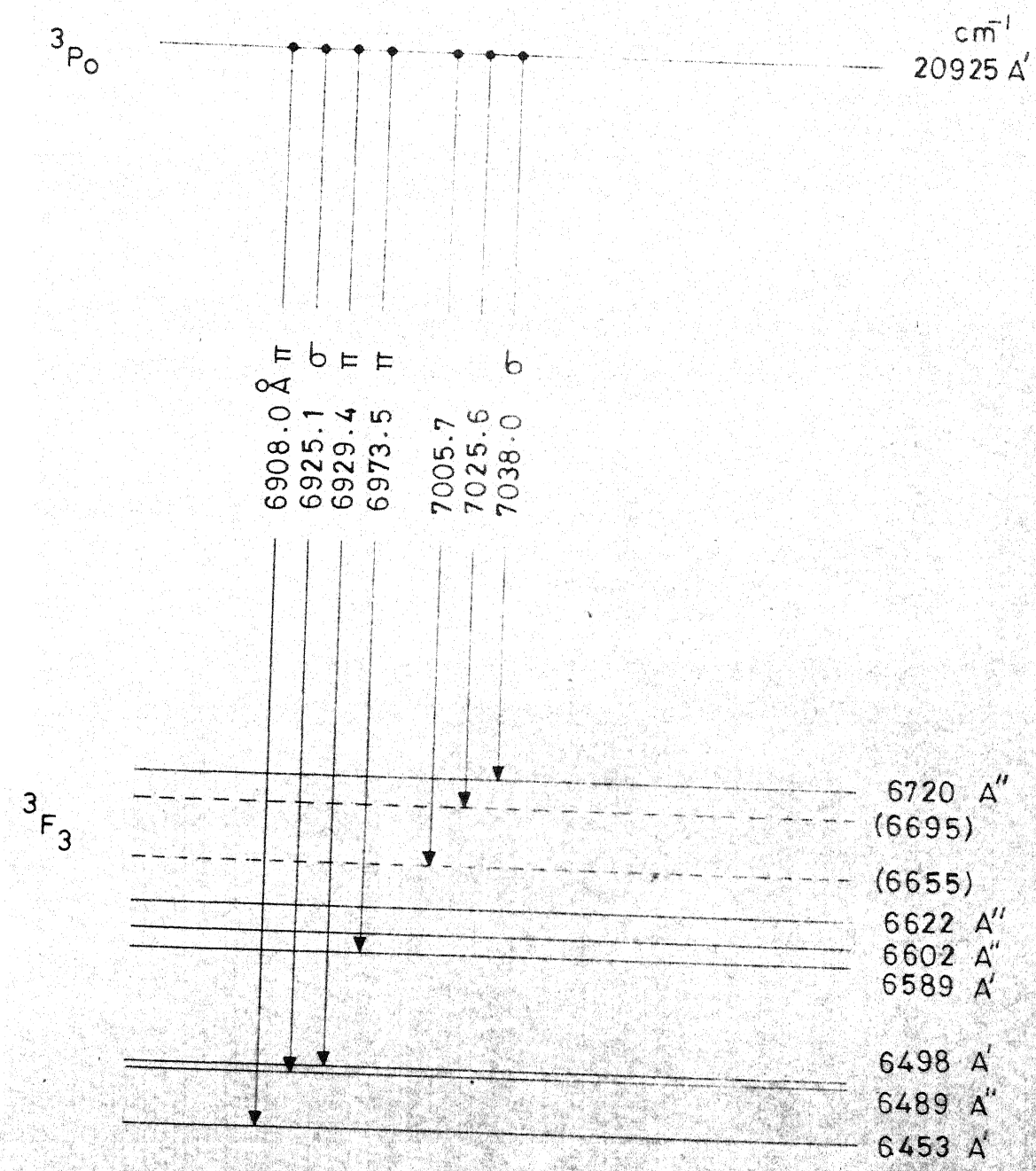


Fig. 3.12 Partial energy level diagram of $LaF_3 : Pr^{3+}$ showing the fluorescence transition group $^3P_o \longrightarrow {}^3F_3$ at LNT.

by A'' . The transitions at 7081.1 (14118) and 7094.5 Å (14092 cm^{-1}) are π polarized and not observed in σ-polarization. Axial spectrum was not recorded. Even then the terminal levels of those transitions are fixed to be A' because a π-polarization (by E. D. and by M. D.) can occur only when the terminal level is an A' . But the Stark levels at 6489 and 6720 cm^{-1} are A'' . Therefore the phonons coupled to those levels at 318 and 113 cm^{-1} are represented by A'' .

(6) Fluorescence terminating in $^3F_4$

The level splits into 9 components in the crystal field. The Stark levels are represented by $5A' + 4A''$ under C_s site and by $5A + 4B$ under C_2 site. The fluorescence group falls in the region 7149-7470 Å (Fig. 3.13 and 3.14). The transitions at 7149.3 (13984) 7177.1 (13929) and 7232.8 Å (13822 cm^{-1}) are σ-polarized and E. D. in nature. So their lower levels at 6941, 6996 and 7103 cm^{-1} are represented by A'' under C_s site and by A under C_2 site. The transitions at 7169.3 (13945) 7192.3 (13900), and 7262.8 Å (13765 cm^{-1}) are π-polarized and M. D. in nature. Their lower levels at 6980, 7025 and 7160 cm^{-1} are represented by A' under C_s site and by A under C_2 site. Only five levels are to be of A type species under C_2 site where as 6 levels are represented by A in the above analysis. So C_2 site fails to explain this

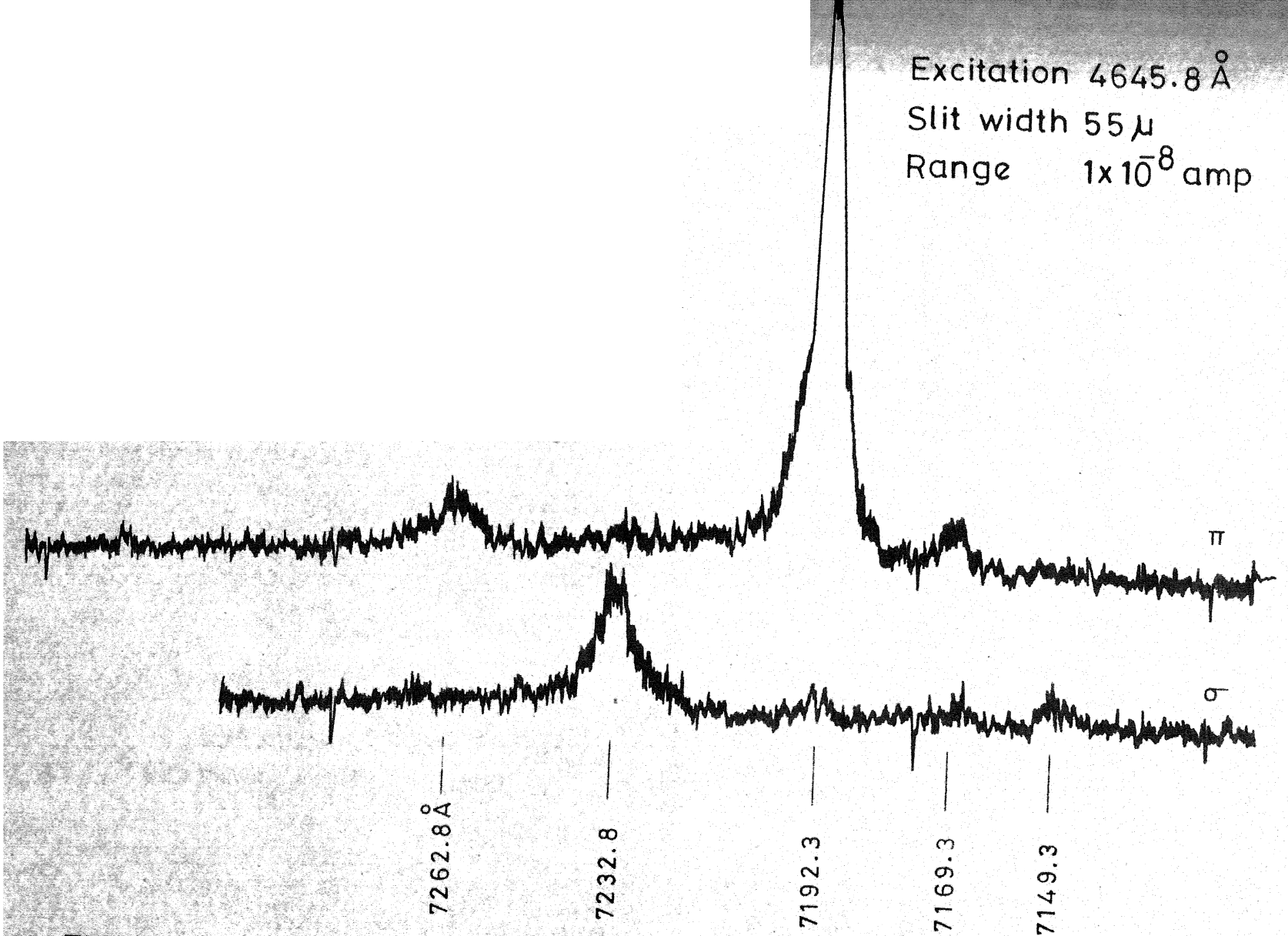
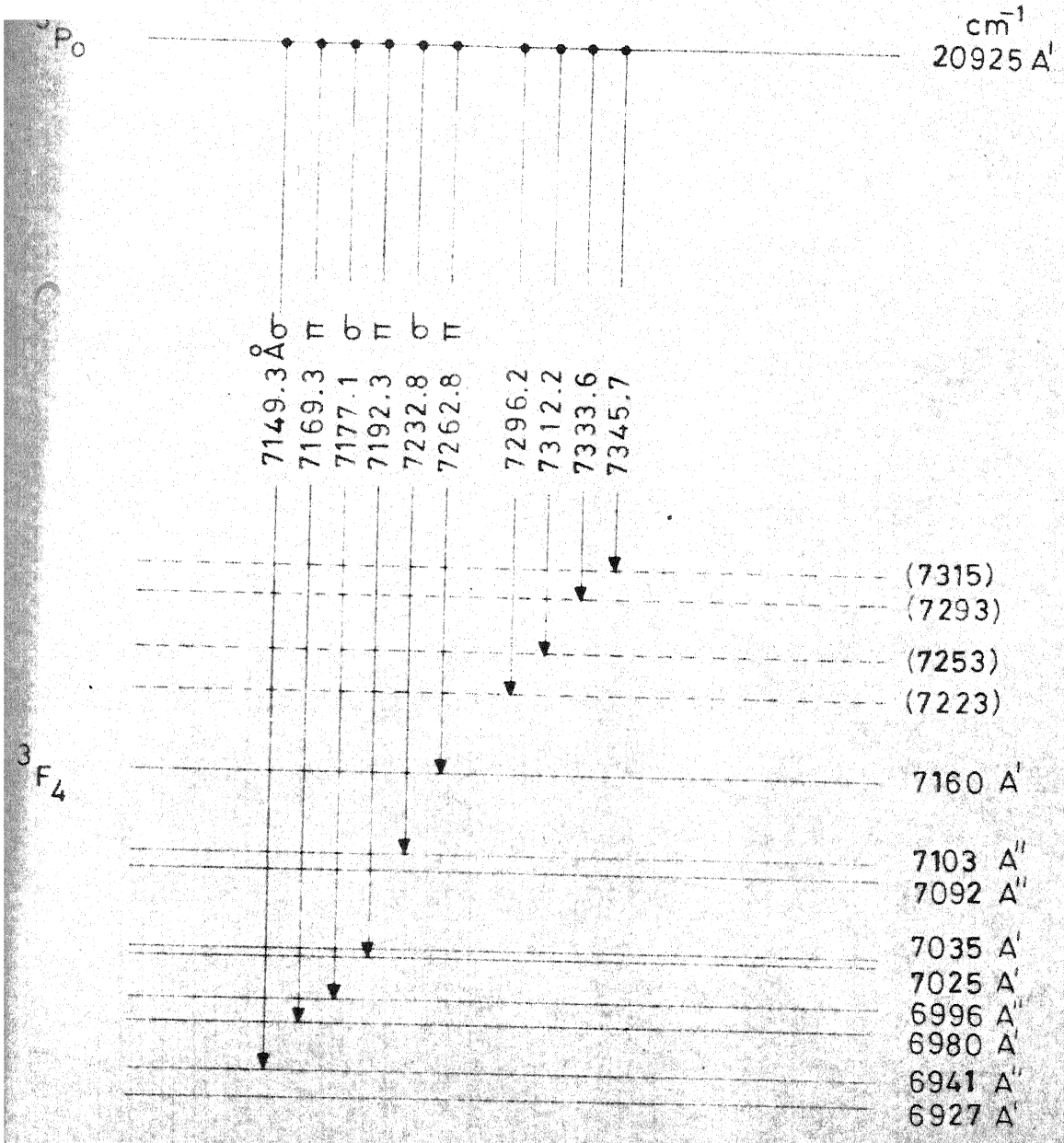


Fig. 3.13 Fluorescence spectrum of $LaF_3:Pr^{3+}$ at LNT, $^3P_0 \longrightarrow {}^3F_4$ group.



ig.3.14 Partial energy level diagram of $LaF_3:Pr^{3+}$ showing the fluorescence transition group $^3P_0 \longrightarrow {}^3F_4$ at LNT.

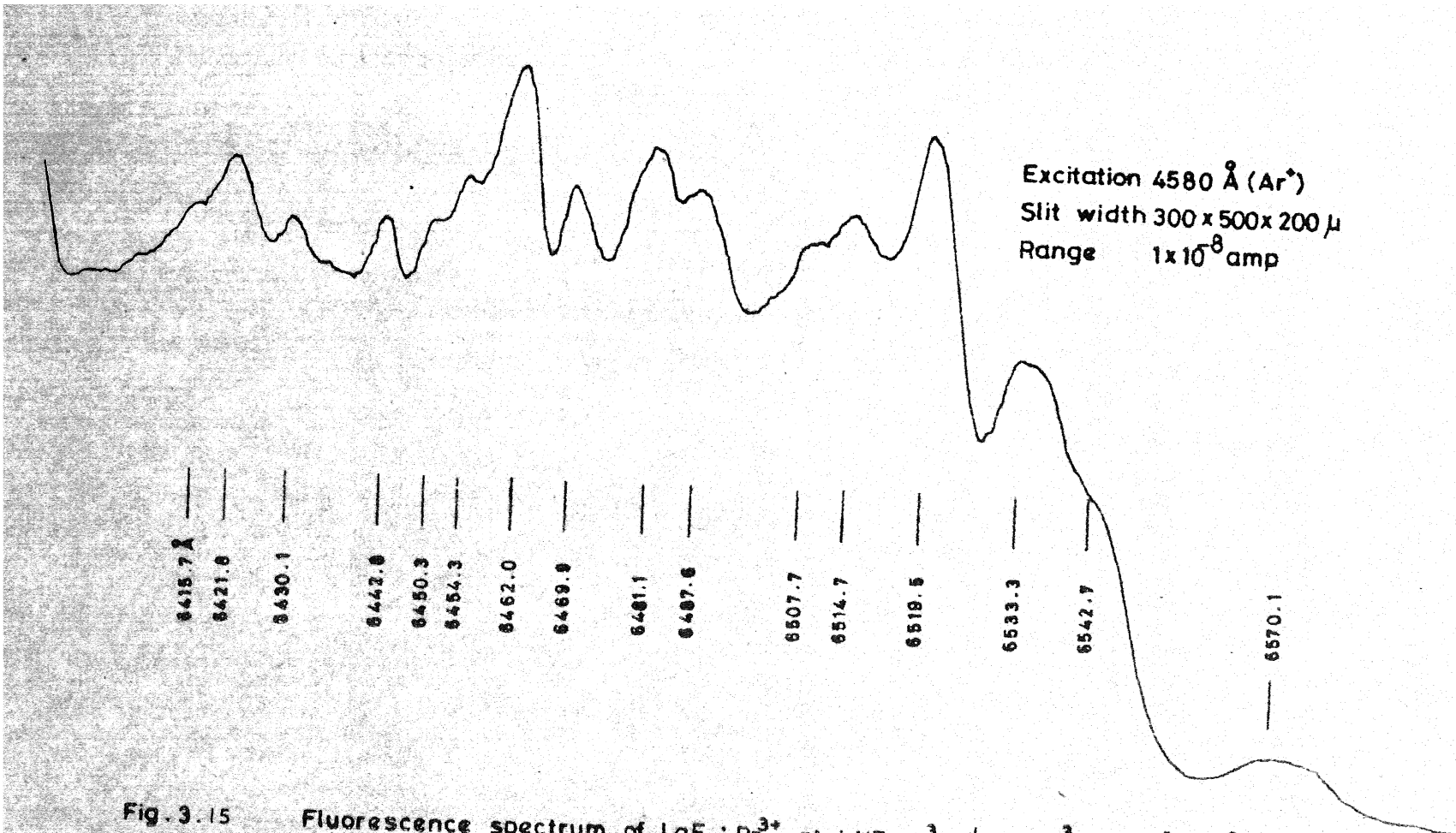


Fig. 3.15 Fluorescence spectrum of $LaF_3 : Pr^{3+}$ at LNT ; $^3P_1 (^1I_6) \longrightarrow {}^3F_3$ and $^3P_2 \longrightarrow {}^3F_4$ groups.

by A', the 340 cm^{-1} phonon coupled to the fluorescing level of the transition is represented by A''. The transition at 6487.6 Å (15410 cm^{-1}) is σ-polarized and E.D. in nature. The fluorescing Stark level of this transition at 21520 cm^{-1} is represented by A' since the level at 6453 is an A' and the phonon at 340 cm^{-1} is an A''. The 6496.1 Å (15390 cm^{-1}) transition is π-polarized and M.D. in nature. Since the phonon at 315 cm^{-1} is A'', the Stark level at 21529 cm^{-1} is an A''. The transition at 6519.5 Å (15334 cm^{-1}) is σ polarized and E.D. in nature. But the Stark level at 6498 cm^{-1} is an A' and the phonon at 315 cm^{-1} is A''. Consequently, the Stark level at 21516 cm^{-1} is represented by A'. The transition at 6542.7 Å (15230 cm^{-1}) is π-polarized and M.D. in nature. But the Stark level at 6589 cm^{-1} is an A', and the 313 cm^{-1} phonon is an A''. Therefore the fluorescing level at 21556 cm^{-1} is represented by A''. The 6570.1 Å (15216 cm^{-1}) is σ-polarized and E.D. in nature. Its terminal level is an A' and the phonon coupled to the upper level is an A''. This suggests that the Stark level at 21487 cm^{-1} is an A'. The terminal Stark level of the 5240 Å (19079 cm^{-1}) transition at 2457 cm^{-1} is an A' and therefore the fluorescing Stark level at 21536 cm^{-1} is an A''.

3.8 Room temperature fluorescence

The fluorescence groups $^3P_1(^1I_6) \rightarrow {}^3H_6$ and $^3P_1(^1I_6) \overset{\varphi}{\rightarrow} {}^3F_3$ in the regions 5763 - 5824 Å and 6625-6893 Å are observed only at room temperature and are given in Table 3.10 and shown in Figs.3.16a and 3.16b. Even the fluorescence transitions in the regions 5156-5293 Å ($^3P_1(^1I_6) \rightarrow {}^3H_5$) and 6443-6570 Å ($^3P_1(^1I_6) \rightarrow {}^3F_3$) are observed only at room temperature in this laboratory‡. (Fluorescence in the region 6625-6893 Å has been published by Venkateswarlu [36] earlier). This suggests that there is fast relaxation at liquid nitrogen temperature from $^3P_1$ (or phonon coupled levels of $^3P_0$) to $^3P_0$ level. At room temperature the population of $^3P_1(^1I_6)$ levels from $^3P_0$ level by thermalization is also considerable. It is interesting to take into account the relative intensities of the fluorescence groups+. The intensity of the group $^3P_1(^1I_6) \rightarrow {}^3H_6$ is weaker than that of $^3P_0 \rightarrow {}^3H_6$. But the intensity of the groups $^3P_1(^1I_6) \rightarrow {}^3H_5$, $^3F_3$ is greater or at least comparable to that of $^3P_0 \rightarrow {}^3H_5$, $^3F_3$ (Fig.3.17).

φ or from the phonon coupled levels of $^3P_0$.

‡ But under CW Ar^+ laser excitation these two groups of lines have been observed by Prof. P. Venkateswarlu even at LNT. So these two groups of transitions are analysed under LNT fluorescence.

\+ The groups $^3P_1(^1I_6) \rightarrow {}^3H_4$, $^3F_2$ are not observed.

Table 3.10

Fluorescence of Pr^{3+} in LaF_3 observed only at RT

Wavelength (Å)	Wavenumber (cm^{-1})	Pol	Transition Initial	Final
5189.0	19266	π	21498	2232
5218.0	19159	π	21458	2298
5248.4	19048	π	21458	2412
5253.9	19028		21458	2430
5264.0	18992		21458	2466
5763.4	17346		21556+55	4266
5784.2	17284	σπ	21536	4222+30
5808.0	17213	π	21516	4303
5823.8	17166	π	21578+31	4443
6625.4	15089		21578	6489
6649.4	15035		21536	6498
6655.6	15021		21516	6498
6660.6	15010	π	21458	6448
6680.1	14966		21556	6489
6700.5	14920		21520	6600
6704.2	14912	πσ	21516	6604
6722.5	14871	π	21458	6587
6753.9	14802	π	21564	6622+140
6760.5	14788		20925+316	6453
6769.8	14767		20925+295	6453
6780.2	14745		20925+273	6453
6788.1	14728		20925+292	6489
6794.5	14714		20925+242	6453
6831.5	14634		20925+198	6489
6886.3	14518		20925+82	6489
6889.6	14511		20925+76	6489
6893.0	14503	πσ	20925+76	6498
6912.2	14463		20925+27	6489

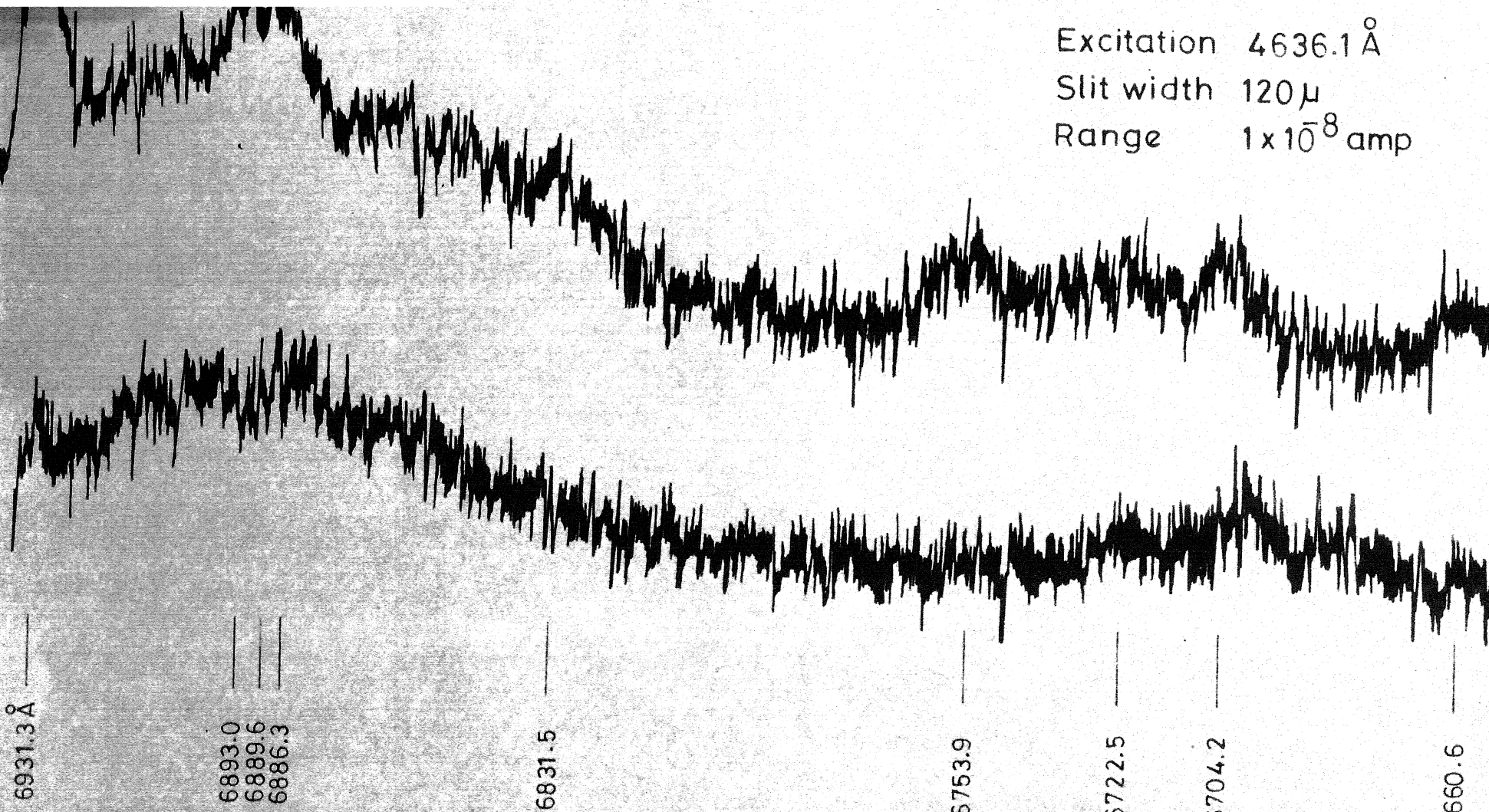


Fig. 3.16 a Fluorescence spectrum of $LaF_3:Pr^{3-}$ observed only at RT showing transitions fro
phonon coupled levels of $^3P_0$ and $^3P_1$ to $^3F_3$ levels.

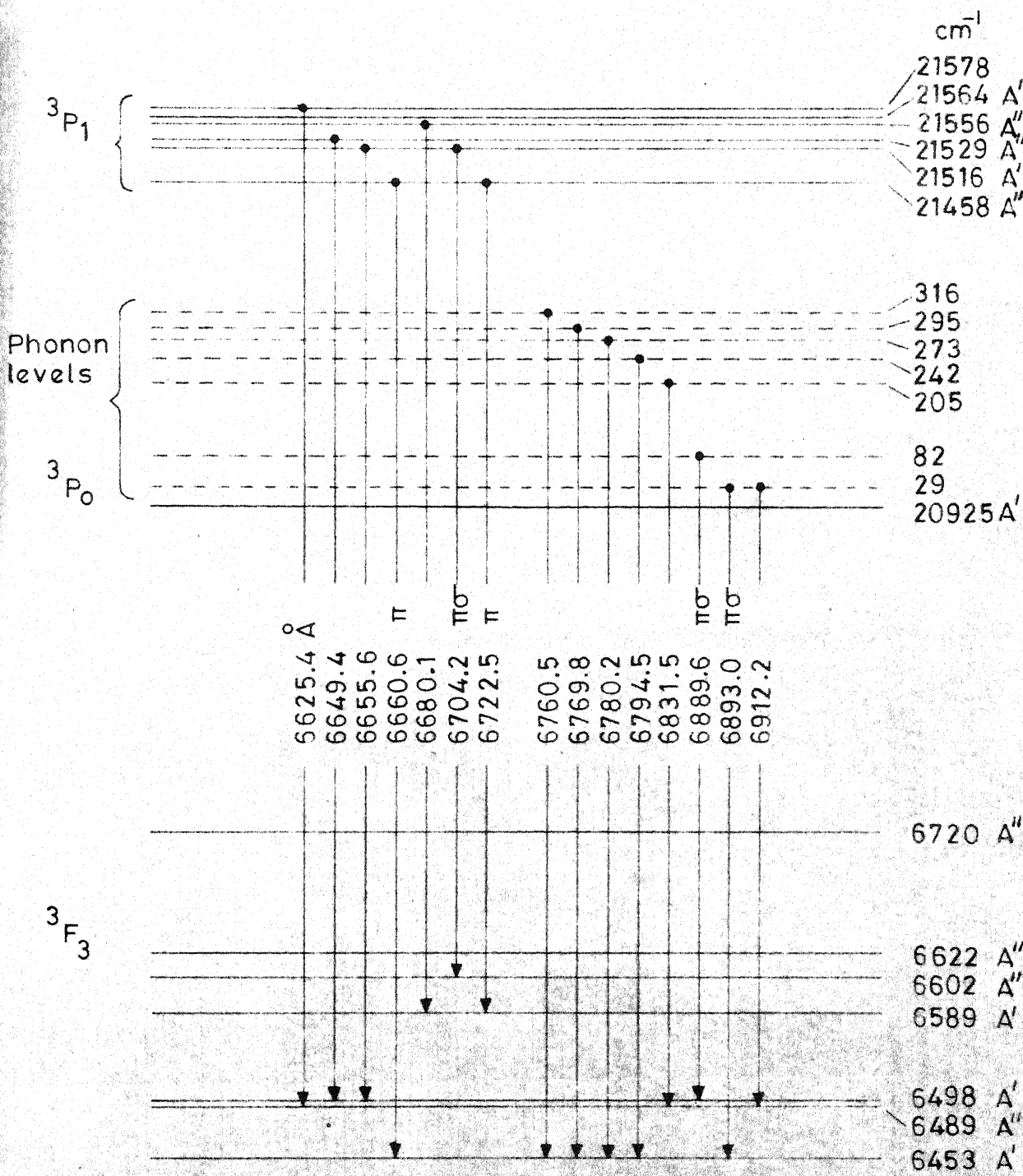


Fig. 3.16 b Partial energy level diagram of $LaF_3:Pr^{3+}$ showing transitions from $^3P_1$ and phonon coupled levels of $^3P_0$ terminating in $^3F_3$ observed at RT.

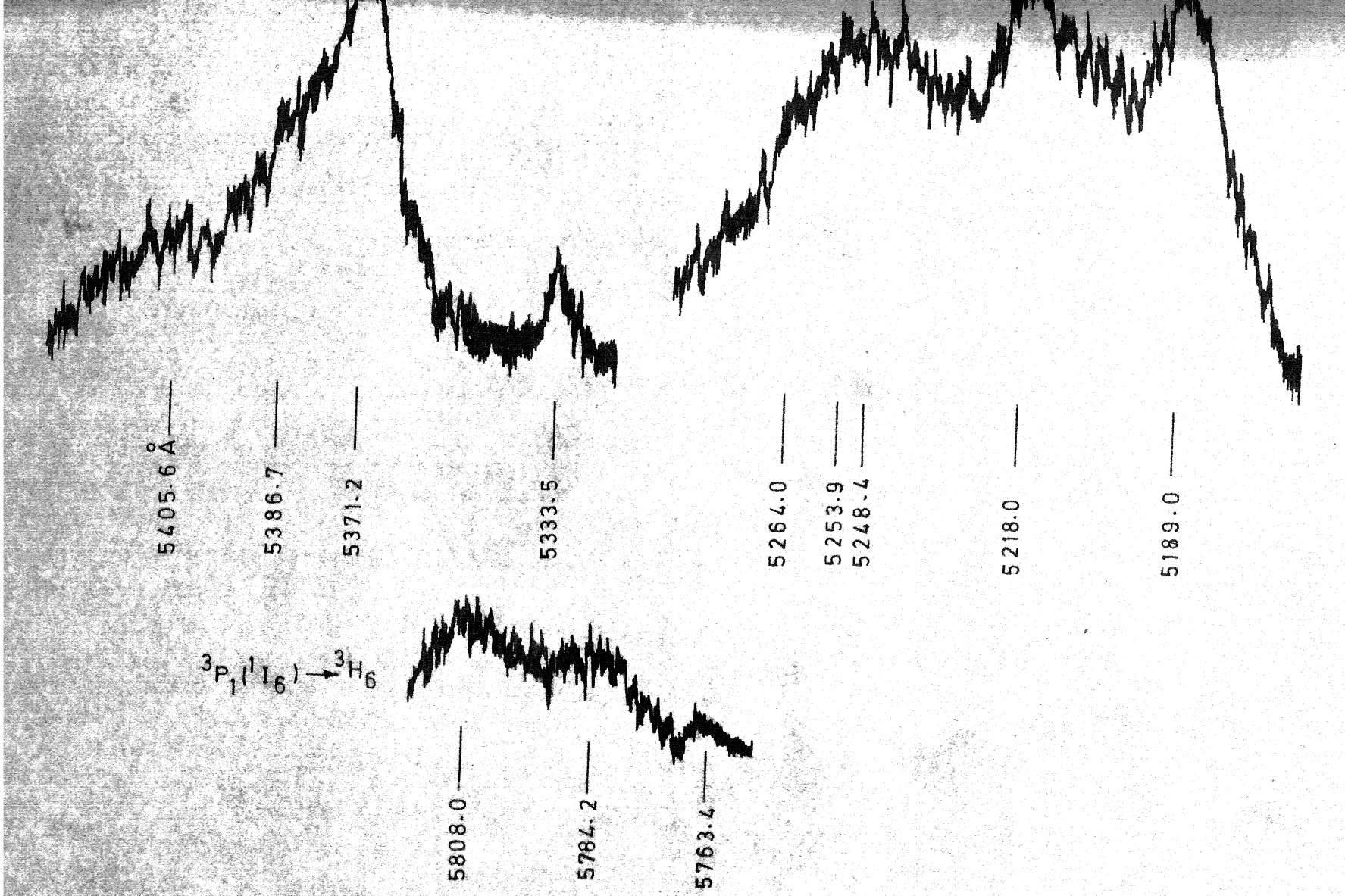


Fig.3.17 Fluorescence spectrum of $LaF_3 : Pr^{3+}$ at RT, $^3P_1 (^1I_6) \rightarrow {}^3H_5$; $^3P_0 \rightarrow {}^3H_5$ and $^3P_1 (^1I_6) \rightarrow {}^3H_6$ groups.

These observations support Ofelt's [3] theory on the intensity of the crystal spectra. The transition at 5189.0 (19266), 5218 (19159) and 5248.4 Å (19048 cm^{-1}) are π-polarized and M.D. in nature. Their initial and final levels are shown in Table 3.10. The level at 21498 cm^{-1} is an A'', since the terminal level of that transition at 2230 cm^{-1} is an A''. The level at 21458 cm^{-1} is an A'' since the terminal level of 5218 Å at 2298 cm^{-1} is an A''. The terminal level of 5248.4 Å at 2412 cm^{-1} is an A'' since the fluorescing level at 21458 cm^{-1} is an A''. The explanation for the other transitions is not given and they are understood from the table.

3.9 Fluorescence originating from $^3P_2$ (LNT)

This level splits into 5 components in the crystal field. The Stark components are represented by $3A' + 2A''$ under C_s site. The fluorescence group falls in the region 6408-6462 Å (Fig.3.15). This fluorescence group is observed only when 4580 Å line of Ar^+ laser is used in exciting the crystal. The transitions at 6421.8 Å (15568 cm^{-1}) and 6430.1 Å (15548 cm^{-1}) are σ-polarized and E.D. in nature. They are terminating in the same Stark ($^3F_4$) level at 7160 (7165) cm^{-1} (A'). So, their fluorescing (initial) Stark levels at 22734 and 22714 cm^{-1} are represented by A''. Since two levels are already assigned with A'' the remaining three Stark levels at 22691, 22772 and 22819 cm^{-1}

are represented by A'. The transition at 6408.7 Å is σ-polarized and M.D. in nature (not observed in axial spectrum). The fluorescing Stark level of this transition at 22691 cm^{-1} is an A'. So its terminal Stark level at 7092 cm^{-1} is of A'' type species.

3.10 Resonance fluorescence from $^1D_2$ Stark multiplet

This level splits into 5 components in the crystal field. The Stark components are represented by $3A' + 2A''$ under C_s symmetry. When $^3P_0$, $^3P_1(^1I_6)$ levels are excited no fluorescence is observed from $^1D_2$ multiplet. Fluorescence is observed from $^1D_2$ multiplet on resonant excitation. Four groups of lines $^1D_2 \rightarrow {}^3H_4$ (Figs.3.18 and 3.19), $^1D_2 \rightarrow {}^3H_5$ (Figs. 3.20 and 3.21), $^1D_2 \rightarrow {}^3H_6$ and $^1D_2 \rightarrow {}^3F_2$ are observed in fluorescence, respectively in the regions 5811-6108 Å, 6793-6923 Å, 7888-8191 Å and 8503-8618 Å. But there is a change in spin multiplicity in the transitions $^1D_2 \rightarrow {}^3H_{4,5,6}$ and $^1D_2 \rightarrow {}^3F_2$. Such transitions are forbidden in the pure Russel-Saunders coupling. But in the intermediate coupling, states with the same J value may be coupled, consequently L and S are no longer good quantum numbers. So, the fluorescence emission originating from $^1D_2$ levels and terminating in $^3H_{4,5,6}$ and $^3F_2$ levels is due to the possible J-mixing of wave functions. Consequently we can express the state function of the $|^1D_2\rangle$ state as

Table 3.11

Resonance Fluorescence from $^1D_2$ levels

Wavelength (Å)	Wavenumber (cm^{-1})	Int.	Pol.	Nat.	Transition Initial	Transition Final
5811	17204	vw			17204	0
5841.6	17114	vw			?	?
5846.9	17098	vw			17204	0+106
5874.7	17017	vw			17183	0+166
5917.9	16893	w	π	M	16893	0
5920.7	16885	w	π	M	17086	204
5939.0	16833	m	σ	E	16893	60
5946.4	16812	m	σ	E	16872	60
5953.8	16791				16872	(81)
5975.1	16731	m	π	E	16872	(141)
5999.2	16664	s	πσ	M	16872	(208)
6023.8	16596				16893	296
6030.7	16577				16872	296
6035.0	16565	w	π	E	16893	317
6039.2	16554	w	π	E	16872	317
6108.0	16367	w	σπ	EM	16872	504
6793.2	14717	vw	π	M	16893	(2181)
6801.4	14699	vw	π	M	16872	(2181)
6817.7	14664	vw			16893	2230
6827.2	14643	vw			16872	2230
6849.9	14595	vw	π	M	16893	2298
6852.5	14589	vw			16893	2305
6885.9	14518	w	πσ	ME	16872	2356

Table 3.11 (contd.....)

Wavelength (Å)	Wavenumber (cm^{-1})	Int.	Pol.	Nat.	Transition Initial	Transition Final
6906.7	14475	vw			16872	2298+99
6914.4	14459	vw			16872 16893	2412 2432
6923.3	14440	vw			16872 16893	2432 (2453)
7539.8	13259	w			?	?
7561.8	13221	w			?	?
7574.7	13198	w			?	?
7888.0	12674	m			16893	4221
7929.4	12608	m			16872	4266
8000.4	12496	vv			17086	4590
8062.8	12399	vv			17183	4785
8116.7	12317	vv			16893	4303+273
8190.5	12206	vv			16893	4443+144
8503.1	11757	vv			16893	5136
8536.4	11711	vv			16893	5182
8566.9	11670	vv			16872	5199
8605.9	11617	vv			16893	5276
8617.6	11601	vv			16872	5276

s	strong	vv	very very weak
m	moderate	E	electric dipole
w	weak	M	magnetic dipole
vw	very weak		

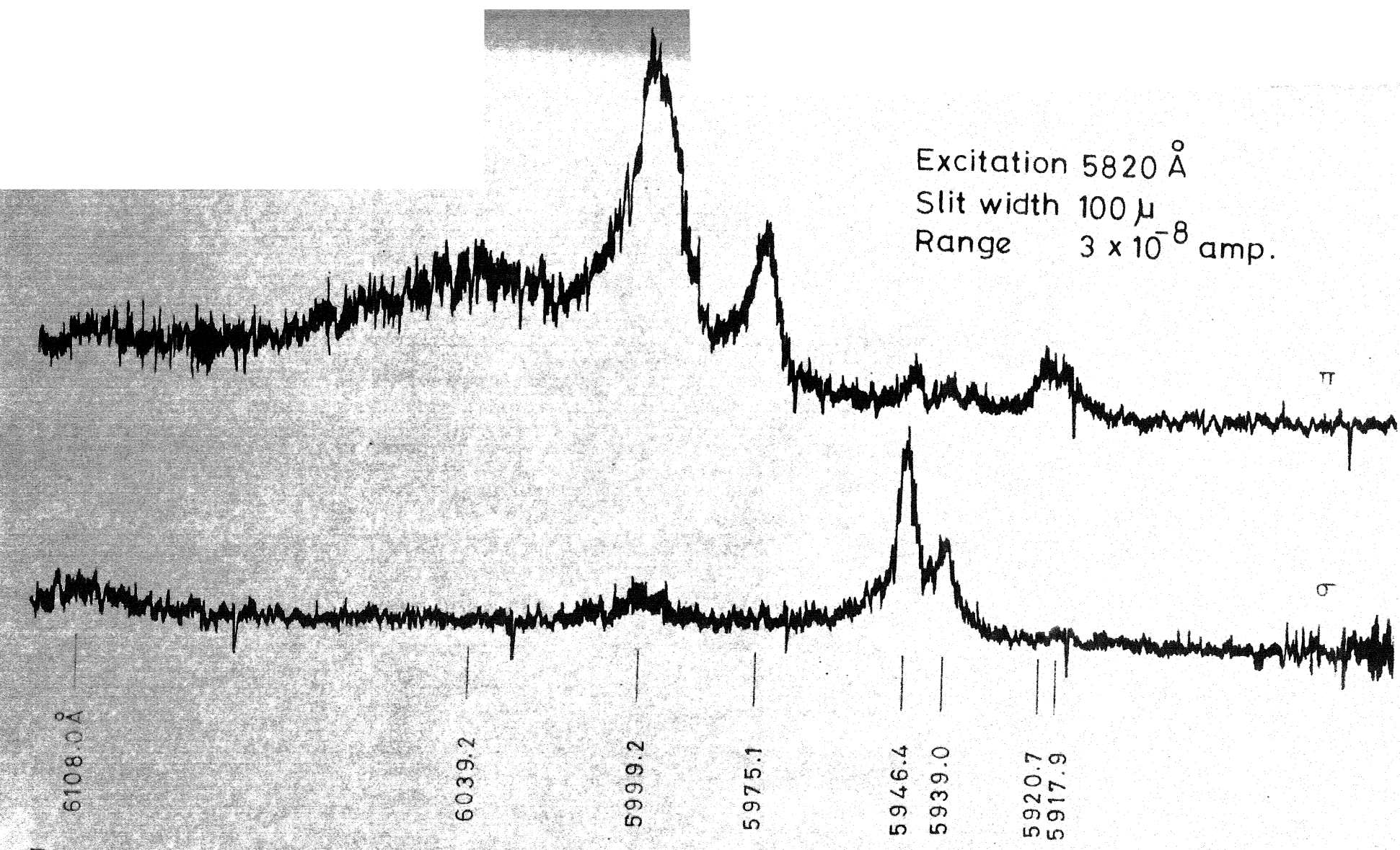


Fig. 3.18 Fluorescence spectrum of $LaF_3 : Pr^{3+}$ at LNT, $^1D_2 \longrightarrow {}^3H_4$ group.

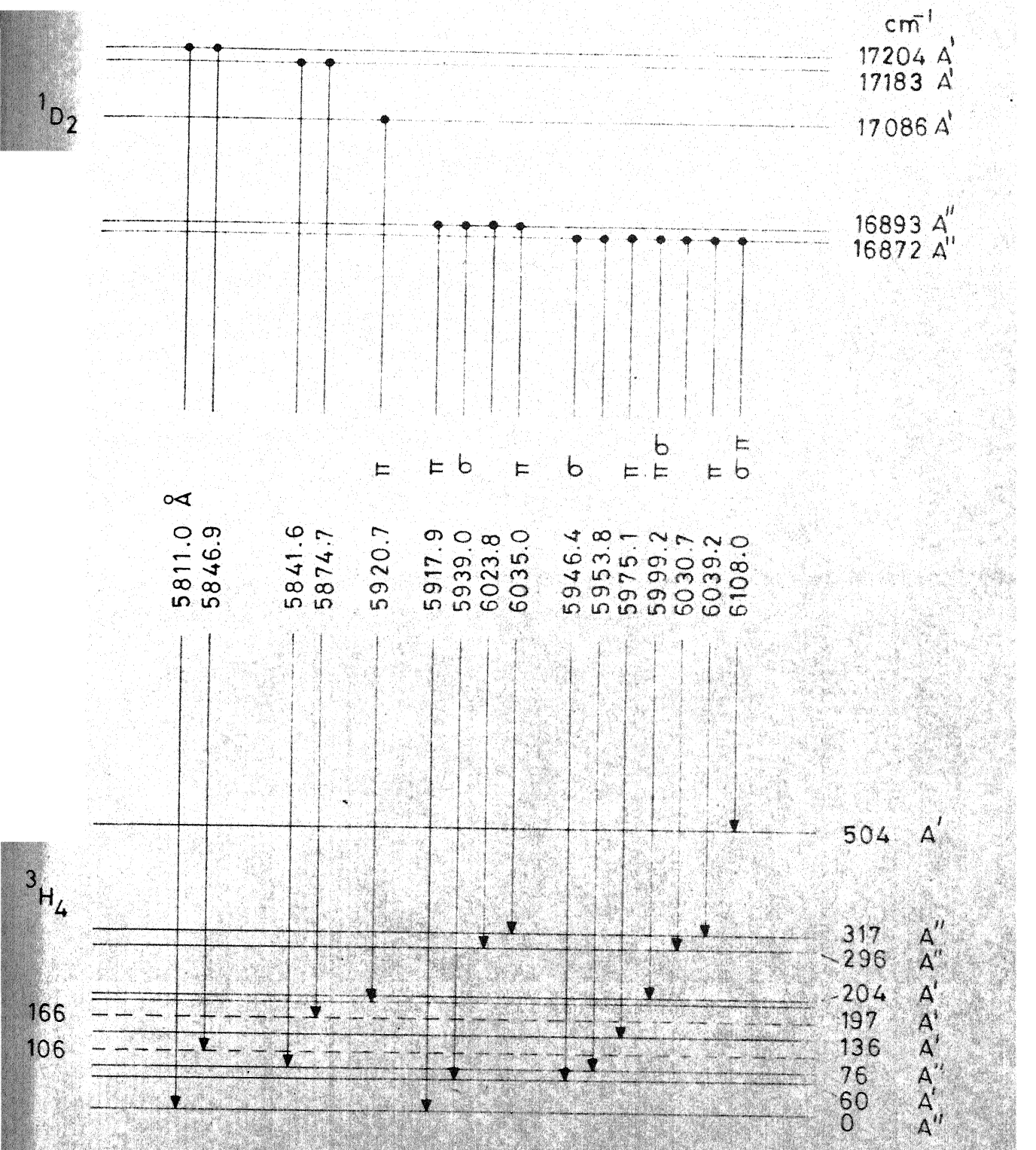


Fig.3.19 Partial energy level diagram of $LaF_3:Pr^{3+}$ showing the fluorescence transition group $^1D_2 \rightarrow {}^3H_4$ at LNT.

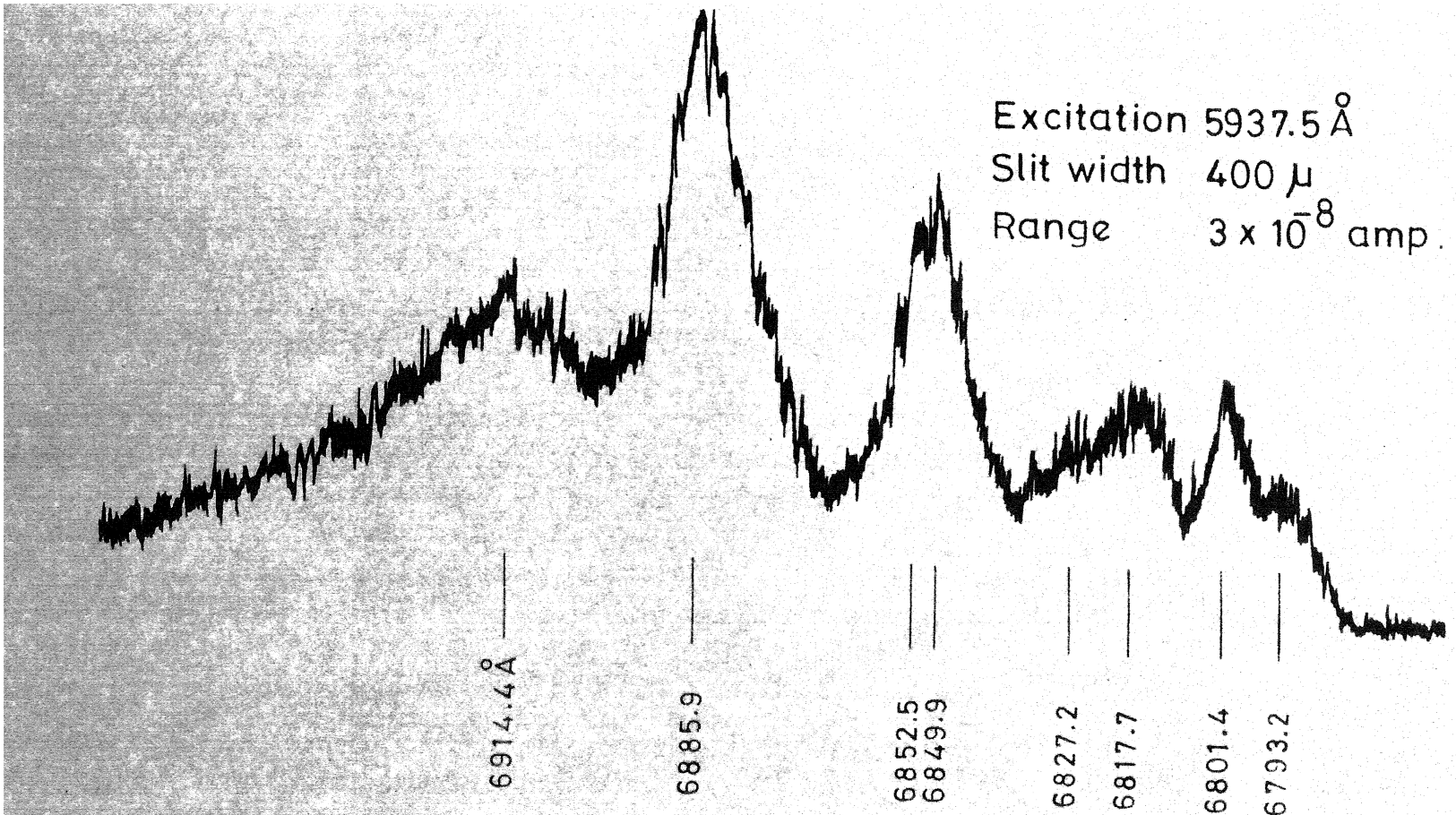


Fig. 3.20 Fluorescence spectrum of $LaF_3 : Pr^{3+}$ at LNT, $^1D_2 \longrightarrow {}^3H_5$ group

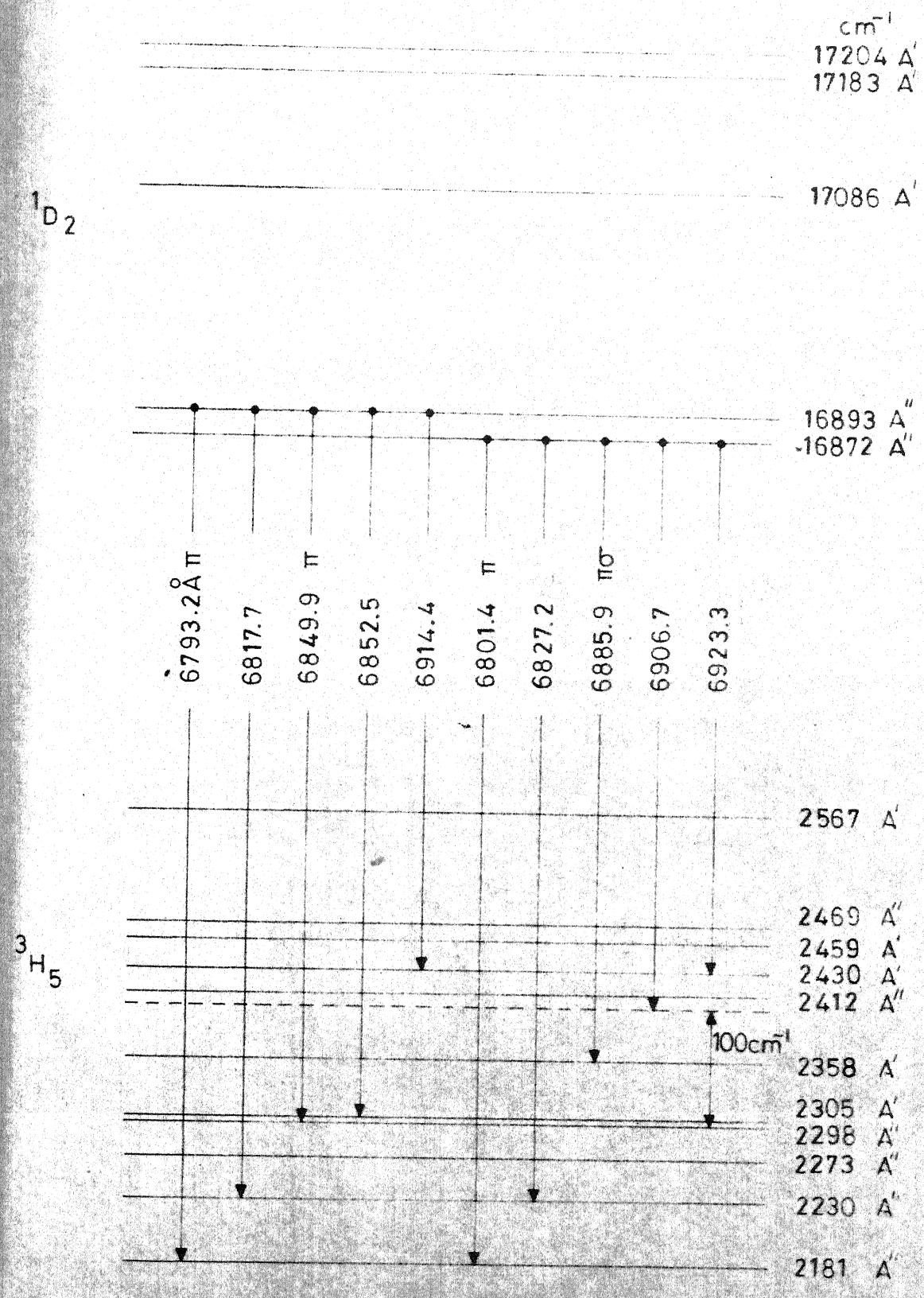


Fig.3.21 Partial energy level diagram of $LaF_3: Pr^{3+}$ showing the fluorescence transition group $^1D_2 \rightarrow {}^3H_5$ at LNT.

$$|^1D_2'\rangle = a\,|^1D_2\rangle + b\,|^3P_2\rangle + c\,|^3F_2\rangle$$

where the sum of the squares of the coefficients, a, b and c is 1 Therefore, these transitions are weak and their intensities would depend on the amount of mixing, that is on the magnitude of the coefficients a, b and c.

Based on fluorescence originating from ^3P levels, representations of $^3H_{4,5,6}$ and $^3F_{2,3,4}$ multiplets have been already assigned. Species assignment is made to $^1D_2$ levels after analysing the fluorescence originating from these ($^1D_2$) levels. The transition 5917.9 Å (16893 cm^{-1}) is π-polarized and M.D. in nature. Its terminal level at 0 cm^{-1} is represented by A'' under C_s symmetry and by $A_1(B_1)$ under C_{2v} symmetry. So, the fluorescing Stark level at 16893 cm^{-1} is A'' under C_s site and $A_2(B_2)$ under C_{2v} site. The transition 5946.4 Å (16812 cm^{-1}) is σ-polarized and E.D. in nature. Its terminal level at 60 cm^{-1} is A' under C_s site and $A_2(B_2)$ under C_{2v} site. Therefore, the fluorescing Stark level at 16872 cm^{-1} is represented by A'' under C_s site and by $A_2(B_2)$ under C_{2v} site. The transition at 5975.1 Å (16731 cm^{-1}) is π-polarized. Its terminal level at 136 (141) cm^{-1} is an A' under C_s site and an $A_2(B_2)$ under C_{2v} site. The initial level of this transition at 16872 cm^{-1} is an A'' under C_s site and $A_2(B_2)$ under

C_{2v} site. Under C_s site π-polarization is possible from A'' to A' but under C_{2v} site π-polarization is not possible from $A_2(B_2)$ to $A_2(B_2)$. So, C_{2v} site symmetry fails to explain the two transitions at 5946.4 Å and 5975.1 Å with their observed polarization. The transition at 5920.7 Å (16885 cm^{-1}) is π-polarized and M. D. in nature. Its terminal level at 204 cm^{-1} is an A'. Therefore the Stark level at 17086 cm^{-1} is represented by A'. Since the two levels are already assigned with A'' and one level with A', the remaining two levels at 17183 cm^{-1} and 17204 cm^{-1} are represented by A'. The transition at 6849.9 Å (14595 cm^{-1}) is π-polarized and M. D. Its terminal level at 2298 cm^{-1} is an A'' since the initial level at 16893 cm^{-1} is also an A''.

Other fluorescence transitions from $^1D_2$ levels to lower multiplets are not dealt in detail to avoid repetition. The Stark levels involved in these transitions are already assigned with irreducible representations. So, they are easily understood from Table 3.11.

3.11 Excitation spectra

Excitation spectrum has been recorded for atleast one fluorescence line of each group. The structure and relative intensity of different peaks in all the excitation spectra have remained the same for fluorescence

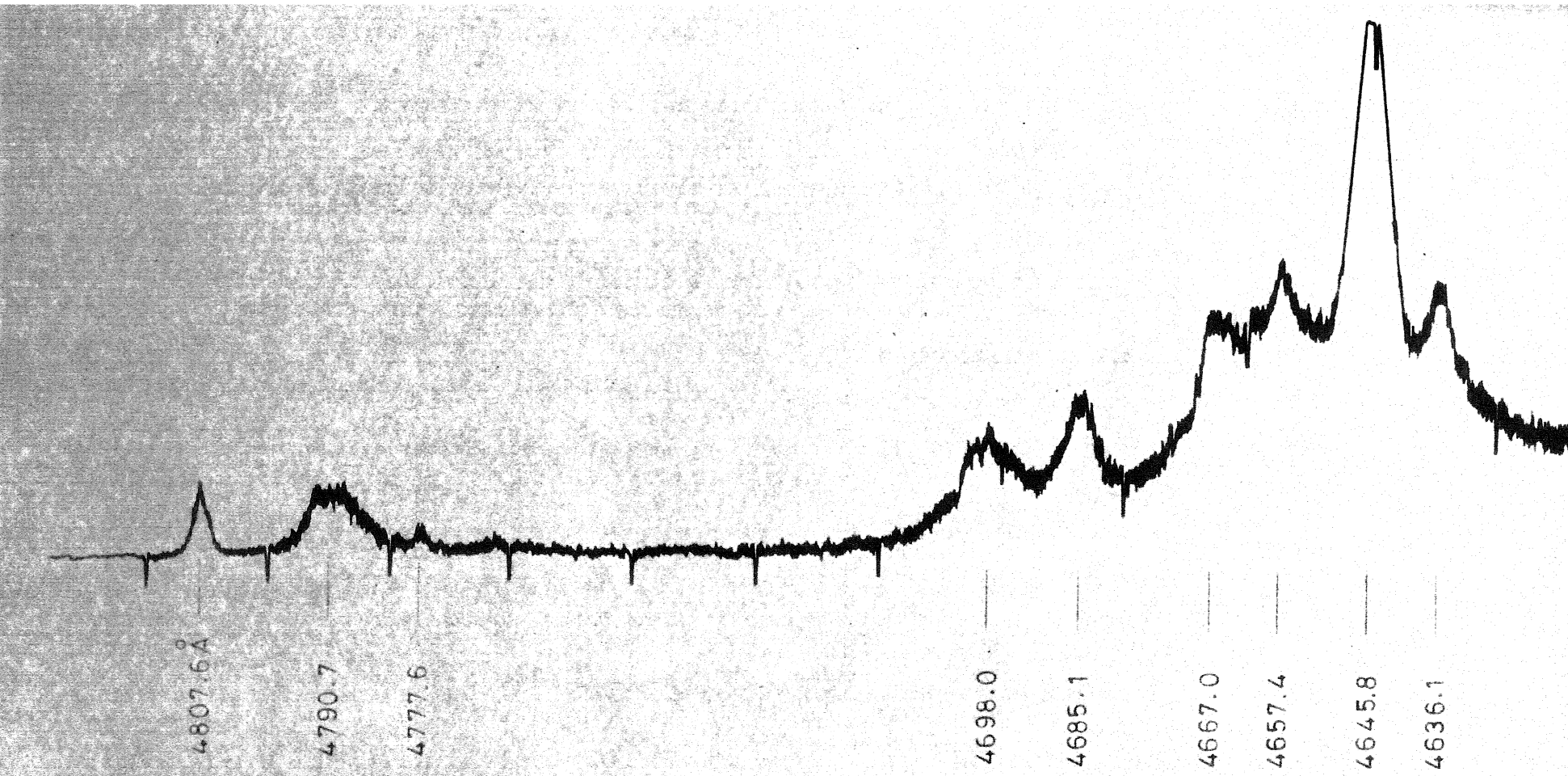


Fig.3.22 Excitation spectrum of 4791.5 Å showing transitions from $^3H_4$ to $^3P_0$, $^3P_1(^1I_6)$ levels at LNT.

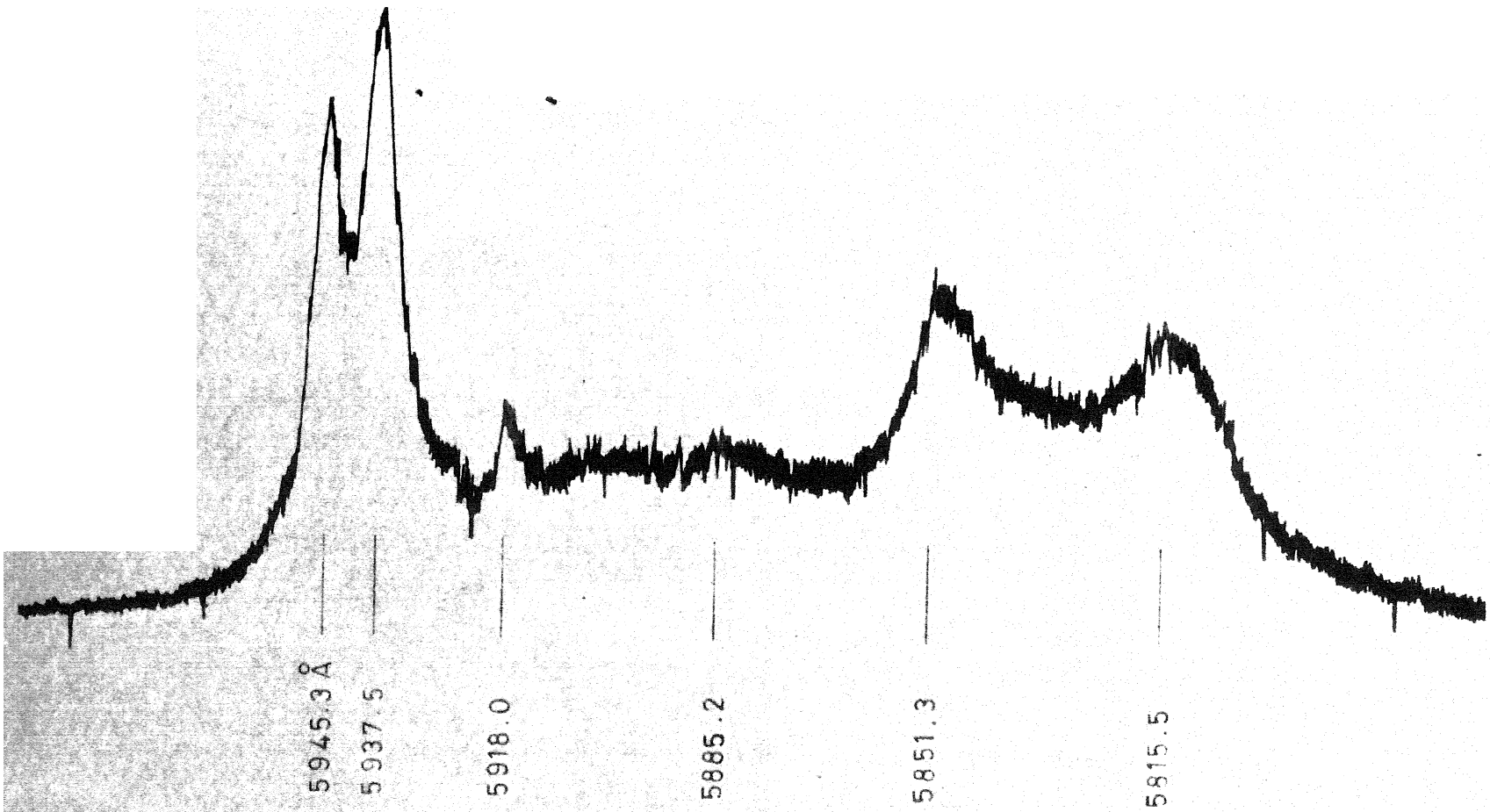


Fig. 3.23 Excitation spectrum of 7888 Å showing transitions from $^3H_4$ to $^1D_2$ levels at LNT.

Table 3.12

$^3H_4 \rightarrow {}^3P_0$, $^3P_1(^1I_6)$ excitation Transitions of $LaF_3:Pr^{3+}$ at LNT

Wavelength (Å)	Wavenumber (cm^{-1})	Transition Initial $^3H_4$	Transition Final $^3P_{0,1}(^1I_6)$
4636.1	21564	0	21564
4645.8	21519	0	21519
4657.4	21465	?	?
4667.0	21421	57	21478
4672.7	21395	76	21471
4685.1	21338	136	21474
4698.0	21280	195	21475
4777.6	20925	0	20925
4790.7	20868	57	20925
4807.6	20795	?	?

Table 3.13

$^3H_4 \rightarrow {}^1D_2$ Excitation Transitions of $LaF_3:Pr^{3+}$ at LNT

Wavelength (Å)	Wavenumber (cm^{-1})	Transition Initial ($^3H_4$)	Transition Final ($^1D_2$)
5815.3	17191	?	?
5851.3	17086	0	17086
5885.0	16988	195	17183
5918.0	16893	0	16893
5937.5	16837	57	16894
5945.3	16815	57	16872
		76	16891

Note: For the initial levels, ($^3H_4$), the values reported by Carnall et al.[4] have been used.

Fig.3.24 Excitation spectrum of 5218 Å showing transitions from $^3H_4$ to $^3P_1$ ($^1I_6$) levels at R.T.

Table 3.14

$^3H_4 \rightarrow {}^3P_1(^1I_6)$ Excitation Transitions of $LaF_3:Pr^{3+}$ at RT

Wavelength (Å)	Wavenumber (cm^{-1})	Transition Initial($^3H_4$)	Transition Final $^3P_1(^1I_6)$
4495.6	22238	0	21564+337x2
4513.5	22150	0	21564+293x2
4531.5	22062	0	21578+242x2
4547.3	21985	0	21578 + 203x2
4551.5	21965	0	21578 +193x2
4563.1	21909	0	21564 + 345
4581.8	21819	0	21578 + 241
4599.7	21734	0	21578 + 156
4616.0	21658	0	21578 + 80
4633.1	21578	0	21578
4637.8	21556	0	21556
4649.5	21502	76	21578
4665.7	21427	57	21484
4682.1	21352	204	21556
4698.8	21276	204	21480
4715.9	21199	322	21521

lines emanating from a particular level. To avoid repetition, excitation spectra of only two transitions, 4791.5 Å (20865 cm^{-1}) originating from $^3P_0$ level and 7929.4 (12608 cm^{-1}) originating from $^1D_2$ level are given in Fig. 3.22 and 3.23. The transitions from ground levels to the upper levels are identified and are given in Tables 3.12 and 3.13. The excitation spectra revealed some of the levels of $^3P_0$, $^3P_1(^1I_6)$ and $^1D_2$ levels. Similarly, at room temperature excitation spectrum has been recorded for atleast one fluorescence line of each group. Excitation spectrum of 5218 Å (19159 cm^{-1}) transition is shown in Fig. 3.24. The transitions corresponding to all the peaks have been identified and are given in Table 3.14. The levels that are identified from the above spectra are compared with those of Caspers et al [3] and Carnall et al [4] in Table 3.8. From the table it is seen that the values obtained by all the workers for the $^3P_0$ and $^3P_1(^1I_6)$ energy levels are in fairly good agreement among themselves within their experimental errors. But among $^1D_2$ level energies there is large discrepancy. There is close agreement among all the workers only for two levels at 16872 and 16893 cm^{-1} . But energy values obtained in the present study for four levels of this multiplet are closely agreeing with those obtained by Carnall et al[4]. There is some discrepancy only for one level at (17191 cm^{-1}). All the excitation transitions are shown in Fig. 3.25.

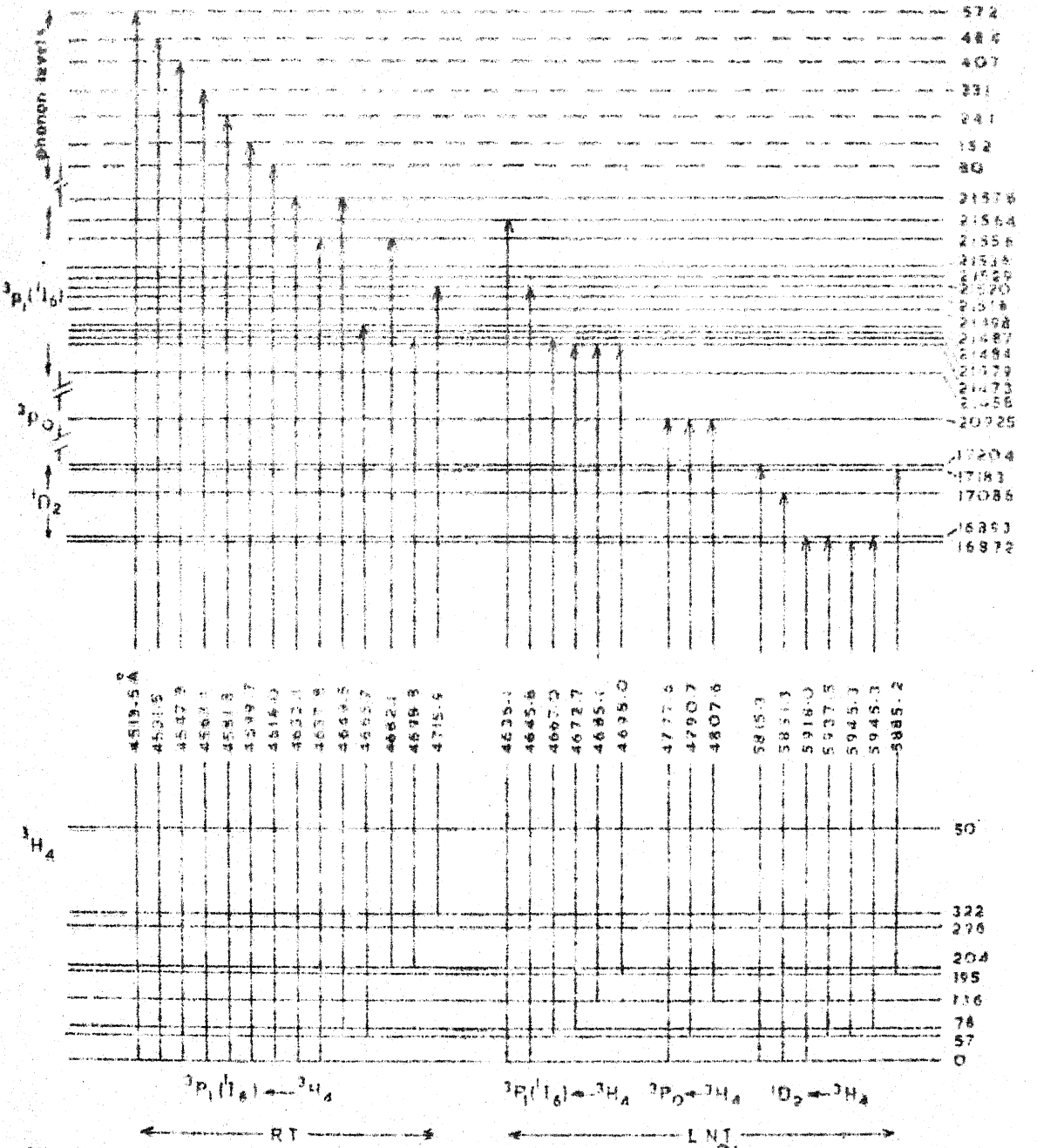


Fig.3.25 Observed excitation transitions of $LaF_3:Pr^{3+}$ at room and liquid nitrogen temperatures

3.12 Conclusion

The values obtained for the energy levels of Pr^{3+} in LaF_3 from the excitation and fluorescence spectra are agreeing with in the experimental errors with those of Caspers et al. and Carnall et al. (Table 3.8). We are able to explain the observed polarized fluorescence transitions using C_s site symmetry. The fluorescence spectra indicate that there is mixing among the wavefunctions of the energy levels. It is also observed that the $^3P_1(^1I_6)$ and $^3P_2$ levels relax very fast to lower level(s) at liquid nitrogen temperature. At room temperature strong fluorescence is observed even from $^3P_1(^1I_6)$ levels. This suggests that the population in these levels is significant at room temperature (At room temperature thermal population of $^3P_1(^1I_6)$ levels from $^3P_0$ is also significant). The intensity of the fluorescence spectra strongly supports Ofelt's theory. Strong M.D. transitions are observed even for $\Delta J = 6$. One may expect weak transitions by mixing of wavefunctions, but the reason for the observed strong M.D. transitions is not known. No fluorescence emission arising from $^1D_2$ multiplet is observed when levels above that are excited.

REFERENCES

1. J. Sugar, Phys. Rev. Letts. 14, 731-732 (1965).
 J. Sugar, J. Opt. Soc. Am. 55, 1058-1061 (1965).
 J. Sugar, J. Opt . Soc. Am. 61, 727 (1971).
2. H.M. Crosswhite, G.H. Dieke and W.J. Carter, J.Chem. Phys. 43, 2047 (1965).
3. H.H. Caspers, H.E. Rast and R.A. Buchanan, J.Chem. Phys. 43, 2124 (1965).
4. W.T. Carnall, P.R. Fields and R. Sarup, J.Chem. Physics 51, 2587 (1969).
5. Wm.S. Heaps, L.R. Elias and W.M. Yen, Phys.Rev.B13, 94 (1976).
6. E.Y. Wong, O.M. Stafsudd and D.R. Johnston, J.Chem. Phys. 39, 786 (1963).
7. W.M. Yen, W.C. Scott and A.L. Schawlow, Phys.Rev. 136, A271 (1964).
8. L.E. Erickson, Opt. Commun. 21, 147 (1977).
9. Y.C. Chen, K. Chiang and S.R. Hartman, Phys.Rev.B21, 40 (1980).
10. W. Pong and C.S. Inouye, J.Opt.Soc.Am. 68, 521 (1978).
11. V.K. Sharma, J. Chem. Phys. 54, 496 (1971).
12. I. Oftedal, Z. Physik Chem. 13B, 190 (1931).
13. J.H. Van Vleck and M.H. Hebb, Phys. Rev.46, 17 (1934).
14. M.L. Afanasiev, S.P. Habuda and A.G. Lundin, Acta Cryst. B28, 2903 (1972).
15. K. Schlyter, Arkiv Kemi 5, 73 (1953).
16. W.F. Krupke and J.B. Gruber, J.Chem.Phys.39, 1024 (1963).
17. M. Mansmann, Z. Krist. 122, 375 (1965).
18. A. Zalkin, D.H. Templeton and T.E. Hopkins, Inorg. Chem. 5, 1466 (1966).
19. R.P. Bauman and S.P.S. Porto, Phys. Rev. 161, 842 (1967).

19a P. Venkateswarlu (unpublished work).

20. H.E. Rast, H.H. Caspers and S.A. Miller and R.A. Buchanan, Phys.Rev. 171, 1051 (1968).

21. R.P. Lowndes, J.F. Parrish and C.H. Perry, Phys. Rev. 182, 913 (1969).

22. A.K. Cheetham and B.E.F. Fender and H. Fuess and A.F. Wright, Acta Cryst. B32, 94 (1976).

23. P.R.W. Hudson, J.Phys.C. (Solid State) 9, L39 (1976).

24. O. Greis and D.J.M. Bevan, J. Sol.Stat.Chem. 24, 113-114 (1978).

25. L.O. Anderson and W.G. Proctor, Z. Kristall.127 , 366-385 (1968).

26. L.O. Anderson and G. Johansson, ibid., 127, 386 (1968).

26. Collete de Rango, G. Tsoucaris and Ch. Zelwer, C.R. Acad. Sci., Ser. C. 263, 64 (1965).

27. K. Lee and A. Sher, Phys. Rev. Letts. 14, 1027 (1965).

28. E.A. Baturin, Yu.A. Luk'Yanychev and O.T. Malyuchkhov, Sov. Phys. Sol. Stat. I 1527 (1965).

29. M. Goldman and L. Shen, Phys. Rev. 144, 321 (1966).

30. J.M. Baker and R.S. Rubins, Proc. Phys. Soc. (London) 78, 1353 (1961).

31. M.B. Schultz and C.D. Deffries, Phys. Rev. 149, 270 (1966).

32. S. Matthies and D. Welsch, Phys. Sol. Stat.(b) 68, 125 (1975).

33. N.V. Starostin, V.N. Ganin and A.K. Gerasyuk, Sov. Phys.Sol.Stat. 19, 285 (1977).

34. D.S. McClure$^{\varphi}$ Optical Properties of Ions in Crystals, pp. 257, Ed. H.M. Crosswhite and H.W. Moos.

35. G.S. Ofelt, J. Chem. Phys. 37, 511 (1962).

36. P. Venkateswarlu, Proceedings of Nuclear Physics and Solid State Physics Symposium, 16C, 138 (1973).

φ R.Meltzer, S.A. Reed, P. Russell and J.W. Stout

CHAPTER 4

ENERGY TRANSFER STUDIES

ABSTRACT

One of the radiative transitions of Pr^{3+} in LaF_3 at 4791.5 Å of the $^3P_0 \rightarrow {}^3H_4$ fluorescence group is found to be self-absorbed in the crystal medium itself. Its oscillator strength is estimated to be $(1.4 \pm 0.2) \times 10^{-6}$. When $^3P_0$ and $^3P_1$ ($^1I_6$) levels of Pr^{3+} in LaF_3 are excited no fluorescence is observed arising from $^1D_2$ levels. But under the same excitation conditions $^1D_2$ fluorescence is observed in LaF_3:Nd^{3+}, Pr^{3+} and LaF_3:Dy^{3+},Pr^{3+} but not in LaF_3:Ho^{3+}, Pr^{3+}. We have found that the emission of $^1D_2$ fluorescence is due to ion-pair relaxation between Pr^{3+} and Nd^{3+} or Dy^{3+}. The absence of $^1D_2$ levels fluorescence in LaF_3:Ho^{3+}, Pr^{3+} is probably due to the absence of overlap between ion-pair transitions of the two ions.

4.1 Radiative energy transfer

4.1.1 General

One of the fluorescence lines of the group $^3P_0 \rightarrow {}^3H_4$ at 4791.5 Å is found to be self-absorbed in the crystal medium itself. When the path traversed by the fluorescence radiation in the crystal medium is negligibly small a single line is observed and as the distance covered in the crystal medium is increased a pronounced double hump is observed in place of a single line (Fig.4.1). This is explained as follows. Consider two atoms A and B of the same kind, one in the excited electronic state , n_2 and the other in the ground state, n_1. When the atom in the excited state comes down to the ground state the difference in energy is emitted in the form of a photon which is in the optical region. If the emitting atom is free, the emitted photon energy is modified by the recoil of the atom. When the fluorescent energy falls on the atom B, the atom B goes from the ground state to an excited state whose energy is equal to the energy of the incident photon modified by the recoil of the atom B. Since the emitting as well as the absorbing atoms are embedded in a solid matrix the recoil energy is negligibly small when compared to the photon energy. Hence this is a kind of resonance radiative

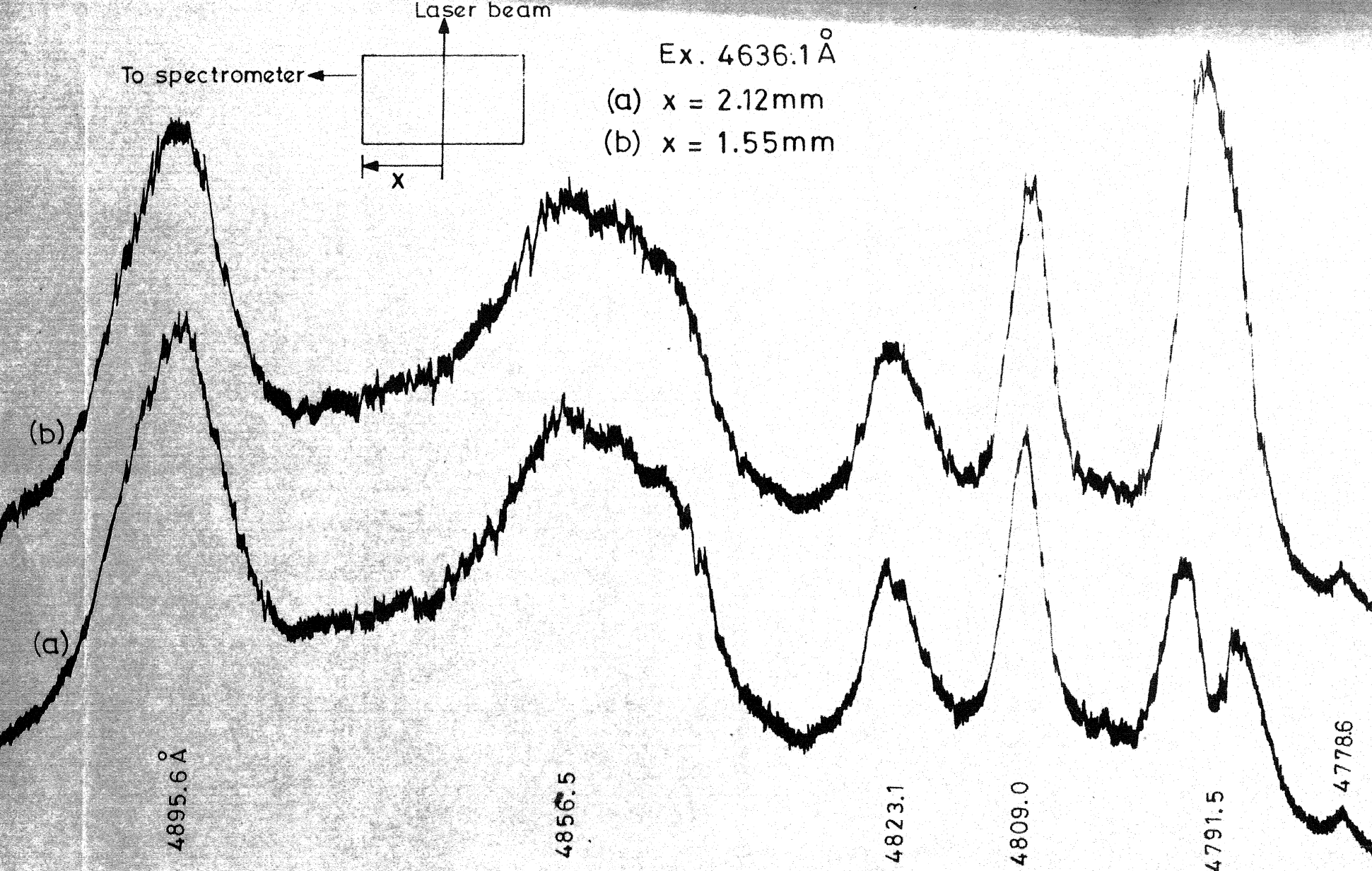


Fig. 4.1 Self-absorption in $LaF_3 : Pr^{3+}$ at LNT (Radiative energy transfer) of 4791.5 Å.

energy transfer between the same two levels.

A mathematical treatment of this phenomenon is available from which oscillator strength of the transition is estimated. This phenomenon was first observed in gases. The double hump nature was termed as self-reversal by spectroscopists to distinguish it from self-absorption. In self-reversal the double hump nature is exhibited where as in self-absorption the line is completely absent. A hypothetical case of self-reversal in gases was described in detail by Bernheim [1]. Self-reversal usually occurs when the lamp is too hot or when there is a high pressure of foreign gas present in the lamp. When the excitation occurs in the central portion of the lamp the resonance light will be absorbed by the unexcited atoms surrounding the excitation region. If the excitation is too hot the resonance lines will be broadened. This phenomenon is serious with Rb, Cs and Hg. A theoretical treatment of this phenomenon was given by Cowan and Dieke [2]. A treatment of this phenomenon in solids was given by Kumar et al [3] which is used to evaluate the f-number (oscillator strength) of the transition 4791.5 Å.

The crystal is irradiated with a laser beam in the $\bar{b}$ direction and fluorescence is collected in the $\bar{a}$ direction. By focussing a telescope on the ab face of the

crystal the path length of the fluorescence streak (to travel before being collected by the monochromator) in the crystal is measured using an OSWA (India) horizontal/ vertical cathetometer whose least count is 0.01 mm.

4.1.2 Oscillator strength (f)

It is often useful to discuss the strength of the transition between two levels in terms of oscillator strength [4] defined as

$$f_{ji} = \frac{2\left|(\Psi_j \mid P_x \mid \Psi_i)\right|^2}{m\hbar w_{ij}}$$

where P_x is the x- component of the dipole moment of the electron. Ψ_j, Ψ_i are the wavefunctions of the two atomic states and $\hbar w_{ji}$ is the difference of their energies.

4.1.3 Evaluation of the f-number

When the fluorescence is excited by a laser beam, only a cylindrical column of the crystal contains emitters and the rest of the crystal contains absorbers. In the figure it is shown that the laser beam is passing through the crystal at a distance, x from one end of the crystal (x being measured along the optic axis of the spectrograph). A one dimensional treatment is given here, since the excitation around the vertical axis is symmetric.

Here x is the positional variable.

The position of the laser beam is taken as the origin (x = 0). Then the intensity of the fluorescence line is given by

$$I_o(\lambda) = A\,\varphi(\lambda) \qquad (1)$$

where A is the amplitude and $\varphi(\lambda)$ is the shape function with the peak at say λ_o. After traversing a distance x through the medium containing absorbers the intensity of the line is given by

$$I_x(\lambda) = A\,\varphi(\lambda)\exp(-\alpha_\lambda x) \qquad (2)$$

The absorption coefficient has the same shape function as the emission line shape and is $\alpha_\lambda = \alpha\,\varphi(\lambda)$, where α is the peak absorption coefficient which depends on the number of absorbers present (concentration) and the transition probability.

Thus $$I_x(\lambda) = A\,\varphi(\lambda)\exp(-\alpha\varphi(\lambda)x) \qquad (3)$$

The positions of extrema are obtained on differentiating the above,

$$\frac{d}{d\lambda} I_x(\lambda) = \frac{d\varphi(\lambda)}{d\lambda}[1-\alpha x\,\varphi(\lambda)]\exp[-\alpha x\,\varphi(\lambda)] = 0 \qquad (4)$$

Since exp [- $\alpha x \varphi(\lambda)$] is not zero, either

$$\frac{d\,\varphi(\lambda)}{d\lambda} = 0 \qquad (5a)$$

or

$$1-\alpha x\, \varphi(\lambda) = 0 \qquad (5b)$$

On differentiating equation (4) once again it is seen that the centre of the line (x=0) is a minimum and on either side of it there are maxima. Since $\varphi(\lambda) \leq 1$, equation 5(b) is satisfied only for $\alpha x > 1$. Also $\varphi(\lambda)$ being symmetric around λ_0, there are two values of λ symmetrically disposed about λ_0 for which this equation is satisfied. A calculation of the second derivative shows that for $\alpha x > 1$, the centre of the line is a minimum and the two maxima are given by 5(b). The line which is absorbed on its way therefore shows double humps. The position and intensities of the humps depend on the exact nature of $\varphi(\lambda)$ but the intensity at the line centre is given by

$$I_x(\lambda_0) = A \exp(-\alpha x) \qquad (6)$$

and is valid for any line shape.

For a Lorentzian line profile

$$\varphi(\lambda) = \frac{1}{1 + a^2(\lambda - \lambda_0)^2} \qquad (7)$$

The hump separation is obtained by substituting the above function in equation 5b giving,

$$1 - \frac{\alpha x}{1 + a^2(\lambda - \lambda_o)^2} = 0$$

That is $$\lambda - \lambda_o = \frac{\pm\sqrt{\alpha x - 1}}{a}$$

The humps are separated by

$$S = 2(\lambda - \lambda_o) = \pm \frac{2}{a}\sqrt{\alpha x - 1} = W\sqrt{\alpha x - 1} \qquad (8)$$

In the above equation $W(= 2/a)$ is the linewidth which is obtained from the plot of S^2 verses x. The intercept on the y-axis is equal to $-w^2$ (for a Gaussian [5] line shape $S^2 = \frac{w^2 \ln \alpha x}{\ln 2}$ and the plot does not give a straight line).

Oscillator strength [6], f is given by the relation

$$Nf = 0.821 \times 10^{17}\ cm^{-3} \frac{n}{(n^2 + 2)^2} \int \alpha(E)\, dE \qquad (9)$$

where N is the number density of the emitting atoms (in units of cm^{-3}), α is the maximum absorption coefficient in cm^{-1} and n is the refractive index of the crystal at the wavelength of the absorbed light. For a line having Lorentzian shape, the integral equals $\frac{\alpha\pi}{a}$ where $\frac{2}{a}$ is the full width at half maximum (FWHM) expressed in eV.

$$Nf = 0.821 \times 10^{17} \frac{n}{(n^2+2)^2} \frac{\alpha\pi}{a} \qquad (10)$$

Equation (10) is valid only if the line width 2/a (=w) is substituted in eV. But the experimentally observed linewidths are in cm^{-1}. To facilitate the substitution of this, equation (10) is divided by the conversion factor 1 eV = 8065.7 cm^{-1}. Therefore equation (10) reduces to

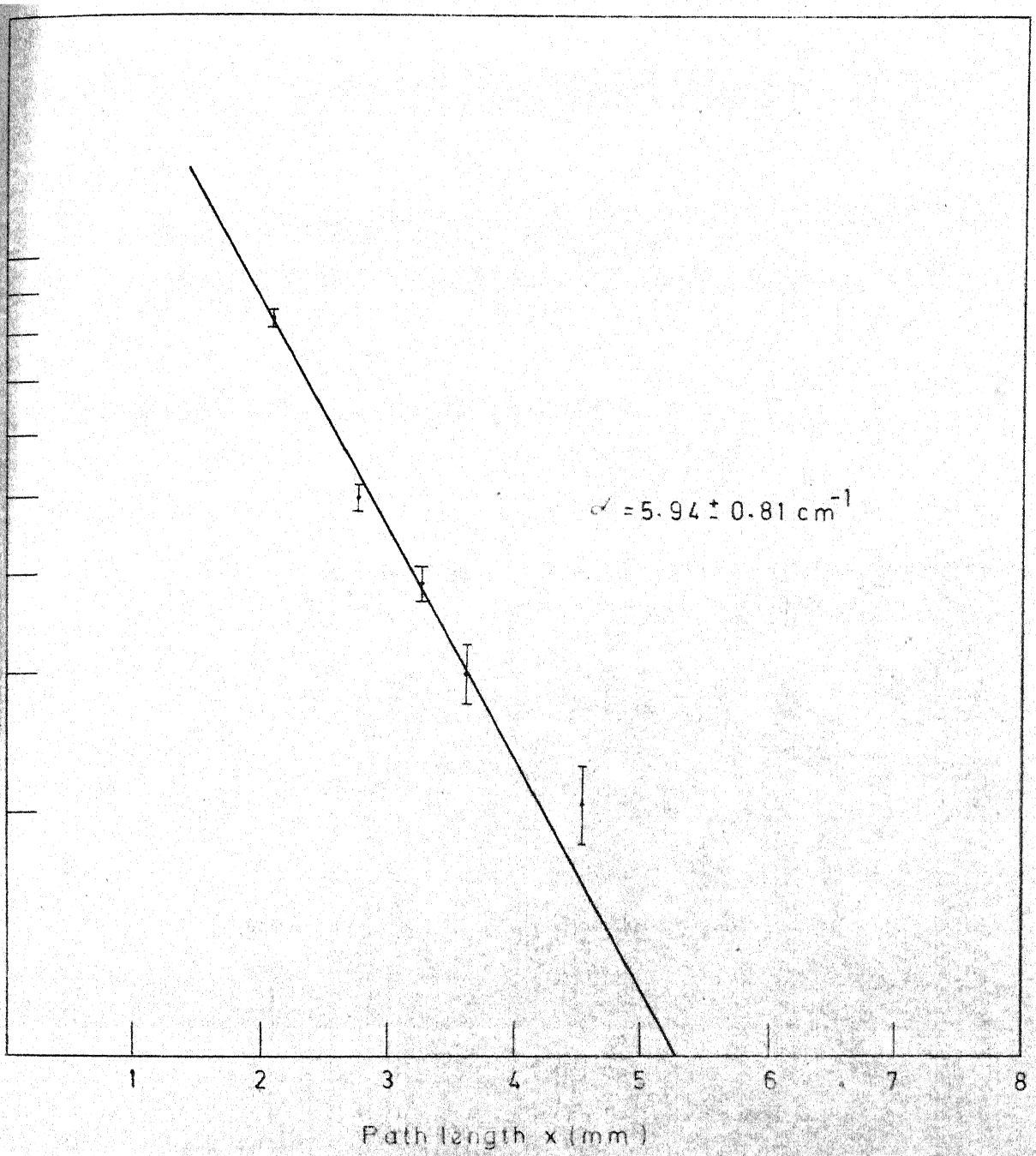
$$Nf = 1.59 \times 10^{13} \frac{n}{(n^2+2)^2} \alpha w \qquad (11)$$

where w is the FWHM expressed in cm^{-1}.

The refractive index [7] of LaF_3 at 4790 Å is 1.60. On substituting this value of n, equation (11) becomes

$$Nf = 1.224 \times 10^{12} \alpha w \qquad (12)$$

α is estimated from equation (6). That is, the intensity of the line centre is measured for different values of X. (X is varied either by moving the crystal for a fixed position of the laser beam or vice versa). In our experiment the position of the crystal is varied which is convenient for us. So the group of fluorescence lines $^3P_0 \rightarrow {}^3H_4$ are recorded for several path lengths and the line centre intensities and hump separations are measured in each case. Since the power output of the laser is not constant all the



ig.4.2 Variation of the line centre intencity of the self reversed line (4791.5 Å) with x at liquid nitrogen temperature.

time, the intensity of the line centre is measured with respect to another line (4809 Å) of the same group in the same run.

A graph is plotted (Fig. 4.2) with logarithmic intensity on the Y-axis and the corresponding path length, x on the X-axis. A straight line is obtained whose gradient is equated to α, and is obtained to be $5.94 \pm 0.8\ cm^{-1}$.

The line width, w is obtained from equation (8). The line width, w is the width of the absorption line. But in fluorescence experiments it is not possible to measure the line widths of the absorption line. So for w, emission line width is substituted. But due to local heating by the laser beam the line width of the emission line may be broadened in relation to absorption line width. If it were the case equation (8) would not be valid. This is checked using the following criterion. Let the absorption line have a width, 2/b different from that of the emission line, 2/a. In this case the intensity of the absorption line is given by

$$I_x(\lambda) = \frac{A}{1 + a^2(\lambda - \lambda_0)^2} \exp\left[\frac{-\alpha x}{1 + b^2(\lambda - \lambda_0)^2}\right] \qquad (13)$$

Proceeding as above [in the derivation of (Eq.8)) in this case, the position of the humps are given by

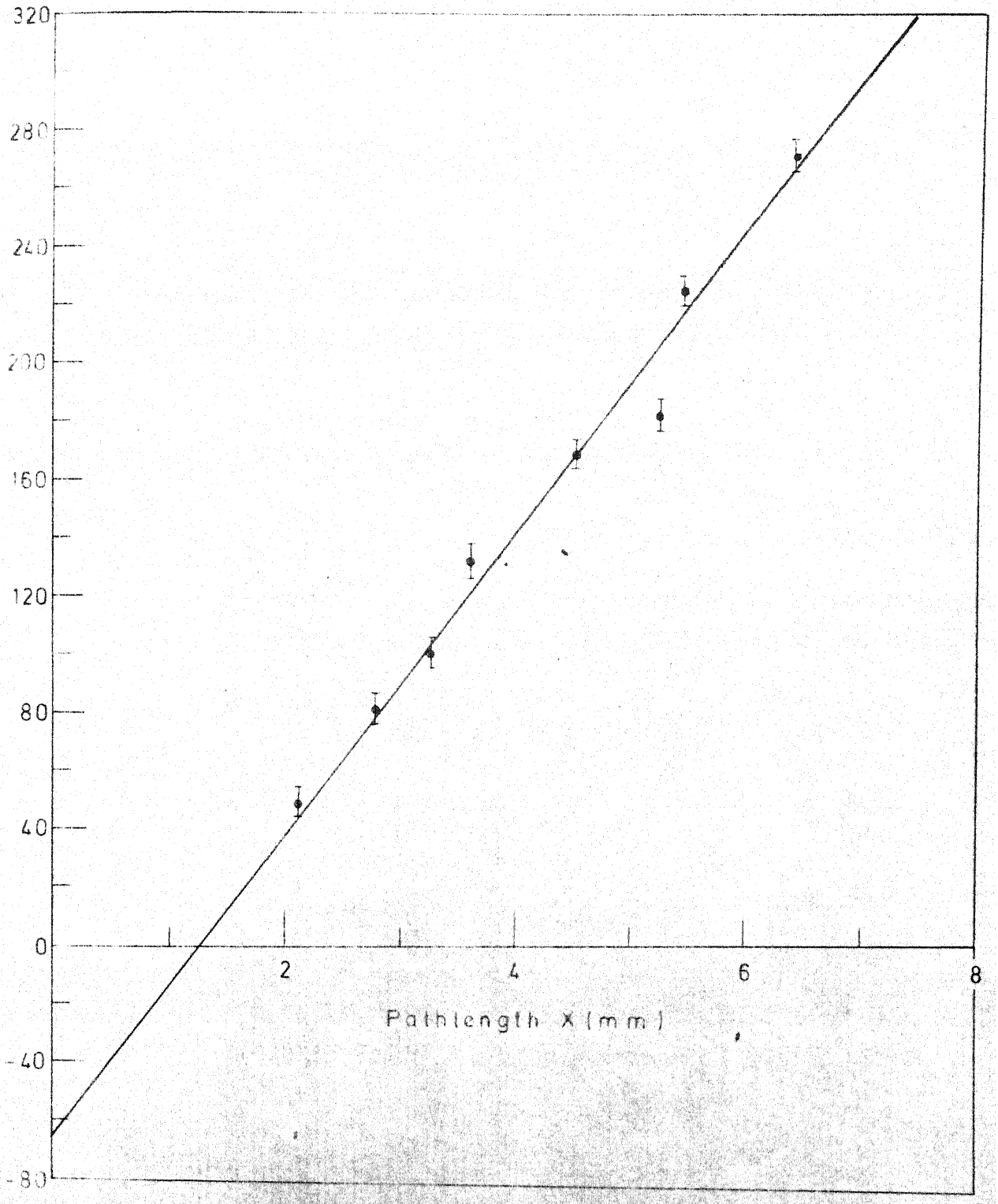


Fig. 4.3 Variation of hump separation $(s)^2$ of the self-reversed line at 4791.5 Å of the $^3P_0 \rightarrow {}^3H_4$ group with x at liquid nitrogen temperature

$$(\lambda - \lambda_o)^2 = \frac{-a(2-\alpha x) \pm \sqrt{a^2\alpha^2x^2 - 4\alpha x(a^2-b^2)}}{2ab^2} \quad (14)$$

A graph is plotted (Fig. 4.3) with S^2(hump separation)^2 on the y-axis and path length on the x-axis. This plot gave a straight line indicating the absence of the effect of nonlinear terms of equation (14). This indicates that equation (8) is valid and no local heating effect is present in the emission line width. From the plot, the intercept on the y-axis, 64 Å^2 is equated with w^2. The line width, w obtained from this plot is 35 ± 2 cm^{-1}. This line width agrees with the FWHM of the line (for x = 0).

The reported unit cell dimensions [8] are a = 7.185 Å and c = 7.350 Å. Volume of the unit cell is 328.6 Å^3. For one percent doping the number density of praseodymium ions is obtained to be 1.825×10^{20} cm^{-3}.

On substituting the above values for α, w and N in equation (12), the oscillator strength, f is obtained to be $(1.40 \pm 0.20) \times 10^{-6}$. This is in good agreement with the value of 0.94×10^{-6} (calculated value 1.04×10^{-6}) obtained by Krupke [9] from absorption measurement at room temperature. The small discrepancy is probably partly because of the error in the Pr^{3+} concentration (1 percent) value used.

4.2 Non-radiative energy transfer

4.2.1 Introduction

Fluorescence spectra of Pr^{3+} in LaF_3 have been recorded at liquid nitrogen and room temperatures. (Tables 9-11 of Chapter 3). The site symmetry of Pr^{3+} in LaF_3 was found to be the lowest symmetry, C_s. Forbidden electric dipole transitions from $^3P_0$ to $^3H_5$ and $^3F_3$ and magnetic dipole transitions for $\Delta J > 2$ have been observed which are probably due to J mixing of wave-functions belonging to $^3P_0$ with $^3P_1$ and $^1I_6$ in crystal field. Fluorescence has been observed from $^3P_1$ and $^1I_6$ to $^3H_{5,6}$ and $^3F_3$ only at room temperature.‡ This indicates a fast relaxation from $^3P_1$ and $^1I_6$ groups of levels to $^3P_0$ level at liquid nitrogen temperature by phonon/multiphonon decay. When $^3P_1$ group of levels was excited no fluorescence was observed from $^1D_2$ Stark multiplet. Fluorescence was observed from $^1D_2$ multiplet only on resonant excitation. This shows that there is no drain mechanism from $^3P_1$, $^1I_6$ and $^3P_0$ levels to $^1D_2$ multiplet in $LaF_3:Pr^{3+}$ crystal. Brown et al[10] observed fluorescence from $^1D_2$ multiplet on the excitation of ^3P levels when there was one of the following additional impurities Ce^{3+}, Eu^{3+}, Tb^{3+} or Yb^{3+}. They explained the drain mechanism

‡ Professor Venkateswarlu observed these fluorescence groups even at liquid nitrogen temperature. He used CW Ar^+ laser for excitation.

to $^1D_2$ levels on the basis of quantum efficiency measurements. They didn't observe any fluorescence from $^1D_2$ multiplet when the additional impurity was Nd^{3+}, Dy^{3+} or Ho^{3+}. The former four ions have one feature in common, namely, the ground states of those ions have the same orbital angular momentum (L=3), that is an F state. So they concluded that the interaction of Pr^{3+} ion with these four ions is through the ground state, therefore dependant on L value of the state (an additional selection rule for interaction mechanism). This is not convincing because (1) the theories developed on ion-ion interaction and energy transfer did not put any such restriction; (2) it is found from the experiments carried out here that there is J mixing of wavefunctions and hence the L value of this fluorescing state is not even uniquely fixed (3) even forbidden transitions are found to be allowed in crystal field (admixture of parity). This shows that interaction mechanism of the Pr^{3+} ion with other ions is not clearly established. Hamilton et al [11] observed decrease in the lifetime of $^3P_0$ state of Pr^{3+} in presence of Nd^{3+} in LaF_3 host. This suggests that further work is needed in this direction. So the crystals of LaF_3:Nd^{3+}(Pr^{3+}), LaF_3:Dy^{3+}(Pr^{3+}) and LaF_3:Ho^{3+}(Pr^{3+})$^{\varphi}$ are chosen for further investigation in this direction. With the advent of intense narrow band laser sources of high excitation densities the study of ion-ion interactions which

$^{\varphi}$ In these crystals Pr^{3+} is present as unintensional dopant.

are very weak in strength have become feasible.

4.2.2 Experimental

The crystals used for this study are (1) $LaF_3:Pr^{3+}$ (1 percent by weight), (2) $LaF_3:Nd^{3+}$ (2 percent by weight), (3) $LaF_3:Dy^{3+}$ (0.5 percent by weight). and (4) $LaF_3:Ho^{3+}$ (0.5 percent by weight). We were trying to record fluorescence from G, F and F multiplets of Nd^{3+}, Dy^{3+} and Ho^{3+} respectively. Then, to our surprise we identified fluorescence groups characteristic of Pr^{3+} ion in addition to the respective impurity fluorescence in all these crystals. This was possible because all these ions have energy levels in the region of our exciting source. The relative positions of the energy levels of the ions, Pr^{3+}, Nd^{3+}, Dy^{3+} and Ho^{3+} in LaF_3 host [12-15] are given in Fig. 4.4. The concentration of Pr^{3+} in crystals (2), (3) and (4) is not known. This Pr^{3+} impurity is present as an unintentional co-dopant in these crystals.

Consider the energy transfer from a sensitizer (or donor) D to an activator (or acceptor) A. The following equation represents energy transfer from an excited donor to a ground acceptor

$$D^* + A \rightarrow D + A^*$$

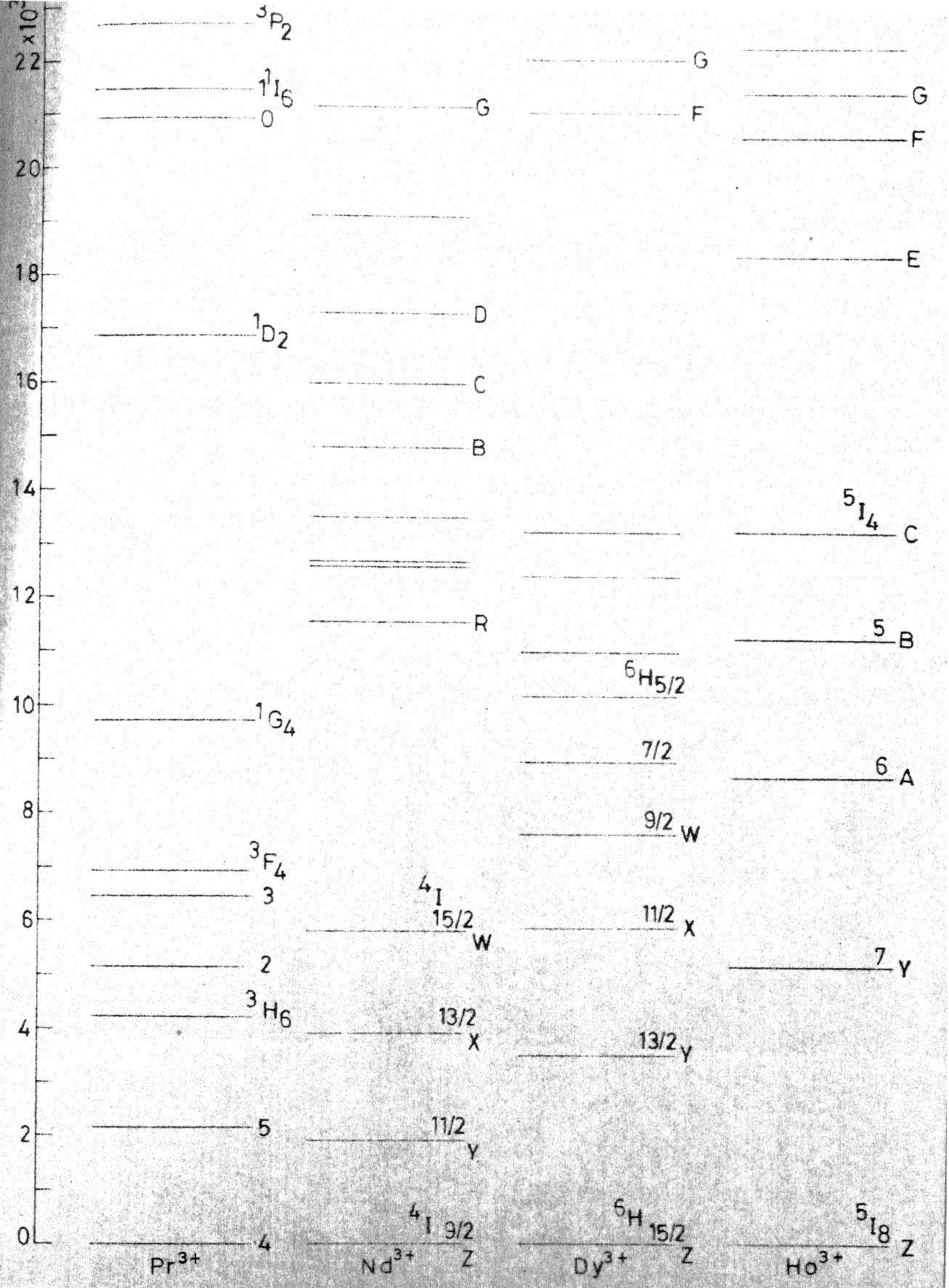


Fig.4.4 Partial energy level diagrams of Pr^{3+}, Nd^{3+}, Dy^{3+} & Ho^{3+} in LaF_3.

where * indicates excited state and ordinary symbol represents ground state of the ion. The efficiency of energy transfer may be determined in the following ways.

(a) Measurement of the emission spectrum and fluorescence quantum yield of the donor (D) and the absorption spectrum of the acceptor (A).

(b) Measurement of the reduction in yield of any process occuring through the excited state D in competition with energy transfer.

(c) Measurement of the effect of energy transfer on the lifetime of the state D.

4.2.3 Results

(a) $LaF_3:Pr^{3+}$

Fluorescence has been recorded using 4636.1 Å laser line as excitation source. At liquid nitrogen temperature fluorescence spectra consists of six groups of lines from $^3P_0$ level to lower multiplets. At room temperature fluorescence is observed from $^3P_1$ ($^1I_6$) to lower levels also. The fluorescence group $^3P_0 \rightarrow {}^3H_6$ is shown in Fig. 4.5. Excitation spectrum of 5985.4 Å line is shown in Fig. 4.6. The excitation spectrum reveals $^3P_0$, $^3P_1$ and $^1I_6$ groups of levels. At liquid nitrogen temperature $^3P_1$ (and $^1I_6$) group of levels relax very

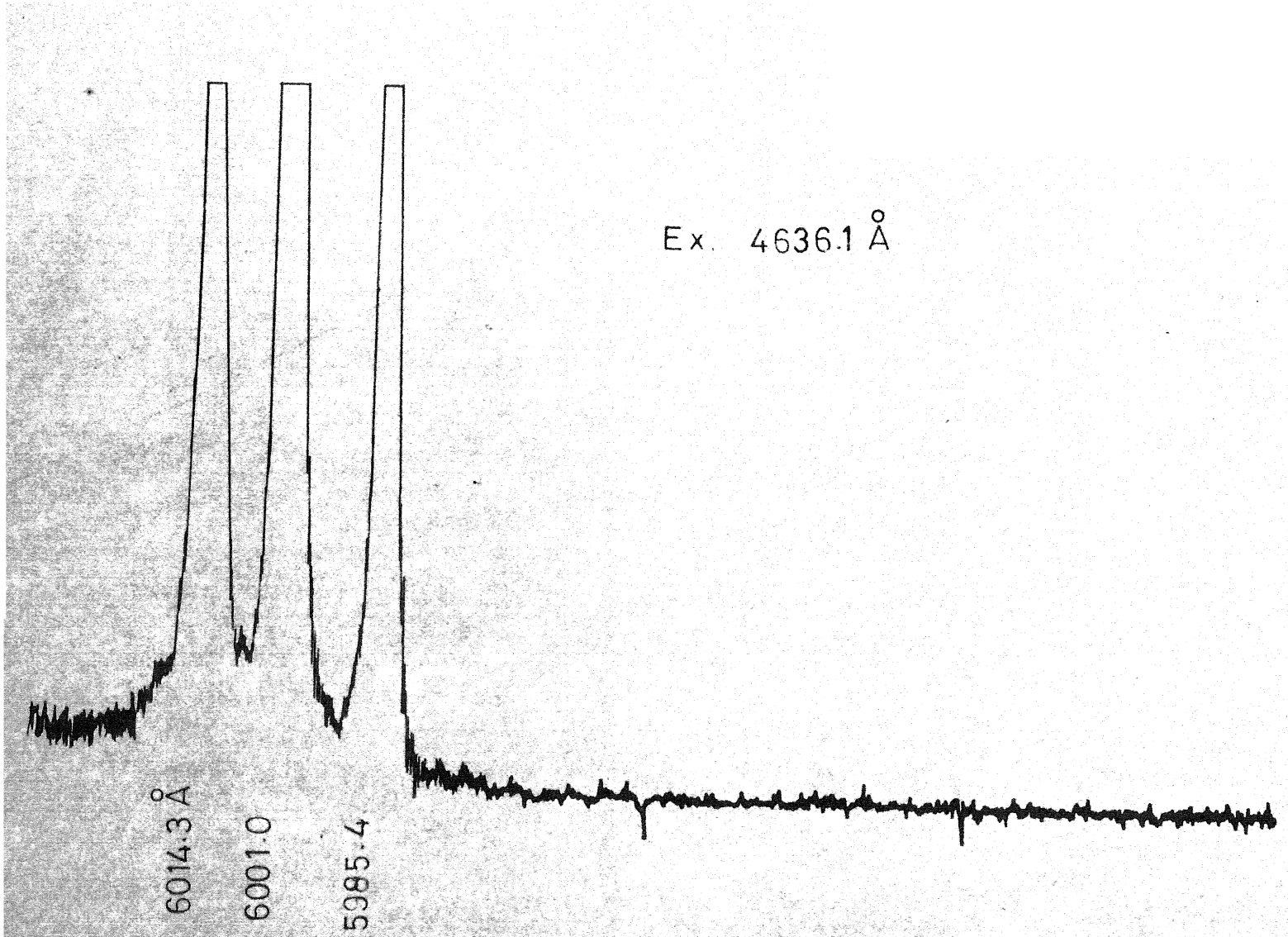


Fig.4.5 Fluorescence spectrum of $LaF_3:Pr^{3+}$ at LNT.

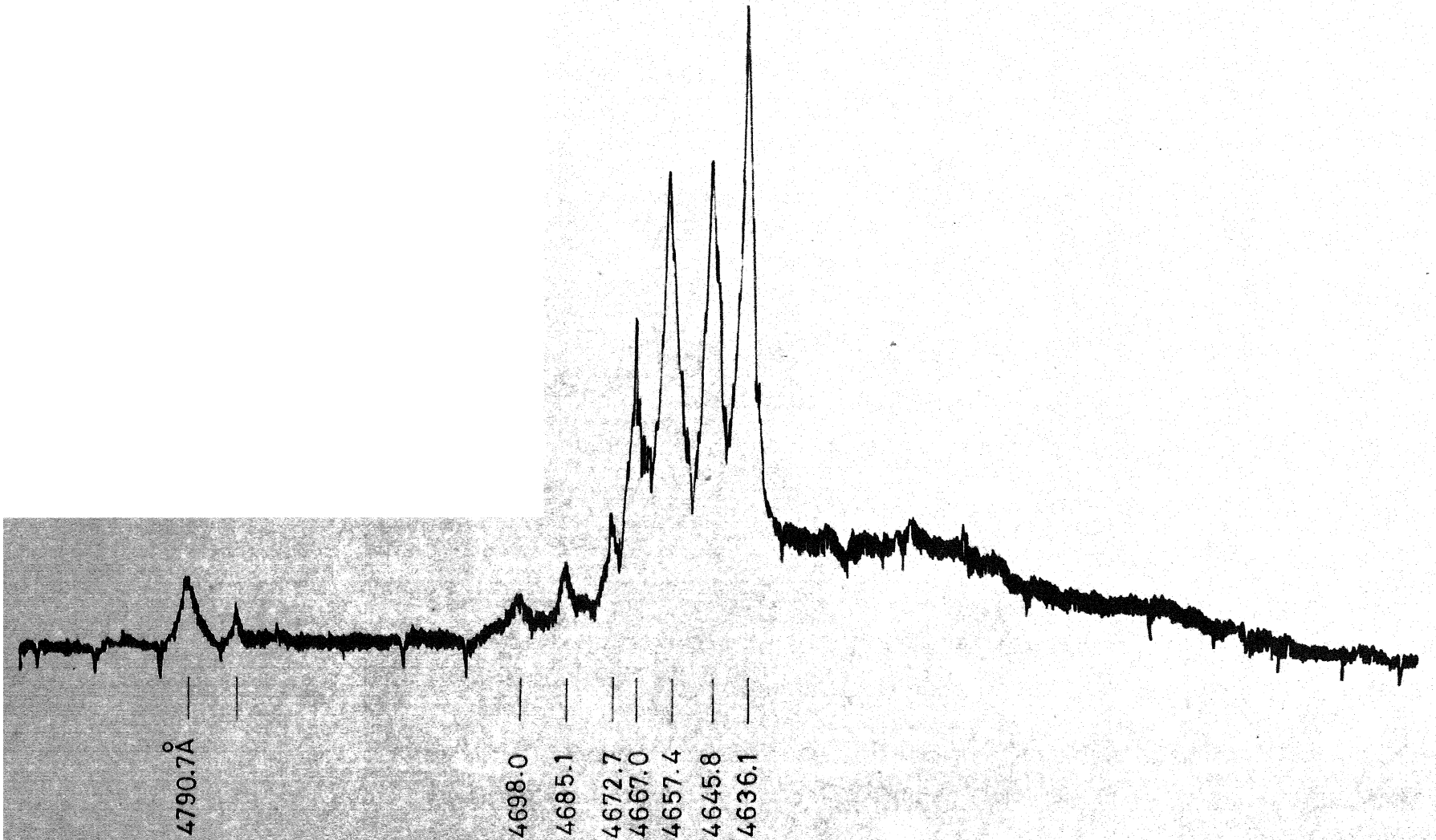


Fig. 4.6 Excitation spectrum of 5985.4 Å transition of $LaF_3:Pr^{3+}$ at LNT

rapidly to $^3P_0$ level. So the excitation spectrum of 5985.4 Å fluorescence line of $^3P_0 \rightarrow {}^3H_6$ contains $^3P_1$ and $^1I_6$ levels also. Lifetime of the $^3P_0$ level is measured using 5985.4 Å transition. The measured value is 50 μsec. for that level at room and liquid nitrogen temperatures. This value is in close agreement with the measured values of $^3P_0$ level lifetime by Barasch and Dieke [16], Brown et al [10] and Zalucha et al [17].

(b) $\underline{LaF_3:Nd^{3+}\ (Impurity\ Pr^{3+})}$

Fluorescence has been recorded using 4636.1 Å laser line as excitation source. At liquid nitrogen temperature fluorescence is observed from $^3P_0$ level to the lower six multiplets and at room temperature fluorescence is observed from $^3P_1$ ($^1I_6$) to lower levels also. In addition, some fluorescence lines originating from $^1D_2$ multiplet and terminating in $^3H_4$ multiplet in the region 5915-5947 Å are observed at both the temperatures. These fluorescence transitions are shown in Fig. 4.7. Excitation spectra of the fluorescence transitions 5946.4 Å ($^1D_2 \rightarrow {}^3H_4$) and 5985.4 Å($^3P_0 \rightarrow {}^3H_6$) have been recorded. The excitation spectra of both the transitions are exactly identical and a typical excitation spectrum is shown in Fig. 4.8. The excitation spectrum of 5946.4 Å(Fig. 4.8) is compared with that

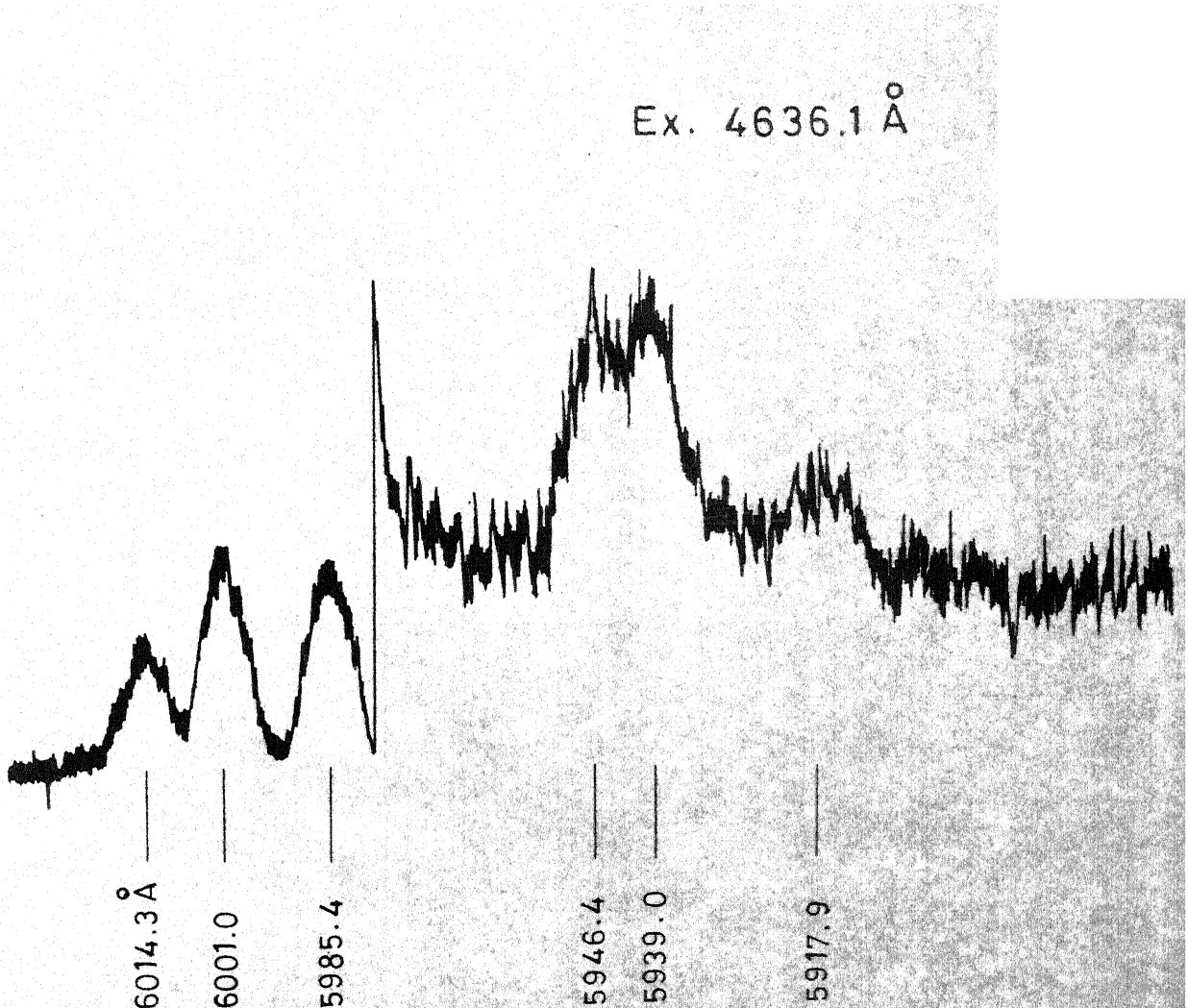


Fig. 4.7 Fluorescence spectrum of $LaF_3:Nd^{3+}$ (IMPURITY Pr^{3+}) at LNT.

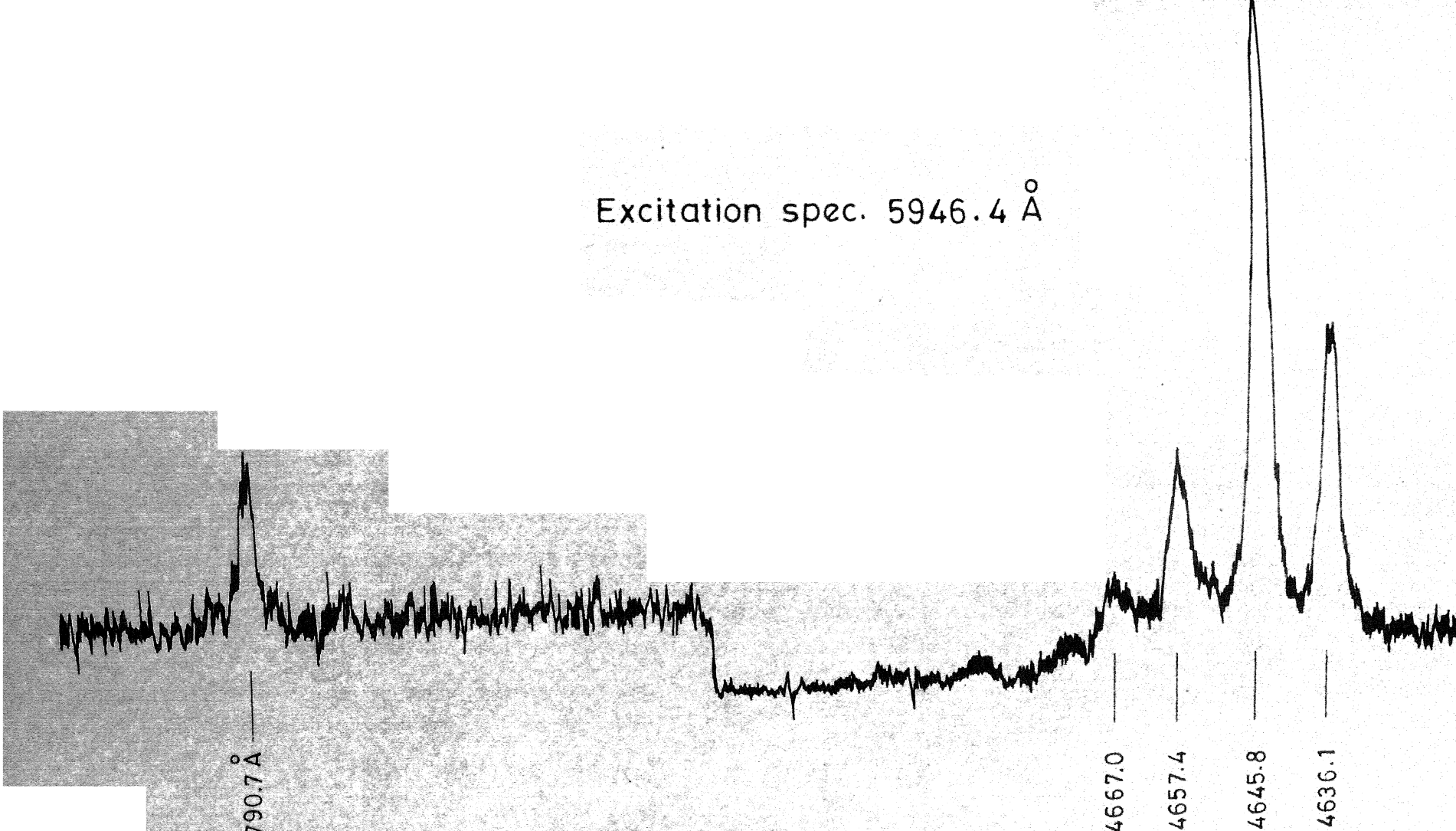


Fig. 4.8 Excitation spectrum of $LaF_3:Nd^{3+}$ (IMPURITY Pr^{3+}) at LNT.

of 5985.4 Å line of the fluorescence observed in $LaF_3:Pr^{3+}$ (Fig. 4.6). Again, the excitation spectra are exactly identical showing only the $^3P_0$ and $^3P_1$ ($^1I_6$) levels of Pr^{3+}. Lifetime of $^3P_0$ level is measured using 5985.4 Å transition. The measured value is 32 μsecs at room and liquid nitrogen temperatures.

(c) $LaF_3:Dy^{3+}$ (Impurity Pr^{3+})

Fluorescence has been recorded using 4636.1 Å laser excitation wavelength. At liquid nitrogen temperature, fluorescence is observed from $^3P_0$ and at room temperature from $^3P_0$ and $^3P_1$ ($^1I_6$) levels. In addition, fluorescence originating from $^1D_2$ multiplet is observed in the region 5915-5947 Å (Fig. 4.9) at LNT and RT. Fluorescence originating from $^4F_{9/2}$ multiplet of Dy^{3+} is also observed (Fig. 4.9). As usual excitation spectra have been recorded of the transitions 5946.4 ($^1D_2 \rightarrow {}^3H_4$), 5985.4 ($^3P_0 \rightarrow {}^3H_6$) of Pr^{3+} and 5695 Å ($^4F_{9/2} \rightarrow {}^6H_{13/2}$) transition of Dy^{3+} and are shown in Fig. 4.10 and Fig. 4.11. The excitation spectrum of 5985.4 Å line is identical with Fig. 4.6, whereas the excitation spectrum of 5946.4 Å transition contains all the levels that are present in the case of 5985.4 Å excitation spectrum and an extra peak at 4540 Å which corresponds to the $^4I_{15/2}$ energy level of Dy^{3+}. The excitation spectrum of 5695 Å transition contains peaks corresponding to the

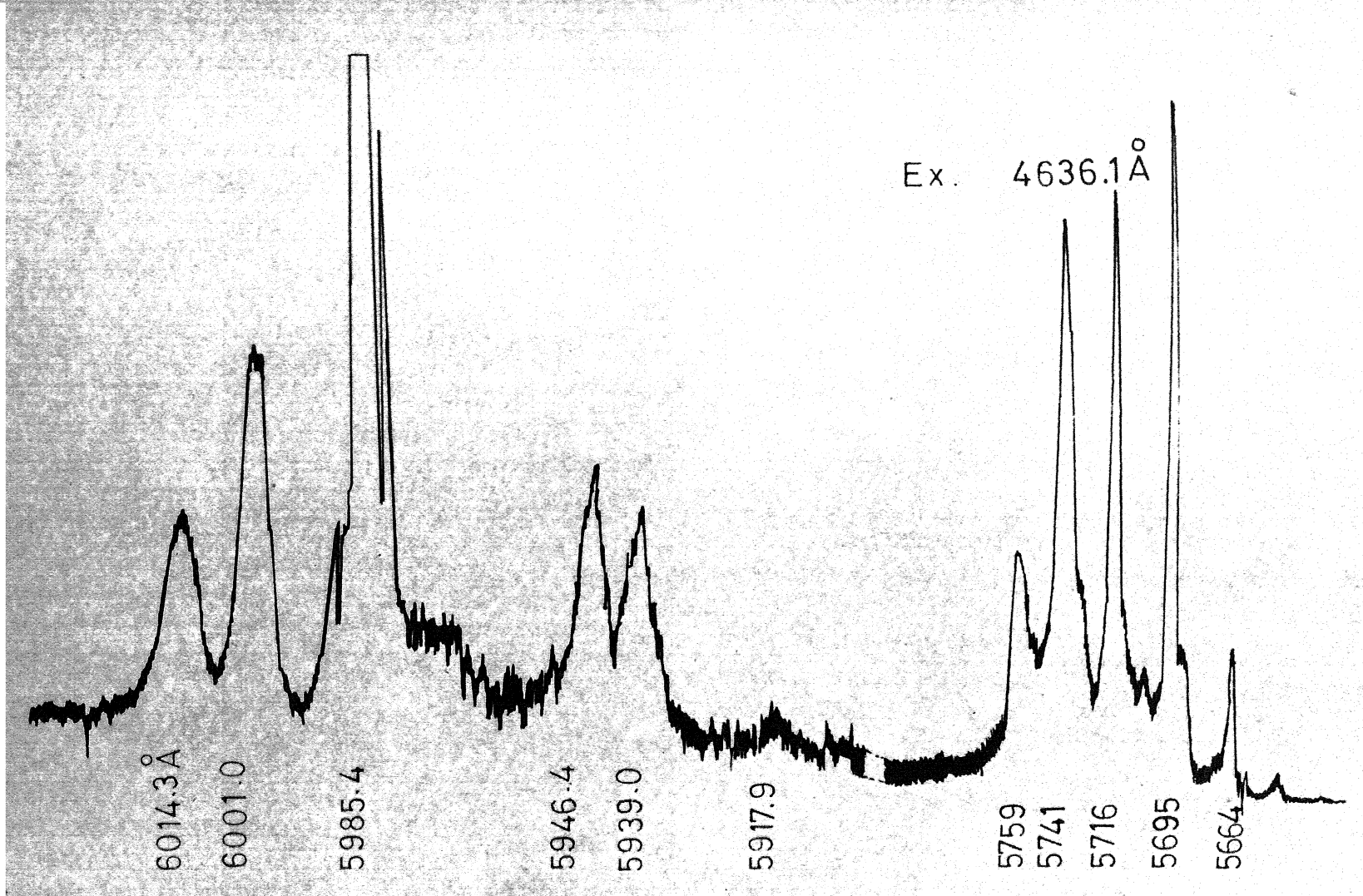


Fig. 4.9 Fluorescence spectrum of $LaF_3 : Dy^{3+}$ (IMPURITY Pr^{3+}) at LNT.

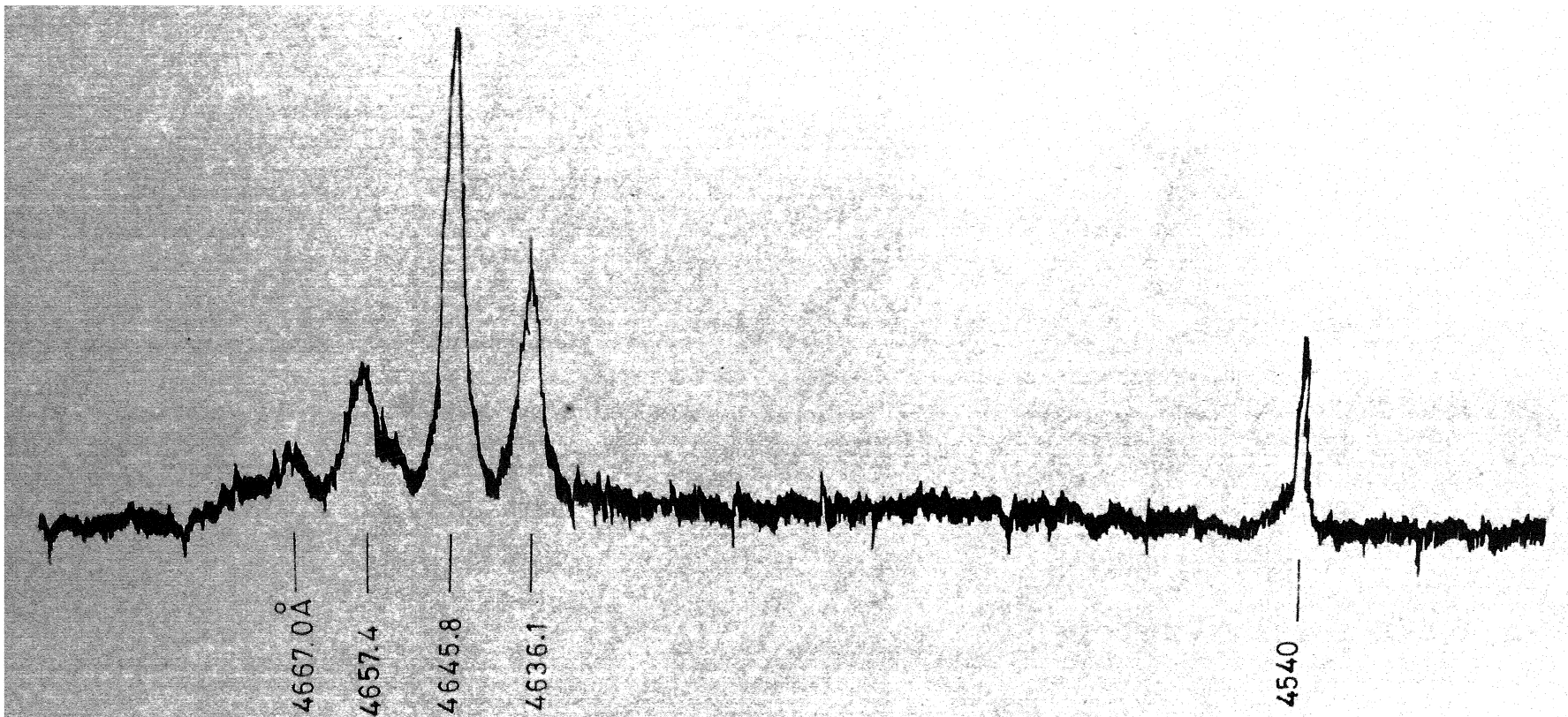


Fig. 4.10 Excitation spectrum of 5946.4Å transition of $LaF_3 : Dy^{3+}$ (IMPURITY Pr^{3+}) at LNT.

energy levels of Dy^{3+} only and there are no levels of Pr^{3+}. Lifetime of $^3P_0$ level of Pr^{3+} is measured using 5985.4 Å which gave a value of 50 μsecs.

(d) $LaF_3:Ho^{3+}$ (Impurity Pr^{3+})

Fluorescence has been recorded using 4636.1 Å laser excitation wavelength. At liquid nitrogen temperature fluorescence is observed from $^3P_0$ level of Pr^{3+}. No fluorescence, characteristic of $^1D_2$ multiplet is observed. In addition fluorescence is observed originating from Ho^{3+} energy levels. Excitation spectrum of 5985.4 Å transition contains only Pr^{3+} energy levels and that of 5492 Å transition contains only Ho^{3+} levels. The measured value for the lifetime of $^3P_0$ is 50 μse in this case also.

4.2.4 Discussion

(i) $LaF_3:Nd^{3+}$

There are many ways in which the $^1D_2$ multiplet can be populated. There can be a drain mechanism from ^3P group of levels to $^1D_2$ Stark multiplet or energy may be transferred from Nd^{3+} ions to $^1D_2$ multiplet of Pr^{3+}. In the case of $LaF_3:Nd^{3+}$ crystal the excitation spectrum of 5946.4 Å line contains only the ^3P group of levels of Pr^{3+}. These clearly indicate that the ^3P group of levels are

responsible for the population of the $^1D_2$ Stark multiplet. There is no energy transfer from Nd^{3+} to Pr^{3+}, because in the excitation spectra of 5946.4 Å and 5985.4Å fluorescence lines, no energy level belonging to Nd^{3+} is present. There are different ways in which the ^3P group of levels can populate the $^1D_2$ multiplet (1) the ^3P group of levels can decay to the $^1D_2$ multiplet by phonon/multiphonon decay (2) ion-pair relaxation among Pr^{3+} ions and between Pr^{3+} and Nd^{3+} ions causing the population of $^1D_2$ levels.

The former mechanism of ^3P levels' decay to $^1D_2$ is improbable on the basis of the following. Non-radiative decay between J multiplets is attributed to phonon emission arising from interactions of the orbital moment of the ion with the fluctuating crystalline field caused by lattice vibrations. The fundamental lattice vibrations (phonons) of LaF_3 as derived from infrared [18] Raman spectra [19] and vibrational side bands [20] only range upto 350-400 cm^{-1}. Therefore decay by single phonon emission is not possible, the minimum energy gap between $^3P_0$ and $^1D_2$ levels being 3721 cm^{-1}. Multiphonon transition rates as a function of energy gap to the lower multiplet in LaF_3 host for Er^{3+} are plotted by Weber [21]. This is shown in Fig.4.12. From the figure it is seen

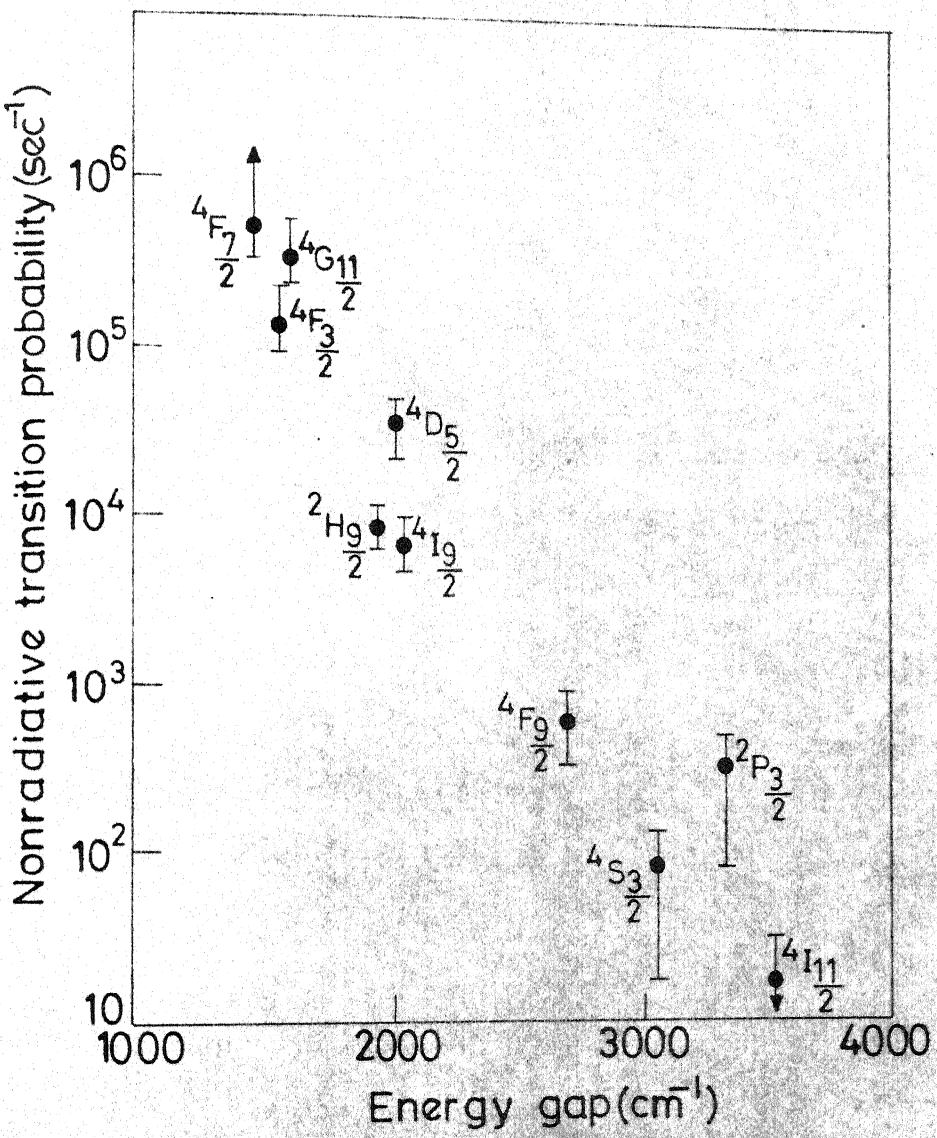


Fig. 4.12 Nonradiative transition probabilities at 77°K for several excited states of Er^{3+} in LaF_3 plotted as a function of energy gap to the next lower multiplet.

(M. J. Weber phys rev. 157, 271 (1967)).

that the transition rate‡ is of the order of 10- 10^2 sec^{-1} for an energy gap of 3700 cm^{-1}. If this were to be the mode of population of $^1D_2$ then the fluorescence intensity would be too weak to be observed. Therefore decay by multiphonon emission is improbable. This is supported by the measured lifetimes of $^3P_0$ level in $LaF_3:Pr^{3+}$ at room and liquid nitrogen temperatures. Spontaneous emission probabilities of Pr^{3+} levels are calculated by Weber [22]. Radiative transition probability from $^3P_0$ to $^1D_2$ levels is also negligibly small. So, this possibility is also ruled out.

The population of $^1D_2$ levels by two photon or sequential two-photon processes is not possible, because the level $^1D_2$ can be reached by a quantum of energy less than a single photon. The only possibility is the ion-pair relaxation [23]. But ion pair relaxation among Pr^{3+} ions to populate $^1D_2$ is improbable because the concentration of Pr^{3+} is very small.φ The only way to populate $^1D_2$ is therefore by ion-pair relaxation between Pr^{3+}

‡ Though the decaying state $^3P_0$ of Pr^{3+} is different from that of Er^{3+}, it would not make significant difference in transition rate. The rates of phonon processes are a function of the modes and the frequencies of vibrations which, inturn, are properties of the host lattice in which the ion is embedded.

φ No $^1D_2$ fluorescence is observed in $LaF_3:Pr^{3+}$(1 percent) on excitation into $^3P_{0,1}$ levels.

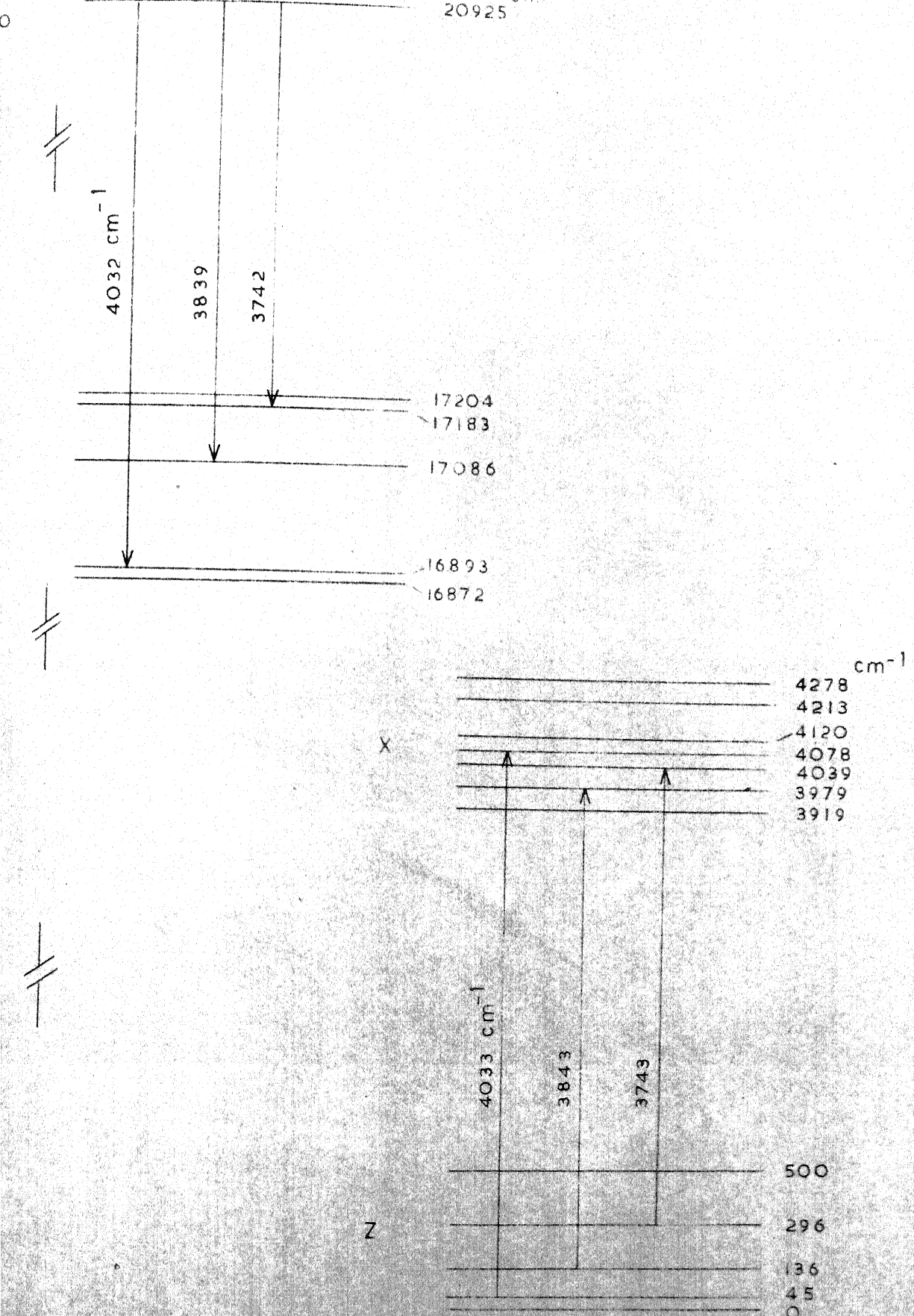
and Nd^{3+} ions. This can be either pure resonant transfer or phonon-assisted resonant transfer. Now, three resonant ion-pair transitions between Pr^{3+} and Nd^{3+} ions in LaF_3 which can be considered are shown in Fig. 4.13. They are,

(1) The down transition from $^3P_0$ (20925 cm^{-1}) to the $^1D_2$ Stark component at 16893 cm^{-1} of Pr^{3+} and the simultaneous companion up transition from the ground level Stark component at 0 cm^{-1} to the excited level Stark component at 4079 cm^{-1} of Nd^{3+}.

(2) The down transition from $^3P_0$ to the $^1D_2$ Stark component at 17086 cm^{-1} of Pr^{3+} and the companion up transition from the ground multiplet Stark component at 136 cm^{-1} to the excited state Stark component at 3979 cm^{-1} of Nd^{3+}.

(3) The down transition from $^3P_0$ to the $^1D_2$ Stark component at 17183 cm^{-1} of Pr^{3+} and the companion up transition from the lower Stark level at 296 cm^{-1} to the excited level Stark component at 4039 cm^{-1} of Nd^{3+}.

Energy transfer can also take place by phonon-assisted resonance. The phonon-assisted transitions together with the resonant transitions are given in Table 4.1. In the table columns 1 to 3 contain respectively the initial



13 Possible ion-pair transitions between energy levels of Pr^3 ($^3P_0 \rightarrow {}^1D_2$) and Nd^3 ($Z \rightarrow X$) in LaF_3

Some Possible Resonant and Non-resonant Ion-pair transitions between Pr^{3+} and Nd^{3+} Ions Doped in LaF_3

Down Transition, $Pr^{3+}(^3P_0 \rightarrow {}^1D_2)$			Up Transition, $Nd^{3+}(Z \rightarrow X)$			Phonon energy (cm^{-1})	Remarks
Initial (cm^{-1})	Final (cm^{-1})	Difference (cm^{-1})	Initial (cm^{-1})	Final (cm^{-1})	Difference (cm^{-1})		
20925	16872	4053	0	4213	4213	- 160	Absorption
20925	16872	4053	0	4278	4278	- 225	Absorption
20925	16872	4053	45	4039	3994	- 59	Absorption
20925	16893	4032	0	4039	4039	7	?
20925	16893	4032	45	4078	4033	-	Resonant
20925	17086	3839	136	3979	3843	4	Resonant
20925	17183	3742	0	3979	3979	- 237	Absorption
20925	17183	3742	45	4039	3994	- 252	Absorption
20925	17183	3742	296	4039	3743	-	Resonant
20925	17204	3721	0	3919	3919	- 198	Absorption
20925	17204	3721	136	3919	3783	- 62	Absorption

and terminal levels of the down transition and the difference in energy. Similarly, columns 4 to 6 contain respectively the initial and final levels of the up transition and the difference in energy. Column 7 contains the phonon involved in the transition and column 8 contains the remarks if any.

The ion-pair relaxation mechanism involved is supported by the measured lifetimes. The lifetime of $^3P_0$ level in $LaF_3:Pr^{3+}$ crystal is 50 μsecs and in $LaF_3:Nd^{3+}$ (Impurity Pr^{3+}) it is 32 μsecs. This decrease in lifetime can be understood in the following way. As the decay proceeds, excited donors having unexcited acceptors in their close neighbourhood tend to become exhausted, since the rate constant, P(R) usually decreases with increasing distance, R. The donors near the acceptors decay very fast exciting the nearby acceptor ions. Therefore, non exponential nature results in the decay curve immediately at short times after excitation resulting in a decrease in lifetime.

(ii) Efficiency of energy transfer

Energy transfer is an additional decay path available to an excited Pr^{3+} ion. The presence of the acceptor, Nd^{3+} does not introduce any structural changes in the crystal. Mathematically, the fluorescence lifetime of the sensitizer, in the presence of activator is given by

$$\frac{1}{\tau} = P_{SA} + \frac{1}{\tau_0}$$

where P_{SA} is the rate of energy transfer and τ_0 is is the intrinsic lifetime. For the $^3P_0$ level of Pr^{3+} in LaF_3 the intrinsic lifetime is 50 μsec (measured value in $LaF_3:Pr^{3+}$(1 percent).+ Its measured lifetime in presence of Nd^{3+} ions (acceptor) is 32 μsec. Therefore, rate of energy transfer is

$$P_{SA} = \frac{1}{\tau} - \frac{1}{\tau_0} = 1.125 \times 10^4/\text{sec.}$$

The efficiency of energy transfer is

$$\eta_T = \frac{P_{SA}}{\frac{1}{\tau_0} + P_{SA}} = 1 - \frac{\tau}{\tau_0} = 0.36$$

(iii) $\underline{LaF_3:Dy^{3+}}$

The excitation spectrum of 5946.4 Å line reveals only $^3P_{0,1}$ levels of Pr^{3+} ion and an extra peak at 4540 Å (22020 cm^{-1}). This peak corresponds to the lowest Stark component of the $^4I_{15/2}$ multiplet of Dy^{3+}. Therefore even in case of $LaF_3:Dy^{3+}$, the energy transfer is from Pr^{3+} to Dy^{3+} as in the case of $LaF_3:Nd^{3+}$. Here, the ion-pair relaxation (or energy transfer) is phonon-assisted and

+ This value is supported by the reported lifetimes for various concentrations of Pr^{3+} in LaF_3 by Brown et al. [10].

Table 4.2

Some Possible Non-resonant (phonon-assisted) Ion-pair Transitions between Pr^{3+} and Dy^{3+} ions Doped in LaF_3

Down Transition, $Pr^{3+}(^3P_0 \rightarrow {}^1D_2)$			Up Transition, $Dy^{3+}(Z \rightarrow Y)$			Phonon energy	Remark
Initial	Final	Difference	Initial	Final	Difference		
20925	16872	4053	0	3695	3695	+ 358	Phonon emission
20925	16893	4032	0	3695	3695	+ 337	Phonon emission
20925	17086	3839	0	3694	3694	+ 144	Phonon emission
20925	17086	3839	17	3695	3678	+ 161	Phonon emission
20925	17183	3742	0	3695	3695	+ 97	Phonon emission
20925	17183	3742	0	3645	3645	+ 97	Phonon emission
20925	17183	3742	17	3645	3628	+ 114	Phonon emission
20925	17204	3721	0	3695	3695	+ 26	Phonon emission
20925	17204	3721	69	3695	3626	+ 95	Phonon emission

the corresponding transitions are given in Table 4.2.‡ The measured lifetime of $^3P_0$ level in this crystal is about 50 μsec. same as the intrinsic lifetime, whereas in $LaF_3:Nd^{3+}$ crystal the lifetime is reduced to 32 μsec. In the latter the acceptor (Nd^{3+}) concentration is 2 percent whereas in the former the acceptor (Dy^{3+}) concentration is only 0.5 percent. Therefore, the donor-acceptor distance is much nearer when the acceptor is Nd^{3+} rather than Dy^{3+}. So, the transfer rate is very efficient when the acceptor is Nd^{3+} and hence appreciable reduction in lifetime could be seen in this case. Therefore it is probable not to see any appreciable reduction in the lifetime of $^3P_0$ level of Pr^{3+} in $LaF_3:Dy^{3+}$ crystal.

The peak at 4540 Å in the excitation spectrum of 5946.4 Å can appear in either of the two ways. (1) There can be Dy^{3+} fluorescence falling in that region (at 5946.4 Å). (2) There can be energy transfer from Dy^{3+} to Pr^{3+}. Fluorescence of Dy^{3+} ion in the region 5946.4 Å is not reported in literature so far. We recorded the Dy^{3+} fluorescence on resonance excitation. We also failed to observe any Dy^{3+} fluorescence at 5946.4 Å. Therefore the former possibility is improbable.

‡ The format of the table is same as in the previous case, except Dy^{3+} ion replacing Nd^{3+} ion in the up transition.

The latter possibility is explained as follows. The excitation spectrum of 5985.4 Å line of Pr^{3+} does not contain any peak characteristic of Dy^{3+}. This implies that there is no energy transfer from Dy^{3+} to ^3P group of levels of Pr^{3+} (or more specifically to $^3P_0$ level). But the presence of a peak at 4540 Å (22020 cm^{-1}) in the excitation spectrum of 5946.4 Å implies that there is energy transfer from Dy^{3+} ion to $^1D_2$ levels of Pr^{3+}. Though the peak corresponding to the lowest component of $^4I_{15/2}$ is present in the excitation spectrum of 5946.4 Å transition, the energy transfer can take place through $^4F_{9/2}$ multiplet. At liquid nitrogen temperature $^4I_{15/2}$ levels relax very fast to $^4F_{9/2}$ levels. The minimum energy gap between the two levels is 800 cm^{-1}. The multiphonon transition rate between them is $\sim 10^6$. Moreover the $^4I_{15/2}$ multiplet is known not to fluoresce [24] at LNT. In the excitation spectrum of 5695 Å fluorescence line of Dy^{3+} ($^4F_{9/2} \rightarrow {}^6H_{13/2}$) the intensity of the peak corresponding to the level 22020 cm^{-1} (of $^4I_{15/2}$) is three times stronger than the most intense excitation peak of the $^4F_{9/2}$ levels. In view of the above points, it is probable for the energy transfer to take place through $^4F_{9/2}$ levels. [But the $^4I_{15/2}$ level appears in the excitation spectrum because it decays to the lower level]. The absence of $^4F_{9/2}$ level in the

Table 4.3

Some Possible Non-resonant Ion-pair Transitions between Dy^{3+} and Pr^{3+} Ions Doped i

Down Transition, Dy^{3+} (F → Y)			Up Transition, Pr^{3+} ($^3H_4 \rightarrow {}^1D_2$)			Phonon energy	Remar
Initial (cm^{-1})	Final (cm^{-1})	Difference (cm^{-1})	Initial (cm^{-1})	Final (cm^{-1})	Difference (cm^{-1})	(cm^{-1})	
21059	3695	17364	0	17183	17183	+ 181	Emiss
21059	3695	17364	0	17086	17086	+ 278	Emiss
21059	3645	17414	0	17204	17204	+ 210	Emiss
21059	3630	17429	0	17204	17204	+ 225	Emissi
21059	3576	17483	0	17204	17204	+ 279	Emissi
21059	3502	17557	0	17204	17204	+ 353	Emissi

excitation spectrum is due to the weaker intensity of the dye in that region. Also, the number of phonons needed in energy transfer from $^4I_{15/2}$ of Nd^{3+} to $^1D_2$ levels of Pr^{3+} are more than those needed from $^4F_{9/2}$ to $^1D_2$ levels. According to Kiel [25] (n+1) phonon process is much weaker than n phonon process. This too supports the above argument. The possible ion-pair transitions are given in Table 4.3. A check of this is made as follows. A series of crystals with concentration of Pr^{3+} ranging from 0.1 to 10 percent for a fixed 1 percent of Dy^{3+} should be chosen and then to measure the lifetimes of Dy^{3+} fluorescing level, $^4F_{9/2}$. A pronounced non-exponential nature in the decay curve of Dy^{3+} level will be noticed with increasing Pr^{3+} concentration if there is energy transfer from $^4F_{9/2}$ level of Dy^{3+} to the $^1D_2$ multiplet of Pr^{3+}.

(iv) $\underline{LaF_3:Ho^{3+}}$

The absence of $^1D_2$ fluorescence in this crystal is justified as follows. The minimum energy gap between $^3P_0$ and $^1D_2$ levels is 3721 cm^{-1} (maximum gap being 4052 cm^{-1}). In Ho^{3+} the ground multiplet extends upto 410 cm^{-1}. The lowest state of the first excited level of Ho^{3+} is at 5192 cm^{-1}. Moreover at liquid nitrogen temperature most of the population is confined to with in 200 cm^{-1}. The energy gap between the down (Pr^{3+}: $^3P_0 \rightarrow {}^1D_2$) and

the up (Ho^{3+}: $^5I_8 \rightarrow {}^5I_7$) transitions is about 1300 cm^{-1}. For ion-pair relaxation to be effective phonons of energy, 1300 cm^{-1} must be supplied by the lattice. Evidently, this would be a third or fourth order process, since the cut-off phonon frequency in LaF_3 is $\sim$ 400 cm^{-1}. It is well known that the higher order process has a very small probability. This explains why no fluorescence is observed from $^1D_2$ levels in this crystal. Energy gap can be reduced by increasing the temperature. But as the temperature increases the net population in any particular level decreases which is another drawback. It may be possible to observe energy transfer (consequently, $^1D_2$ fluorescence) between Pr^{3+} and Ho^{3+} ions if one chooses a LaF_3 crystal, with 1 percent Pr^{3+} and 2 percent Ho^{3+} and at the same time choosing a laser with very high excitation densities and the experiment is performed above liquid nitrogen temperature.

4.2.5 Conclusion

The drain mechanism to $^1D_2$ multiplet of Pr^{3+} is only from $^3P_0$ level, in all the crystals so far observed by us, as well as by Brown et al. The conclusion drawn by Brown et al appears to be wrong on the basis of our observations. The absence of $^1D_2$ fluorescence in LaF_3:Ho^{3+} (impurity Pr^{3+}) is probably due to the large energy

gap between the down and the companion up transitions (lack of resonance). The energy transfer efficiency between Pr^{3+} and Nd^{3+} ions is found to be 36 percent.

REFERENCES

1. R. Bernheim, 'Optical Pumping An Introduction' p.22 Publ. W.A. Benjamin Inc. N.Y. (1965).

2. R.D. Cowan and G.H. Dieke, Rev.Mod. Phys. 20, 418 (1948).

3. U.V. Kumar, D.R. Rao and P. Venkateswarlu, J.Chem. Phys. 67, 3448 (1977).

4. F. Stern, 'Solid State Physics' Vol.15, Ed.F.Seitz and D. Turnbull, pp.375 (Academic Press, N.Y.)

5. U.V. Kumar, Ph.D. Thesis, IIT Kanpur (1975).

6. D.L. Dexter, Phys.Rev. 101, 48 (1956).

7. G. Hass, J.B. Ramsay and R.Thun, J.Opt.Soc.Am. 49, 116 (1959).

8. A. Zalkin, D.H. Templeton and T.E. Hopkins, Inorg.Chem. 5, 1466 (1966).

9. W.F. Krupke, Phys. Rev. 145, 325 (1966).

10. M.R. Brown, J.S.S. Whiting and W.A. Shand, J.Chem. Phys. 43, 1 (1965).

11. D.S. Hamilton, P.M. Selzer, D.L. Huber and W.M. Yen, Phys. Rev. B14, 2183 (1976).

12. W.T. Carnall, P.R. Fields and R. Sarup, J.Chem. Phys. 51, 2587 (1969).

13. U.V. Kumar, H. Jagannath, D.R. Rao and P. Venkateswarlu, Ind. J. Phys. 50, 90-99 (1976).

14. J.L. Fry, H.H. Caspers, H.E. Rast and S.A. Miller, J.Chem.Phys. 48, 2342 (1968).

15. H.H. Caspers, H.E. Rast and J.L. Fry, J.Chem.Phys. 53, 3208 (1970).

16. G.E. Barasch and G.H. Dieke, J. Chem.Phys. 43, 988 (1965).

17. D.J. Zalucha, J.C. Wright and F.K. Fong, J.Chem.Phys. 59, 997 (1973).

18. H.E. Rast, H.H. Caspers and S.A. Miller, Phys. Rev. 171, 1051 (1968).

19. R.P. Bauman and S.P.S. Porto, Phys. Rev. 161, 842 (1967).

20. W.M. Yen, W.C. Scott and A.L. Schawlow, Phys. Rev. 136, A271 (1964).

21. M.J. Weber, Phys. Rev. 157, 262 (1967).

22. M.J. Weber, J. Chem. Phys. 48, 4774 (1968).

23. D.L. Dexter and J.H. Schulman, J. Chem. Phys. 22, 1063 (1954) also Ref. 10.

24. A. Sivaram, Ph.D. thesis, IIT Kanpur (1977).

25. A. Kiel, 'Quantum Electronics', Ed.P. Grivet and N. Bloembergen (Columbia University Press), N.Y. (1964) p. 765.

CHAPTER 5

ENERGY UP-CONVERSION STUDIES

ABSTRACT

When the D levels of Nd^{3+} doped in LaF_3 are resonantly excited fluorescence is observed from R, S, A, D, E, K and L levels. Fluorescence originating from S and A levels is observed only at room temperature, where as that originating from other levels is observed at room and liquid nitrogen temperatures. Decay times have been measured for the R and L level fluorescence at room temperature. The methods of population of the above levels are discussed separately. A rate equation model has been developed which explains the delayed nature of emission from L levels.

5.1 Introduction

The phenomenon of 'Energy Up-conversion' has generated considerable interest among scientists in the recent years. The processes such as Infrared quantum counters(IRQC)[1],Sequential two photon excitation (STEP)[2] and Energy up-conversion(ETU)[3]are important not only from the physics point of view but also have practical relevance. General Electric Co.[4]obtained a visible light source of practical interest by using a GaAs:Si light emitting diode as a pump source. Fong [5]stated that this phenomenon acted as the catalyst for a sequence of deductions that eventually led to a molecular model for the primary process in photosynthesis. These schemes facilitated the detection of infrared[1] signals and the measurement of lifetimes[6]of infrared (low-lying) levels. Estimation of oscillator strengths[7] is possible without the knowledge of dopant concentration. Much work has already been done on up-conversion phenomena[8]. The following observations are helpful in distinguishing the various up-conversion phenomena.

1. The respective energy level positions and their differences.
2. The power law dependance of emission versus sensitizer concentration.

3. The power law dependance of emission versus excitation.

4. Rise and decay times of the emission.

These criteria permit us to distinguish between a single ion and two ion processes, but the experimental results are same whether the two ion process is of the multiple successive transfer type or of the cooperative type.

Barasch and Dieke [9] carried out lifetime measurements of some of the fluorescing energy levels of most of the rare earth ions in different hosts. Asawa and Robinson [10] studied the concentration quenching of R level fluorescence of Nd^{3+} in LaF_3 and $LaCl_3$ hosts. Asawa [11] measured the delayed emission times of R level fluorescence when levels above that are excited in Nd^{3+} doped pure $LaCl_3$ and $LaCl_3$ containing Ce^{3+}. The transitions [12] $R \rightarrow Z$, $R \rightarrow Y$ and $R \rightarrow X$ are known to lase in glass hosts. Energy levels of $LaF_3:Nd^{3+}$ have been established by Caspers et al [13] and by Kumar et al [14] and are given in Table 5.1. Kumar et al [15] studied the fluorescence on excitation into R levels using CW Ar^+ laser. They observed fluorescence from L and K levels also. They found that fluorescence intensity of these groups was proportional to $P^{1.75}$, where P was incident laser power. Jagannath et al [16] measured the decay times of L and K levels using N_2 laser for excitation.

Table 5.1

The Energy Levels of $LaF_3:Nd^{3+}$

SLJ	Stark level designation	Energy (cm^{-1})	SLJ	Stark level designation	Energy (cm^{-1})
$^4I_{9/2}$	Z_1	0	$^4I_{15/2}$	W_1	5817
	Z_2	45		W_2	5876
	Z_3	136		W_3	5989
	Z_4	296		W_4	6142
	Z_5	500		W_5	6173
				W_6	6320
$^4I_{11/2}$	Y_1	1978		W_7	6448
	Y_2	2037		W_8	6551
	Y_3	2068	$^4F_{3/2}$	R_1	11592
	Y_4	2091		R_2	11634
	Y_5	2187			
	Y_6	2223	$^4F_{5/2}$	S_1	12596
				S_2	12613
				S_3	12621
$^4I_{13/2}$	X_1	3919			
	X_2	3979	$^2H_{9/2}$	S_4	12675
	X_3	4039		S_5	12693
	X_4	4078		S_6	12755
	X_5	4120		S_7	(12842)
	X_6	4213		S_8	(12904)
	X_7	4278			

Table 5.1 (contd....)

SLJ	Stark level designation	Energy (cm^{-1})
$^4S_{3/2}; {}^4F_{7/2}$	A_1	13515
$^4F_{7/2}$	A_2	13591
	A_3	13671
	A_4	13677
	A_5	13710
	A_6	13714
$^4F_{9/2}$	B_1	14835
	B_2	14860
	B_3	14891
	B_4	14927
	B_5	14958
$^2H_{11/2}$	C_1	15998
	C_2	16033
	C_3	16045
	C_4	16059
	C_5	16103
$^4G_{5/2}; {}^2G_{7/2}$	D_1	17304
	D_2	17315
	D_3	17364
	D_4	17512
	D_5	17570
	D_6	17601
$^4G_{7/2}$	E_1	19147
	E_2	19235
	E_3	19251
	E_4	19323
$^4G_{9/2}$	F_1	19568
	F_2	19617
	F_3	19651
	F_4	19685
	F_5	19702
	F_6	19739
	F_7	19801
	F_8	19839
$^2K_{15/2}; {}^2G_{9/2}$	G_1	21158
	G_2	21176
	G_3	21201
	G_4	21234
	G_5	21254
	G_6	21302
	G_7	21339
	G_8	21351

Table 5.1 (contd....)

SLJ	Stark level designation	Energy (cm^{-1})	SLJ	Stark level designation	Energy (cm^{-1})
$^2D_{3/2}; {}^4G_{11/2}$	H_1	(21550)		L_7	28929
	H_2	(21634)		L_8	28970
	H_3	(21776)		L_9	29404
	H_4	(21847)		L_{10}	29551
	H_5	(22001)	$^2I_{13/2}, {}^4D_{7/2}$	M_1	30113
$^2P_{1/2}$	I_1	23468	$^2L_{17/2}$	M_2	30203
$^2D_{5/2}$	I_2	23991		M_3	30245
$^2P_{3/2}$	K_1	26364	$^2D_{3/2}$	O_1	33565
	K_2	26404		O_2	33610
				O_3	33642
$^2I_{11/2}; {}^4D_{1/2};$	L_1	28295			
$^4D_{3/2}, {}^4D_{5/2};$	L_2	28340	$^2H_{11/2}, {}^2D_{5/2}$	P_1	34387
$^2L_{15/2}$	L_3	28371	$^2F_{5/2}$	Q_1	39411
	L_4	28525			
	L_5	28544			
	L_6	28823			

In a continuous programme of studying such systems in this laboratory we were interested to see whether there was any energy transfer from Nd^{3+} to Pr^{3+} or vice versa in LaF_3:Nd^{3+} (Impurity Pr^{3+}) crystal. In the course of our experiment we encountered fluorescence originating from R levels of Nd^{3+}. We subsequently resonantly excited the D levels of Nd^{3+} and recorded the fluorescence spectra. We observed the fluorescence spectrum of Nd^{3+} (fluorescence originating from L, K, E, D, A^+, S^+ and R levels), and no characteristic transitions of Pr^{3+} were observed. We were interested to understand the processes by which the L, E, S and R levels were populated. So we chose a series of single crystals of LaF_3 doped with Nd^{3+} (0.1, 0.5, 2.0 and 5.0 percent by weight) as impurity. These crystals were procured from Optovac Inc. All the crystals are of size 8 x 6 x 4 mm^3 except the 2 percent crystal. The original crystal (2 percent by weight of Nd^{3+}) was of size 10 x 7 x 4 mm^3. It was cut into parts. The one which has been used in our measurements is of size 4 x 3 x 2 mm^3. We have also tried to look for up-converted L fluorescence by exciting the B and C groups of levels. We didn't observe any L fluorescence transitions probably due to the weak dye laser output.

+ Fluorescence originating from S and A levels is observed only at room temperature.

Table 5.2

Fluorescence of $LaF_3:Nd^{3+}$

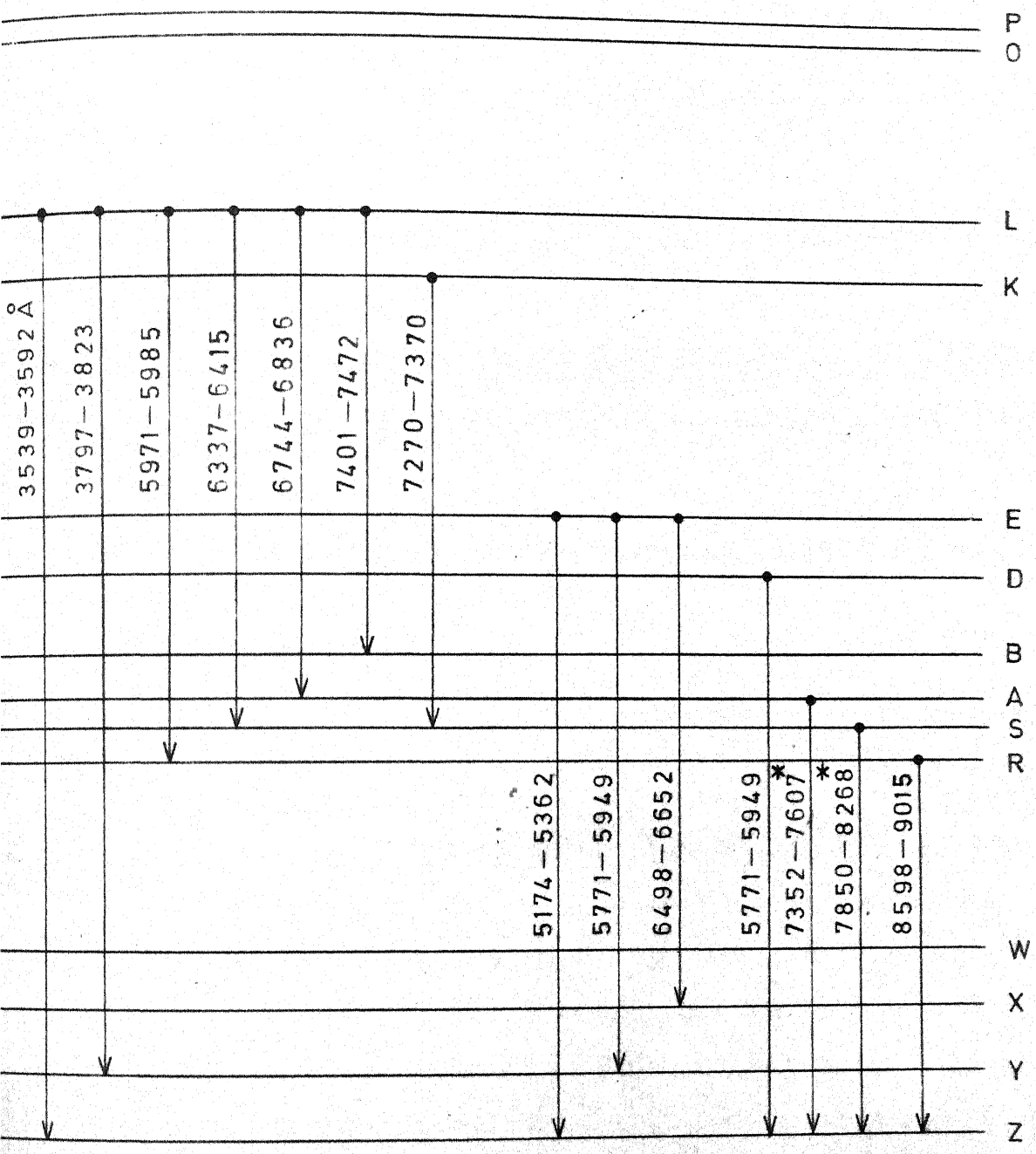
Wavelength (Å)	Wavenumber (cm^{-1})	Transition
3539.3$^{\varphi}$	28246	$L_5 - Z_4$
3592.5$^{\varphi}$	27828	$L_4 - Z_5$+196
3797.9	26324	$L_3 - Y_2$
3801.6	26297	$L_2 - Y_2$
		$L_3 - Y_3$
3818.4	26182	$L_3 - Y_5$
3823.5	26147	$L_2 - Y_5$
		$L_3 - Y_6$
5174.0	19322	$E_4 - Z_1$
5196.6	19238	$E_2 - Z_1$
5208.6	19194	$E_2 - Z_2$
5220.7	19149	$E_1 - Z_1$
5232.2	19107	$E_1 - Z_2$
5259.0	19009	$E_1 - Z_3$
5276.5	18947	$E_2 - Z_4$
5301.6	18857	$E_1 - Z_4$
5335.5	18737	$E_2 - Z_5$
5362.2	18644	$E_1 - Z_5$
5771.8	17321	$D_3 - Z_2$
5791.0	17263	$D_1 - Z_2$
		$E_2 - Y_1$
		$E_4 - Y_3$
5824.2	17165	$D_1 - Z_3$
		$E_3 - Y_4$
		$E_2 - Y_3$
		$E_1 - Y_1$
5843.2	17109	$E_1 - Y_2$
5875.3	17016	$E_2 - Y_6$
		$D_4 - Z_5$
		$D_5 - Z_5$
5894.3	16961	$E_1 - Y_5$
5949.0	16805	$D_1 - Z_5$
5971.8	16741	$L_3 - R_2$
		$L_2 - R_1$
5984.3		
6337.5	15775	$L_3 - S_1$
6348.3	15748	$L_3 - S_2$
		$L_3 - S_3$
		$L_2 - S_1$

Table 5.2 (contd...)

Wavelength (Å)	Wavenumber (cm^{-1})	Transition	Wavelength	Wave-number (cm^{-1})	Transition
6357.0	15726	$L_2 - S_2$	6835.5	14625	$L_2 - A_6$
6377.8	15675	$L_1 - S_3$	6837.4	14621	$L_1 - A_3$
6382.6	15663	$L_2 - S_4$	7269.9	13751	$K_1 - S_2$
6388.1	15650	$L_2 - S_5$	7345.8	13609	$K_1 - S_6$
6414.6	15585	$L_2 - S_6$	7399.0φ	13512	$A_1 - Z_1$
6498.2	15385	$E_3+53 - X_1$	7402.3	13505	$L_2 - B_1$
6519.8	15334	$E_3 - X_1$			$L_3 - B_2$
6544.1	15277	$E_3 - X_2$	7417.9	13477	$L_2 - B_2$
6564.4	15229	$E_1 - X_1$	7422.3φ	13469	$L_3 - B_3$ $A_1 - Z_2$
6590.8	15168	$E_1 - X_2$	7434.7	13447	$L_3 - B_4$
6614.6	15114	$E_2 - X_5$			$L_2 - B_3$
6629.6	15029	$E_1 - X_3+28$	7440.0	13437	$L_1 - B_2$
6652.0	15029	$E_1 - X_5$	7453.6	13413	$L_2 - B_4$
6744.7	14822	$L_2 - A_1$	7471.9	13380	$L_2 - B_5$
6779.1	14747	$L_2 - A_2$	7499.6	13330	$L_2 - B_5+152$
6821.0	14657	$L_3 - A_6$	7534.6	13270	$L_2 - B_5+112$

Wavelength (Å)	Wavenumber (cm^{-1})	Transition	Wavelength (Å)	Wave number (cm^{-1})	Transition
7580.0	13189	$L_2 - B_5 + 193$	8121.7φ	12309	?
7599.5	13155	$L_2 - B_5 + 227$	8214.3φ	12171	$S_4 - Z_5$
7776.1	12856	?	8253.7φ	12112	$S_2 - Z_5$
7850.9φ	12735	$S_7 - Z_2 + 62$	8264.0φ	12097	$S_1 - Z_5$
7879.5φ	12688	$S_5 - Z_1$	8593.8	11633	$R_2 - Z_1$
7886.0φ	12677	$S_4 - Z_1$	8624.8	11591	$R_1 - Z_1$
7905.3φ	12646	$S_5 - Z_2$			$R_2 - Z_2$
7919.6φ	12623	$S_1 + 27 - Z_1$	8656.0	11549	$R_1 - Z_2$
7935.6φ	12598	$S_1 - Z_1$	8696.0	11496	$R_2 - Z_3$
7961.4φ	12557	$S_2 - Z_1 + 56$	8729.0	11453	$R_1 - Z_3$
8013.0φ	12476	$S_2 - Z_3$	8846.0	11301	$R_1 - Z_4$
8026.0φ	12456	$S_1 - Z_3$	8978.0	11135	$R_2 - Z_5$
			9013.0	11092	$R_1 - Z_5$

Lines marked φ are observed only at room temperature.



51 Partial energy level diagram of $LaF_3:Nd^{3+}$ showing the observed fluorescence groups at room and /liquid nitrogen temperatures when D levels are resonantly excited. (* observed only at RT)

5.2 Experimental results and discussion

The observed fluorescence transitions are given in Table 5.2 and the fluorescence groups are shown in Fig.5.1.

1. Fluorescence from D multiplet

The D multiplet of $LaF_3:Nd^{3+}$ is resonantly excited using 5774.7 Å laser line. Resonance fluorescence, D → Z is observed in the region 5771-5949 Å.

2a Fluorescence from R multiplet

When D levels are excited fluorescence is observed from R levels at room and liquid nitrogen temperatures which falls in the region 8598-9015 Å. It is identified to be R→Z transition group and is shown in Fig.5.2. The excitation spectrum of 8656 Å is shown in Fig.5.3. The excitation spectrum shows peaks at 5748.6, 5757.8, 5774.7, 5778.4, 5789.5, 5793.5, 5824.8, 5856.7 and 5928.5 Å which correspond to the transitions from Z levels to D levels and the Stark components are identified in Table 5.3. The R levels can be populated in the following ways. (1) An ion in the D levels may decay to the R levels in cascade manner as D → C → B..... R. (2) An ion in the D levels may directly relax to R levels exciting a nearby ion from the ground Z level to a W level, i.e. $D_{(1)}+Z_{(2)} \rightarrow R_{(1)}+W_{(2)}$. This is an ion-pair energy transfer mechanism.

.2 Fluorescence spectrum of $LaF_3:Nd^{3+}$ at LNT, $R \rightarrow Z$ group.

Fig. 5.3 Excitation spectrum of $LaF_3:Nd^{3+}$ at LNT

Table 5.3

Excitation Transitions of $LaF_3:Nd^{3+}$ at LNT

Wavelength (Å)	Wavenumber (cm^{-1})	Transition
5748.6	17391	$Z_1 - D_3+27$
5757.8	17363	$Z_1 - D_3$
5774.7	17312	$Z_1 - D_2$
5778.4	17301	$Z_1 - D_1$
5789.5	17268	$Z_2 - D_2$
5793.5	17256	$Z_2 - D_1$
5824.8	17163	$Z_3 - D_1$
5856.7	17070	$Z_4 - D_3$
5928.5	16863	$Z_5 - D_3$

Table 5.4

Decay Times of R and S Levels Measured at room Temperature

Concentration of Nd^{3+} percent by-weight	Decay times R level (μs)	S level (μs)
0.5	600 ± 30	600 ± 60
2.0	400 ± 20	400 ± 40
5.0	150 ± 8	150 ± 15

Table 5.5

Some Possible Ion-pair Transitions between Energy Levels of $LaF_3:Nd^{3+}$ (D-R; Z-W)

Down Transition (D - R)	Up Transition (Z - W)	Remark (phonon assisted)
17315 - 11634	136 - 5817	Resonant
17364 - 11592	45 - 5817	Resonant
17304 - 11592	105 - 5817	105 cm^{-1}
17304 - 11634	147 - 5817	147 cm^{-1}
17315 - 11592	153 - 5876	153 cm^{-1}
17520 - 11592	61 - 5989	61 cm^{-1}
17520 - 11634	103 - 5989	103 cm^{-1}

(3) The excited ion from the D levels may relax to W levels at the same time exciting the nearby ion from Z levels to R level i.e. $D_{(1)}+Z_{(2)} \rightarrow W_{(1)}+R_{(2)}$.[φ]

(4) The last way is by the interaction between two ions in W levels i.e. $W + W \rightarrow R + Z$.

Only decay time measurements will indicate which of the mechnnisms is important. The measured lifetimes at room temperature fall in the region 600-150 μsecs (Table 5.4) for the concentrations 0.5, 2.0 and 5.0 percent Nd^{3+} employed and agree well with the values (with in the experimental errors) measured by Asawa and Robinson [10]. The slight decrease in decay times from those of Asawa and Robinson can be due to the up conversion mechanism [see L level fluorescence] that is taking place simultaneously in the system. We didn't observe significant delay (or rise) times for the R level fluorescence.

From the decay time measurements, the first and last modes of drain mechanisms can be easily ruled out becau e these processes show significant rise time. The fact that the measured decay times are of the order of the values obtained on resonant excitation case suggests that the second possibility is the dominant mode of decay. Two possible resonant ion-pair transitions for the population of R levels are shown in Fig.5.4. The phonon-assisted

φ The subscript indicate the ion.

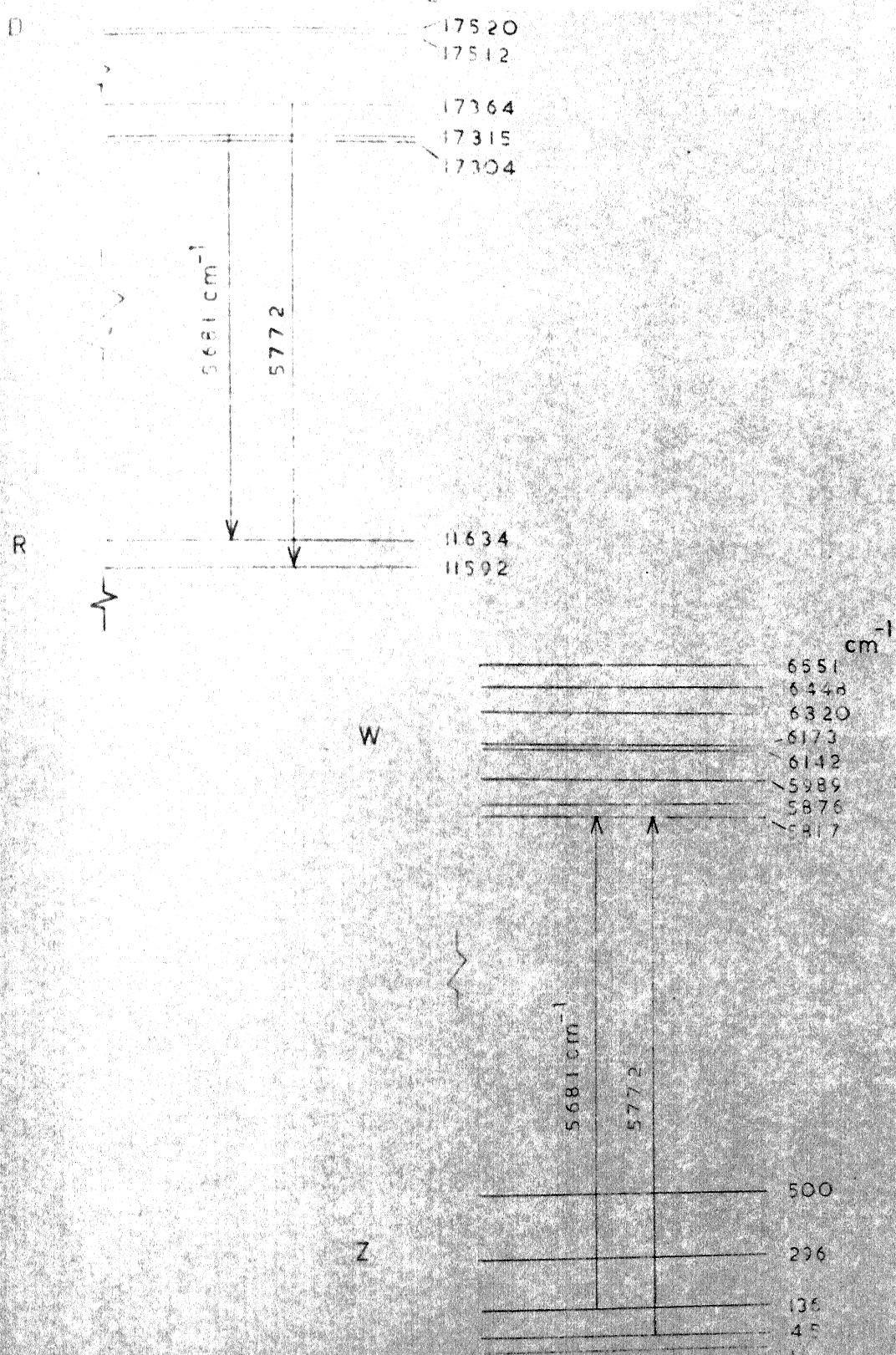


Fig. 5.4 Possible ion-pair transitions between the energy levels of $LaF_3:Nd^{3+}$ (D → R ; Z → W)

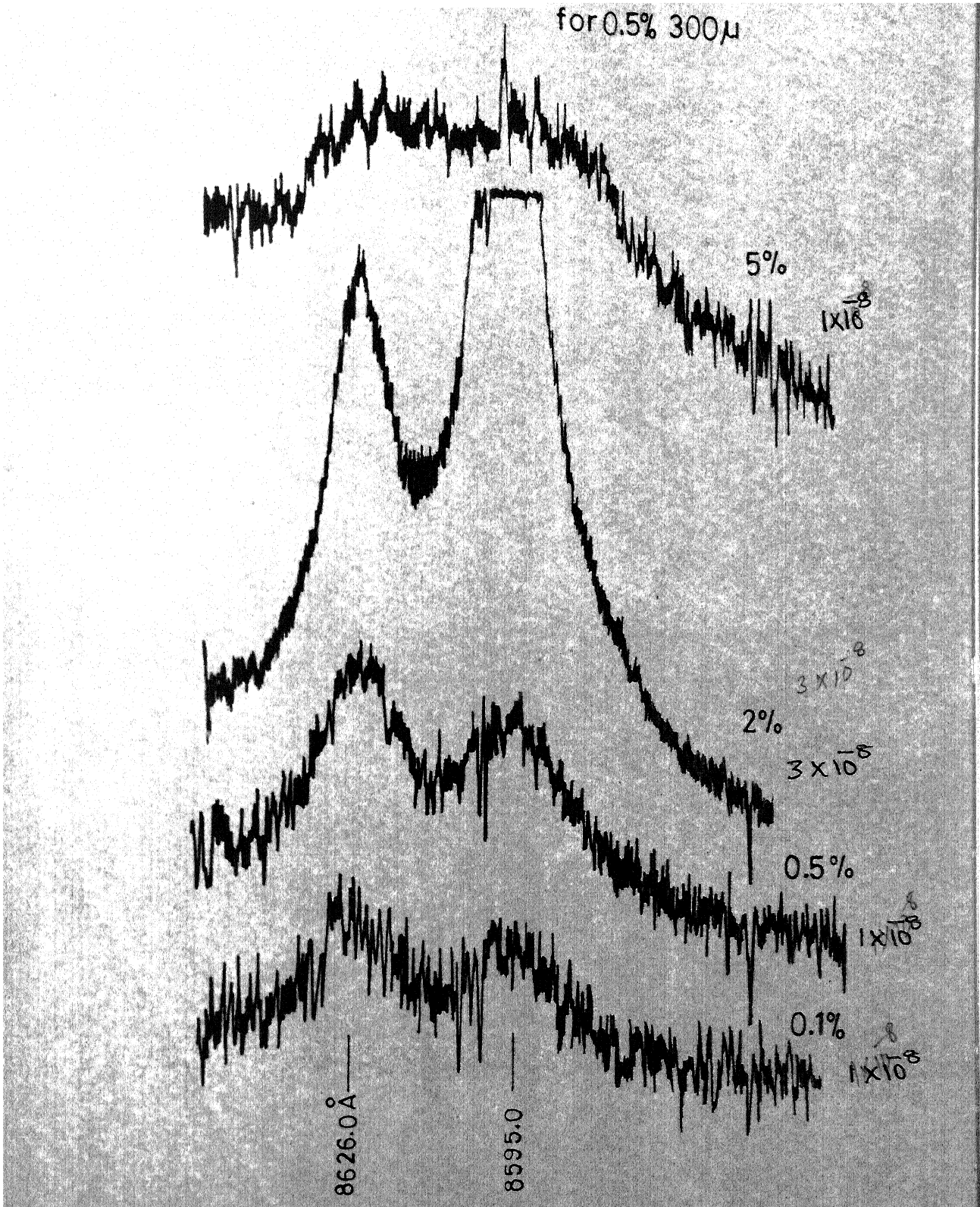
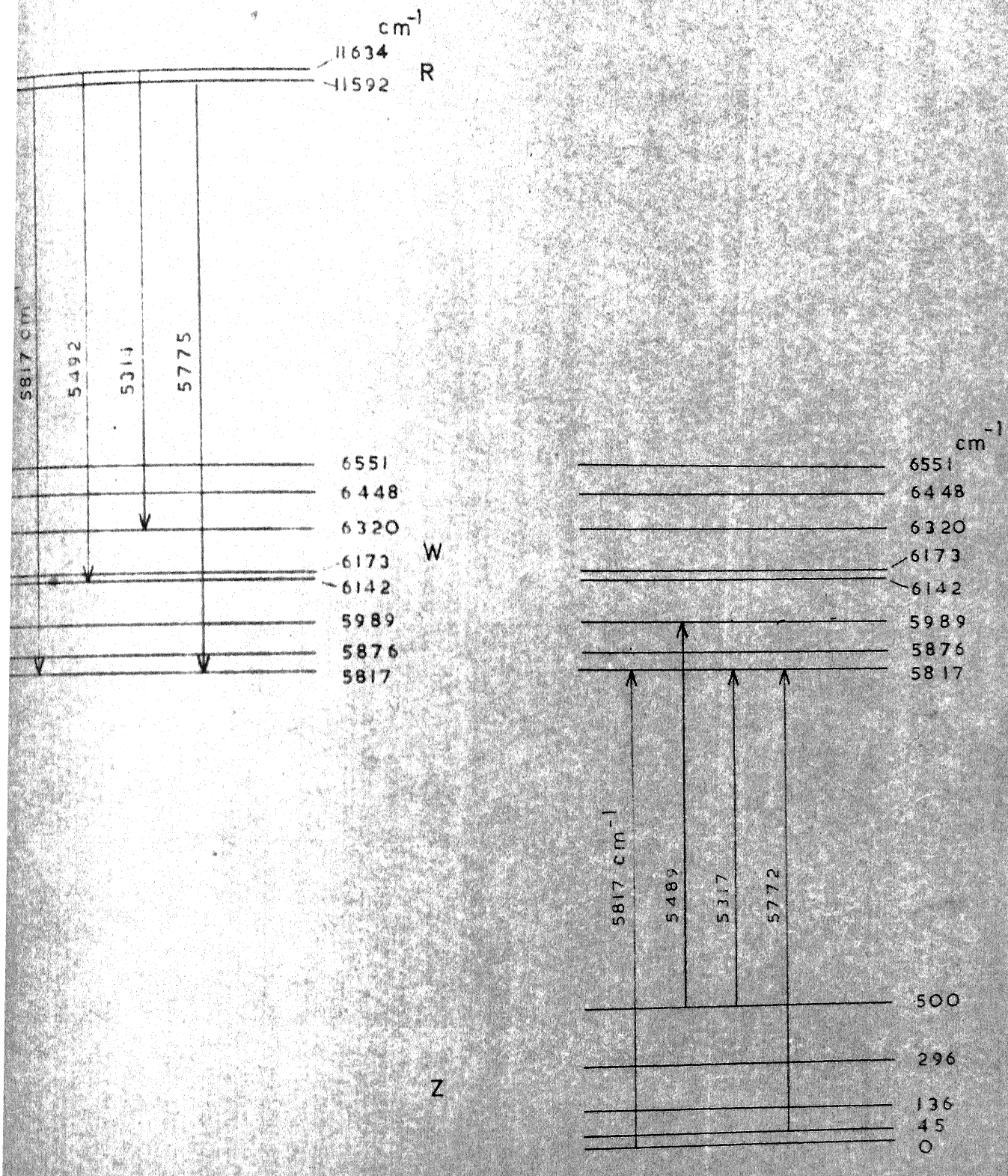


Fig.5.5 Fluorescence spectrum of $LaF_3:Nd^{3+}$ for four different concentrations at room temperature, R→Z group. (concentrations are by weight of NdF_3).



5.6 Possible ion-pair transitions between the energy levels of $LaF_3:Nd^{3+}$ (R → W ; Z → W).

Table 5.6

Possible Ion-pair Transitions between Energy Levels of $LaF_3:Nd^{3+}$ (R-W; Z-W)

Down Transition (R - W)	Up Transition (Z - W)	Phonon assisted (cm^{-1})
11592 - 5817	45 - 5817	3 (Resonant)
11634 - 5817	0 - 5817	- (Resonant)
11634 - 6142	500 - 5989	3 (Resonant)
11634 - 6320	500 - 5817	3 (Resonant)
11592 - 5876	101 - 5817	101
11592 - 5989	136+78 - 5817	78
11592 - 6142	367 - 5817	367
11634 - 5876	59 - 5817	59
11634 - 6142	296+28 - 5817	29
11634 - 6173	296+60 - 5817	60

The possible resonant ion-pair transitions are shown in Fig.5.6. The phonon-assisted ion-pair transitions along with the resonant transitions are given in Table 5.6. From Fig.5.5 it is seen that the intensity is maximum for 2 percent of Nd^{3+}. At higher concentrations the intensity is smaller because of concentration quenching of R level fluorescence. At lower concentrations, it is because of (1) the longer ion-ion distance, consequently weaker ion-ion interaction and hence lower population of R level [since D + Z = R + W] and (2) to a small extent due to the lower number of Nd^{3+} ions.

3. Fluorescence from S multiplet (Room temperature)

The D levels of Nd^{3+} in LaF_3 are resonantly excited using 5772 Å laser line. Only at room temperature fluorescence is observed from S to Z in the region 7850-8268 Å and is shown in Fig.5.7. The excitation spectrum of 7905.3 Å is shown in Fig.5.8 and the transitions from lower levels to upper levels are identified (Table 5.7). The fact that the fluorescence is observed only at room temperature (and not at liquid nitrogen temperature), suggests two ways for the population of S levels. (1) At room temperature the S levels can be populated thermally from R levels (Boltzman distribution). A simple estimation shows that the population of S levels increases by a few orders at room

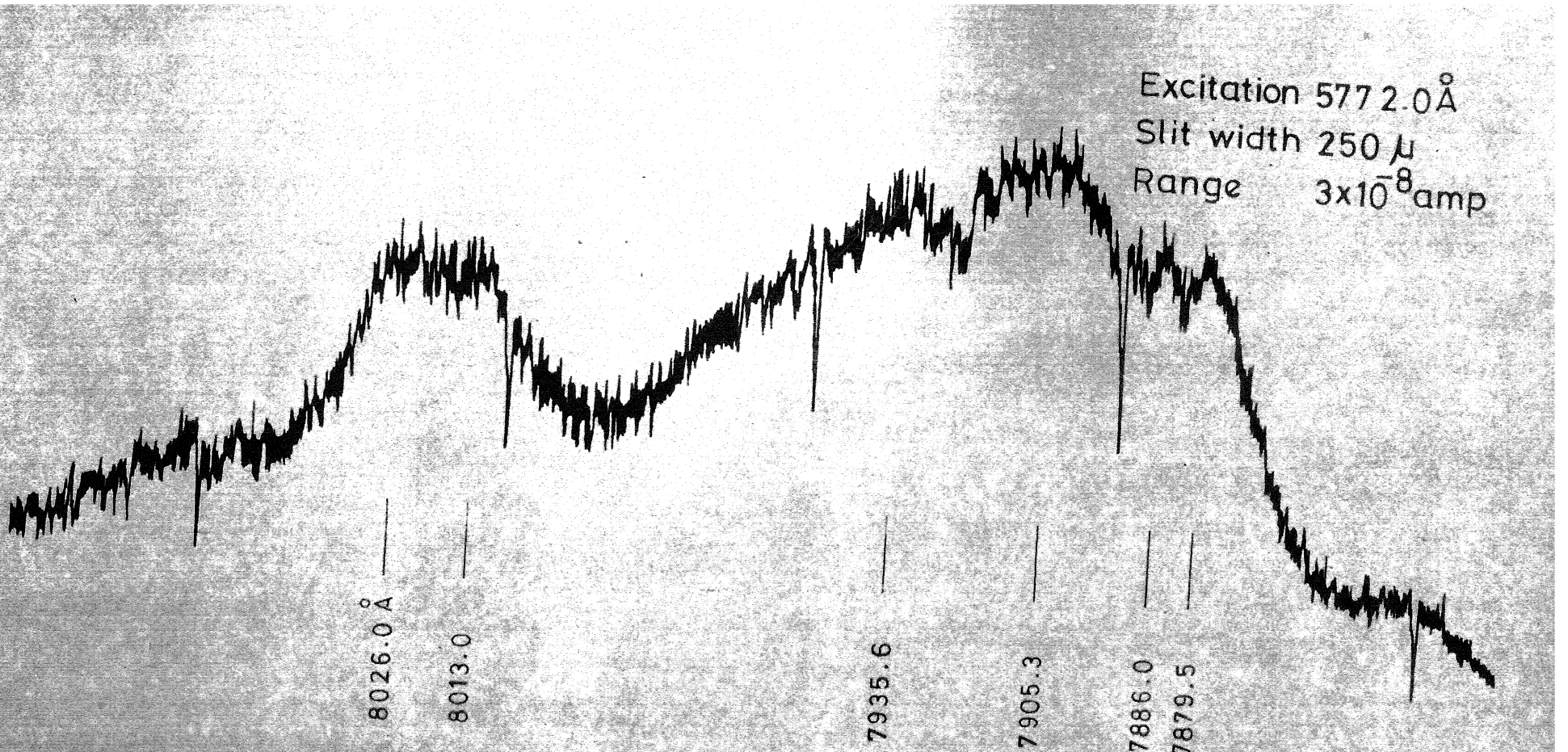


Fig. 5.7 Fluorescence spectrum of $LaF_3: Nd^{3+}$ observed only at room temperature, S ⟶ Z group.

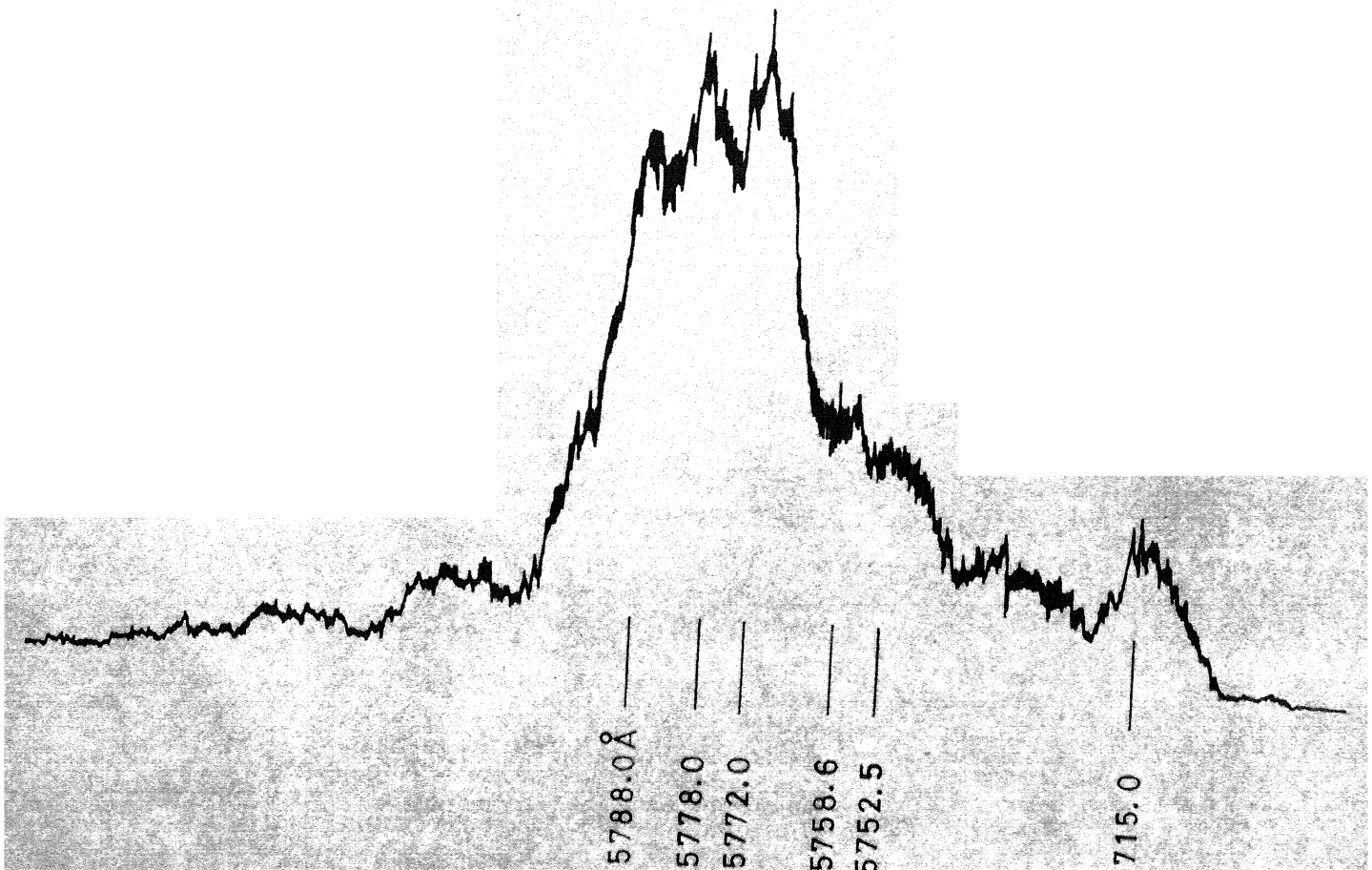


Fig. 5.8 Excitation spectrum of 7905.3 Å (S → Z) at RT showing transitions from Z to D levels.

Table 5.7

Excitation Transitions of $LaF_3:Nd^{3+}$ at RT

Wavelength (Å)	Wavenumber (cm^{-1})	Transition Z - D
5715.0	17493	Z_1+ 27 - D_5
5752.5	17379	Z_3 - D_4
5758.6	17361	Z_1 - D_3
5772.0	17320	Z_2 - D_3
5778.0	17302	Z_1 - D_1
5788.0	17272	Z_2 - D_2

temperature than that at liquid nitrogen temperature. (2) We have already suggested while discussing R level fluorescence that an ion from D level can come down to R level exciting the nearby ion to W level. So two nearby ions in W levels can undergo energy transfer interaction leaving one ion in higher S level and the other in the ground level. i.e. $W^{\varphi} + W^{\varphi} \rightarrow S + Z$, where φ indicates the higher levels of W multiplet. The second mechanism is not possible at liquid nitrogen temperature because of energy level restrictions. At liquid nitrogen temperature the ion immediately relaxes to the lowest level of W multiplet (stokes shift). Therefore, even if two ions in W levels undergo energy transfer interaction only R levels can be populated.

There are two ways to distinguish the above possibilities. (1) To measure the S level decay times for different concentrations of Nd^{3+} ion and (2) to find the relation between fluorescence intensity and excitation flux density.

The measured decay times are given in Table 5.4. It is observed that the measured decay times are identical for R and S levels. This means so long as R level population exists, so does the S level population. This observation strongly suggests that the population of S levels is only due to thermal contribution from that of R levels.

4. Energy up-converted fluorescence from E multiplet

When the D multiplet of Nd^{3+} in LaF_3 is resonantly excited, fluorescence is observed from E levels at room and liquid nitrogen temperatures. The room temperature fluorescence is very week and buried under noise. Three fluorescence groups of lines, E → Z, E → Y and E → X falling respectively in the regions 5174-5362 Å 5771-5949 Å and 6498-6652 Å are observed. E → Z and E → X groups are shown in Figs.5.9 and 5.10. The fact that the intensity of the fluorescence groups E → X, Y, Z is much weaker at room temperature than at liquid nitrogen temperature suggests that the population of E levels by the process of multiphonon/thermalization is ruled out. The fluorescence groups E → Y and D → Z are found to be superimposed. The excitation spectrum of 5232.2 Å is shown in Fig.5.11. The excitation spectrum contains five peaks at 5757.8, 5774.7, 5778.4, 5789.5 and 5793.5 Å which correspond to transitions from Z_1 and Z_2 to D_1, D_2 and D_3 levels. The excitation spectrum indicates that the D levels are responsible for the population of E levels and is discussed below. A direct two photon excitation is not possible because of E energy level restrictions. There are two possibilities by which E levels can be populated. (1) The ion in the excited D level immediately relaxes to the lower Y level, which is further excited to E level by

Fig. 5.9 Fluorescence spectrum of LaF_3 : Nd^{3+} at LNT, E → Z group

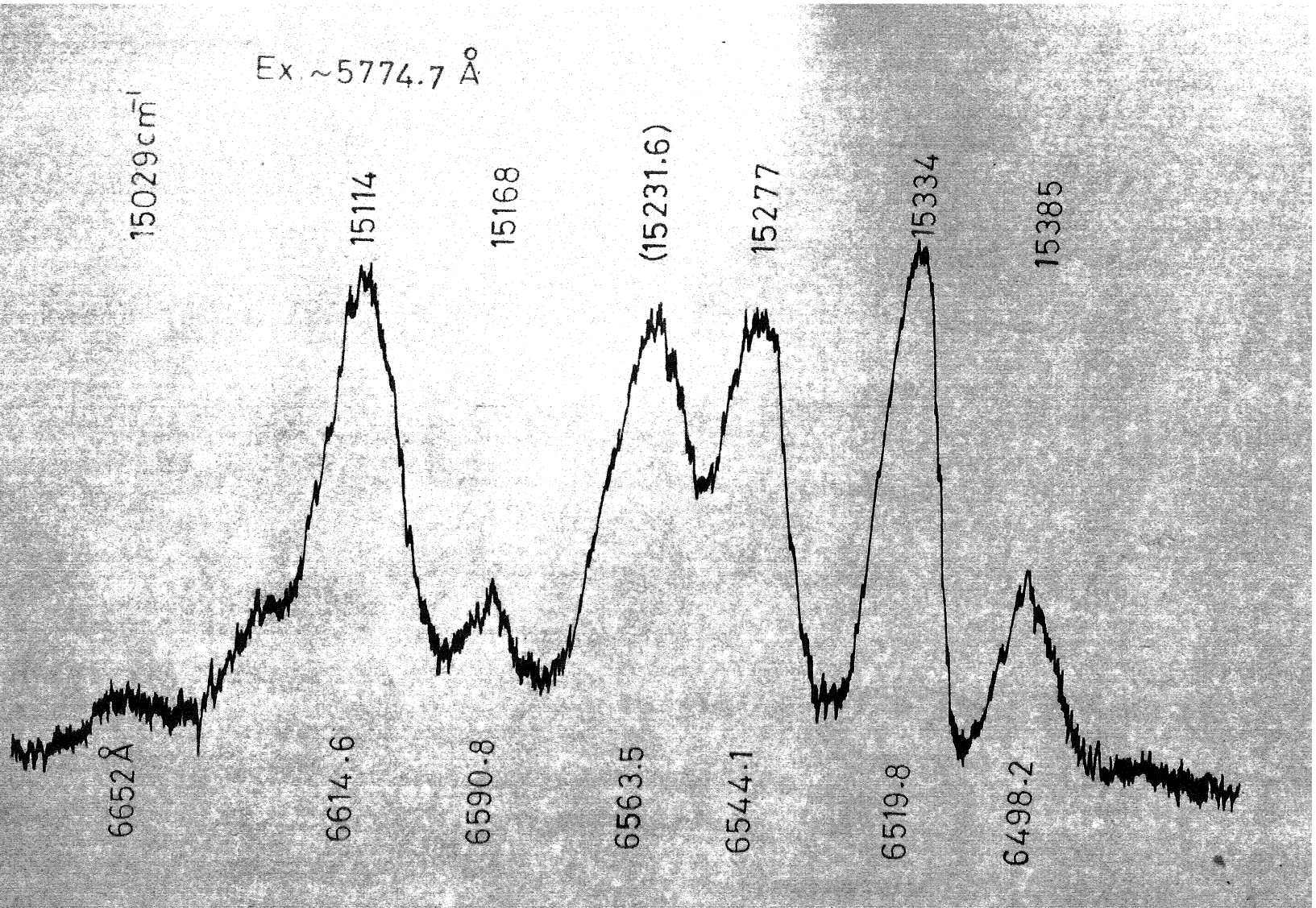


Fig. 5.10 Fluorescence spectrum of $LaF_3:Nd^{3+}$ at LNT, E $\longrightarrow$ X group.

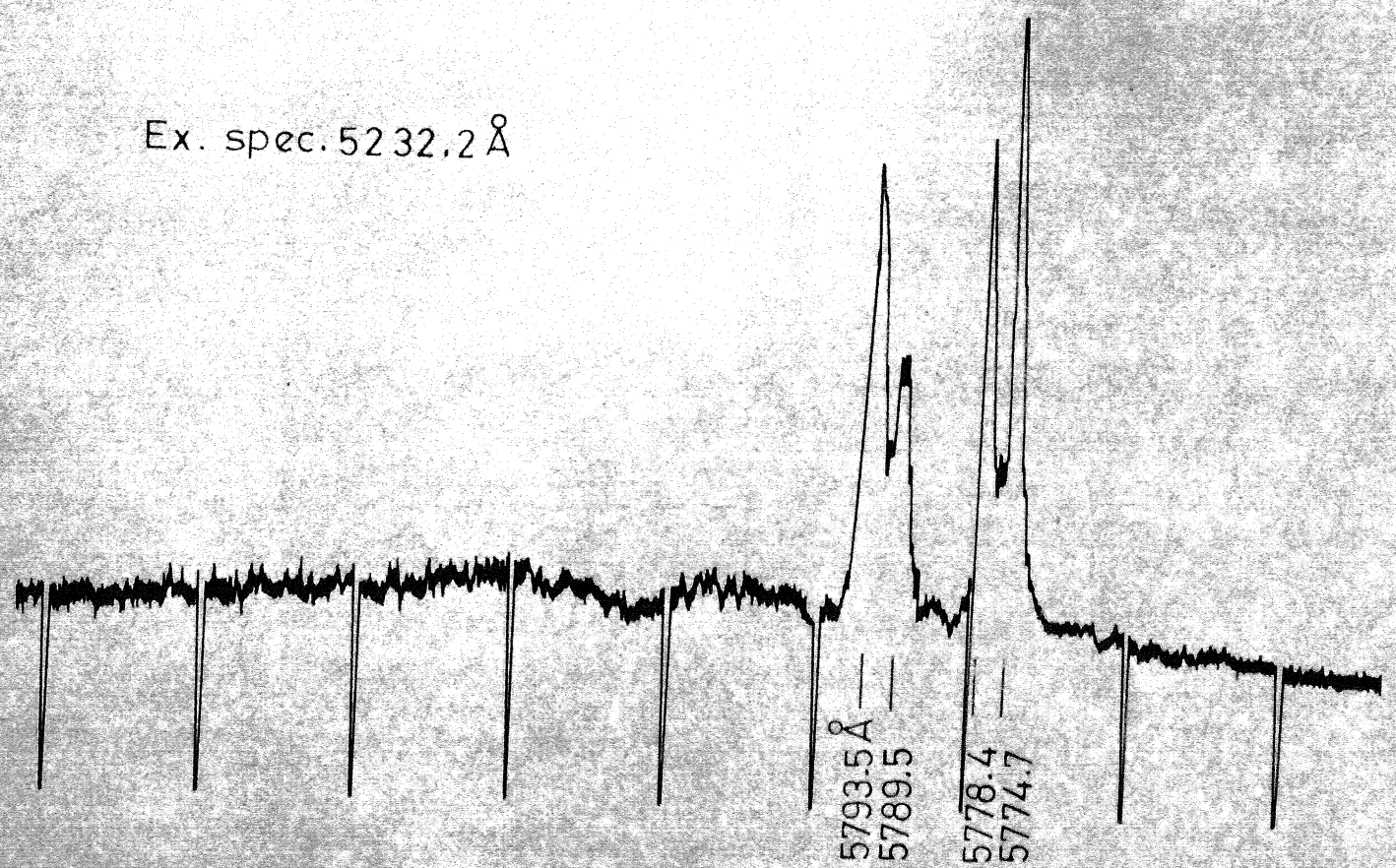


Fig.5.11 Excitation spectrum of $LaF_3:Nd^{3+}$ at LNT.

another photon of the same excitation pulse. In this mechanism only one ion is participating but the number of photons involved is two and is termed, Sequential two photon excitation (STEP) process. (2) In the second possibility the ion which is excited to the D level immediately relaxes to the Y level. Two nearby ions one in the D level and the other in the Y level undergo an energy transfer interaction leaving one ion in the E level and the other in the ground level. This mode of interaction is called Energy transfer up-conversion (ETU) process. ETU process involves the participation of two ions as well as two photons.

Therefore, the measurement of fluorescence intensity versus flux will not distinguish the above two processes. The only way to distinguish the above two is by measuring the decay times. At room temperature the signals are not only weak but also buried under noise. So decay times measurement was not possible. Therefore the above mentioned two possibilities, STEP and ETU processes are suggested for the population of E levels and are shown in Fig.5.12. Some possible ion-pair transitions in ETU process are shown in Table 5.8. The possible energy level matchings in STEP process are shown in Table 5.9. It is seen from Table 5.9 that the exciting wavelengths at 5793.5 Å (17259 cm^{-1}) and 5789.5 Å (17270 cm^{-1}) are resonant

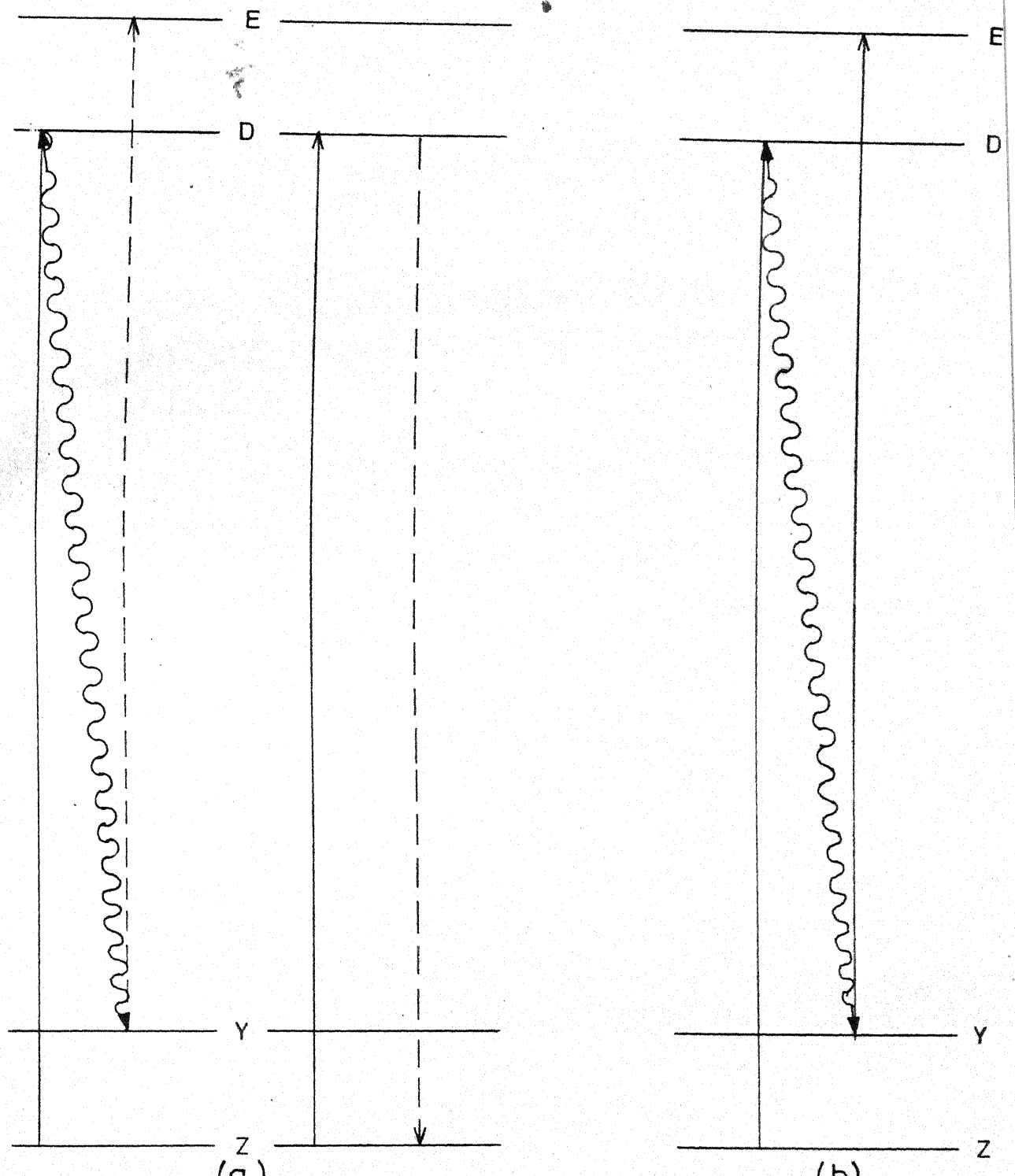


Fig. 5.12 Two probable mechanisims for the production of up converted fluorescence (a) The ETU process in which two excitations on nearby ions annihilate each othe leaving one ion in a higher excited state and the oth in a lower state The dashed line allows represent transitions caused by inter-ionic coupling.

(b) The STEP process in which two sequential excitatio

Table 5.8

Possible Energy Matchings for ETU Process
(D+Y - Z+E)

Initial Levels (D + Y)	Final Levels (Z + E)	Energy mismatch (phonon) cm^{-1}
$D_2(17315) + Y_1(1978) = Z_1(0) + E_2(19235)+58$		58
$D_1(17304) + Y_1(1978) = Z_2(45)+ E_2(19237)$		- (Resonant)
$D_2(17315) + Y_1(1978) = Z_2(45)+ E_3(19248)$		- (Resonant)
$D_1(17304) + Y_1(1978) = Z_3(136)+E_1(19146)$		- (Resonant)
$D_2(17315) + Y_1(1978) = Z_3(136)+E_1(19157)$		6 (Resonant)
$D_2(17315) + Y_2(2037) = Z_1(0) + E_4(19323)+29$		29
$D_1(17304) + Y_2(2037) = Z_2(45)+ E_2(19235)+61$		61
$D_1(17304) + Y_2(2037) = Z_3(136)+E_1(19147)+58$		58

Table 5.9

Possible Energy Matchings for STEP Process
(Z-D ; Y-E)

Excitation Wavelength	Wavenumber (cm^{-1})	Z - D	Y - E
5774.7	17312	Z_1 - D_2	Y_1 +33 - E_4
5778.4	17301	Z_1 - D_1	Y_1 - E_3 +28
5789.5	17268	Z_2 - D_2	Y_1 - E_3
5793.5	17256	Z_2 - D_1	Y_1 - E_2

with $Z \rightarrow D$ as well as $Y \rightarrow E$ transitions.

5. Energy up-converted fluorescence from L multiplet

On exciting the D multiplet resonantly using 5774.7 Å (17312 cm^{-1}) laser line, fluorescence is observed from L multiplet at room and liquid nitrogen temperatures. The observed fluorescence falls in the region 3539-7472 Å. The observed fluorescence groups termin in Z,Y,R,S,A and B multiplets and some of the groups are shown in Fig.5.13-5.15. Excitation spectra have been recorded for 3798, 6348, 6821, and 7472 Å transitions which contain peaks corresponding to the transitions from Z_1 and Z_2 to D_1 and D_2 levels. The excitation spectrum of 3801.6 Å is shown in Fig.5.16. The L levels are populated in one (or more) of the following ways. (1) Two photons may be absorbed simultaneously exciting the ion to P multiplet. Subsequently, L levels are populated by cascade decay or by ion-pair decay. (2) An ion in the excited D level may relax immediately to R level, which, then is picked up by another photon of the same pulse to L level. (STEP). (3) Two nearby excited ions, one in the D level and the other in the R level undergo an energy transfer interaction leaving one ion in a higher excited L level and the other in the ground Z level (ETU). Two photons are involved in the above mentioned three processes. Therefo

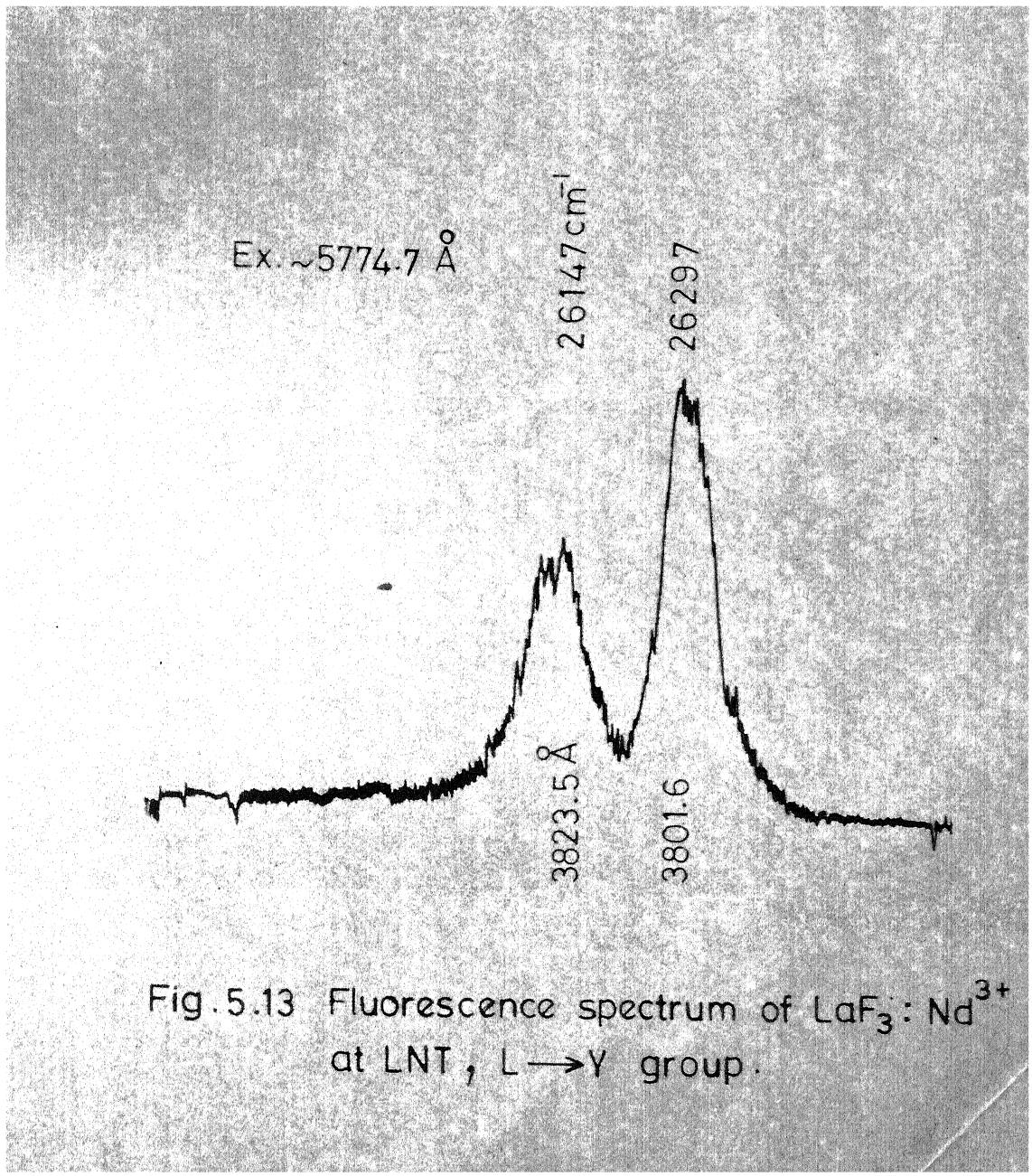


Fig. 5.13 Fluorescence spectrum of $LaF_3 : Nd^{3+}$ at LNT, L ⟶ Y group.

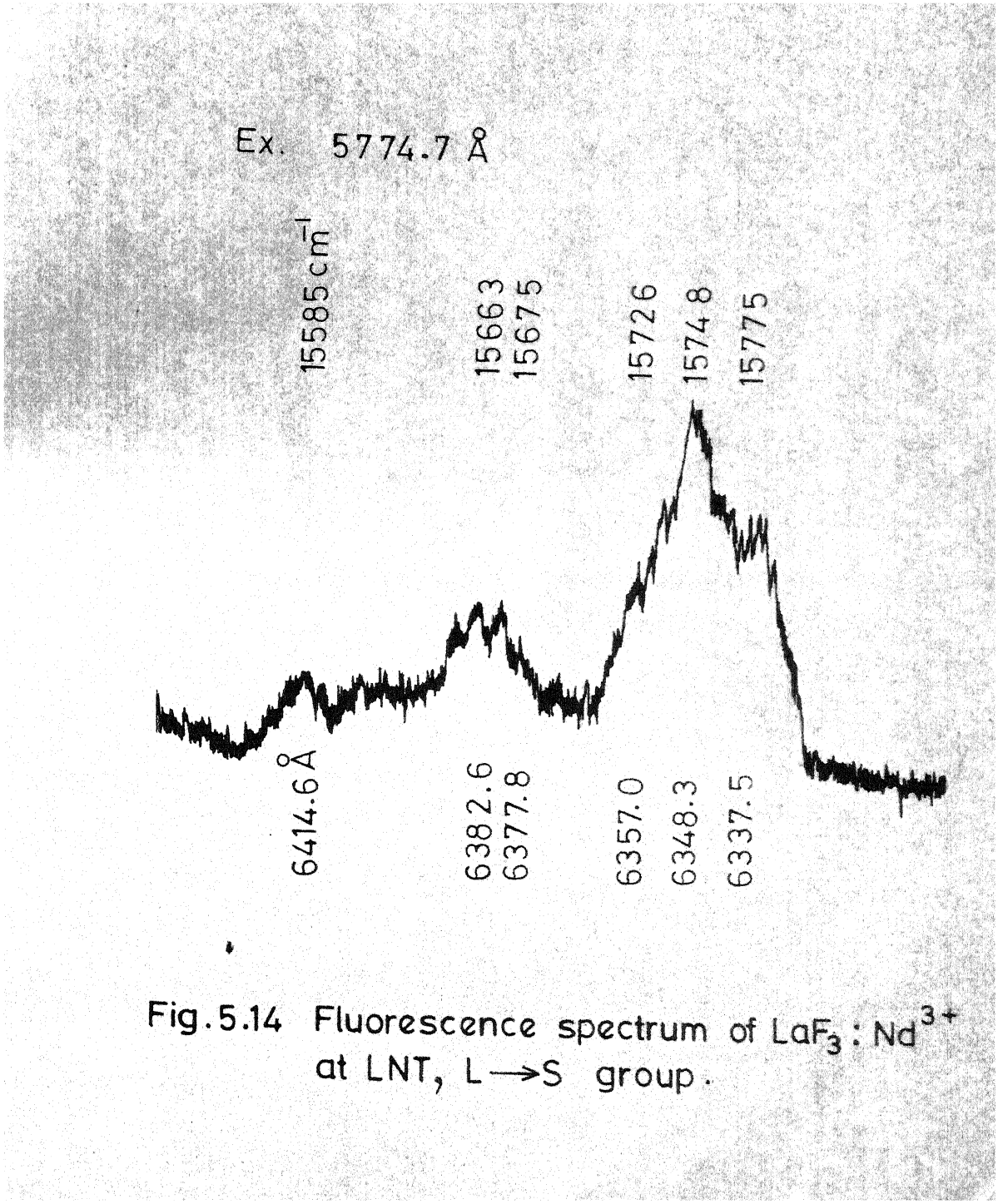


Fig. 5.14 Fluorescence spectrum of $LaF_3 : Nd^{3+}$ at LNT, L → S group.

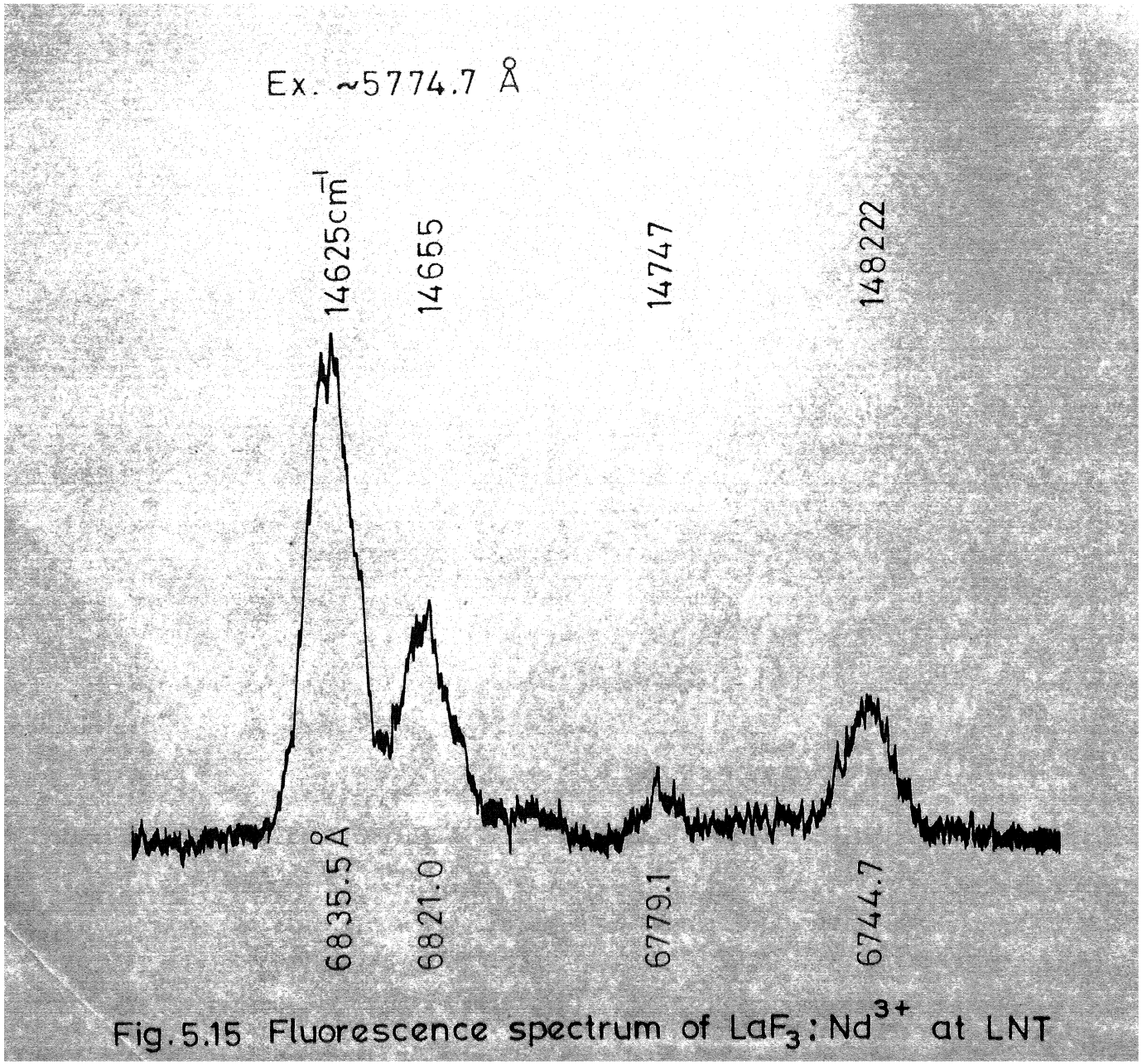


Fig. 5.15 Fluorescence spectrum of $LaF_3:Nd^{3+}$ at LNT



Fig. 5.16 Excitation spectrum of $LaF_3:Nd^{3+}$ at LNT.

the fluorescence intensity from L levels will show quadratic dependance on the pump power[9] in every case. So, the above mentioned experiment (fluorescence intensity versus flux) is not suitable to find the exact process. The only way is to measure the delay (or rise) and decay times of the L fluorescence for various concentrations of Nd^{3+} ion. At room temperature delay times of the induced L fluorescence fall in the region 16-.4 μsec. for the concentrations used (0.1 percent, 0.5 percent, 2.0 percent and 5.0 percent of Nd^{3+}) and the decay times varied from 20 μsecs to 8 μsecs (Table 5.10)and are plotted in Fig.5.17. Among the three possibilities in populating the L levels the first one is very complicated. If the ions were to be excited to P multiplet and then consequently populated L levels by cascade decay only, the delay time should not vary with concentration. But if the ion from P multiplet were to decay to L level by ion-pair relaxation, then L fluorescence would be too weak to be observed under the exciting pump power. But experimentally reasonably intense fluorescence is observed from L levels which is comparable to that of E levels. Based on this, the first process is eliminated. If the STEP process is the only mechanism, then L level decay times should be same as those pertaining to the E level.

[9] Based on limiting steady state equations Zalucha et al found that the intensity of the induced fluorescence will linear in flux and concentration if the ETU processes is most important path for the depopulation of the lower (interacting) levels otherwise (ETU process is slow) it w be quadratic in flux and concentration.

Table 5.10

Delay and Decay Times of L Levels Measured at Room Temperature

Concentration of Nd^{3+} percent by weight	Measured time	
	Delay time (μsec)	Decay time (μsec)
0.1	16 ± 0.8	20 ± 1.0
0.5	10 ± 0.5	20 ± 1.0
2.0	6 ± 0.4	19 ± 1.0
5.0	4 ± 0.2	8 ± 0.4

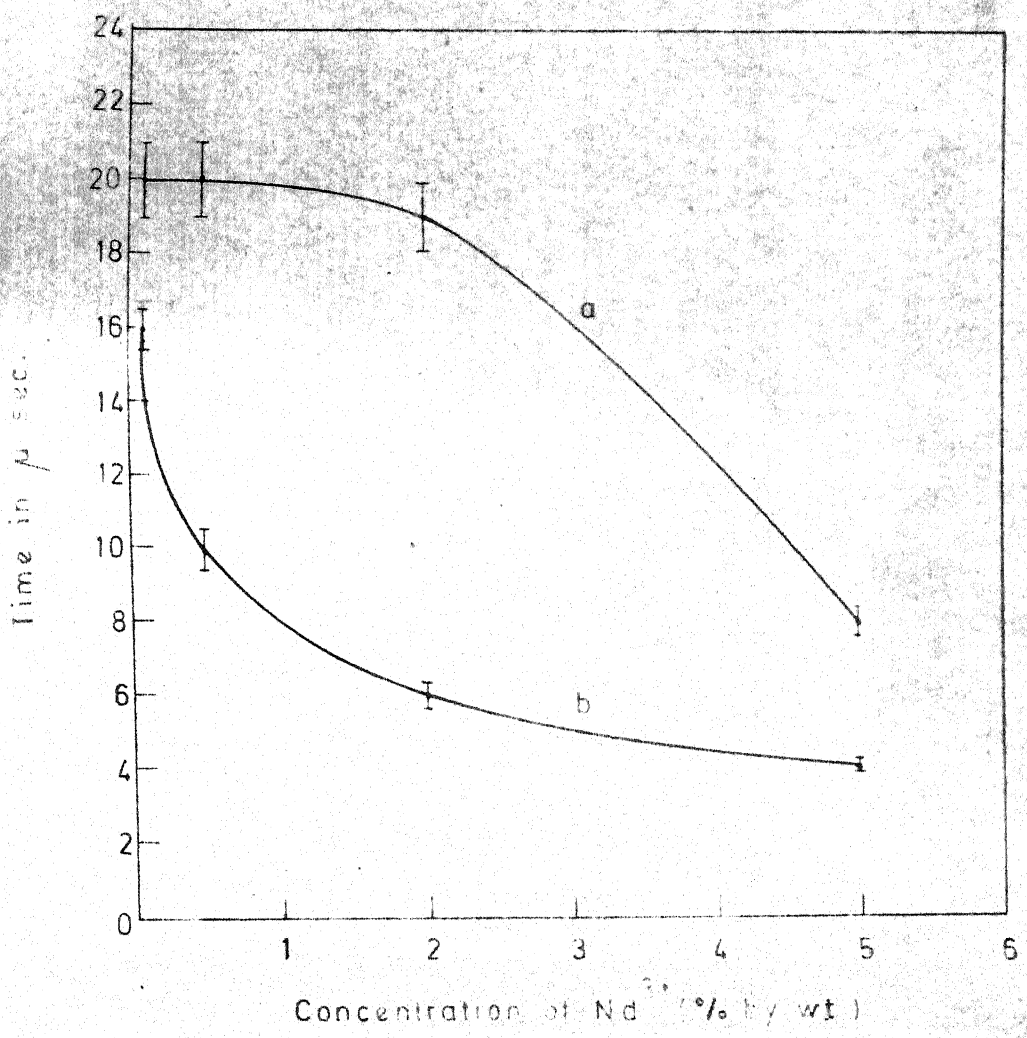


Fig.5.17 Observed (a) decay and (b) delay times respecti
for several concentrations of $LaF_3 : Nd^{3+}$ measur
room temperature of the up-converted L fluore

as those measured by exciting the levels resonantly. And more over there should not be any delay time because the pulse width of the exciting laser line is in nanoseconds. The fact that the delay time decreased from 16 μsecs to 4 μsecs clearly rules out the STEP process. So, ETU process is the only way that can populate the L levels. ETU process can explain the observed delay and decay times times of the induced L level fluorescence. This process is designated as, $D + R \rightarrow L + Z$ and is depicted in Fig.5.18. Under this mechanism of population the induced L level decay times depend on the intrinsic decay times of the D and R levels. Energy transfer interaction between ions in D and R levels causes the population of L levels even after the laser excitation has been turned off. So, there exists a delay (or ris time for the induced L fluorescence. As the concentration of Nd^{3+} is increased, the interaction[φ] between the ions is strengthened and hence the delay (or rise) time of the induced L fluorescence decreases. This argument supports the ETU process in populating the L levels. ETU process can be explained as due to interaction among three ions also. In this process two ions in D and R levels may interact with a third ion in the ground level, Z such that ions which are initially excited will be left in the ground levels, (Z), and the initially unexcited ion in L levels.

φ Energy transfer phenomena are discussed in detail in introductory chapter.

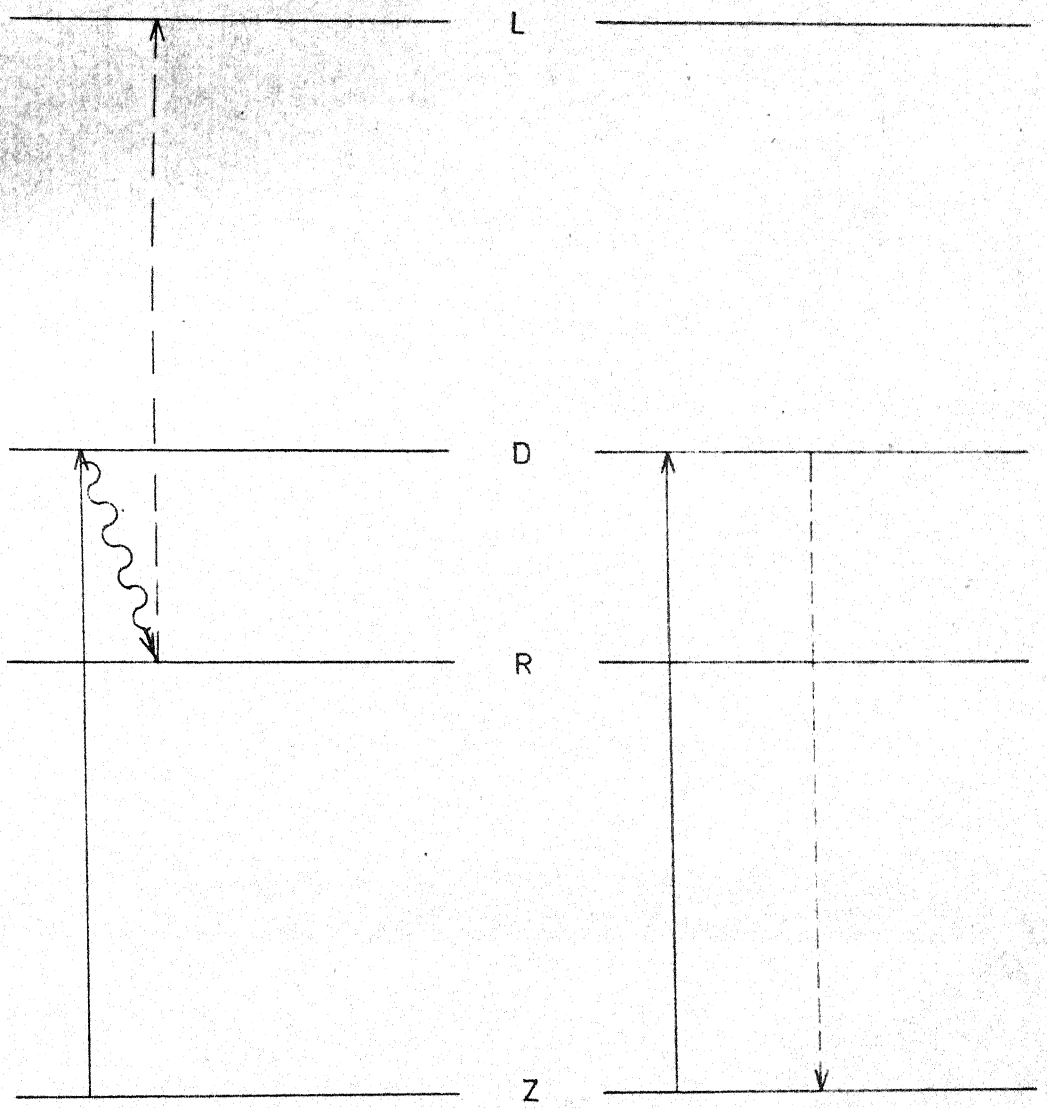


Fig 5.18 ETU process. An ion relaxes from D level to R level. Then two excitations on nearby ions in D and R level annihilate each other leaving one ion in a higher exc state (L) and the other in a lower state (Z)

Table 5.11

Energy Combinations for ETU Process
(D+R - Z+L)

Initial Levels	Final Levels	Energy mismatch (phonon)
D(17304) + R(11592)	= Z(500)+L(28371)+25	25 cm^{-1}
''	= Z(500)+L(28340)+56	56
''	= Z(296)+L(28544)+56	56
''	= Z(136)+L(28525)+235	235
''	= Z(136)+L(28544)+216	216
''	= Z(45) +L(28823)+28	28
''	= Z(0) +L(28544)+352	352
D(17315)+ R(11592)	= Z(296)+L(28525)+86	86
''	= Z(136)+L(28544)+227	227
''	= Z(45) +L(28525)+337	337
''	= Z(45) +L(28544)+318	318
''	= Z(0) + L(28823)+84	84
D(17304) + R(11634)	= Z(500)+L(28340)+98	98
''	= Z(296)+L(28544)+98	98
''	= Z(136)+L(28544)+258	258
''	= Z(45) +L(28544)+349	349
''	= Z(0) + L (28938)	-
D(17315) + R(11634)	= Z(500)+L(28371)+78	78
''	= Z(296)+L(28544)+109	109
''	= Z(136)+L(28544) + 269	269
''	= Z(45) +L(28823)+81	81
''	= Z(0) +L(28823)+126	126

Table 5.12

Energy Combinations for ETU Process

Down Transitions (D-Z, R-Z)		Up Transitions (Z-L)		Energy mismatch (phonon)
D(17304) R(11592)	Z(45) Z(0)	Z(0)	L(28823) + 28	28 cm^{-1}
D(17315) R(11592)	Z(136) Z(296)	Z(45)	L(28525)	5
D(17315) R(11592)	Z(45) Z(0)	Z(45)	L(28823) + 84	84
D(17315) R(11592)	Z(136) Z(0)	Z(45)	L(28823)	7
D(17315) R(11592)	Z(296) Z(45)	Z(0)	L(28544) + 22	22
D(17304) R(11592)	Z(500) Z(0)	Z(0)	L(28371) + 25	25
D(17315) R(11592)	Z(136) Z(500)	Z(0) + 25	L(28295)	-25
D(17315) R(11592)	Z(296) Z(296)	Z(0) + 25	L(28340)	-

Some possible ion-pair transitions are given in Tables 5.11 and 5.12.

6. Rate equation model

The population of the induced L level is estimated from the populations of D and R levels in the following way. Let $N_G(t)$, $N_R(t)$, $N_D(t)$, and $N_L(t)$ represent respectively the populations of the ground, R, D, and L levels at time t; τ_R, τ_D and τ_L be the total intrinsic or 'natural' decay times ; σ_{DR} the rate constant of the initial state D to the final state R and σ_U the rate constant for the ETU process. Also, assume that at time t = 0, only D level is populated since the pulse duration is very much less than the relaxation time and the 'off' period is much longer than the relaxation times.

The lowest order rate equations which can describe excited-state annihilation for pulsed excitation, are given by

$$\frac{dN_D}{dt} = -\frac{N_D}{\tau_D} - \sigma_U N_D N_R \qquad (5.1)$$

$$\frac{dN_R}{dt} = -\frac{N_R}{\tau_R} + \sigma_{DR} N_D - \sigma_U N_D N_R \qquad (5.2)$$

$$\frac{dN_L}{dt} = -\frac{N_L}{\tau_L} + \sigma_U N_D N_R \qquad (5.3)$$

In deriving the above equations it is assumed that the population of levels D and R is not significant by the decay from L level. Also, assume that

$$\sigma_U N_D N_R \ll \frac{N_D}{\tau_D} \tag{5.4}$$

$$\sigma_U N_D N_R \ll \frac{N_R}{\tau_R} \tag{5.5}$$

The rate equations can be written as

$$\frac{dN_D}{dt} = - \frac{N_D}{\tau_D} \tag{5.6}$$

$$\frac{dN_R}{dt} = - \frac{N_R}{\tau_R} + \sigma_{DR} N_D \tag{5.7}$$

$$\frac{dN_L}{dt} = \sigma_U N_D N_R - \frac{N_L}{\tau_L} \tag{5.8}$$

At this stage it is important to note that the laser is on for a time which is much less than the relaxation times of the levels involved. So at time $t = 0$; $N_R(0) = N_L(0) =$ and $N_D(0) \neq 0$. Solution of equation 5.6 (population of D level) can be written as

$$N_D(t) = N_D(0)\, e^{-t/\tau_D} \tag{5.9}$$

Substituting the value of $N_D(t)$ in equation 5.7 and solving it for $N_R(t)$, it gives

$$N_R(t) = \frac{\sigma_{DR} N_D(0)}{\frac{1}{\tau_R} - \frac{1}{\tau_D}} \left(e^{-t/\tau_D} - e^{-t/\tau_R} \right) \quad (5.10)$$

The product of equations 5.9 and 5.10 is

$$N_L(t)N_R(t) = \frac{\sigma_{DR} N_D^2(0)}{\frac{1}{\tau_R} - \frac{1}{\tau_D}} \left(e^{-\frac{2t}{\tau_D}} - e^{-(\frac{1}{\tau_R} + \frac{1}{\tau_D})t} \right) \quad (5.11)$$

Substituting the value of $N_D(t)N_R(t)$ in equations 5.8 and solving it for $N_L(t)$ it gives,

$$N_L(t) = \frac{\sigma_U \sigma_{DR} N_D^2(0)}{\tau_R^{-1} - \tau_D^{-1}} \left(\frac{e^{-2t/\tau_D}}{\tau_L^{-1} - 2\tau_D^{-1}} - \frac{e^{-t/\tau_R} \cdot e^{-t/\tau_D}}{\tau_L^{-1} - \tau_D^{-1} - \tau_R^{-1}} + \right.$$

$$\left. + \frac{(\tau_R^{-1} - \tau_D^{-1})\, e^{-t/\tau_L}}{(\tau_L^{-1} - 2\tau_D^{-1})(\tau_L^{-1} - \tau_D^{-1} - \tau_R^{-1})} \right) \quad (5.12)$$

Equation 5.12 represents delayed emission from state L, under pulsed excitation of D level. For simultaneous and sequential two-photon excitation, state L would have had single exponential decay with time constant τ_L. We now consi the following limiting cases to have a direct physical insight into the actual situation though these are not rigorously valid.

Assume $\tau_R \gg \tau_D$, $\tau_R \gg \tau_L$ and for $t > \tau_D$

$$N_D(t) = N_D(0) \; e^{-t/\tau_D} \tag{5.9}$$

And

$$N_R(t) = \sigma_{DR} \, N_D(0) \, \tau_D \; e^{-t/\tau_R} \tag{5.13}$$

The second term in equation 5.10, is much smaller and hence neglected.

$$N_D(t)N_R(t) = \sigma_{DR} \, N_D^2(0) \, \tau_D \; e^{-t\left(\frac{1}{\tau_R} + \frac{1}{\tau_D}\right)}$$

$$\simeq \sigma_{DR} \, N_D^2(0) \, \tau_D \; e^{-t/\tau_D} \tag{5.14}$$

Then the solution of equation 5.8 is

$$N_L(t) = \frac{\sigma_U \sigma_{DR} N_D^2(0)}{\tau_D^{-1}(\tau_L^{-1} - \tau_D^{-1})} \left(e^{-t/\tau_D} - e^{-t/\tau_L} \right) \tag{5.15}$$

Case (i) : Say $\tau_D \gg \tau_L$, now equation 5.15 becomes

$$N_L(t) = \frac{\sigma_U \sigma_{DR} N_D^2(0)}{\tau_D^{-1} \, \tau_L^{-1}} \; e^{-t/\tau_D} \tag{5.16}$$

This implies that the state L decays with the time constant τ_D. This type of situation has been encountered by Partlow [3] and Zalucha et al [3].

Case(ii) : Say $\tau_L \gg \tau_D$, now equation 5.15 becomes

$$N_L(t) = \frac{\sigma_U \sigma_{DR} N_D^2(0)}{(\tau_D^{-1})^2} e^{-t/\tau_L} \qquad (5.17)$$

That is the state L decays with its time constant.

Case (iii) : Say $\tau_L > \tau_D$; In this case equation 5.15 retains both the terms

$$N_L(t) = \frac{\sigma_U \sigma_{DR} N_D^2(0)}{\tau_D^{-1}(\tau_D^{-1} - \tau_L^{-1})} \left(e^{-t/\tau_L} - e^{-t/\tau_D} \right) \qquad (5.15)$$

Equation 5.15 represents a case in which there will be some delay which depends on τ_D and τ_L and which decays with the time constant$^{\varphi}$ τ_L. The measured delay and decay times of L level fluorescence support this case. The fact that the induced decay times are approximately of the same magnitude as if measured intrinsically [16] and that the delay times are less than the decay times suggests that the decay time of D level is less than that of L level.

Equation 5.12 or 5.15 shows that the L level population, $N_L(t)$ is proportional to square of the population of D level $N_D^2(0)$. But the D level population itself is proportional to the intensity of the exciting laser. This shows that the L level population and hence its fluorescence will show quadratic dependance on incident pump power.

φ Eqn.5.15 actually indicates that the decay time should depend upon both τ_D and τ_L, but the experimental value is nearly equal to τ_L.

The above mathematical treatment and the measured delay and decay times of L fluorescence clearly support the Energy transfer up-conversion (ETU) process in populating the L levels when D levels are resonantly excited.

5.3 Conclusion

It has been observed that the R levels are populated by ion-pair relaxation of the type, $D(1) + Z(2) \rightarrow R(1) + W(2)$. The S levels, whose fluorescence is observed only at room temperature are found to be populated due to thermal contribution from R levels. Two processes, STEP and ETU have been suggested for the population of E levels. From the measured delay and decay times of L fluorescence it has been concluded that these levels are populated by energy transfer interaction between two ions, one in D and the other in R levels. A rate equation model has been developed for the population of L levels which could explain the delayed emission from these levels.

REFERENCES

1. J.C. Wright, D.J. Zalucha, N.V. Lauer, D.E. Cox and F.K. Fong, J. Appl. Phys. 44, 781 (1973).

2. D.J. Zalucha, J.A. Sell and F.K. Fong, J.Chem.Phys. 60, 1660 (1974).

3. W.D. Partlow, Phys. Rev. Lett. 21, 90 (1968).

 D.J. Zalucha, J.C. Wright and F.K. Fong, J.Chem.Phys. 59, 997 (1973).

4. F.E. Auzel, Proc. IEEE 61, 758 (1973)

 R.A. Hewes and J.F. Sarver, Phys.Rev. 182,427 (1969).

5. F.K. Fong, Theory of Molecular Relaxation, Chapt. 9 (John Wiley Sons (1975)).

6. W.B. Gandrud and H.W. Moos, J. Chem. Phys.49, 2170 (1968).

7. J.A. Sell and F.K. Fong, J.Chem.Phys. 62, 4161 (1975).

8. All the above references and
 M.R. Brown and W.A. Shand, 'Advances in Quantum Electronics, Vol.1, Ed. D.W. Goodwin.
 R.J. Woodward, T.A. Williams and M.R. Brown, Phys.Lett. 22, 435 (1966).

 L.D. Livanova, I.G. Saitkulov and A.L. Stolov, Sov. Phys. Sol.Stat.11, 750 (1969).

 T. Miyakawa and D.L. Dexter, Phys.Rev. B1, 70 (1970).

 M. Haeskaylo, J. Appl. Phys. 48, 4803 (1977).

 P.P. Feofilov and V.V. Ovsyankin, Appl.Opt. 6, 1828 (1967).

 M.R. Brown, W.A. Shand and J.S.S. Whiting, Brit.J.Appl. Phys. 16, 619 (1965).

 M.R. Brown, and W.A. Shand, IEEE Journal of Quant.Elec. QE-2, 8 (1966).

 J.P. van der Ziel, F.W. Ostemayer Jr., and L.G. Van Uitert Phys. Rev. B2, 4432 (1970).

9. G.E. Barasch and G.H. Dieke, J.Chem.Phys.43, 988 (1965).

10. C.K. Asawa and M. Robinson, Phys.Rev. 141, 251 (1966)

11. C.K. Asawa, Phys. Rev. 155, 188 (1967).

12. R. Reisfeld and C.K. Jorgensen, 'Lasers and Excited States of Rare Earths' (Springer-Verlag Berlin, 1977) pp. 94.

13. H.H. Caspers, H.E. Rast and R.A. Buchanan, J.Chem. Phys. 42, 3214 (1965).

14. U.V. Kumar, H. Jagannath, D. R. Rao and P. Venkateswarlu Ind. J. Phys. 50, 90 (1976).

15. U.V. Kumar, D.R. Rao and P. Venkateswarlu, J.Chem. Phys. 67, 3448 (1977).

16. H. Jagannath, S.K. Basu and P. Venkateswarlu, Chem.Phys.Lett. 66, 313 (1979).

A 67014

Date Slip

This book is to be returned on the date last stamped.

CD 6.72.9

PHY- 1980-D-RED-2AS